



# University of Sheffield

**Investigating Dipeptide Repeat Interactions  
and Hypoxia as Mechanisms of Toxicity in a  
*Drosophila* model of *C9orf72* Frontotemporal  
Dementia and Amyotrophic Lateral Sclerosis**

**Duncan R. Garner**

Thesis submitted for the degree of  
Doctor of Philosophy (PhD)  
in the Department of Neuroscience

**April 2024**

# Table of Contents

<b>List of Figures</b>	<b>8</b>
<b>List of Tables</b>	<b>10</b>
<b>List of Abbreviations</b>	<b>12</b>
<b>Abstract</b>	<b>16</b>
<b>Acknowledgements</b>	<b>17</b>
<b>1. Introduction</b>	<b>18</b>
<b>1.1. Rationale</b>	<b>18</b>
<b>1.2. Frontotemporal dementia and amyotrophic lateral sclerosis</b>	<b>19</b>
1.2.1 Overview	19
1.2.2. Clinical characteristics	20
1.2.2.1. FTD	20
1.2.2.2. ALS	21
1.2.3. Neuropathology	22
1.2.4. Epidemiology and aetiology	26
1.2.5. Genetic causes	27
<b>1.3. <i>C9orf72</i></b>	<b>30</b>
1.3.1. Discovery of the <i>C9orf72</i> expansion	31
1.3.2. Features of the <i>C9orf72</i> expansion	32
1.3.2.1 Clinical	32
1.3.2.2. Pathology	32
1.3.2.3. Epidemiology	33
1.3.3. Impact of <i>C9orf72</i> repeat length	34

1.3.4. Mechanisms of disease	35
1.3.4.1. Loss of C9orf72 function through haploinsufficiency	36
1.3.4.2. RNA foci	37
1.3.4.3. Dipeptide repeat proteins (DPRs)	38
<b>1.4. Gene/Environment/Time hypothesis</b>	<b>44</b>
<b>1.5. Hypoxia</b>	<b>45</b>
1.5.1. Physiological response to hypoxia	45
1.5.2. Hypoxia in neurodegenerative disease	48
<b>1.6. Drosophila melanogaster as a model organism</b>	<b>50</b>
1.6.1 UAS/Gal4	50
1.6.2. Modelling neurodegenerative disease	51
1.6.3. Modelling C9orf72 FTD/ALS	52
1.6.4. Modelling hypoxia	56
<b>1.7. Aims of research</b>	<b>56</b>
<b>2. Materials and Methods</b>	<b>58</b>
<b>2.1. Drosophila husbandry</b>	<b>58</b>
<b>2.2. Generation of transgenic flies</b>	<b>63</b>
<b>2.3. Genetic interaction eye screens</b>	<b>63</b>
<b>2.4. Behavioural assays</b>	<b>64</b>
2.4.1. Startle-induced negative geotaxis (SING) assay	64
2.4.2. Locomotor activity monitoring assay	65
2.4.3. Sleep analysis	66
<b>2.5. Hypoxia</b>	<b>66</b>
2.5.1. Hypoxic exposure	66

2.5.2. Hypoxic stupor assay	66
2.5.3. Intermittent hypoxic exposure	67
2.5.4. Continuous hypoxic exposure	67
<b>2.6. Immunohistochemistry (IHC)</b>	<b>68</b>
2.6.1. Salivary gland dissection	68
2.6.2. Adult brain dissections	70
2.6.3. TUNEL Assay	70
2.6.4. Imaging apparatus	71
<b>2.7. Biochemistry</b>	<b>71</b>
2.7.1. Protein extraction	71
2.7.2. Protein quantification	72
2.7.3. Western blotting	72
2.7.4. Co-immunoprecipitation and sample preparation for tandem mass spectrometry	73
2.7.5. Protein identification	74
2.7.6. Protein Ontology	74
2.7.7. Trizol extraction of RNA	75
2.7.8. DNase treatment and reverse transcription	75
2.7.9. RT-qPCR	76
2.7.10 RT-qPCR primers	78
2.7.11 Primer optimisation	79
2.7.12 Analysis	79
2.7.13 Amplex Red H <sub>2</sub> O <sub>2</sub> assay	80
<b>2.8. Generation of graphics, statistics and figures</b>	<b>80</b>
<b>2.9. Antibodies</b>	<b>81</b>

<b>3.</b>	<b>Identification of DPR interacting proteins using 1000-repeat DPR models</b>	<b>82</b>
<b>3.1.</b>	<b>Introduction</b>	<b>82</b>
<b>3.2.</b>	<b>Results</b>	<b>83</b>
	3.2.1. 1000-repeat DPR-interacting proteins are identified by mass tandem spectrometry following co-immunoprecipitation	83
	3.2.2. 1000-repeat DPRs interactomes are enriched in distinct profiles of biological processes	85
	3.2.3. XPO1 and CNOT1 are potential modifiers of GR1000 toxicity	92
<b>3.3.</b>	<b>Discussion</b>	<b>98</b>
	3.3.1. Identification of physiologically-relevant DPR-proteins interactions	98
	3.3.2. Distinct protein interaction profiles between DPRs	98
	3.3.3. Localisation of DPR interactomes aligns with DPR localisation	102
	3.3.4. GA exhibits a length dependent interactome	104
	3.3.5. AP1000 exhibits a small but novel interactome	105
	3.3.6. PR exhibits a length dependent interactome	106
	3.3.7. GR1000 exhibits many, novel protein interactions	108
	3.3.8. DNMT1 and NSF are key proteins but do not modify GR1000 toxicity	109
	3.3.9. mROH1 and GANAB represent novel GR interactors but do not modify GR1000 toxicity	110
	3.3.10. CNOT1 is a potential modifier of GR1000 toxicity	111
	3.3.11. XPO1 is relevant to C9 disease and a potential modifier of GR1000 toxicity	112
<b>3.4.</b>	<b>Conclusions</b>	<b>114</b>

<b>4.</b>	<b>Characterisation of XPO1 as a GR1000-interacting protein</b>	<b>115</b>
<b>4.1.</b>	<b>Introduction</b>	<b>115</b>
<b>4.2.</b>	<b>Results</b>	<b>116</b>
	4.2.1. Knockdown of XPO1 modifies age-related GR1000 motor deficits	116
	4.2.2. GR1000 motor activity deficits are not modified by knockdown of XPO1	119
	4.2.3. XPO1 is a modifier of GR1000 sleep phenotypes	121
	4.2.4. Interaction with GR1000 does not disrupt XPO1 localisation or function	124
<b>4.3.</b>	<b>Discussion</b>	<b>132</b>
	4.3.1. Severe knockdown of XPO1 is detrimental	132
	4.3.2. Partial knockdown of XPO1 delays the onset of age-related GR1000 phenotypes	133
	4.3.3. XPO1 localisation and function is unaffected by the GR1000-XPO1 interaction	134
	4.3.4. Study of the GR1000-XPO1 interaction is hampered by the lack of appropriate tools in <i>Drosophila</i>	136
	4.3.5. GR1000 does not significantly damage the nuclear envelope	137
<b>4.4.</b>	<b>Conclusions</b>	<b>139</b>
<b>5.</b>	<b>Investigating the role of hypoxia and HIF1<math>\alpha</math> in GR1000 toxicity</b>	<b>140</b>
<b>5.1.</b>	<b>Introduction</b>	<b>140</b>
<b>5.2.</b>	<b>Results</b>	<b>141</b>
	5.2.1. HIF1a as a modifier of GR1000 toxicity	141

5.2.2. Intermittent hypoxia does not cause or exacerbate motor phenotypes	147
5.2.3. GR1000 disrupts the sensing of and/or response to hypoxia	150
5.2.4. Continuous hypoxia does not potentiate GR1000 motor deficits	158
5.2.5. Knockdown of HIF1 $\alpha$ does not facilitate hypoxia-induced effects on GR1000 motor phenotypes	163
<b>5.3. Discussion</b>	<b>166</b>
5.3.1. Basal activity of HIF1 $\alpha$ under normoxic conditions is unaffected by GR1000	166
5.3.2. GR1000 perturbs the hypoxic stupor response	166
5.3.3. GR1000 motor phenotypes are unaffected by intermittent hypoxia	168
5.3.4. GR1000 perturbs the transcriptional response to continuous hypoxia	169
5.3.5. Hypoxia may be associated with molecular changes in brains expressing GR1000	171
5.3.6. Uncovering the effects of GR1000 on HIF1 $\alpha$ protein localisation and abundance	172
5.3.7. GR1000 motor phenotypes are unaffected by continuous hypoxia	173
5.3.8. NF- $\kappa$ B activity is modulated by GR1000	174
<b>5.4. Conclusions</b>	<b>174</b>
<b>6. Discussion</b>	<b>176</b>
<b>6.1. Role of hypoxia in <i>C9orf72</i> FTD/ALS</b>	<b>177</b>
6.1.1. Exposure to hypoxia	177
6.1.2. HIF1 $\alpha$ -mediated response to hypoxia	178

6.1.3. Tissue level hypoxia	179
6.1.4. Hypoxia and astrocytes	180
<b>6.2. Role of XPO1 in <i>C9orf72</i> FTD/ALS</b>	<b>181</b>
<b>6.3. Hypothesis of the GR-mediated aberrant response to hypoxia</b>	<b>181</b>
<b>6.4. Implications for patients</b>	<b>182</b>
<b>6.5. Conclusions</b>	<b>183</b>
<b>6.6. Summary of key findings</b>	<b>184</b>
<b>7. Appendices</b>	<b>185</b>
<b>7.1. Proteins identified by tandem mass spectrometry as present in DPR but not GFP</b>	<b>185</b>
<b>7.2. Proteins identified by tandem mass spectrometry as significantly higher in DPR than GFP</b>	<b>209</b>
<b>7.3. Whole blots for Figure 4.5</b>	<b>215</b>
<b>8. Bibliography</b>	<b>217</b>

## List of figures

Figure 1.1. Frontotemporal dementia (FTD) and amyotrophic lateral sclerosis (ALS) exist on a single disease spectrum	29
Figure 1.2. Mechanisms of disease in <i>C9orf72</i> FTD/ALS.	36
Figure 1.3. Repeat-associated non-AUG (RAN) translation of sense and antisense hexanucleotide repeat RNA, in every reading frame, produces five toxic dipeptide repeat proteins (DPRs)	39
Figure 1.4. DPRs disrupt cellular processes to cause neurotoxicity.	43
Figure 1.5. HIF1 is the transcriptional master regulator of the cellular response to hypoxia	47
Figure 1.6. Expression of EGFP-tagged 1000-repeat DPRs in <i>Drosophila</i> using the GAL4/UAS system	53
Figure 2.1. Cartoon representations of wildtype <i>Drosophila</i> and scored eye phenotypes used in eye screen scoring system	64
Figure 2.2. Startle induced negative geotaxis assay	65
Figure 2.3. Locomotor activity monitoring assay	66
Figure 2.4 Hypoxic stupor assay	67
Figure 2.5 Nuclear/Cytoplasmic fluorescence analysis	69
Figure 2.6 RT-qPCR experimental conditions	77
Figure 3.1. Isolation and identification of DPR-interacting proteins	84
Figure 3.2. The GA1000 interactome is significantly enriched in cytoskeletal, metabolic and RNA processes	88
Figure 3.3. The AP1000 interactome is significantly enriched in cytoskeletal and signalling processes	89
Figure 3.4. The PR1000 interactome is significantly enriched in multiple transport and localisation processes	90

Figure 3.5. The GR1000 interactome is significantly enriched in multiple transport and localisation processes	91
Figure 3.6. Genetic manipulation of shortlisted genes modifies GFP- and GR1000-induced phenotypes in the <i>Drosophila</i> eye	97
Figure 4.1. Knockdown of XPO1 delays age-related motor decline in flies pan-neuronally expressing GR1000	118
Figure 4.2. Knockdown of XPO1 does not modify activity deficits in flies pan-neuronally expressing GR1000	120
Figure 4.3. Total sleep is increased in flies pan-neuronally expressing GR1000	122
Figure 4.4. Pan-neuronal expression of GR1000 causes changes in sleep bout duration that are modified by knockdown of XPO1	123
Figure 4.5. Cytoplasmic 120 kDa band intensity does not change with GR1000 expression	126
Figure 4.6. Localisation of anti-XPO1 signal and its cargoes, exd and YAN, is not significantly affected by GR1000 expression	128
Figure 4.7. Anti-XPO1 signal localises predominantly to the neuronal cell body in <i>in vitro</i> <i>Drosophila</i> primary neurons	130
Figure 4.8. Nuclear envelope abnormalities are not significantly more common in flies expressing GR1000	131
Figure 5.1. HIF1 $\alpha$ is a modifier of GR1000 toxicity in the <i>Drosophila</i> eye	142
Figure 5.2. Genetic manipulation of HIF1 $\alpha$ modifies <i>Drosophila</i> climbing phenotypes	144
Figure 5.3. Genetic manipulation of HIF1 $\alpha$ does not modify activity deficits in flies pan-neuronally expressing GR1000	146
Figure 5.4. Intermittent hypoxia does not cause or exacerbate motor phenotypes in <i>Drosophila</i>	149
Figure 5.5. The <i>Drosophila</i> hypoxic stupor response is perturbed by pan-neuronal expression of 1000-repeat DPRs	151

Figure 5.6. Pan-neuronal expression of GR1000 perturbs the transcriptional response to hypoxia in <i>Drosophila</i>	154
Figure 5.7. Pan-neuronal expression of GR1000 does not affect activity under hypoxia in <i>Drosophila</i>	155
Figure 5.8. Pan-neuronal expression of GR1000 does not significantly exacerbate hypoxia-induced DNA damage or oxidative stress	157
Figure 5.9. Regime for repeated hypoxic exposure in <i>Drosophila</i>	159
Figure 5.10. Pan-neuronal expression of GR1000 prevents hypoxia-induced increases in climbing ability	161
Figure 5.11. Repeated exposure to hypoxia does not modify activity deficits in flies pan-neuronally expressing GR1000	162
Figure 5.12. Knockdown of HIF1 $\alpha$ does not affect <i>Drosophila</i> climbing ability following exposure to hypoxia	164
Figure 5.13. Knockdown of HIF1 $\alpha$ does not affect <i>Drosophila</i> motor activity following exposure to hypoxia	165

## List of tables

Table 1.1. Summary of FTLD-TDP subtypes and their associated pathology, clinical syndromes, and genetics	25
Table 1.2. FTLD-FUS subtypes and the characteristics of FET-positive inclusions	26
Table 1.3. <i>Drosophila</i> models of <i>C9orf72</i> -mediated frontotemporal dementia and amyotrophic lateral sclerosis	54
Table 2.1. <i>Drosophila</i> stocks used in this study	59
Table 2.2. Filter cubes used in this study	71
Table 2.4. RT-qPCR primers used in this study	78
Table 2.5. Antibodies used in this study	81

Table 3.1. GR-interacting proteins shortlisted for genetic modifier screening	94
Table 3.2. Summary of DPR interactome studies and their findings	99

## List of Abbreviations

ALS	Amyotrophic lateral sclerosis
AMPK	AMP-activated protein kinase
ANG	Angiogenin
AP	Alanine-proline
ATP	Adenosine tri-phosphate
BIBD	Basophilic inclusion body disease
BSA	Bovine serum albumin
bvFTD	behavioural variant FTD
C9	C9orf72
C9orf72	Chromosome 9 open reading frame 72
CHMP2B	Charged multivesicular body protein 2B
CNOT1	CCR4-NOT transcription complex subunit 1
CNS	Central nervous system
co-IP	Co-immunoprecipitation
CSF	Cerebrospinal fluid
CTC/N/BF	corrected total cytoplasmic/nuclear/brain fluorescence
CYLD	Cylindromatosis (Human)
dCYLD	Cylindromatosis ( <i>Drosophila</i> )
Dif	Dorsal-related immunity factor
DNM1	Dynamin 1
DENN	differentially expressed in normal and neoplastic cells
DEPC	Diethyl pyrocarbonate
dpe	Days post eclosion
DPR	Dipeptide repeat protein
DSHB	Developmental studies hybridoma bank
EWS	Ewing's sarcoma protein
EGFP	Enhanced green fluorescent protein
emb	Embargoed
EPO	Erythropoietin
exd	Extradenticle
fALS	Familial ALS

FET	FUS, EWS, TAF15
FIH-1	Factor inhibiting HIF1
FTD	Frontotemporal dementia
FTLD	Frontotemporal lobar degeneration
FUS	Fused in sarcoma
GA	Glycine-alanine
GANAB	Glucosidase II $\alpha$ subunit (human)
GCS2 $\alpha$	Glucosidase II $\alpha$ subunit ( <i>Drosophila</i> )
GDP/GTP	Guanosine di-/tri-phosphate
GEF	Guanine nucleotide exchange factor
GLUT1	Glucose transporter 1
GMR	Glass multimer reporter
GP	Glycine-proline
GR	Glycine-arginine
GRN	Granulin
GWA	Genome wide association
HIF1 $\alpha$	Hypoxia-inducible factor 1 $\alpha$
hnRNP	Heterogeneous nuclear ribonucleoproteins
HRE	Hypoxia reactive element
HRP	Horseradish peroxidase
ICC	Immunocytochemistry
IHC	Immunohistochemistry
iNPC	Induced neural progenitor cell
iPSC	Induced pluripotent stem cell
LDH	Lactate dehydrogenase
MAPT	Microtubule-associated protein tau
MND	Motor neuron disease
mROH1	Maestro heat like repeat family member 1
MS	Mass spectrometry
NCT	Nucleocytoplasmic transport
NF- $\kappa$ B	Nuclear factor kappa B
NIFID	Neuronal intermediate filament inclusion disease

nfvPPA	Non-fluent variant primary progressive aphasia
Nsf2	N-ethylmaleimide sensitive factor 2
NSF	N-ethylmaleimide sensitive factor
nSyb	Neuronal synaptobrevin
Nup107	Nucleoporin 107kD
ODDD	Oxygen-dependent degradation domain
PBS	Phosphate-buffered saline
PDK	Pyruvate dehydrogenase kinase
PERK	Protein kinase RNA-like endoplasmic reticulum kinase
PHD	HIF-prolyl hydroxylase
PR	Proline-arginine
Pvf1	PDGF- and VEGF- related factor 1
RAN	Repeat associated non-AUG translation
RBP	RNA-binding protein
RFP	Red fluorescent protein
RIPA	Radioimmunoprecipitation assay
RO	RNA only
ROI	Region of interest
ROS	Reactive oxygen species
RT-qPCR	Reverse transcriptase quantitative polymerase chain reaction
sALS	Sporadic ALS
SG	Stress granule
Shi	Shibire
SING	Startle-induced negative geotaxis
SMCR8	Smith-Magenis syndrome chromosome region 8
SNP	Single nucleotide polymorphism
SOD1	Superoxide dismutase 1
SRSF1/2	Serine and arginine rich splicing factor 1/2
SQSTM1	Sequestosome 1
svPPA	Semantic variant primary progressive aphasia
TAF15	TATA-box binding protein associated factor 15
TBS	Tris-buffered saline

TCA	Tricarboxylic acid
TDP-43	TAR DNA binding protein 43
TREM2	Triggering receptor expressed on myeloid cells 2
TUNEL	Terminal deoxynucleotidyl transferase dUTP nick end labelling
UAS	Upstream activating sequence
UBQLN2	Ubiquilin 2
UPS	Ubiquitin-proteasome system
VCP	Valosin containing protein
VEGF	Vascular endothelial growth factor
VHL	Von-Hippel Lindau
WDR41	WD repeat domain 41
XPO1	Exportin 1
Zfp106	Zinc finger protein 106

## Abstract

Frontotemporal dementia (FTD) and amyotrophic lateral sclerosis (ALS) are two devastating neurodegenerative diseases, with a high degree of clinical, pathological and genetic overlap. There are currently limited treatment options and no known cure for either disease. The most common genetic cause of FTD/ALS is a G<sub>4</sub>C<sub>2</sub> hexanucleotide repeat expansion in the *C9orf72* gene, with affected individuals carrying up to 1000s of repeats. There are three proposed mechanisms leading to neurodegeneration downstream of the expansion: 1) haploinsufficiency, 2) formation of toxic RNA foci by repeat RNA and 3) non-canonical translation of the expansion to produce 5 toxic dipeptide repeat proteins (DPRs): poly-GR, PR, GA, AP and GP. While all three of these mechanisms may contribute to disease, DPRs have been identified as the most prominent driver of neurodegeneration. However, specific mechanisms underlying DPR toxicity remain unclear. The emerging gene/environment/time hypothesis implicates the combined effects of genetic susceptibility, environmental factors, and aging in causing disease. Evidence points to a role of hypoxia and hypoxia signalling across the ALS spectrum, but they have not been linked to *C9orf72* FTD/ALS. Here, we model *C9orf72* FTD/ALS in *Drosophila* by expressing DPRs of a physiologically relevant length in the fly nervous system. Using proteomics, we aimed to identify DPR-interacting proteins and screen them for modifiers of DPR toxicity using the excellent genetic toolkit of *Drosophila*. We identify Exportin 1 (XPO1) as interacting with GR1000 and modifying its toxicity and downstream motor deficits. By exposing flies expressing GR1000 to hypoxia by incubation in a hypoxia chamber, we demonstrate an aberrant molecular and behavioural response to hypoxia in our model. Our findings indicate that poly(GR) disrupts the ability of the *Drosophila* nervous systems to sense and/or respond to hypoxia. This disruption provides a possible mechanism of neurodegeneration in *C9orf72* FTD/ALS.

## **Acknowledgements**

Firstly, I would like to thank my supervisor Dr Ryan West for all his support throughout my project. Thank you for helping and encouraging me through, even when everything refused to work. Thank you for your knowledge and guidance in planning experiments and shaping this project. Your support has been truly invaluable to me and this project.

I would also like to thank Dr Scott Allen for kindly letting me use his equipment and for his help with planning and performing hypoxia experiments, which formed a crucial part of this project.

Thank you to Dr Amy Keerie for teaching me everything about RT-qPCR and for always being a positive and supportive influence since the start of my project.

Many thanks as well to Dr Joanne Sharpe for teaching me so much about fly work and for always keeping me company in the fly lab.

Thank you to the University of Sheffield for kindly providing funding for this project, without which it would not have been able to happen.

I would like to thank my family and friends for their continued support through my project. Most of all I must thank Emily for supporting me through the most difficult times, keeping me calm and smiling and for always laughing at all my silly science words. Finally, I would like to thank my cat Cleo for her strict enforcement of a work/life balance.

# 1. Introduction

## 1.1. Rationale

Neurodegenerative diseases are among some of the most devastating human diseases for patients and relatives. These relatively untreatable and incurable diseases affect millions of people worldwide and are responsible for significant human, emotional and socioeconomic costs. Neurodegenerative disease is characterised by progressive loss of neurons, leading to functional impairments in the nervous system, manifesting in a range of cognitive and motor deficits. While there is a strong association of genetic and environmental factors with many neurodegenerative diseases, the most common risk factor is invariably increasing age. Therefore, as life expectancies increase worldwide, incidence of neurodegenerative disease is set to increase in tandem. Dementia is the most globally prevalent neurodegenerative disease, is the seventh leading cause of death worldwide and second leading cause of death in high-income countries (World Health Organization, 2020). In 2015 it was estimated that 651,000 individuals were currently living with dementia in the UK, with that figure set to increase to 1.35 million by 2040. Accompanying this increased prevalence is an estimated increase in the economic costs of dementia from £23 billion to £80.1 billion (Wittenberg *et al.*, 2020). In 2019 dementia cost the global economy \$1.3 trillion, with roughly half of that cost attributed to family and close friends acting as informal carers (World Health Organization, 2023). It is also important to consider the high but unquantifiable social and emotional costs of dementia on patients and their families.

Early-onset neurodegenerative disease, affecting individuals under the age of 65, is particularly devastating to society since it is more likely to disrupt the financial and family life of an individual. Frontotemporal dementia (FTD) is the third most common form of early-onset dementia (Vieira *et al.*, 2013), and often co-occurs with amyotrophic lateral sclerosis (ALS) which carries a particularly severe survival time of 2-4 years (Marin *et al.*, 2015). As in many other neurodegenerative diseases, limited understanding of FTD/ALS pathogenesis has hindered the development of therapeutic agents. In fact, treatments for FTD are limited to management of symptoms and ALS treatments typically only improve survival by a few months (Fang *et al.*, 2018).

Study of FTD/ALS revealed that the most common genetic cause of both diseases is a G<sub>4</sub>C<sub>2</sub> hexanucleotide repeat expansion in the *C9orf72* gene, in which patients can carry 1000s of G<sub>4</sub>C<sub>2</sub> repeats (DeJesus-Hernandez *et al.*, 2011; Renton *et al.*, 2011). Extensive research surrounding the *C9orf72* mutation has identified dipeptide repeat proteins (DPRs), produced by the bidirectional, repeat-associated non-AUG (RAN) translation of repeat RNA, as the most prominent driver of *C9orf72*-mediated neurodegeneration. These DPRs form inclusions

within cells of the central nervous system (CNS), disrupting cellular processes and causing neurotoxicity (Ash *et al.*, 2013; Mori, Arzberger, *et al.*, 2013). Despite extensive research into DPR toxicity, exact mechanisms of toxicity remain unclear: in part due to disparity in repeat length between patients and the models used. Recently, West *et al.* (2020) developed and characterised a *Drosophila* model of physiologically relevant 1000-repeat DPR toxicity, with which we hope to better study and understand mechanisms of DPR toxicity.

Recently, a gene/environment/time model of FTD/ALS pathogenesis has been proposed. In this model, the combined effects of genetic predisposition, environmental factors and aging cross a threshold of toxicity that causes neurodegeneration. Environmental factors that have been linked to ALS include smoking, physical exercise and occupations such as firefighters and professional athletes (Vanacore *et al.*, 2010; Julian *et al.*, 2021; Westeneng *et al.*, 2021). Hypoxia represents a common underlying mechanism between these environmental factors, which may form the molecular basis of their contribution to FTD/ALS. In fact, hypoxia and hypoxia signalling have previously been implicated in various forms of ALS but not *C9orf72*-associated FTD/ALS (Ilieva *et al.*, 2003; Lambrechts *et al.*, 2003). This research aims to identify and characterise mechanisms of DPR toxicity, with a particular focus on the potential role of hypoxia and hypoxia signalling, at the organism, cellular and molecular level. This will be achieved using our previously established, physiologically relevant *Drosophila* model of DPR toxicity: the first animal model to model DPRs of a length comparable to those in patients (>1000 repeats).

## **1.2. Frontotemporal dementia and amyotrophic lateral sclerosis**

### **1.2.1 Overview**

Frontotemporal dementia (FTD) and amyotrophic lateral sclerosis (ALS) are two devastating neurodegenerative diseases with limited treatment options and no known cure. FTD is characterised by degeneration of the frontal and temporal lobes of the brain, leading to cognitive impairment, behaviour and language defects (Neary *et al.*, 1994). ALS is characterised by degeneration of upper and lower motor neurons in the brain and spinal cord, leading to a progressive decline in motor function (Rowland, 1998). FTD and ALS share a high degree of clinical, pathological, and genetic overlap (Ringholz *et al.*, 2005; Mackenzie *et al.*, 2007; Burrell *et al.*, 2011; DeJesus-Hernandez *et al.*, 2011; Renton *et al.*, 2011; Sieben *et al.*, 2012). Therefore, they are now considered as existing at either end of a single disease spectrum.

## 1.2.2. Clinical characteristics

### 1.2.2.1 FTD

First described by Pick in 1892, frontotemporal dementia (FTD) is now used to refer to a clinically, pathologically and genetically heterogeneous group of syndromes associated with frontotemporal lobar degeneration (FTLD), which is progressive atrophic degeneration of the frontal and temporal lobes. FTD is the third most common form of early-onset dementia (Vieira *et al.*, 2013), accounting for up to 16 % of cases under 65 years of age and up to 9 % of all dementia cases (Hogan *et al.*, 2016). Age-of-onset is between 45-64 years in 60 % of patients (Bang, Spina and Miller, 2015), however cases have been reported in patients as young as 30 (Snowden, Neary and Mann, 2002). Survival time from onset of symptoms typically ranges from 6-11 years, however this varies between subtypes (Bang, Spina and Miller, 2015).

The frontal and temporal lobes function predominantly in emotional and sensory processing, social conduct, voluntary motor control, language comprehension and speech. As such, neurodegeneration in these regions causes symptoms such as behavioural changes, language deficits, and cognitive dysfunction (Neary *et al.*, 1994). While frontal and temporal degeneration is the common feature in FTD, a heterogeneous topology of neurodegeneration results in distinct clinical disease manifestations (Neary *et al.*, 1998). These have been categorised into behavioural variant FTD (bvFTD) and primary progressive aphasia (PPA), which is categorised further into semantic variant PPA (svPPA), non-fluent variant PPA (nfvPPA) and logopenic PPA (IPPA) (Gorno-Tempini *et al.*, 2011; Rascovsky *et al.*, 2011). Clinical presentations vary even within these subtypes, depending on the specific brain regions affected (Snowden, Neary and Mann, 2002).

bvFTD is the most common subtype, constituting 60-80 % of all FTD diagnoses (Johnson *et al.*, 2005; Hogan *et al.*, 2016). bvFTD initially presents as behavioural disinhibition, apathy, lack of empathy, compulsive and ritualistic behaviour and hyperorality (Rascovsky *et al.*, 2011; Bang, Spina and Miller, 2015). While behavioural symptoms distinguish bvFTD from Alzheimer's disease (AD) (Snowden, Neary and Mann, 2002), their presence in other psychiatric illnesses often leads to bvFTD patients being misdiagnosed with depression or schizophrenia (Woolley *et al.*, 2011). As the disease progresses and degeneration becomes more widespread, patients may also develop executive dysfunction and wider cognitive impairment (Rascovsky *et al.*, 2011; Lashley *et al.*, 2015). These symptoms are not only detrimental to the patient, but also particularly detrimental to patient's family and carers.

nfvPPA patients initially present with slow, effortful speech (Gorno-Tempini *et al.*, 2004) that progressively declines even to the point of mutism (Gorno-Tempini *et al.*, 2006). Other

symptoms include inconsistent speech sound errors (Gorno-Tempini *et al.*, 2011), of which the patient remains unaware; and agrammatism, initially subtle and only present in speech but appearing more severely and in written language over time (Gorno-Tempini *et al.*, 2004). Comprehension remains generally unaffected, although patients may have difficulty understanding syntactically complex sentences (Gorno-Tempini *et al.*, 2004).

svPPA is characterised by asymmetric degeneration of the temporal lobes, resulting in two categories of initial symptoms: linguistic and behavioural. Left temporal lobe variant (LTLV) is associated with linguistic symptoms, such as word-finding difficulties; surface dyslexia; anomia for nouns; and loss of semantic knowledge of objects (Thompson, Patterson and Hodges, 2003; Seeley *et al.*, 2005). Right temporal lobe variant (RTLTV) is associated with mild linguistic symptoms, such as impaired word comprehension, but more predominantly with behavioural changes, such as irritability; emotional distance; social deficits; and disrupted sleep, appetite and libido (Edwards-Lee *et al.*, 1997; Seeley *et al.*, 2005). Patients with both forms of svPPA can later develop new compulsions and abilities, potentially stemming from a heightening of the hemisphere in which degeneration is less severe (Seeley *et al.*, 2005). For example, left svPPA patients may develop compulsions towards visual or non-verbal stimuli such as painting, drawing and gardening. Right svPPA patients, however, tend towards verbal stimuli such as writing, word games and card games (Edwards-Lee *et al.*, 1997; Seeley *et al.*, 2005). LTLV is estimated to be roughly 3 times more common than RTLTV (Thompson, Patterson and Hodges, 2003).

These distinct clinical classification criteria of FTD subtypes have been established primarily based on the early or initial symptoms shown by patients. While there is a degree of overlap in these symptoms, patients ultimately converge on a shared set of FTD symptoms as the disease progresses and the primary focal atrophy spreads throughout the frontal and temporal lobes (Bang, Spina and Miller, 2015). Studies of ALS symptoms in FTD patients found that up to 13 % of FTD patients had concomitant ALS, with 27 % of patients demonstrating some form of motor dysfunction (Lomen-Hoerth, Anderson and Miller, 2002; Burrell *et al.*, 2011). It was also found the bvFTD is the FTD subtype most strongly associated with concomitant ALS (Johnson *et al.*, 2005).

#### **1.2.2.2 ALS**

Motor neuron disease (MND) is used to describe several adult-onset conditions characterised by progressive degeneration of motor neurons. Amyotrophic lateral sclerosis (ALS) is characterised by degeneration of both upper and lower motor neurons, which is observed in 95 % of cases (Rowland, 1998). As such, ALS is now used to refer to both ALS

and MND. The mean age-of-onset is typically between 60-65 years for sporadic ALS, while cases of familial ALS onset roughly 5 years earlier (Mehta *et al.*, 2019). ALS prognosis is especially poor, with a median survival of 2-4 years (Marin *et al.*, 2015).

ALS is clinically heterogeneous, with differences arising from the focal point of onset and the degree of upper and lower motor neuron degeneration (Feldman *et al.*, 2022). Upper motor neuron (UMN) degeneration leads to reduced muscle contraction speed, reduced muscle activation and spasticity. Lower motor neuron (LMN) degeneration leads to muscle atrophy, fasciculations and loss of muscle and force (Kent-Braun *et al.*, 1998).

ALS cases are broadly categorised into spinal, bulbar and respiratory onset ALS, based upon the initial clinical presentation. The hallmark symptom of ALS is progressive muscle weakness, associated with muscle atrophy, with a focal onset that typically spreads as the disease progresses. This pattern of focal onset that subsequently spreads is associated with the pattern of motor neuron degeneration. Spinal onset ALS constitutes 70 % of ALS cases and weakness is initially observed in the upper or lower limbs, leading to difficulties performing manual tasks like buttoning a shirt or writing. Bulbar onset ALS constitutes 25 % of ALS cases and weakness presents initially in the bulbar muscles in the neck and jaw, leading to dysarthria, dysphagia and/or dysphonia (Masrori and Van Damme, 2020). Respiratory onset is much rarer and is characterised by initial weakness in the respiratory muscles (Feldman *et al.*, 2022). As all forms of the disease progress, motor neuron dysfunction and muscle weakness becomes more widespread: ultimately leading to respiratory failure and death (Chiò *et al.*, 2015).

While spinal, bulbar and respiratory onset ALS represent more classical ALS phenotypes, recent research is uncovering a significant non-motor component to the disease. 30-50 % of all ALS cases exhibit cognitive impairment, with up to 15 % meeting the diagnostic criteria for FTD (Ringholz *et al.*, 2005; Phukan *et al.*, 2012).

### **1.2.3. Neuropathology**

Frontotemporal lobar degeneration (FTLD) is the neuropathological mechanism underlying multiple clinical disorders, including clinical FTD and some ALS phenotypes. FTLD is characterised by neuronal loss, gliosis, microvacuolar changes, and white matter myelin loss within and adjacent to the frontal and temporal lobes (Neary *et al.*, 1994). The majority of FTLD cases, as in other neurodegenerative disorders, are considered proteinopathies, meaning they are associated with aberrant intracellular protein deposition and aggregation. As such, FTLD cases can be classified into subtypes based upon the presence of specific

intracellular protein inclusions (MacKenzie *et al.*, 2010). Nearly all FTLD cases contain TAR DNA-binding protein with molecular weight 43 kDa (TDP-43), microtubule-associated protein tau (MAPT), or fused-in-sarcoma (FUS) inclusions and are therefore classified as FTLD-TDP, FTLD-tau, or FTLD-FUS respectively (MacKenzie *et al.*, 2010). The few remaining cases have ubiquitin- and p62-positive inclusions (FTLD-UPS) or, even rarer, no inclusions at all (FTLD-ni) (MacKenzie *et al.*, 2010). There is no one-to-one association between pathological subtype of FTLD and clinical subtypes of FTD.

FTLD-TDP is the most common subtype of FTLD, accounting for up to 50 % of all FTLD cases (Sieben *et al.*, 2012). Encoded by the TARDBP gene, the RNA-binding protein TDP-43 belongs to the heterogeneous nuclear ribonucleoprotein (hnRNP) family and functions in alternative splicing; regulation of mRNA stability and transport; and miRNA processing (Baralle, Buratti and Baralle, 2013). Under pathological conditions, TDP-43 is relocated to the cytoplasm, hyperphosphorylated, ubiquitinated and cleaved into C-terminal fragments which form TDP-43 inclusions (Neumann *et al.*, 2006a). Based on the intracellular localisation, distribution, density, and morphology of the inclusions, FTLD-TDP pathology can be categorised further in subtypes (Table 1.1.). TDP-43 inclusions are not exclusive to FTLD, they are also found in affected tissues in other neurodegenerative diseases including sporadic ALS (Neumann *et al.*, 2006a; Higashi *et al.*, 2007; Miklossy *et al.*, 2008).

FTLD-tau is the 2<sup>nd</sup> most common subtype of FTLD (Sieben *et al.*, 2012), and is included in the wider group of neurodegenerative diseases, characterised by depositions of hyperphosphorylated tau, known as tauopathies. 44 mutations in the MAPT gene, which encodes tau, have been linked to FTLD-tau pathology (Cruts, Theuns and Van Broeckhoven, 2012). These mutations account for a strong familial component in FTLD-tau, although sporadic cases of FTLD-tau are also common. MAPT can be alternatively spliced into 6 isoforms, containing either 3 (3R) or 4 (4R) microtubule binding domain repeats (Mandelkow and Mandelkow, 2012). FTLD-tau pathologies are classified as 3R or 4R, based upon the predominant tau isoform contained within tau inclusions. Clinical FTD is most commonly associated with 3R tauopathy, although there is some overlap with 4R (Dickson *et al.*, 2011). Pick's disease is the pathology associated with 3R tau, and most commonly presents as bvFTD in patients although svPPA and nvPPA phenotypes have also been recorded (Graff-Radford *et al.*, 1990; Irwin *et al.*, 2016). Pathological hallmarks of Pick's disease include ballooned neurons, known as Pick's cells, and large spherical tau inclusions, known as Pick bodies, in the neuronal cytoplasm (Dickson, 1998).

FTLD-FUS accounts for roughly 10 % of all FTLD cases (MacKenzie *et al.*, 2011) and is comprised of 3 pathological subtypes: atypical FTLD-U (aFTLD-U), neuronal intermediate

filament inclusion disease (NIFID) and basophilic inclusions body disease (BIBD) (MacKenzie *et al.*, 2010). FUS-positive neuronal and glial inclusions are present in all three subtypes (Munoz *et al.*, 2009; Neumann, Rademakers, *et al.*, 2009; Neumann, Roeber, *et al.*, 2009; Urwin *et al.*, 2010), however morphology, localisation and composition varies between subtypes (Table 1.2). FUS belongs to the FET family of DNA/RNA binding proteins, along with Ewing's sarcoma protein (EWS) and TATA-binding protein associated factor 15 (TAF15) (Law, Cann and Hicks, 2006). All 3 FET proteins have been identified in FUS-positive inclusions in FTLD-FUS (Neumann *et al.*, 2011), leading to a proposed renaming of FTLD-FUS to FTLD-FET (MacKenzie and Neumann, 2012). FUS-positive neuronal and glial inclusions have also been identified in ALS, however these inclusions do not contain the other FET proteins (Neumann *et al.*, 2011). ALS cases demonstrating FUS pathology typically also carry familial *FUS* mutations, while FTLD-FUS is associated with sporadic disease, providing a potential explanation for the differences observed in pathology (Snowden *et al.*, 2011).

FTLD-UPS encompasses the few remaining cases of FTLD in which the major pathological protein remains unknown, but the involvement of the ubiquitin-proteasome system (UPS) is apparent. These cases have ubiquitin- and p62-positive inclusions that test negative for TDP-43, tau and FUS. Most of these cases are associated with rare *CHMP2B* mutations, although sporadic cases also exist (Urwin *et al.*, 2010). *CHMP2B* mutations have also been reported in ALS patients (Parkinson *et al.*, 2006).

The pathological hallmarks of ALS are degeneration of upper and lower motor neurons accompanied by surrounding astrogliosis. In the majority of cases, cytoplasmic inclusions of ubiquitinated TDP-43 are seen in surviving neurons and glia in the primary motor cortex, brainstem motor nuclei and spinal cord (Mackenzie *et al.*, 2007). Given the prevalence of TDP pathology in ALS, it is widely considered a pathological hallmark of ALS. Despite the clear disease relevance of TDP-43, mutations in *TARDBP* are an uncommon cause of ALS (Kabashi *et al.*, 2008; Van Deerlin *et al.*, 2008). TDP-43 inclusion morphology is either compact and round or skein-like (Leigh *et al.*, 1991). In ALS associated with *SOD1* and *FUS* mutations, TDP-43 pathology is replaced with *SOD1* or *FUS* pathology respectively (Bruijn *et al.*, 1997; Mackenzie *et al.*, 2007; Vance *et al.*, 2009; Blair *et al.*, 2010). *SOD1* and *FUS* pathology has also been seen in other cases of ALS, not associated with mutations in either gene (Forsberg *et al.*, 2019). Another characteristic pathological feature of ALS is the presence of Bunina bodies in the spinal cord and brain stem (Okamoto, Mizuno and Fujita, 2008). These are small, round eosinophilic intraneuronal inclusions which are highly variable in number and can form clusters or chains (Saber *et al.*, 2015). They are positive for cystatin

C and transferrin, but negative for proteins commonly involved in neurodegeneration, such as TDP-43, tau and p62 (Saber *et al.*, 2015).

**Table 1.1. Summary of FTLD-TDP subtypes and their associated pathology, clinical syndromes, and genetics** as reviewed by Mackenzie *et al.* (2011); E. B. Lee *et al.* (2017). NCI = neuronal cytoplasmic inclusions, NII = neuronal intranuclear inclusions.

<b>Type</b>	<b>TDP-43 pathology</b>	<b>Associated clinical syndromes</b>	<b>Associated genetic mutations</b>
A	Round/crescent-like NCI Short dystrophic neurites Rare lentiform NII Present only in upper cortical layers	bvFTD, nfvPPA	<i>GRN</i> <i>C9orf72</i>
B	Less frequent NCI Dystrophic neurites Present in all cortical layers	bvFTD, FTD/ALS	<i>C9orf72</i> Chromosome 9p
C	Long tortuous dystrophic neurites Few NCI Present only in upper cortical layers	svPPA, bvFTD	
D	Frequent lentiform NII Short dystrophic neurites Rare NCI Present in all cortical layers	Inclusion body myopathy with Paget's disease of bone and FTD	<i>VCP</i>
E	Granulofilamentous neuronal inclusions Fine, dot-like neuropil aggregates Present in all cortical layers	bvFTD	

**Table 1.2. FTL-D-FUS subtypes and the characteristics of FET-positive inclusions**, as reviewed by MacKenzie *et al.* (2011). NCI = neuronal cytoplasmic inclusions, GCI = glial cytoplasmic inclusions, NII = neuronal intranuclear inclusions.

<b>Subtype</b>	<b>FET pathology</b>	<b>Clinical phenotype</b>
aFTLD- U	Round, oval or crescent-like NCI Ovoid or flame-shaped GCI Long, thick filamentous NII	Early onset bvFTD
BIBD	Small, round NCI containing RNA Ovoid or flame-shaped GCI	sALS, fALS, FTD/ALS, pure FTD
NIFID	Small, round NCI containing neuronal filaments Small, round or tangle-like GCI Vermiform NII	sFTD with movement disorder

#### 1.2.4. Epidemiology and aetiology

Estimates of FTD prevalence range widely between studies but are reported at 1-180 per 100,000, with no difference between men and women (Hogan *et al.*, 2016). However, as previously discussed, FTD cases are often missed or misdiagnosed so these estimates likely underestimate the true prevalence (Knopman and Roberts, 2011; Woolley *et al.*, 2011; Landqvist Waldö *et al.*, 2015; Lanata and Miller, 2016). Family history is observed in up to 40 % of FTL-D cases, with 10 % of cases following an autosomal dominant pattern of inheritance (Chow *et al.*, 1999; Rohrer *et al.*, 2009). ALS has an estimated global prevalence of 4.42 per 100,000, and is 50 % more prevalent in men than in women (Xu *et al.*, 2020). Familial disease constitutes a lower proportion of ALS than FTD, with only 5 % of ALS cases being classified as familial (Byrne *et al.*, 2011) although evidence does point towards the potential misclassification of a proportion of sporadic cases (Van Blitterswijk *et al.*, 2012).

### 1.2.5. Genetic causes

While the majority of cases of FTD and ALS are sporadic in nature, both diseases have a strong familial association. There is a high degree of overlap in disease pathology between sporadic and familial cases, highlighting that common mechanisms may underlie both sporadic and familial cases. A number of genetic mutations responsible for familial cases have been identified, including genes that are heavily involved in sporadic pathology. Several of these mutations are also found in sporadic cases (Le Ber, 2013). It is important to note that, although most of these mutations can be identified in cases across the world, prevalence does vary between regional populations.

Up to 40% of FTLD patients have a familial history, with 10 % of those demonstrating an autosomal dominant pattern of inheritance (Rohrer *et al.*, 2009). Mutations in *MAPT*, *GRN* and *C9orf72* account for up to 15, 22 and 25 % of familial FTLD cases respectively (Hutton *et al.*, 1998; Cruts *et al.*, 2006; DeJesus-Hernandez *et al.*, 2011; Renton *et al.*, 2011). Mutations in *VCP*, *TARDBP*, *FUS*, *SQSTM1*, *TREM2*, *CHMP2B* and *UBQLN2* are rarer, each accounting for 1-3 % of FTLD cases (Watts *et al.*, 2004; Skibinski *et al.*, 2005; Benajiba *et al.*, 2009; Broustal *et al.*, 2010; Elisa *et al.*, 2012; Gellera *et al.*, 2012; Guerreiro *et al.*, 2013).

Familial history is less common in ALS, with familial ALS (fALS) comprising 5 % of all ALS cases (Byrne *et al.*, 2011). To date over 40 genes have been implicated in ALS, explaining up to 50 % of fALS cases and even up to 10 % of apparent sporadic ALS (sALS) cases (Zou *et al.*, 2017; Gregory *et al.*, 2020). *SOD1* mutations represent the most common genetic cause of ALS in Asian populations and the second most common in European populations, accounting for 30 and 15 % of cases respectively (Zou *et al.*, 2017). The *C9orf72* mutation is the most common in European populations, accounting for 34 % of fALS cases and found in up to 5 % of sALS cases (Zou *et al.*, 2017). *TARDBP* and *FUS* mutations are rarer but not insignificant: they constitute roughly 5 % of all fALS cases each (Zou *et al.*, 2017).

Autosomal dominant, autosomal recessive and X-linked inheritance patterns have been observed in fALS, frequently with low disease penetrance (Andersen and Al-Chalabi, 2011). ALS mutations have been identified in sALS cases and multiple ALS mutations have been identified in single ALS families. Altogether these observations evidence an oligogenic basis of ALS and potential for many sALS cases to be recategorised as fALS (Van Blitterswijk *et al.*, 2012).

It is worth noting that the genetic mutations discussed above are all associated with different pathologies and clinical presentations. This heterogeneity is what underpins the genetic basis of the FTD/ALS spectrum (Fig. 1.1.). For example, *SOD1* mutations are associated

with 'pure' ALS without FTD phenotypes (Chio *et al.*, 2012) while *GRN* mutations are associated with 'pure' FTD without ALS phenotypes (Schymick *et al.*, 2007). Other mutations, such as the *C9orf72* mutation are associated with clinical presentations across the spectrum (Boeve *et al.*, 2012).

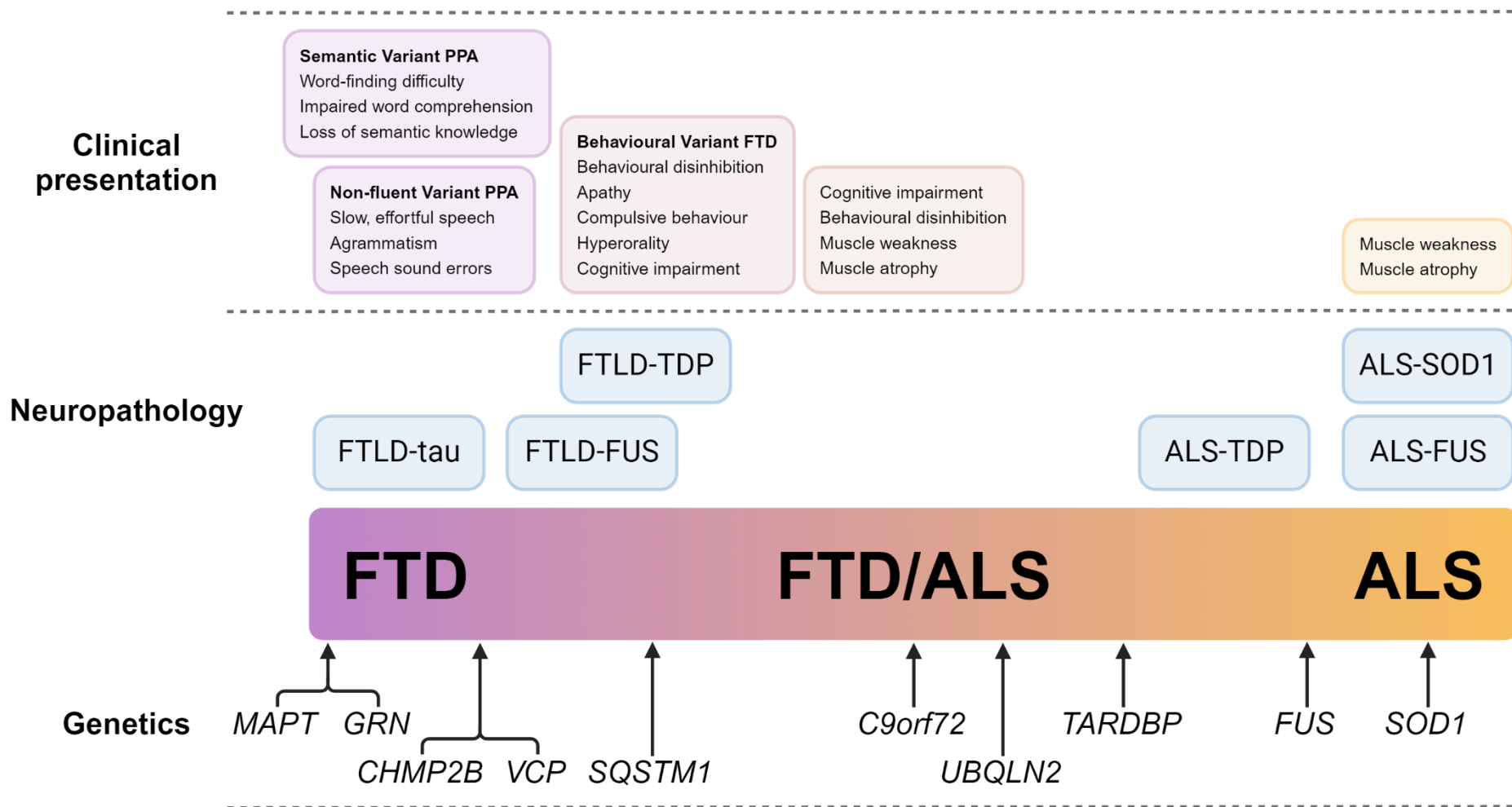


**Figure 1.1. Frontotemporal dementia (FTD) and amyotrophic lateral sclerosis (ALS) exist on a single disease spectrum.** Clinical presentations, underlying neuropathology, associated genetic mutations and their location along the spectrum are shown. Adapted from Lee and Huang (2017).

### 1.3. C9orf72

A single hexanucleotide repeat expansion mutation in the *C9orf72* gene is the most common genetic cause of both FTD and ALS (DeJesus-Hernandez *et al.*, 2011). The human *C9orf72* gene is located on the reverse strand of the short arm of chromosome 9 at position 21.2 and is comprised of over 27,000 base pairs. The gene itself is comprised of 2 non-coding exons (1a and 1b) and 10 coding exons (2-11) which give rise to 3 coding variants. Variant 1 (V1) is the shortest transcript, including only non-coding exon 1a and coding exons 2-5. V2 and V3 include coding exons 2-11 but differ in their inclusion of non-coding exons 1b or 1a respectively (DeJesus-Hernandez *et al.*, 2011). Alternative splicing of the 3 RNA variants produces two isoforms of the C9orf72 protein: C9-short (222 amino acids, 24 kDa) and C9-long (481 amino acids, 54 kDa). While expressed throughout a range of tissues, C9orf72 is particularly abundant in the CNS and immune system (Smeyers, Banchi and Latouche, 2021).

Bioinformatics studies revealed that C9orf72 shows homology to the DENN (differentially expressed in normal and neoplasia) domain family of proteins, in both primary and secondary structure (Levine *et al.*, 2013). DENN domain proteins tend to be guanine nucleotide exchange factors (GEFs) for Rab GTPases (Yoshimura *et al.*, 2010). Rab GTPases act as master regulators of membrane trafficking, that activate when bound to guanosine triphosphate (GTP) and become inactivated once they hydrolyse GTP to guanosine diphosphate (GDP) (Zerial and McBride, 2001). GEFs are crucial to GTPase function, as they facilitate the binding of GTP and thus GTPase activation. C9orf72, in addition to its homology to DENN domain proteins, has been shown to interact with a number of Rab GTPases involved in pathways such as autophagy and endosomal transport (Farg *et al.*, 2014; Sellier *et al.*, 2016; Webster *et al.*, 2016; Shi *et al.*, 2018). C9orf72 has also been shown to form a complex with other DENN domain proteins, SMRC8 (Smith-Magenis chromosome region 8) and WDR41 (WD40-repeat containing protein 41). This complex can act as a GEF and has been shown to interact with the autophagy initiation complex to control autophagic flux (Sullivan *et al.*, 2016; Yang *et al.*, 2016).

C9orf72 has also been implicated in nucleocytoplasmic transport (NCT), through interactions with Importin  $\beta$ 1 and Ran-GTPase at the nuclear membrane (Xiao *et al.*, 2015). The role of C9orf72 in autophagy pathways has been shown to have downstream effects on stress granules (Maharjan *et al.*, 2017; Chitiprolu *et al.*, 2018). C9orf72 has also been shown to interact with regulators of actin dynamics, such as cofilin, Arp2/3 and coronin. This involvement in actin dynamics may explain axonal growth and maintenance phenotypes that have been observed in studies of C9orf72 function (Sivadasan *et al.*, 2016).

The cellular localisation of C9orf72 has been studied extensively but with somewhat contrasting results. Isoform-specific antibodies revealed that C9-long is the most abundant and shows diffuse, cytoplasmic localisation with some speckling in neurites that is indicative of synaptic localisation. Conversely, C9-short appears to localise at the nuclear membrane (Xiao *et al.*, 2015; Frick *et al.*, 2018). C9orf72 has also been observed at the Golgi apparatus (Aoki *et al.*, 2017), stress granules (Maharjan *et al.*, 2017; Chitiprolu *et al.*, 2018), mitochondria (Wang *et al.*, 2021) and multiple compartments of the endolysosomal pathway (Farg *et al.*, 2014; Amick, Rocznik-Ferguson and Ferguson, 2016; Sellier *et al.*, 2016; Frick *et al.*, 2018; Shi *et al.*, 2018; Wang *et al.*, 2020).

### **1.3.1. Discovery of the C9orf72 expansion**

For years it had been established that both FTD and ALS had a genetic component, but the majority of familial cases bore no association to the genetic mutations that had been discovered. This raised the possibility of prominent FTD- and ALS-associated genetic mutations that remained undiscovered. Also, families had been described with autosomal dominant FTD/ALS that could not be explained by the previously identified disease-associated genetic mutations. Linkage analysis in these families identified a 3.7 Mb region on chromosome 9p21 as a major FTD/ALS locus (Morita *et al.*, 2006; Vance *et al.*, 2006). This same genomic region had also been identified as linked to 'sporadic' FTD and ALS in genome-wide association (GWA) studies (Van Es *et al.*, 2009; Laaksovirta *et al.*, 2010; Shatunov *et al.*, 2010). Two independent research groups, using distinct techniques, performed targeted sequencing of this region in autosomal dominant FTD/ALS families: revealing a G<sub>4</sub>C<sub>2</sub> hexanucleotide repeat expansion in the intron between exons 1a and 1b of the C9orf72 gene (Fig. 1.2.) (DeJesus-Hernandez *et al.*, 2011; Renton *et al.*, 2011). Despite evidence implicating this genomic region in FTD/ALS arising as early as 2006, the discovery of the mutation was delayed due to its repetitive nature. The highly-repetitive, GC-rich nature of the mutation causes it to often be missed by typical screening and bioinformatic tools, making it highly elusive (Depienne and Mandel, 2021).

### **1.3.2. Features of the *C9orf72* expansion**

#### **1.3.2.1 Clinical**

Clinical presentations of individuals carrying the *C9orf72* hexanucleotide repeat expansion are relatively heterogeneous, although some common features do stand out. While there is variation between cohorts, >60 % of *C9orf72*-associated FTD (C9FTD) present with bvFTD (Simón-Sánchez *et al.*, 2012; Snowden *et al.*, 2012; Galimberti *et al.*, 2013; Kaivorinne *et al.*, 2013). C9FTD patients are also much more likely to develop neuropsychiatric symptoms, such as psychosis, delusions and hallucinations (Dobson-Stone *et al.*, 2012). In *C9orf72*-associated ALS (C9ALS), some studies have shown that bulbar-onset ALS is more common (Ratti *et al.*, 2012; Stewart *et al.*, 2012; Debray *et al.*, 2013). C9ALS patients typically have a later age-of-onset, although conflicting results have also been published, and reduced survival (Cooper-Knock *et al.*, 2012; Ratti *et al.*, 2012; Debray *et al.*, 2013). In studies of FTD and ALS, *C9orf72* hexanucleotide repeat expansion carriers presenting with one disease are more likely to develop the other concomitantly (Dobson-Stone *et al.*, 2012; Ratti *et al.*, 2012; Stewart *et al.*, 2012; Kaivorinne *et al.*, 2013).

#### **1.3.2.2. Pathology**

In *C9orf72* hexanucleotide repeat expansion carriers, clinical presentations correlate strongly with the degree of degeneration in respective regions of the CNS. Despite the heterogeneity of clinical phenotypes and topology of degeneration, the underlying pathology in these individuals is relatively homogeneous. Affected regions consistently show major TDP-43 pathology (DeJesus-Hernandez *et al.*, 2011; Boeve *et al.*, 2012; Stewart *et al.*, 2012).

In cases with clinical symptoms of FTD, there is severe atrophy of the frontal and temporal lobes with greater atrophy in the right fronto-insular, thalamus, cerebellum and bilateral parietal regions compared to non-*C9orf72* FTD (Irwin *et al.*, 2013). FTLTDP type B is the prevalent pathology in the majority of cases (Cairns *et al.*, 2007; Boxer *et al.*, 2011; Hsiung *et al.*, 2012; Stewart *et al.*, 2012; MacKenzie *et al.*, 2013). FTLTDP type B is associated with the clinical syndromes of bvFTD and ALS (Mackenzie *et al.*, 2011), in line with what is observed in *C9orf72* hexanucleotide repeat expansions carriers. A significant number of C9 disease cases, often pure FTD rather than FTD/ALS, have concomitant or pure FTLTDP type A pathology. However, type B pathology is believed to be the primary pathology associated with *C9orf72*, with type A pathology possibly only developing in a genetically susceptible subset of patients as they age (Hsiung *et al.*, 2012).

The pathology of C9ALS is almost entirely indistinguishable from that of sALS, which is characterised by degeneration and TDP-43 inclusions in upper and lower motor neurons. Cases presenting as clinically pure ALS demonstrate minimal extramotor pathology (Murray *et al.*, 2011; Stewart *et al.*, 2012), although p62-positive neuronal cytoplasmic inclusions have been reported in the hippocampi of affected individuals (Murray *et al.*, 2011; Cooper-Knock *et al.*, 2012). It is also worth noting that, even in the absence of clinical motor dysfunction, TDP-43 positive neuronal cytoplasmic inclusions are often present in the lower motor neurons of those with C9 disease (MacKenzie, Frick and Neumann, 2014).

Unlike other cases of FTLT-DTP and ALS, those associated with the hexanucleotide repeat expansion in *C9orf72* have ubiquitin- and p62-positive but TDP-43 negative inclusions in the CNS (Al-Sarraj *et al.*, 2011). These inclusions primarily consist of dipeptide repeat proteins (DPRs), produced by non-canonical translation of the expanded *C9orf72* hexanucleotide repeat, which aggregate with protein components of the UPS (Ash *et al.*, 2013; Gendron *et al.*, 2013; MacKenzie *et al.*, 2013; Mann *et al.*, 2013; Mori, Arzberger, *et al.*, 2013; Mori, Weng, *et al.*, 2013). For the most part these inclusions are neuronal cytoplasmic, although neuronal intranuclear and dystrophic neurites are also found (MacKenzie *et al.*, 2013). Irrespective of clinical phenotype, these inclusions are consistently found in the frontal and temporal lobes, hippocampus and cerebellum (Schipper *et al.*, 2016). They are also found, at a much lower frequency, in motor neurons, spinal cord and skeletal muscle (Gomez-Deza *et al.*, 2015; Cykowski *et al.*, 2019).

Another unique pathological feature of C9 disease is the presence of RNA foci, comprised of G<sub>4</sub>C<sub>2</sub> repeat RNA transcripts aggregated together with RNA-binding proteins (RBPs) (DeJesus-Hernandez *et al.*, 2011; Cooper-Knock *et al.*, 2014). These RNA foci are found in up to 50 % of neurons in the frontal cortex, hippocampus and cerebellum and at reduced frequency in the spinal cord and glia. RNA foci are mostly intranuclear and found only rarely in the cytoplasm (DeJesus-Hernandez *et al.*, 2011; Lagier-Tourenne *et al.*, 2013; Mizielinska *et al.*, 2013).

### **1.3.2.3. Epidemiology**

Epidemiological data on the *C9orf72* mutation is highly variable between cohorts, based on the region and genealogy of individuals studied. The highest prevalence of the mutation is found in European, especially Scandinavian, populations. The mutation is found at a much lower frequency in Asian populations (Ishiura and Tsuji, 2015; Zou *et al.*, 2017). Meta analysis by Zou *et al.* (2017) and Marogianni *et al.* (2019) found that the *C9orf72* mutation was associated with 34 % of fALS and 5 % of sALS cases in individuals of European

descent, but only 2.3 % of fALS and 0.3 % of sALS cases in individuals of Asian descent. C9 FTD is less commonly studied in epidemiological studies, however the few studies in this field found that *C9orf72* mutation carriers accounted for 15-57 % of fFTLD and up to 23 % of sFTLD patients in Europe (Ishiura and Tsuji, 2015). Females were found to have a 16% higher prevalence of C9 ALS, but no difference was observed in C9 FTD (Curtis *et al.*, 2017). SNP analysis revealed a common risk haplotype among many *C9orf72* mutation carriers, suggesting a possible single Scandinavian founder that caused the higher prevalence in European cohorts (Laaksovirta *et al.*, 2010).

### 1.3.3. Impact of *C9orf72* repeat length

There is no definitive boundary between what is considered 'healthy' and what is considered pathogenic repeat length. Repeat lengths under 24 are found in almost all 'healthy' controls (DeJesus-Hernandez *et al.*, 2011; Renton *et al.*, 2011), although repeat lengths up to 35 are not uncommon (Ratti *et al.*, 2012; Simón-Sánchez *et al.*, 2012). As such, there is a consensus that individuals carrying <30 repeats be classified as 'healthy' controls. Despite these limits of 24-30 repeats for 'healthy' controls, individuals have been identified carrying up to 400 repeats but showing no clinical phenotype (Beck *et al.*, 2013), and repeat lengths of 20-30 have been associated with C9 disease (Gómez-Tortosa *et al.*, 2013; Iacoangeli *et al.*, 2019). While unaffected individuals typically carry <30 repeats, affected individuals typically carry 100s-1000s of repeats (Beck *et al.*, 2013; Dobson-Stone *et al.*, 2013)

Much of the variability and disparity in studies of repeat length likely arises from the difficulty of accurately quantifying higher repeat lengths. The expanded repeats themselves are difficult to sequence owing to their 100 % GC content and repetitive nature (Ebbert *et al.*, 2018). Intra-individual repeat variability is also observed as a result of somatic mosaicism and repeat instability (van Blitterswijk *et al.*, 2013; Waite *et al.*, 2014). This means that repeat length can vary between tissues and even within tissues, for example shorter repeats are found in blood and cerebellum compared to the frontal lobe (van Blitterswijk *et al.*, 2013).

Evidence towards the association of repeat length with clinical presentations remains conflicted. Some studies have found that ALS patients carry longer repeats than FTD patients (Dols-Icardo *et al.*, 2014; Suh *et al.*, 2015), but these findings have not been replicated by similar studies (Beck *et al.*, 2013; van Blitterswijk *et al.*, 2013; Nordin *et al.*, 2015). With regards to age of onset, both a higher (van Blitterswijk *et al.*, 2013; Nordin *et al.*, 2015) and lower (Gijssels *et al.*, 2015) repeat length have been linked to a later age of onset. While Dols-Icardo *et al.* (2014) found no association between repeat length and

survival, a reduced survival has been linked to longer repeats in the cerebellum and parietal lobe by van Blitterswijk *et al.* (2013) and Nordin *et al.* (2015) respectively.

#### **1.3.4. Mechanisms of disease**

After the discovery of the *C9orf72* hexanucleotide expansion and its strong association with FTD/ALS, researchers set out to identify and characterise pathogenic mechanisms of the mutation. Three mechanisms have been proposed as contributors to the neurodegeneration seen in C9 FTD/ALS (Fig. 1.2): 1) *C9orf72* loss-of-function through haploinsufficiency (Therrien *et al.*, 2013); 2) G<sub>4</sub>C<sub>2</sub> repeat RNA-mediated toxicity, whereby transcription of the repeat produces RNA that forms toxic foci which sequester RNA-binding proteins (DeJesus-Hernandez *et al.*, 2011); 3) DPR-mediated toxicity, whereby non-canonical translation of repeat RNA produces toxic DPRs (Mori, Arzberger, *et al.*, 2013). Importantly, there is evidence towards each of these three mechanisms and it is likely the case that all three contribute towards neurodegeneration individually. However, evidence points towards DPRs as being the most prominent driver of toxicity and neurodegeneration (Mizielinska *et al.*, 2014; Wen *et al.*, 2014; Tran *et al.*, 2015; Moens *et al.*, 2018; Solomon *et al.*, 2018). Despite the establishment of these three mechanisms and the subsequent research surrounding them, their contribution to disease at the cellular and molecular level remain somewhat unclear. This highlights the need for further research, to identify and characterise disease processes downstream of the *C9orf72* hexanucleotide repeat expansion.

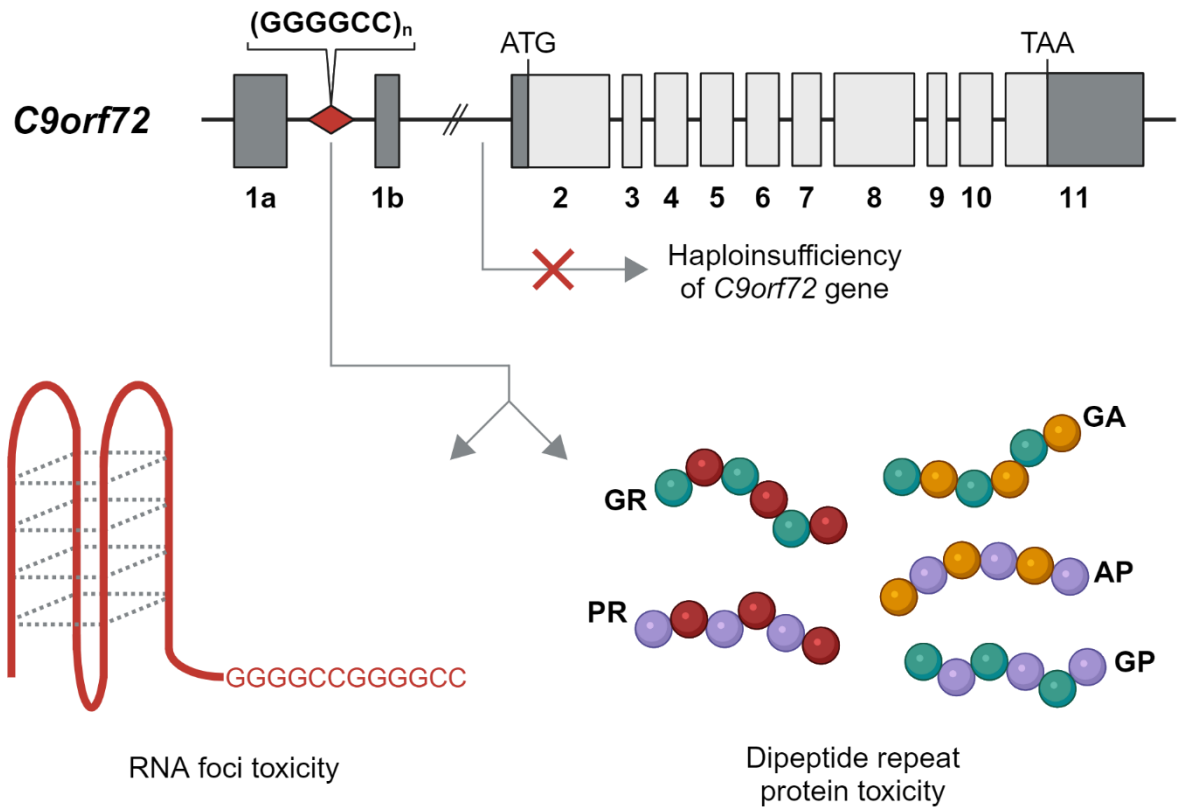


**Figure 1.2. Mechanisms of disease in *C9orf72* FTD/ALS.** The  $G_4C_2$  hexanucleotide repeat expansion between intron 1a and 1b of *C9orf72* results in: haploinsufficiency through reduced *C9orf72* expression; transcription of the repeat to form toxic RNA structures; and RAN translation of repeat RNA to produce five toxic DPRs.

#### 1.3.4.1. Loss of *C9orf72* function through haploinsufficiency

Studies of patients carrying the expansion have consistently shown a reduction in *C9orf72* mRNA transcripts of up to 50 % across the cortices, cerebellum and spinal cord (DeJesus-Hernandez *et al.*, 2011; Belzil *et al.*, 2013; Donnelly *et al.*, 2013; Waite *et al.*, 2014; van Blitterswijk *et al.*, 2015; Rizzu *et al.*, 2016). This reduction appears to arise mostly from a reduction in V2 transcripts, which are also the most abundant in non-mutation carriers (Tran *et al.*, 2015; van Blitterswijk *et al.*, 2015; Rizzu *et al.*, 2016). This reduction in transcript levels is thought to arise from epigenetic changes, mostly methylation of the  $G_4C_2$  repeat and surrounding CpG islands, which suppress gene transcription (Belzil *et al.*, 2013). While methylation is associated with haploinsufficiency through reduced *C9orf72* expression, it is also associated with reduced accumulation of RNA foci and DPR inclusions in human brains (Liu *et al.*, 2014). This may explain the pleiotropic effects of *C9orf72* methylation: increased methylation is associated with earlier age-of-onset (Gijssels *et al.*, 2015; Zhang *et al.*,

2017) but also associated with slower disease progression and neurodegeneration (McMillan *et al.*, 2015; Russ *et al.*, 2015).

The decrease in *C9orf72* transcripts corresponds with a decrease of up to 50 % at the protein level in the cortices and up to 20 % in the cerebellum and spinal cord (Xiao *et al.*, 2015; Frick *et al.*, 2018; Saberi *et al.*, 2018). This decrease is primarily driven by a decrease in C9-long, the most abundant isoform (Viodé *et al.*, 2018). As discussed above, evidence points to a role of *C9orf72* in many biological processes, all of which may be adversely affected by a decrease in *C9orf72* expression and function. Despite this, studies of haploinsufficiency have produced conflicting results on the contribution of haploinsufficiency to C9 disease.

Loss of *C9orf72* function leads to locomotor deficits and motor neuron degeneration in *C. elegans* (Therrien *et al.*, 2013) and zebrafish (Ciura *et al.*, 2013). *C9orf72* ablation caused mild motor deficits in mice but was more prominently characterised by inflammatory and immune phenotypes (Koppers *et al.*, 2015; Atanasio *et al.*, 2016). Patients who are homozygous for the *C9orf72* mutation do not exhibit more severe disease, indicating that *C9orf72* expression and function are not tied to disease severity (Fratta *et al.*, 2013). Additionally, no loss-of-function mutations in *C9orf72* have been reported in association with FTD/ALS (Harms *et al.*, 2013). While evidence points towards haploinsufficiency being insufficient for neurodegeneration, an emerging hypothesis is that it contributes to disease by exacerbating the toxicity of RNA foci and DPRs. One study in cultured motor neurons found that *C9orf72* contributed towards DPR clearance via lysosomal pathways (Shi *et al.*, 2018). *C9orf72* expression has also been shown to be neuroprotective against the toxicity of RNA foci and DPRs in mice (Shao *et al.*, 2019).

#### **1.3.4.2. RNA foci**

RNA foci are a pathological hallmark of C9 disease that precede TDP-43 pathology, detected throughout the frontal cortex, hippocampus, cerebellum and spinal cord (DeJesus-Hernandez *et al.*, 2011; Lagier-Tourenne *et al.*, 2013; Mizielinska *et al.*, 2013). They are predominantly found within the nucleus but are also seen in the cytoplasm at a reduced frequency. G<sub>4</sub>C<sub>2</sub> repeats are bi-directionally transcribed to produce sense and antisense repeat RNA that, because of its repetitive nature, forms stable secondary structures such as hairpins, RNA duplexes, and G-quadruplexes (Fratta *et al.*, 2012). These RNA structures aggregate into foci and sequester RBPs such as Pur- $\alpha$ , FUS, hnRNPs, SRSF1/2, Zfp106 and nucleolin (Fratta *et al.*, 2012; Xu *et al.*, 2013; Cooper-Knock *et al.*, 2014; Haeusler *et al.*, 2014; Celona *et al.*, 2017; Česnik *et al.*, 2019). Importantly, RNA foci have not been shown

to interact TDP-43. Sequestration of RBPs disrupts their function (Xu *et al.*, 2013), with downstream effects on RNA metabolism, nucleocytoplasmic transport and nucleolar dynamics (Xu *et al.*, 2013; Haeusler *et al.*, 2014).

Studies of RNA toxicity report contrasting results on the contribution of RNA foci to disease. Cooper-Knock *et al.* (2015) found that the presence of antisense RNA foci in the motor neurons of C9ALS patients was associated with accompanying TDP-43 pathology. However, increased antisense RNA foci burden in the frontal cortex was associated with a later age-of-onset (DeJesus-Hernandez *et al.*, 2017). In the same study, patient RNA foci burden was found to not correlate with clinical features such as age, survival or clinical phenotype.

Models of G<sub>4</sub>C<sub>2</sub> toxicity have demonstrated toxicity in rat primary neurons (Wen *et al.*, 2014) and in *Drosophila* (Xu *et al.*, 2013; Zhang *et al.*, 2015). RBP expression was found to modulate G<sub>4</sub>C<sub>2</sub> toxicity in some of the models, implicating RNA as the toxic species (Xu *et al.*, 2013; Celona *et al.*, 2017; Swinnen *et al.*, 2018). In contrast, Tran *et al.* (2015) showed that G<sub>4</sub>C<sub>2</sub> toxicity correlated with DPR production but not RNA foci in *Drosophila*. To delineate toxicity of RNA from DPRs, RNA only models were established. While these demonstrated toxicity in zebrafish (Swinnen *et al.*, 2018), no such toxicity was observed in *Drosophila* (Mizielinska *et al.*, 2014; Moens *et al.*, 2018).

The disparity between these studies likely arises from differences in methodology, model organisms and repeat lengths used. For example, *Drosophila* may lack homologues to the consequential human RBPs in RNA toxicity, resulting in the general lack of RNA toxicity seen in *Drosophila* models. While many studies using G<sub>4</sub>C<sub>2</sub> models took steps to confirm an absence of DPRs, difficulties in DPR detection make it impossible to rule out their presence entirely. Therefore, it becomes difficult to attribute observed toxicity entirely to RNA foci rather than the combined effects of RNA and DPRs. As such, the role of RNA foci in C9 disease remains unclear.

#### **1.3.4.3. Dipeptide repeat proteins (DPRs)**

The non-canonical, repeat associated non-AUG (RAN) translation of repeat RNA, across each open reading frame of both sense and antisense directions, produces five distinct dipeptide repeat proteins. Poly-glycine-alanine (GA), poly-glycine-proline (GP), and poly-glycine-arginine (GR) are produced from the sense strand. GP, poly-alanine-proline (AP), and poly-proline-arginine (PR) are produced from the antisense strand (Fig. 1.3). These DPRs are found in inclusions in post-mortem brain samples from C9 patients, but their role in C9 disease is somewhat unclear. DPR inclusions are found across affected and

unaffected regions of the brain and do not correlate with TDP-43 pathology or neurodegeneration (Davidson *et al.*, 2014; Mackenzie *et al.*, 2015). However, DPRs appear to be more prominent drivers of neurodegeneration than RNA foci (Mizielinska *et al.*, 2014; Wen *et al.*, 2014; Tran *et al.*, 2015; Moens *et al.*, 2018; Solomon *et al.*, 2018). It is also important to note that soluble DPRs are also likely to play a role in C9 disease but, due to difficulties visualising and quantifying their burden, our understanding of them is limited (Quaegebeur *et al.*, 2020). DPR pathology precedes TDP-43 pathology in patients, so DPRs have been proposed to cause TDP-43 pathology (Baborie *et al.*, 2015). To provide more insight into the role of DPRs in C9 disease, numerous studies have investigated the effects of the five individual DPRs in model systems.

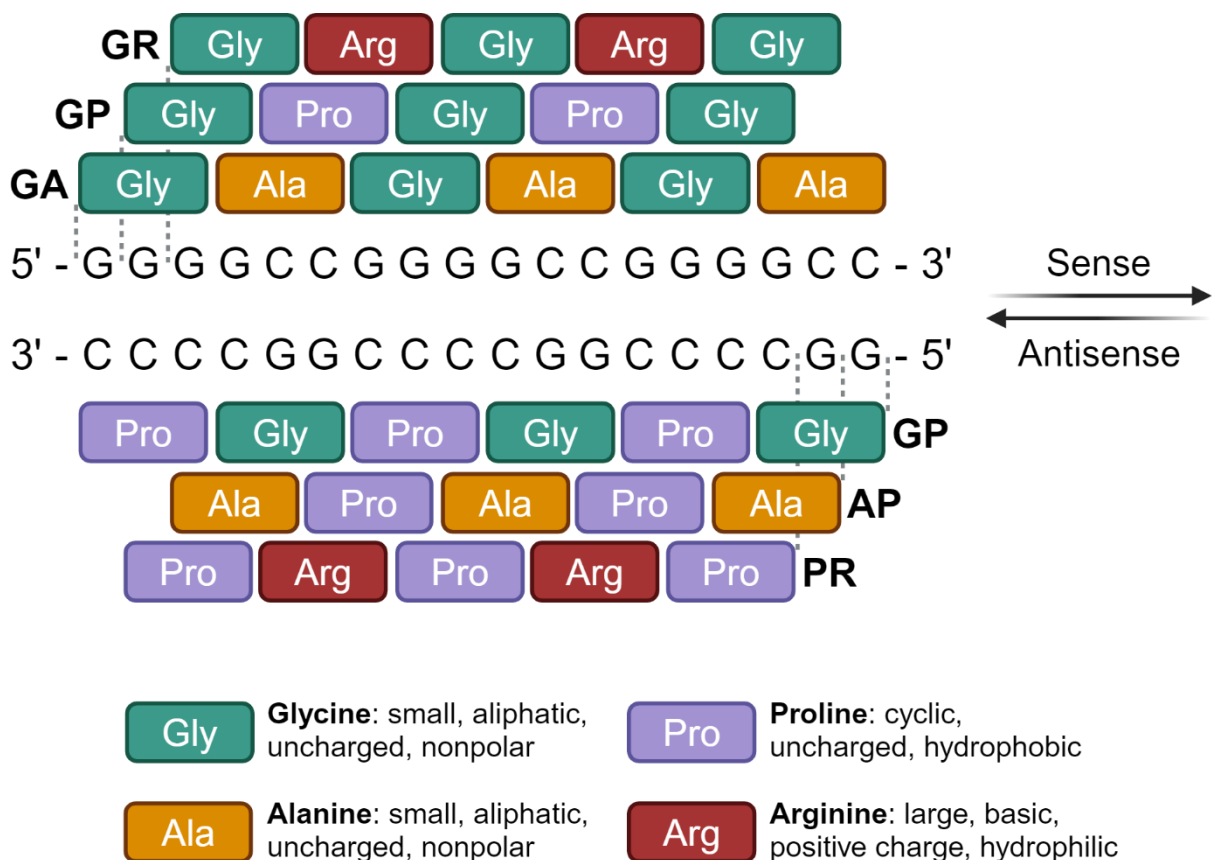


**Figure 1.3. Repeat-associated non-AUG (RAN) translation of sense and antisense hexanucleotide repeat RNA, in every reading frame, produces five toxic dipeptide repeat proteins (DPRs).** Poly-glycine-alanine (GA), poly-glycine-proline (GP) and poly-glycine-arginine (GR) are produced from the sense strand. Poly-glycine-proline (GP), poly-alanine-proline (AP) and poly-proline-arginine (PR) are produced from the antisense strand.

GA is the DPR seen most frequently in inclusions in patient brain tissue, followed by GP and GR which are followed by AP and PR (Mackenzie *et al.*, 2015). This is likely due to its high propensity to aggregate, arising from its composition and ability to form beta sheets. GA is also capable of spreading, demonstrated as neuron-to-neuron and astrocyte-to-neuron transmission (Khosravi *et al.*, 2020; Marchi *et al.*, 2022). Due to its prevalence in patients, GA has been studied extensively. It has been shown to be toxic in HEK293 cells, chick embryonic spinal cord, mouse and rat primary neurons (May *et al.*, 2014; Zhang *et al.*, 2014; Lee *et al.*, 2017). GA has been shown to sequester numerous proteins to DPR inclusions, including transport, proteasomal and nucleocytoplasmic transport proteins; and even GP and AP DPRs (May *et al.*, 2014; Lee *et al.*, 2017). As a result, downstream disruption is observed as proteasomal impairment, ER stress and nucleocytoplasmic transport defects resulting in TDP-43 pathology and apoptosis (Zhang *et al.*, 2014; Khosravi *et al.*, 2017; Lee *et al.*, 2017; Nonaka *et al.*, 2018) (Fig. 1.4). However, this disruption is not always associated with toxicity: Schludi *et al.* (2017) showed that GA expressed in mice formed inclusions in spinal cord, brainstem and cerebellum, associated with TDP-43 pathology and motor deficits but no outright toxicity. GA also shows length-dependent morphological, mechanistic and toxic effects. The short repeat models discussed above show spherical inclusions of GA, unlike the stellate or fern-like inclusions observed in patients and recapitulated by 1000 repeat models (Callister *et al.*, 2016; West *et al.*, 2020). GA-induced TDP-43 pathology and GA spreading were associated with longer repeat lengths (Nonaka *et al.*, 2018; Morón-Oset *et al.*, 2019). These observation may provide an explanation for GA toxicity in 1000 but not 100 repeat GA *Drosophila* models (Mizielinska *et al.*, 2014; West *et al.*, 2020).

Despite being one of the more prevalent DPRs in patients, GP has been studied the least. This is partly due to difficulties in cloning its alternative codon sequence past 50 repeats (Callister *et al.*, 2016). Studies that have examined GP toxicity found negligible toxicity in *Drosophila* or chick embryonic spinal cord (Freibaum *et al.*, 2015; Lee *et al.*, 2017). This is likely in part due to its flexible coil structure that prevents it from aggregating on its own (Yamakawa *et al.*, 2015). However, it is difficult to make conclusions about GP toxicity and its contribution to disease without further study.

Studies have shown that the arginine-containing DPRs, GR and PR, are the most toxic DPRs in HEK293 cells, *Drosophila*, rat primary neurons, and iPSC-derived cortical and motor neurons (Mizielinska *et al.*, 2014; Wen *et al.*, 2014; Freibaum *et al.*, 2015; Tao *et al.*, 2015; Lee *et al.*, 2016). Both GR and PR have also proven neurotoxic when expressed individually in mice, causing FTD/ALS phenotypes (Zhang *et al.*, 2018, 2019; Choi *et al.*, 2019; Hao *et al.*, 2019). Similar results have also been reported when PR is expressed in

monkeys (Xu *et al.*, 2023). Their toxicity likely arises from their arginine content conferring positive charge and high polarity.

Mechanisms of PR toxicity tend to centre on its presence in the nucleus and disruption of nuclear processes. PR has been shown to interact with RNA, RBPs, and nucleolar proteins (Hartmann *et al.*, 2018; Suzuki and Matsuoka, 2021; Balendra *et al.*, 2023); disrupt nuclear lamins and heterochromatin (Zhang *et al.*, 2019); and promote phase separation (White *et al.*, 2019; Balendra *et al.*, 2023). These all contribute to the nucleolar dysfunction that is observed in models of PR toxicity (Mizielinska *et al.*, 2017; White *et al.*, 2019) (Fig. 1.4). However, it is important to note that these studies were performed in short repeat models in which PR mostly localises to the nucleus. In patient tissue and longer repeat models, PR is found in both the nucleus and cytoplasm (Mackenzie *et al.*, 2015; Callister *et al.*, 2016; West *et al.*, 2020).

GR is the only DPR that has been correlated with neurodegeneration and clinical severity in patients (Saber *et al.*, 2018; Sakae *et al.*, 2018; Quaegebeur *et al.*, 2020), and is generally regarded as the most toxic of all the DPRs. GR has been shown to sequester stress granule (SG) proteins and impair SG dynamics (Hartmann *et al.*, 2018; Zhang *et al.*, 2018; Park *et al.*, 2023) (Fig. 1.4). GR binding of mitochondrial and mitochondrial ribosomal proteins, leading to mitochondrial dysfunction, have also been implicated in GR toxicity (Lopez-Gonzalez *et al.*, 2016; Choi *et al.*, 2019) (Fig. 1.4). Disruption of nucleocytoplasmic transport (Fig. 1.4), resulting in TDP-43 mislocalisation, has also been identified as a mechanism of GR toxicity (Mizielinska *et al.*, 2017; Cook *et al.*, 2020), although a direct link is disputed (Vanneste *et al.*, 2019). Interestingly, one study identified DNA damage and oxidative stress in patient iPSC-derived motor neurons that was replicated by expression of GR in control motor neurons (Lopez-Gonzalez *et al.*, 2016) (Fig. 1.4). Studies with short GR repeats have shown its localisation to the nucleolus (Hartmann *et al.*, 2018), but cytoplasmic localisation is more commonly seen in patients and longer repeat models (Mackenzie *et al.*, 2015; Callister *et al.*, 2016; West *et al.*, 2020). Both PR and GR also demonstrate length-dependent toxicity. In a 100-repeat *Drosophila* model both DPRs had pan-neuronal expression induced in adults to avoid lethality during development (Mizielinska *et al.*, 2014), but in a 1000-repeat model both DPRs can be pan-neuronally expressed throughout the fly lifetime (West *et al.*, 2020). In this model, the arginine-containing DPRs, especially GR, cause age-related neurodegeneration and decline in motor function.

AP is one of the least frequently observed DPRs in patient tissue (Mackenzie *et al.*, 2015). This infrequency, combined with a lack of toxicity in early, short repeat *Drosophila* and cell models (Mizielinska *et al.*, 2014; Wen *et al.*, 2014; Boeynaems *et al.*, 2016; Xu and Xu,

2018), has resulted in limited study of AP. However, in 1000-repeat cell and *Drosophila* models AP causes electrophysiological defects, motor deficits, toxicity and neurodegeneration (Callister *et al.*, 2016; West *et al.*, 2020) (Fig. 1.4).

Recent studies have highlighted length-dependent effects of DPRs in models of FTD/ALS. Morón-Oset *et al.* (2019) demonstrated that GA200 spreads to a greater extent than GA100 through the *Drosophila* brain, while GA36 does not spread at all. Such effects have also been demonstrated with the arginine-containing DPRs, which cause ribosomal stalling when expressed at 101 repeats, but not 10 repeats (Radwan *et al.*, 2020). Liquid-liquid phase separation by PR has also been shown to occur only in longer repeats (White *et al.*, 2019; Jafarinia, van der Giessen and Onck, 2020). At 1000-repeats, GA, AP, PR and GR are all toxic and causes motor deficits in both *Drosophila* and zebrafish models (Swaminathan *et al.*, 2018; West *et al.*, 2020), despite some of the DPRs previously showing little to no toxicity in shorter repeat models. These length-dependent effects likely arise due to the length-dependent morphology and localisation of the DPRs demonstrated by Callister *et al.* (2016) and West *et al.* (2020). The disparity in DPR toxicity between studies not only arises from difference in repeat length, but also from model system used. This highlights the need for standardised models in future research. Common mechanisms of toxicity for individual DPRs can be seen between studies and there is clearly a potential role of DPRs, especially GA and GR, in causing TDP-43 pathology. However, translating these findings to patients is complicated by a number of factors: different DPR species can coexist within individual cells and can interact with each other (Darling *et al.*, 2019; West *et al.*, 2020); chimeric DPRs can be produced by frameshifts during RAN translation (McEachin *et al.*, 2020; Latallo *et al.*, 2023); and potential interplay between DPRs, RNA foci and *C9orf72* haploinsufficiency.

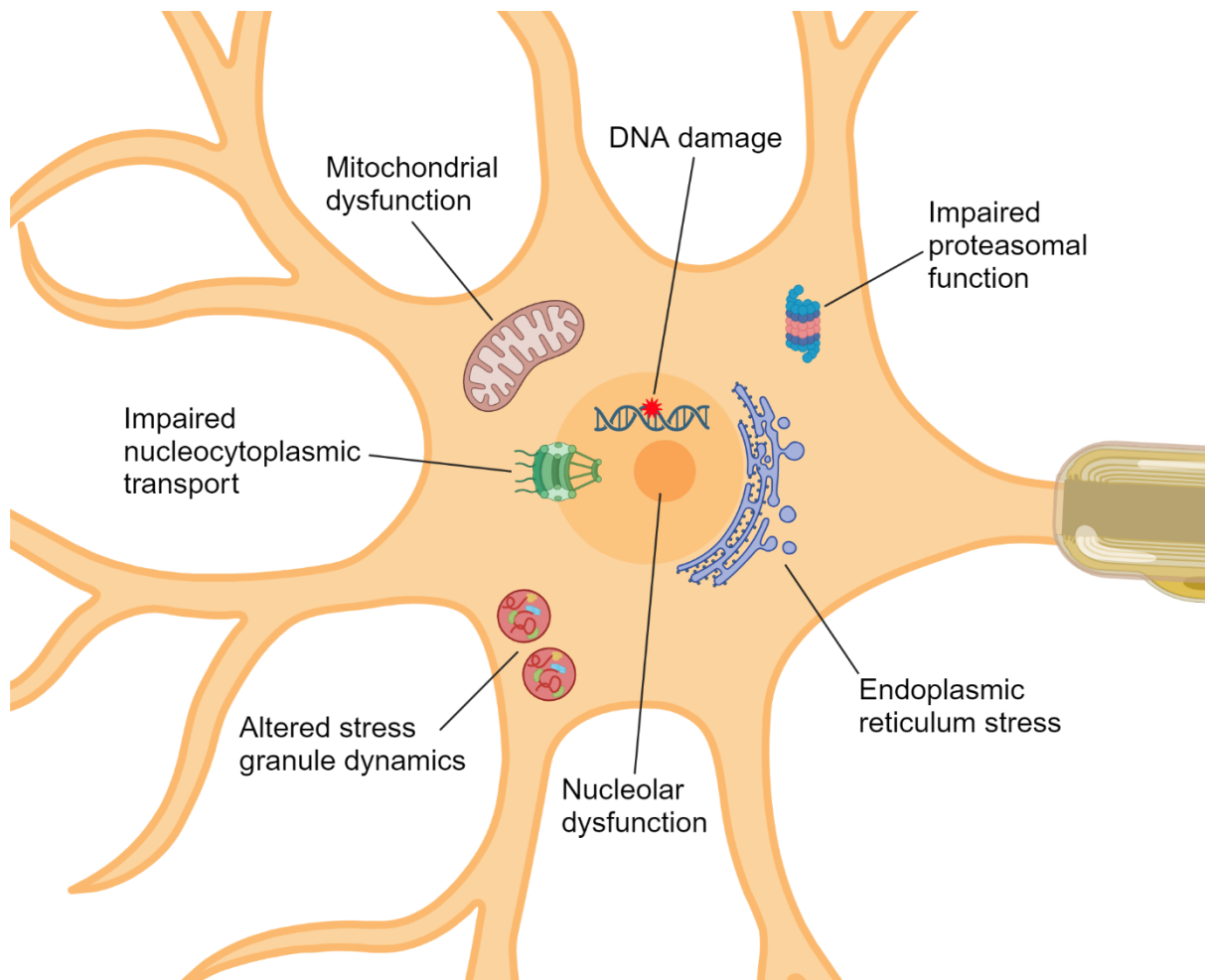


**Figure 1.4. DPRs disrupt cellular processes to cause neurotoxicity.** Models of DPR toxicity have identified DPR-induced disruption in biological processes, which mediates DPR toxicity.

#### 1.4. Gene/Environment/Time hypothesis

Despite the clear genetic component of FTD/ALS, incomplete penetrance and a remarkable sporadic component leaves many cases that cannot be explained by genetics alone (McLaughlin, Vajda and Hardiman, 2015). ALS has also been shown to be a multistep process, whereby disease develops in stages (Chiò *et al.*, 2018; Vucic *et al.*, 2020). These findings support a gene/environment/time hypothesis, whereby disease is caused by the interplay between genetic vulnerability, environmental risk factors and aging (Al-Chalabi and Hardiman, 2013). Under this hypothesis, age-associated accumulation of CNS damage; environmental stressors of the CNS; and genetic predisposition towards disease all combine to reach a 'tipping point', past which disease pathology and neurodegeneration begin to occur.

With the emerging prominence of this hypothesis, research has begun to focus on the FTD/ALS exposome. The exposome is defined as the cumulative lifetime effect of environmental and lifestyle factors (Feldman *et al.*, 2022). To date, environmental factors such as high toxin pollution and blood metals have been shown to correlate with increased disease risk and shortened survival (Su *et al.*, 2016; Goutman *et al.*, 2019; Figueroa-Romero *et al.*, 2020; Peters *et al.*, 2021). Lifestyle factors such as smoking, alcohol consumption and low BMI have also been associated with ALS risk (Westeneng *et al.*, 2021). Somewhat surprisingly, strenuous physical exercise has also been linked to an increased ALS risk (Julian *et al.*, 2021; Westeneng *et al.*, 2021), especially in professional athletes (Daneshvar *et al.*, 2021). Despite the identification of these disease-contributing environmental and lifestyle factors, we have limited understanding of how they mechanistically increase susceptibility to disease. By developing our understanding of these underlying mechanisms, we can better understand disease pathogenesis and identify opportunities for treatment. One mechanism with potential to underly factors such as smoking and physical exercise is hypoxia, which has already been linked to ALS. Importantly hypoxia relates to genetic, aging (time) and environmental factors under the gene/environment/time hypothesis.

Environmental factors, such as occupational low oxygen exposure; physical exercise; and smoking, are the most apparent in causing hypoxia. However, aging and genetic factors may also play a causative role through impairment of the physiological response to hypoxia (Kim *et al.*, 2003; Weil, 2003; Benderro and Lamanna, 2011) and increasing the likelihood of conditions such as ischemia that can also lead to hypoxia (Cai *et al.*, 2017). Hypoxia can also modulate aging pathways, potentially accelerating the time aspect of the gene/environment/time hypothesis (Kim *et al.*, 2016).

## 1.5. Hypoxia

Oxygen is an essential molecule in many biological processes, especially aerobic respiration. As such, oxygen homeostasis is an important process for all aerobic organisms. Hypoxia is a state of limited oxygen availability at the tissue level, below the homeostatic range of that tissue (Cafaro, 1960). In humans, hypoxia can occur for a number of reasons, including reduced environmental oxygen; impaired supply of oxygen to tissues, through breathing or vascular impairment; and in periods of particularly high oxygen consumption, such as physical exercise (Hopkins, 2007; Cloutier and Thrall, 2009). Limited oxygen supply disrupts oxygen-consuming biological processes, leading to reduced electron transport and ATP production; increased ROS production; and apoptosis (Sendoel and Hengartner, 2014). This cumulates as an overall state of cellular stress, highlighting the importance of an appropriate cellular response to hypoxia to prevent injury.

### 1.5.1. Physiological response to hypoxia

The cellular response to hypoxia is mediated by the transcription factor Hypoxia Inducible Factor 1 (HIF1). HIF1 is a highly conserved heterodimeric complex consisting of the constitutively expressed HIF1 $\beta$  and continuously translated HIF1 $\alpha$  (Gorr, Gassmann and Wappner, 2006). Both subunits are required for transcriptional activity and are retained in the cytoplasm under normoxic conditions (Fig. 1.5). HIF1 $\alpha$ , which can be replaced in the complex by HIF2 $\alpha$  or HIF3 $\alpha$  (Ema *et al.*, 1997; Gu *et al.*, 1998), is considered the oxygen-sensing subunit. Under normoxic conditions, prolyl hydroxylase domain (PHD) proteins catalyse the O<sub>2</sub>-dependent hydroxylation of two prolyl residues in the oxygen-dependent degradation domain (ODDD) of HIF1 $\alpha$  (Bruick and McKnight, 2001; Epstein *et al.*, 2001) (Fig. 1.5). Hydroxylation of these residues permits binding of HIF1 $\alpha$  to von Hippel-Lindau (VHL) (Jaakkola *et al.*, 2001; Yu *et al.*, 2001), which acts as part of a ubiquitin ligase complex (Fig. 1.5). This binding facilitates poly-ubiquitination of HIF1 $\alpha$ , leading to its degradation by the proteasome (Huang *et al.*, 1998; Kallio *et al.*, 1999; Maxwell, Patrick H. Wiesener *et al.*, 1999) (Fig. 1.5). However, under hypoxic conditions the PHD-mediated, O<sub>2</sub>-dependent hydroxylation of HIF1 $\alpha$  prolyl residues can no longer occur (Fig. 1.5). Because HIF1 $\alpha$  is continuously translated, HIF1 $\alpha$  now rapidly accumulates in the cytoplasm (Huang *et al.*, 1998), where it dimerises with HIF1 $\beta$  and moves into the nucleus (Manalo *et al.*, 2005). In the nucleus, HIF1 binds to hypoxia reactive element (HRE) sequences in the DNA and promotes downstream gene transcription (Wenger, Stiehl and Camenisch, 2005) (Fig. 1.5). This system of continuous degradation enables rapid (<5 minutes) switching on and off of the hypoxia response (Huang *et al.*, 1998; Jewell *et al.*, 2001). HIF1 $\alpha$  also undergoes O<sub>2</sub>-

dependent inhibition: under normoxia, hydroxylation of an asparagine residue by factor inhibiting HIF1 (FIH-1) disrupts HIF1 interactions with transcriptional co-activators (Lando *et al.*, 2002).

It is estimated that HIF1 regulates the transcription of up to 5 % of human genes (Manalo *et al.*, 2005). However, the most well characterised are those which are directly involved in the response to hypoxia. One major category is genes involved in cellular metabolism, such as glycolytic enzymes, pyruvate dehydrogenase kinase (PDK), lactate dehydrogenase (LDH), and glucose transporter 1 (GLUT1). Upregulation of these genes promotes a shift to anaerobic respiration over aerobic respiration, to maintain ATP production while minimising ROS generation by the TCA cycle and mitochondrial respiration. This facilitates short term adaptation of cellular energy metabolism to the hypoxic conditions. For longer term adaptation, genes such as vascular endothelial growth factor (VEGF) and angiogenin (ANG) promote vascularisation in order to increase oxygen supply to the hypoxic tissue.

Other aspects of the cellular response to hypoxia are not directly regulated by HIF1-induced transcription. Hypoxia-induced mitochondrial ROS production leads to calcium release from the ER and activation of multiple kinases, triggering signalling cascades and downstream effects. Activation of PKR-like endoplasmic reticulum kinase (PERK) leads to a reduction in protein translation (Koumenis *et al.*, 2002). Calcium release and AMP kinase (AMPK) activation leads to endocytosis and degradation of Na<sup>+</sup>/K<sup>+</sup>-ATPase from the cell membrane (Gusarova *et al.*, 2011). Both protein translation and Na<sup>+</sup>/K<sup>+</sup>-ATPase activity are ATP demanding processes, so these cascades function to reduce cellular ATP consumption during the shift to anaerobic respiration.

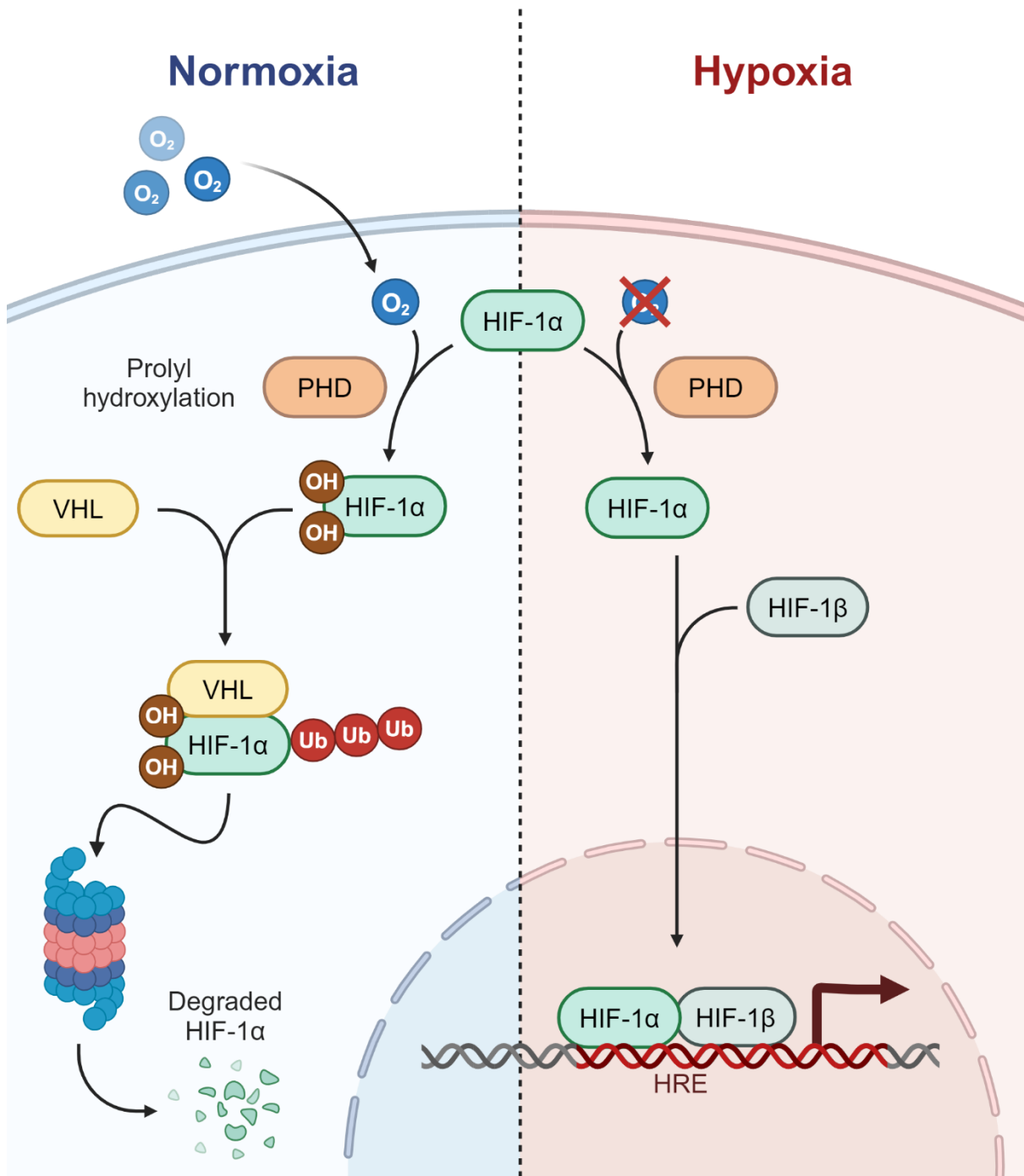


**Figure 1.5. HIF1 is the transcriptional master regulator of the cellular response to hypoxia.** HIF1 activity is regulated through the oxygen-dependent degradation of HIF1 $\alpha$ . In normoxia, the presence of oxygen causes HIF1 $\alpha$  degradation via the ubiquitin-proteasome system (UPS). In hypoxia, limited oxygen availability prevents this degradation, allowing HIF1 $\alpha$  to dimerise with HIF1 $\beta$  and promote transcription downstream of hypoxia response elements (HRE). Figure adapted from BioRender

### 1.5.2. Hypoxia in neurodegenerative disease

The human brain constitutes only 2 % of the body's mass but uses 20 % of its resting energy production (Kety, 1957), manifesting as high glucose and oxygen demand. It is therefore unsurprising that the brain is particularly susceptible to hypoxia (Cervos-Navarro and Diemer, 1991). Indeed, healthy individuals demonstrated cognitive impairment after periods in altitude-induced hypoxia (Nelson *et al.*, 1990; Hornbein, 1992). Hypoxia and hypoxia signalling have also been linked to neurodegenerative disease, such as Parkinson's disease, Alzheimer's disease, Huntington's disease, multiple sclerosis and ALS (Correia *et al.*, 2013; Mitroshina *et al.*, 2021).

Occupational exposure to hypoxia, as a firefighter or professional athlete, have both been identified as ALS risk factors (Belli and Vanacore, 2005; Chiò *et al.*, 2005; Vanacore *et al.*, 2010; Julian *et al.*, 2021). Interestingly, intermittent hypoxia has been shown to have an accelerative role by aggravating motor neuronal loss and ALS phenotypes in SOD1 ALS mice (Kim *et al.*, 2013). Altogether, these findings point to a causative or accelerative role of occupational/intermittent exposure to hypoxia in ALS. This is in line with the gene/environment/time hypothesis, in that hypoxia may increase disease risk and accelerate disease progression in individuals who are genetically predisposed. Importantly, early-onset muscle weakness in the diaphragm leads to intermittent hypoxia in many ALS patients, and disease progression leads to chronic respiratory difficulties and chronic hypoxia (Lyll *et al.*, 2001). Therefore, hypoxic exposure may be an environmental factor that is relevant to patients at both presymptomatic and symptomatic stages of disease.

In addition to environmental hypoxia, there also appears to be a role of tissue-level hypoxia in ALS. Vascular and blood flow changes in the spinal cord characterise ALS pathogenesis and precede motor neuron degeneration (Zhong *et al.*, 2008; Miyazaki *et al.*, 2012; Pronto-Laborinho, Pinto and De Carvalho, 2014). These changes have been linked to tissue-level hypoxia in the spinal cord of SOD1 ALS mice (Sato *et al.*, 2012). Similarly, hypoxic stress has been observed in the spinal cord of ALS patients and was closely associated with disease progression (Yamashita *et al.*, 2021). When spinal cord hypoxic stress was treated in SOD1 mice, ALS symptoms and survival were improved (Zheng *et al.*, 2004; Tada *et al.*, 2019). These findings indicate that tissue-level hypoxia in affected tissues is detrimental and likely plays a role in ALS disease progression.

Tissue-level hypoxia undoubtedly leads to activation of the HIF1-mediated protective response to hypoxia in affected cells. However, dysregulation of HIF1 $\alpha$  has been identified in ALS model systems and patient tissues. HIF1 $\alpha$  expression has been shown to be increased in the motor neurons of ALS patients and mouse models, perhaps in response to tissue-level

hypoxia (Sato *et al.*, 2012; Nagara *et al.*, 2013; Nomura *et al.*, 2019). These studies also demonstrate changes in HIF1 $\alpha$  expression throughout disease progression, although there is conflicting evidence towards the direction of these changes (Sato *et al.*, 2012; Nomura *et al.*, 2019). Alongside perturbed HIF1 $\alpha$  expression, dysfunctional hypoxia signalling has also been demonstrated in ALS. Despite elevated HIF1 $\alpha$  expression in SOD1 mice, expression of HIF1 $\alpha$  transcriptional targets, erythropoietin (EPO) and VEGF, was decreased (Sato *et al.*, 2012). This suggests a disconnect between HIF1 $\alpha$  expression and transcriptional activity, which may occur due to the impaired nuclear import of HIF1 $\alpha$  demonstrated in these models by Nagara *et al.* (2013). Additionally, VEGF expression was not increased in response to hypoxic exposure in SOD1 mice, sALS monocytes and sALS fibroblasts (Murakami *et al.*, 2003; Moreau *et al.*, 2011; Raman *et al.*, 2015). Importantly, similar effects have also been demonstrated in hypoxic sALS patients, who exhibited increased levels of EPO but not VEGF in cerebrospinal fluid (CSF) (Moreau *et al.*, 2006; Just *et al.*, 2007). Interestingly, survival signalling pathways mediated by p-AKT and p-ERK, rather than HIF1 $\alpha$ , have been shown to be sustained following exposure to hypoxia in SOD1 mice (Ilieva *et al.*, 2003). Altogether, these findings point towards dysregulation of hypoxia signalling and the response to hypoxia across the ALS spectrum.

Dysfunction in hypoxia signalling is particularly relevant to neurodegenerative disease, considering the neuroprotective effects of HIF1 $\alpha$ -induced genes. VEGF in particular has been demonstrated as neuroprotective and neurotrophic in motor neurons (Lambrechts *et al.*, 2003; Van Den Bosch *et al.*, 2004). Due to these effects, VEGF has been trialled as a treatment for ALS, delaying disease progression in mouse models (Zheng *et al.*, 2004; Ismailov *et al.*, 2014). However, VEGF treatment is yet to be utilised in patients. Despite this, VEGF treatment may hold promise for patients as reduced VEGF expression has been observed post-mortem in motor neurons of ALS patients (Brockington *et al.*, 2006) and VEGF expression has been shown to be positively correlated with age of onset in C9 patients (Dickson *et al.*, 2019). Interestingly, deletion of the HRE in the VEGF promoter has been shown to be sufficient to cause motor neuron degeneration and ALS phenotypes in mice (Oosthuysen *et al.*, 2001). It is therefore unsurprising that genetic variation in VEGF and ANG has been associated with ALS (Lambrechts *et al.*, 2003; Cronin *et al.*, 2008).

There is clear evidence for a link between an aberrant response to hypoxia and ALS, however the role of hypoxia signalling in disease pathogenesis remains unclear. While most of this research has been performed in SOD1 models of ALS, the observations may represent common features and mechanisms across different forms of the disease.

## 1.6. *Drosophila melanogaster* as a model organism

*Drosophila melanogaster*, commonly known as the fruit fly, is a powerful model organism for the study of genetics and molecular biology of human diseases. *Drosophila* were used in the founding of the field of classical genetics in the early 1900s, and *Drosophila* research has been awarded six Nobel prizes for physiology and medicine to date. Several characteristics make *Drosophila* an attractive model for scientific research. They can be cultured at low cost and in high numbers, facilitating screening and high-throughput experiments which are often key in genetic studies. Their short life span and 10 day generation time from fertilisation to adult fly (at 25°C) means *Drosophila* research can progress much faster than zebrafish and mammalian models.

*Drosophila* are especially useful for modelling neurodegenerative disease. Their 50-90 day lifespan permits the study of disease alongside aging, which is extremely relevant to neurodegenerative disease. The adult fly nervous system is also remarkably complex, the brain alone contains 200,000 neurons, leading to complex behaviours such as courtship, sleep, aggression, learning and memory (Raji and Potter, 2021). This relative complexity makes *Drosophila* a suitable model of the human nervous system.

Having been used in research for decades, an extensive set of research tools have been developed in *Drosophila*. The fly genome has been completely sequenced and annotated, identifying roughly 14,000 genes. Many of these are homologous to human genes, in fact up to 75 % of human disease-associated genes have a homologue in *Drosophila* (Reiter *et al.*, 2001). Flies also have high genetic tractability, as such a plethora of fly lines have been generated with endogenous mutations, transgenic reporters, overexpression constructs and RNA interference (RNAi) constructs integrated into their genome.

### 1.6.1 UAS/Gal4

One of the most commonly used genetic tools in *Drosophila* is the GAL4/UAS system, a modular expression system endogenous to yeast. First developed for *Drosophila* in 1993 by Brand and Perrimon, this system permits the expression of desired constructs in a tissue-specific manner. It is based upon the finding that GAL4 protein, encoded by the *GAL4* gene, binds to Upstream Activating Sequence (*UAS*) and activates downstream gene expression (Kakidani and Ptashne, 1988; Webster *et al.*, 1988). In *Drosophila* this is utilised by generating *GAL4* fly lines, by inserting the *GAL4* gene under the control of endogenous promoters, and *UAS* lines, by inserting the *UAS* sequence upstream of transgenic constructs. By crossing a *GAL4* line with a *UAS* line, the offspring will carry both elements

and thus the *UAS*-linked transgene will be expressed in the presence of GAL4. Extensive libraries of both GAL4 and *UAS* lines have been generated. For example, GAL4 lines may express GAL4 under the control of a tissue-specific promoter. Additionally, *UAS* lines may carry *UAS*-driven RNAi constructs for gene knockdown or *UAS*-driven endogenous genes for overexpression. These extensive and widely available libraries facilitate much of the research carried out using *Drosophila*.

### 1.6.2. Modelling neurodegenerative disease

*Drosophila* have been incredibly useful in generating models of various human neurodegenerative diseases, including Alzheimer's disease (Cao *et al.*, 2008), Parkinson's disease (Feany and Bender, 2000), FTD (West *et al.*, 2020) and ALS (Watson *et al.*, 2008). These models are especially useful for studying neurodegenerative disease, since cell models do not recapitulate whole organism systems and patient samples are only available post-mortem and thus represent only end-stage disease. Using these models, researchers have been able to develop our understanding of disease aetiology, mechanisms and pathogenesis. Flies are particularly useful for studying the genetic contribution to disease, owing to their robust genetic toolkit.

*Drosophila* models of the poly-glutamine (polyQ) disorders, spinocerebellar ataxias (SCAs), have been used to identify molecular mechanisms of toxicity downstream of causative genetic expansions (Li *et al.*, 2008; McGurk *et al.*, 2021). These models have subsequently been used to identify modifiers of polyQ-induced degeneration (Cushman-Nick, Bonini and Shorter, 2013). *Drosophila* models of Parkinson's, carrying mutations in DJ-1, has been used to study of interactions between genetic susceptibility and environmental risk factors of disease (Meulener *et al.*, 2005, 2006). One study modelling *MAPT*-linked FTD used the genetic capabilities of *Drosophila* to identify modifiers of tau-mediated neurodegeneration (Shulman and Feany, 2003). Given the involvement of tau in many neurodegenerative disorders, findings from this study may have far-reaching implications. Using a *Drosophila* model of FTD caused by the *CHMP2B*<sup>intron5</sup> mutation, West *et al.* (2018) were able to identify modifiers of *CHMP2B*<sup>intron5</sup> toxicity and elucidate neuropathological cascades. Various other genetic causes of FTD/ALS have been also modelled in *Drosophila*, including TDP-43, FUS, VCP, and Ataxin-2 (Ritson *et al.*, 2010; Elden *et al.*, 2011; Lanson *et al.*, 2011).

### 1.6.3. Modelling *C9orf72* FTD/ALS

Due to an absence of a *C9orf72* homologue in *Drosophila*, it is not possible to use flies to study haploinsufficiency as a disease mechanism. The lack of homologue also means that models must rely on transgenic constructs, rather than mutation of an endogenous gene. To date, there are three categories of *Drosophila* model of *C9orf72* FTD/ALS: 1) pure repeat models, carrying the G<sub>4</sub>C<sub>2</sub> repeat and producing both RNA foci and DPRs; 2) RNA-only models, consisting of G<sub>4</sub>C<sub>2</sub> repeats interspersed with stop codons to prevent translation; and 3) DPR-only models, consisting of codon-switched repeat constructs that encode individual DPR species. While pure repeat models most accurately replicate what is occurring in patients, the inability to delineate RNA- and DPR-mediated effects limits the understanding we can develop from their study. For this reason, RNA- and DPR-only models were established. To best develop our understanding of C9 disease as it occurs in patients, it is key to utilise all three categories of model for their individual strengths. Current *Drosophila* models of *C9orf72* FTD/ALS are summarised in Table 1.3.

Until recently, DPR-only models have been limited by their short repeat length, generally limited to 100 repeats. The difficulty of cloning repetitive sequences *in vivo* prevented longer repeat models from being generated, until West *et al.* (2020) generated *Drosophila* DPR-only models of 1000-repeat length (Fig. 1.6), akin to the longer repeats observed in patients. The length-dependent properties of DPRs seen in this and other models raises the question of whether short repeat models accurately represent what is occurring in patients. Importantly, key DPR-mediated pathology may be missing in short repeat models. Where 100-repeat DPRs are extremely toxic, if not lethal, 1000-repeat DPRs demonstrate reduced toxicity in *Drosophila* (West *et al.*, 2020). This permits pan-neuronal expression of DPRs throughout the fly lifetime, without drastic reduction in fly lifespan. This is particularly important for models of FTD/ALS, given the key role of aging in neurodegeneration. Importantly, the differences in toxicity do not arise from changes in expression but from the nature of the 1000-repeat DPRs themselves, potentially in DPR-protein interactions or in *de novo* synthesis rates (West *et al.*, 2020).

As a result, this project uses this novel *Drosophila* model of *C9orf72* FTD/ALS which utilises the GAL4/UAS system to express individual DPRs in a tissue-specific manner, throughout the fly lifetime. Extensive characterisation of these 1000-repeat DPR lines and their associated distinct pathological phenotypes, by West *et al.* (2020), provides an excellent platform for the research of this project.

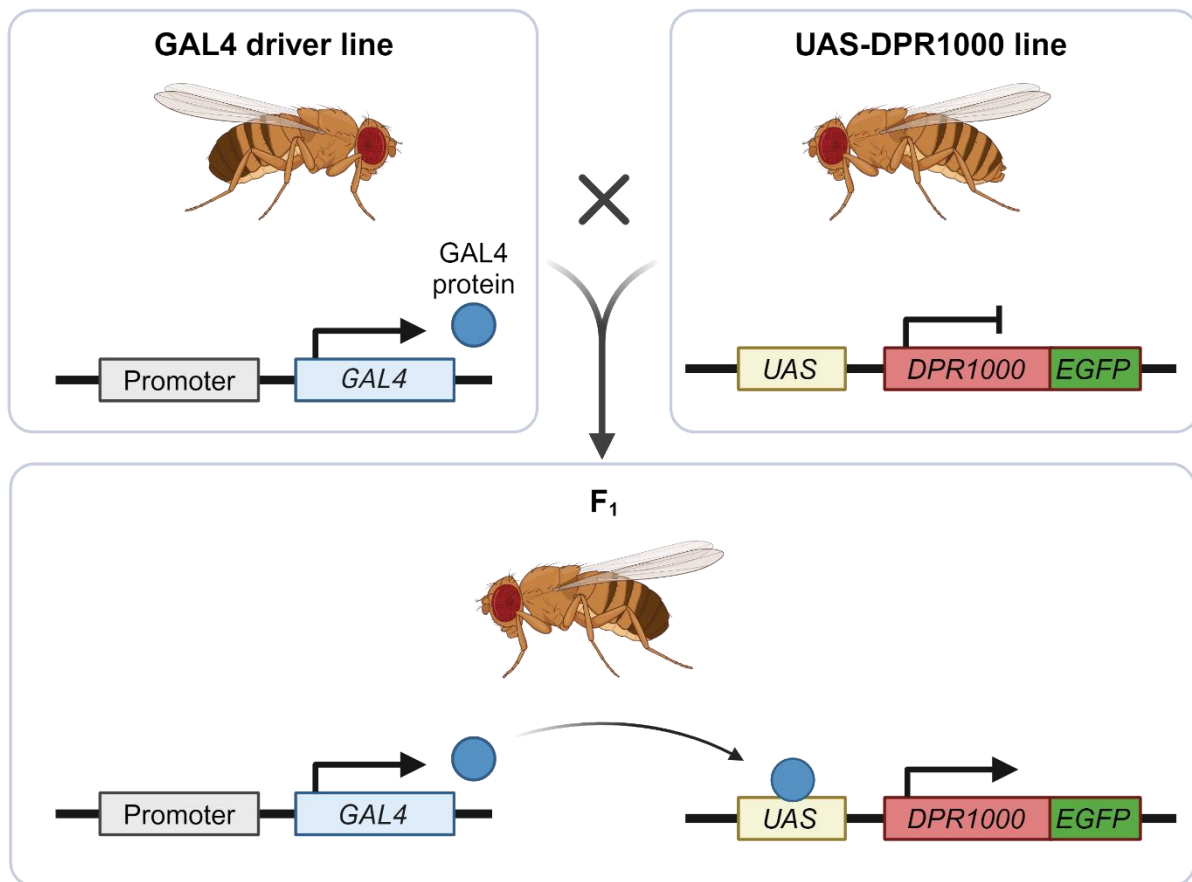


**Figure 1.6. Expression of EGFP-tagged 1000-repeat DPRs in *Drosophila* using the GAL4/UAS system.** GAL4 driver line expresses the transcriptional activity GAL4 under the control of a tissue-specific promoter. UAS-DPR1000 line carries UAS-driven DPR1000-EGFP, not expressed in the absence of GAL4. Crossing these lines produces F<sub>1</sub> which express GAL4 in a tissue specific manner, driving UAS expression of DPR1000-EGFP in the same manner.

**Table 1.3. *Drosophila* models of *C9orf72*-mediated frontotemporal dementia and amyotrophic lateral sclerosis, summarised in (Sharpe *et al.*, 2021).**

<b><i>Drosophila</i> model</b>	<b>Repeat length</b>	<b>Reference</b>
<b>Pure repeat</b>		
UAS-G <sub>4</sub> C <sub>2</sub>	3, 36, 103	Mizielinska <i>et al.</i> (2014)
	8, 28, 58	Freibaum <i>et al.</i> (2015)
	8, 29, 49	Goodman <i>et al.</i> (2019)
UAS-G <sub>4</sub> C <sub>2</sub> (intronic)	5, 80, 160	Tran <i>et al.</i> (2015)
UAS-G <sub>4</sub> C <sub>2</sub> -EGFP	3, 30	Xu and Xu (2018)
UAS-DsRed-G <sub>4</sub> C <sub>2</sub>	8, 32, 38, 56, 64, 128	Solomon <i>et al.</i> (2018)
UAS-LDS-(G <sub>4</sub> C <sub>2</sub> ) <sub>44</sub> .GR-GFP	44	Goodman <i>et al.</i> (2019)
<b>RNA only (RO)</b>		
UAS-G <sub>4</sub> C <sub>2</sub> RO	38, 108, 288	Mizielinska <i>et al.</i> (2014)
	48	Burguete <i>et al.</i> (2015)
	800, 1000, >1000	Moens <i>et al.</i> (2018)
UAS-G <sub>4</sub> C <sub>2</sub> RO (intronic)	106, 1152	Moens <i>et al.</i> (2018)
UAS-C <sub>4</sub> G <sub>2</sub> RO	107	Moens <i>et al.</i> (2018)
UAS-C <sub>4</sub> G <sub>2</sub> RO (intronic)	108	Moens <i>et al.</i> (2018)
<b>DPR only</b>		
<b>AP</b>		
UAS-AP	36, 100	Mizielinska <i>et al.</i> (2014)
	8, 64	Solomon <i>et al.</i> (2018)
UAS-FLAG-EGFP-AP	50	Wen <i>et al.</i> (2014)
UAS-FLAG-AP	25, 50	Boeynaems <i>et al.</i> (2016)
UAS-EGFP-AP	50	Freibaum <i>et al.</i> (2015)
	36	Xu and Xu (2018)
UAS-AP-EGFP	1024	West <i>et al.</i> (2020)
<b>PR</b>		
UAS-PR	36, 100	Mizielinska <i>et al.</i> (2014)
	8, 64	Solomon <i>et al.</i> (2018)
UAS-FLAG-EGFP-PR	50	Wen <i>et al.</i> (2014)
UAS-FLAG-PR	25, 50	Boeynaems <i>et al.</i> (2016)

	80	Yang <i>et al.</i> (2015)
UAS-EGFP-PR	50	Freibaum <i>et al.</i> (2015)
	36	Xu and Xu (2018)
UAS-PR-EGFP	1100	West <i>et al.</i> (2020)
<b>GR</b>		
UAS-GR	36, 100	Mizielinska <i>et al.</i> (2014)
	8, 64	Solomon <i>et al.</i> (2018)
UAS-FLAG-EGFP-GR	50	Wen <i>et al.</i> (2014)
UAS-FLAG-GR	25, 50	Boeynaems <i>et al.</i> (2016)
	80	Yang <i>et al.</i> (2015)
UAS-EGFP-GR	50	Freibaum <i>et al.</i> (2015)
	36	Xu and Xu (2018)
UAS-GR-EGFP	1136	West <i>et al.</i> (2020)
<b>GA</b>		
UAS-GA	36, 100	Mizielinska <i>et al.</i> (2014)
	8, 64	Solomon <i>et al.</i> (2018)
UAS-FLAG-EGFP-GA	50	Wen <i>et al.</i> (2014)
UAS-FLAG-GA	25, 50	Boeynaems <i>et al.</i> (2016)
	80	Yang <i>et al.</i> (2015)
UAS-EGFP-GA	50	Freibaum <i>et al.</i> (2015)
	36	Xu and Xu (2018)
UAS-GA-mCherry	36, 100, 200	Morón-Oset <i>et al.</i> (2019)
UAS-GA-EGFP	1020	West <i>et al.</i> (2020)
<b>GP</b>		
UAS-EGFP-GP	47	Freibaum <i>et al.</i> (2015)

#### 1.6.4. Modelling hypoxia

In addition to the previously discussed advantages of using *Drosophila* in neurodegeneration research, *Drosophila* models are well suited to studies of hypoxia, due to the fact that flies are relatively resistant to hypoxia. In fact, flies suffer little to no brain damage after 4 hours in anoxia (complete absence of oxygen) (Krishnan *et al.*, 1997). While this is a notable difference from mammals, this facilitates the study of hypoxia response processes with ease.

Like humans, flies live under mostly atmospheric conditions (21 % O<sub>2</sub>). However, the respiratory and circulatory systems of the fly differ morphologically from those of mammals. Flies take in air through spiracles, small orifices throughout their body, which are connected to the tracheal network. The tracheal network transports gases to and from tissues through epithelial-like tubes (trachea), and shares a number of cellular features with the mammalian circulatory system (Christos Samakovlis *et al.*, 1996). Soluble nutrients are transported via haemolymph ("blood") which fills the entire body cavity and is continuously pumped around by a heart.

Many of the signalling pathways involved in the response to hypoxia are well conserved, even in *Drosophila*. HIF1 $\alpha$  and  $\beta$  have homologues in *Drosophila*, namely similar (*sima*) and tango (*tgo*) (Lavista-Llanos *et al.*, 2002). Functionally, *sima* is regulated through the same molecular mechanisms of O<sub>2</sub>-dependent hydroxylation and degradation by homologues to human proteins (Wappner *et al.*, 2003; Irisarri *et al.*, 2009). Additionally, many of the transcriptional targets of *sima* are homologous to human HIF1-induced genes. However, in some cases their function may differ slightly, for example *Drosophila* Pvf1 (VEGF) does not promote vascularisation because flies do not possess vasculature.

While *Drosophila* do have some differences to humans that are important in the study of hypoxia and its effect on the CNS, their similarity at the molecular level makes them an excellent model to study changes at the cellular and molecular level. Given that hypoxia-induced neurotoxicity and impaired hypoxia signalling are the proposed mechanisms in the link between hypoxia and ALS, *Drosophila* make a suitable model for studying this association.

#### 1.7. Aims of research

The overall aim of this project is to identify and characterise mechanisms of DPR toxicity, with a particular focus on GR toxicity. From this we hope to provide disease mechanisms and processes as opportunities for targeting with therapeutics, in order to improve outcomes for *C9orf72* FTD/ALS patients.

Mechanisms of DPR toxicity have previously been described in shorter repeat DPR models, but evidence from patients and 1000-repeat models highlights that short repeat models may not bear sufficient physiological relevance to translate these findings into patients. Therefore, we will use the physiologically relevant 1000-repeat DPR *Drosophila* models in this research. Sequestration of proteins is arguably the most direct manner through which DPRs can disrupt biological processes. Therefore, we hypothesise that DPR-protein interactions mediate disruption of biological processes and thus DPR toxicity. Manipulating expression of DPR-interacting proteins may reveal modifiers of DPR toxicity, which we believe are likely to be mediators of DPR toxicity. By studying the effects of the DPR interaction on these mediating proteins, we may gain insight into the mechanisms underlying their mediation of DPR toxicity.

Importantly, previous research into mechanisms of toxicity in C9 FTD/ALS has identified a potential role of a number of proteins. However, for some proteins, such as Exportin 1 (XPO1), evidence has been particularly conflicting between models. Therefore, we hypothesise that by modelling DPRs of a length similar to those observed in patients, we can clarify the role of such proteins in DPR toxicity in patients.

The gene/environment/time hypothesis highlights that the combined effects of genetic susceptibility, environmental stress and aging contribute to disease. As such, DPR toxicity may be exacerbated by the interplay between environmental stress and mechanisms of DPR toxicity. We hypothesise that environmental risk factors of FTD/ALS, such as hypoxia, may be linked to underlying mechanisms of DPR toxicity.

The key aims of this research are to:

1. Identify GR1000-interacting proteins, such as XPO1, that act as modifiers of GR1000 toxicity *in vivo*
2. Characterise the effects of the GR1000-XPO1 interaction on XPO1 physiology
3. Investigate the effects of GR1000 expression on hypoxia signalling, a process downstream of XPO1
4. Elucidate the role of hypoxia and hypoxia signalling in GR1000 toxicity

## 2. Materials and Methods

### 2.1. *Drosophila* husbandry

*Drosophila* stocks were purchased from Bloomington *Drosophila* Stock Centre (Indiana University, Bloomington, USA). UAS-DPR stocks were generated previously by West *et al.* (2020). Additional stocks were kindly gifted by external *Drosophila* researchers. Details of *Drosophila* stocks, including source, can be found in Table 2.1.

Unless otherwise stated, *Drosophila* stocks were maintained on standard yeast-agar media at 25°C with constant humidity and a 12h:12h light:dark cycle. Fly food was prepared by the University of Sheffield Fly Facility (Sheffield, UK) according to a standard recipe (80 g/l cornmeal, 18 g/l dried yeast, 10 g/l soya flour, 80 g/l malt extract, 40 g/l molasses, 8 g/l agar, 0.25 % nipagin, 0.4 % propionic acid). Adult flies were transferred to fresh media every 10 days. Where necessary, media was supplemented with a yeast-water paste to increase egg laying.

To determine genotype, sex and virginhood of adult *Drosophila*, flies were anaesthetised on a porous pad emitting a constant stream of CO<sub>2</sub>. Males and virgin females were collected for establishing genetic crosses. At 25 °C newly eclosed females will remain virgins for approximately 8 hours. Virgin females were selected based on the presence of meconium, folded wings or having eclosed in the previous 8 hours. Unless otherwise stated, genetic crosses were maintained at the same conditions as stocks. Genetic crosses were transferred to fresh media every 3 to 4 days. At 25 °C the average generation time, from fertilised egg to eclosed adult, is 10 days. To prevent collection of flies with incorrect genotypes, F1 progeny were collected in a 9 day period immediately following the eclosion of the first fly.

**Table 2.1. *Drosophila* stocks used in this study.** Only primary sourced stocks are listed here. Stocks generated by combining multiple genetic elements or double balanced stocks are not listed for concision.

Stock	Chromosome	Source	Description
<b>Wildtype lines</b>			
CantonS	N/A	University of Manchester Fly Facility	Wildtype
OregonR	N/A	University of Manchester Fly Facility	Wildtype
<b>UAS-DPR lines</b>			
<i>UAS-GR1000-EGFP/TM6B, Tb<sup>1</sup>, Hu, e<sup>1</sup></i>	3 <sup>rd</sup>	Generated in West <i>et al.</i> (2020)	EGFP-tagged GR1000 under UAS promoter
<i>UAS-PR1000-EGFP/TM6B, Tb<sup>1</sup>, Hu, e<sup>1</sup></i>	3 <sup>rd</sup>	Generated in West <i>et al.</i> (2020)	EGFP-tagged PR1000 under UAS promoter
<i>UAS-AP1000-EGFP/TM6B, Tb<sup>1</sup>, Hu, e<sup>1</sup></i>	3 <sup>rd</sup>	Generated in West <i>et al.</i> (2020)	EGFP-tagged AP1000 under UAS promoter
<i>UAS-GA1000-EGFP/TM6B, Tb<sup>1</sup>, Hu, e<sup>1</sup></i>	3 <sup>rd</sup>	Generated in West <i>et al.</i> (2020)	EGFP-tagged GA1000 under UAS promoter
<i>UAS-mCD8-EGFP/TM6B, Tb<sup>1</sup>, Hu, e<sup>1</sup></i>	3 <sup>rd</sup>	RRID:BDSC_32184	Membrane-localised EGFP under UAS promoter

### Gal4 lines

<i>GMR-Gal4/CyO-GFP</i>	2 <sup>nd</sup>	Gift from Professor Sean Sweeney (University of York, UK)	Glass multimer reporter, eye-specific driver
<i>GMR-Gal4, UAS-mCD8-EGFP/CyO-GFP</i>	2 <sup>nd</sup>	Generated in this study	Eye-specific expression of membrane-localised EGFP
<i>GMR-Gal4/CyO-GFP; UAS-GR1000-EGFP/TM6B, Tb<sup>1</sup>, Hu, e<sup>1</sup></i>		Generated in this study	Eye-specific expression of GR1000-EGFP
<i>nSyb-Gal4/CyO-GFP</i>	2 <sup>nd</sup>	Gift from Dr. Chris Elliott (University of York, UK)	Neuronal Synaptobrevin, pan-neuronal driver
<i>nSyb-Gal4/CyO-GFP; UAS-mCD8-EGFP/TM6B, Tb<sup>1</sup>, Hu, e<sup>1</sup></i>	2 <sup>nd</sup> and 3 <sup>rd</sup>	Generated in this study	Pan-neuronal expression of membrane-localised EGFP
<i>nSyb-Gal4/CyO-GFP; UAS-GR1000-EGFP/TM6B, Tb<sup>1</sup>, Hu, e<sup>1</sup>, Gal80</i>	2 <sup>nd</sup> and 3 <sup>rd</sup>	Generated in this study	Pan-neuronal expression of GR1000-EGFP
<i>nSyb-Gal4/TM6B, Tb<sup>1</sup>, Hu, e<sup>1</sup></i>	3 <sup>rd</sup>	RRID:BDSC_51635	Neuronal Synaptobrevin, pan-neuronal driver
<i>OK6-Gal4/CyO-GFP</i>	2 <sup>nd</sup>	RRID:BDSC_64199	RapGAP1, larval salivary gland driver
<b>RNAi lines</b>			
<i>UAS-mCherry-RNAi</i>	3 <sup>rd</sup>	RRID:BDSC_35785	dsRNA for RNAi of mCherry under UAS control in the VALIUM20 vector, RNAi control
<i>UAS-c11.1-RNAi/CyO</i>	2 <sup>nd</sup>	RRID:BDSC_61204	dsRNA for RNAi of c11.1 (mROH1) under UAS control in the VALIUM20 vector

<i>UAS-GCS2α-RNAi</i>	3 <sup>rd</sup>	RRID:BDSC_34334	dsRNA for RNAi of GCS2α (GANAB) under UAS control in the VALIUM20 vector
<i>UAS-shi-RNAi</i>	3 <sup>rd</sup>	RRID:BDSC_28513	dsRNA for RNAi of Shi (DNM1) under UAS control in the VALIUM10 vector
<i>UAS-Nsf2-RNAi</i>	3 <sup>rd</sup>	RRID:BDSC_34914	dsRNA for RNAi of Nsf2 (NSF) under UAS control in the VALIUM20 vector
<i>UAS-Not1-RNAi</i>	3 <sup>rd</sup>	RRID:BDSC_28681	dsRNA for RNAi of Not1 (cNot1) under UAS control in the VALIUM10 vector
<i>UAS-emb-RNAi</i>	3 <sup>rd</sup>	RRID:BDSC_34021	dsRNA for RNAi of emb (XPO1) under UAS control in the VALIUM20 vector
<i>UAS-emb-RNAi</i>	3 <sup>rd</sup>	RRID:BDSC_31353	dsRNA for RNAi of emb (XPO1) under UAS control in the VALIUM10 vector
<i>UAS-sima-RNAi</i>	3 <sup>rd</sup>	RRID:BDSC_33894, gift from Professor Joseph Bateman (King's College London)	dsRNA for RNAi of sima (HIF1α) under UAS control in the VALIUM20 vector
<b>Other UAS lines</b>			
<i>UAS-sima</i>	2 <sup>nd</sup>	RRID:BDSC_9582, gift from Professor Joseph Bateman	Wildtype sima (HIF1α) under UAS promoter
<i>UAS-Vc-emb</i>	3 <sup>rd</sup>	Gift from Dr. Samir Merabet (Institut de Génomique Fonctionnelle de Lyon)	Venus(C-terminus)-tagged emb (XPO1) under UAS promoter

<i>UAS-CNOT1<sup>WT</sup></i>	3 <sup>rd</sup>	Gift from Professor Rold Bodmer (Sanford Burnham Prebys Medical Discovery Institute)	Wildtype human Not1 (CNOT1) under UAS promoter
<b>Balancer lines</b>			
<i>If/CyO-GFP</i>	2 <sup>nd</sup>	University of York	
<i>TM3, Sb, e1/TM6B, Tb<sup>1</sup>, Hu, e<sup>1</sup></i>	3 <sup>rd</sup>	University of York	
<i>If/CyO-GFP; MKRS/TM6B, Tb<sup>1</sup>, Hu, e<sup>1</sup></i>	2 <sup>nd</sup> and 3 <sup>rd</sup>	University of York	
<b>Other lines</b>			
<i>wg[Sp-1]/CyO; RFP-Nup107</i>	2 <sup>nd</sup> and 3 <sup>rd</sup>	RRID:BDSC_35517	RFP-tagged Nup107 under control of Nup107 regulatory sequences
<i>OK6-Gal4/CyO; RFP-Nup107/TM6B, Tb<sup>1</sup>, Hu, e<sup>1</sup></i>	2 <sup>nd</sup> and 3 <sup>rd</sup>	Generated in this study	RFP-tagged Nup107 and RapGAP1, larval salivary gland driver

## 2.2. Generation of transgenic flies

*UAS-DPR1000-EGFP* lines were established by West *et al.* (2020) prior to this study. In brief, short units of semi-randomised alternative codons were generated, consisting of 22 or 36 repeats of six bases/two amino acids. Using semi-randomised alternative codons permits DPR expression in the absence of G<sub>4</sub>C<sub>2</sub> RNA, while also reducing the repetitive nature of the DNA to enhance construct stability. Units were repeatedly cloned into the pEGFP-N1 vector in tandem, to form a final construct containing a minimum of 1000 repeats (Callister *et al.*, 2016). This generated four C-terminal EGFP-tagged 1000-repeat DPR constructs: AP-1024, PR-1100, GR-1136, and GA-1020. Cloning of GP was unsuccessful, as has been documented previously by other groups. Constructs were subcloned from the pEGFP-N1 vector into the pUAS<sub>attB</sub> vector to create *UAS-DPR1000-EGFP* constructs suitable for expression in *Drosophila*. pUAS<sub>attB</sub>-DPR1000-EGFP constructs were individually microinjected into *Drosophila* embryos, facilitating PhiC31-mediated insertion of each construct into the same genomic site. Positive transformants were screened for presence and full repeat length of the DPRs.

For simplicity, *UAS-DPR1000-EGFP* constructs will be referred to as DPR1000 (e.g. *UAS-GR1000-EGFP* as GR1000) throughout. As a control for the EGFP tag and UAS-driven expression of protein, *UAS-mCD8-EGFP* has been used as a control for the DPR1000 constructs and will be referred to as GFP.

## 2.3. Genetic interaction eye screens

Eye screen crosses were maintained at 29 °C to increase activity of the UAS/Gal4 system and therefore DPR expression and phenotype severity. Expression of all constructs was driven in the eye using *GMR-Gal4*. Flies were collected no later than 3 days post eclosion (dpe) and eyes were examined using a Stemi 305 light microscope (Zeiss, Germany). Eye phenotypes were scored using a 9-point scoring system used by West *et al.* (2020) adapted from Pandey *et al.* (2007); Ritson *et al.* (2010); and He *et al.* (2014). In short, flies are awarded 1 point for each of the following phenotypes: size alteration, pigmentation defect, gross morphological disruptions, ommatidial disorganisation, ommatidial fusion, abnormal interommatidial bristle orientation, abnormal interommatidial bristle number, melanised patches (Fig 2.1). 9 points are awarded for embryonic or pharate lethality. Images were captured using an Axiocam 208 colour camera (Zeiss) and Zen 3.7 capture software (Zeiss). A minimum of 120 flies, combined from 3 separate crosses, were scored per genotype.

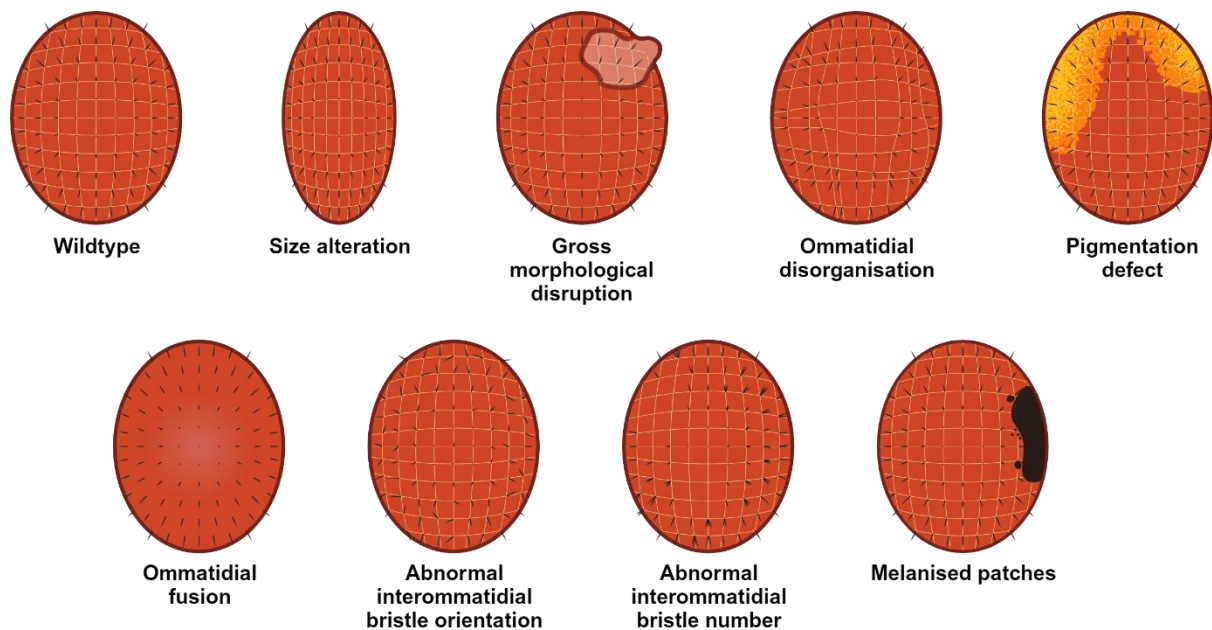


**Figure 2.1. Cartoon representations of wildtype *Drosophila* and scored eye phenotypes used in eye screen scoring system.** Yellow lines represent the ommatidial array, black lines represent interommatidial bristles.

## 2.4. Behavioural assays

### 2.4.1. Startle-induced negative geotaxis (SING) assay

All SING assays were performed at 20 °C and within the same 30 minute window every day to eliminate circadian effects. Male flies were transferred, without anaesthetisation, into glass boiling tubes in a custom climbing apparatus with a white, backlit background. After a 1 minute acclimatisation period, the assay apparatus was banged down on the bench 4 times to elicit the SING response in the flies. Banging of the climbing apparatus was performed in a manner consistent between experiments (Fig. 2.2). Video capture, using a C920 Pro HD webcam (Logitech) and VirtualDub capture software, was started immediately after banging and continued for 60 seconds. Each climbing assay was performed 3 times in brief succession in case of technical problems with video capture, and the first video was used where possible. A minimum of 20 flies per condition, combined from 3 independent crosses, were assayed.

Climbing video analysis was performed in ImageJ. Furthest distance reached in 10 seconds was measured manually.

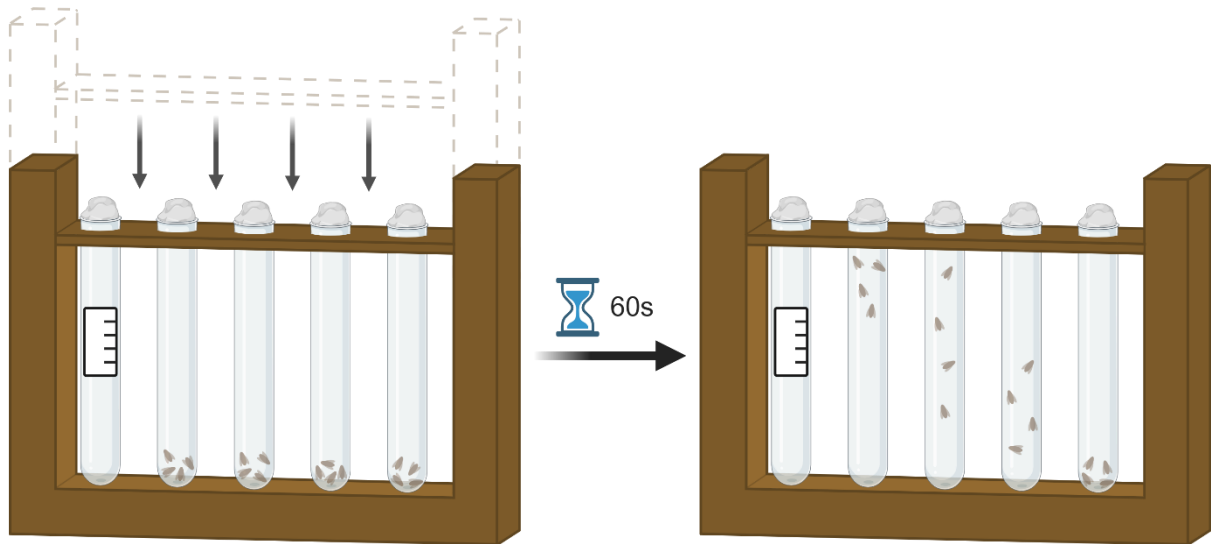


**Figure 2.2. Startle induced negative geotaxis assay.** Schematic of assay apparatus. Flies from different conditions are assayed in separate boiling tubes in a tube rack. The rack and tubes are banged down to knock flies to the bottom and induce the SING response, which is filmed using a webcam.

#### 2.4.2. Locomotor activity monitoring assay

Activity assays were performed at 25 °C on a 12h:12h light:dark cycle. Male flies were CO<sub>2</sub> anaesthetised before being individually transferred into activity monitor tubes containing 5 % sucrose, 2 % agar food at one end (Fig. 2.3). Tubes were sealed with cotton bungs and loaded into DAM5H activity monitors (Trikinetics, USA). Flies were allowed a minimum of 8 hours to recover from anaesthesia before data collection. Activity was monitored midnight-midnight on the day of monitoring.

Data was collected using DAMSystem3 software (Trikinetics) and processed using DAMFileScan113 software (Trikinetics). Acquisition settings: Reading interval = 1 min, Acquire = All, Save = Total, Beam.

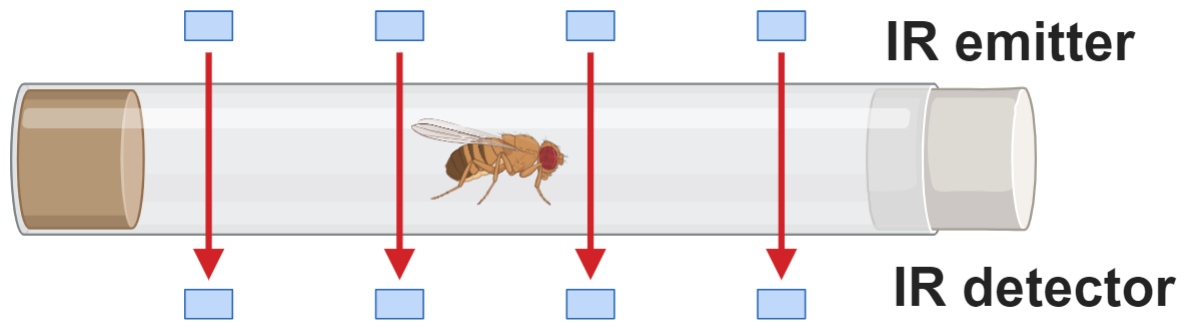


**Figure 2.3. Locomotor activity monitoring assay.** Schematic of fly in an activity monitor tube with infrared (IR) beams passing through the tube. When a fly breaks a beam, it is recorded by the DAMSystem3 activity monitoring software.

### 2.4.3. Sleep analysis

Sleep analysis was performed using Rtivity v1.2 (Silva *et al.*, 2022). Data from locomotor activity assays was used for analysis. Sleep was measured from 8 am on the day of activity monitoring to 8 am the following day. For analysis, sleep was defined as a period of inactivity lasting at least 5 min.

## 2.5. Hypoxia

### 2.5.1. Hypoxic exposure

Hypoxic exposure was performed using an H35 HEPA Hypoxystation (Don Whitley Scientific, UK). Conditions in hypoxic environments were consistently maintained at 30 °C, 65 % humidity, 0 % CO<sub>2</sub>. Oxygen levels were maintained as stated per experiment. Normoxic control conditions were matched entirely to hypoxic conditions with the exception of being maintained at 21 % O<sub>2</sub>.

### 2.5.2. Hypoxic stupor assay

Flies were transferred, without anaesthesia, to 90 mm cages (Flystuff) with no food at 20 °C under normoxia. Cages were placed mesh-side down, with a gap to allow gas exchange, and left for 15 minutes to allow flies to acclimatise and collect at the top of the cage (Fig. 2.3). Petri dish lids were placed over the mesh, preventing gas exchange, before the cages were moved into a 1 % O<sub>2</sub> environment. Once all cages were positioned in hypoxia, petri dish lids were removed, and cages were balanced between lids to allow gas exchange. Flies were filmed for 6 minutes using a phone camera. Videos were analysed using VLC. Flies

were recorded as fallen when they reached the bottom of the cage without subsequently ascending.

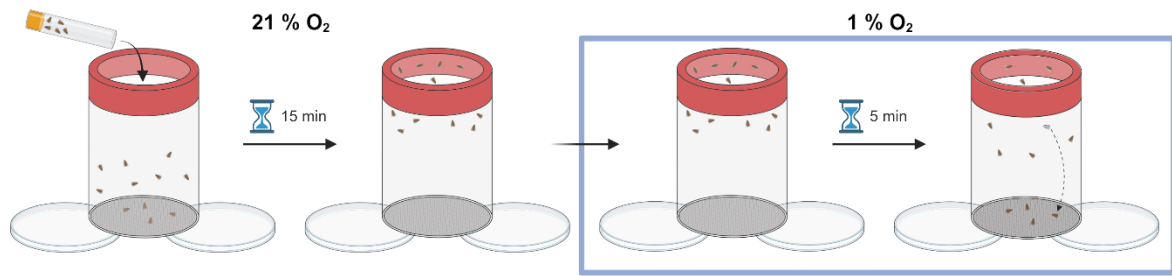


**Figure 2.4 Hypoxic stupor assay.** Schematic of hypoxic stupor assay apparatus and protocol. Left to right: flies are transferred in to cages and left for 15 minutes to collect at the top of the cage, cages are transferred into a 1 % O<sub>2</sub> environment and filmed for 5 minutes as they enter a hypoxic stupor and fall to the bottom of the cage. Cages are balanced between petri dish lids at all times to allow gas exchange through the mesh bottom, except when transferring into hypoxia when the mesh is covered with a lid (not shown) to allow control over the initiation of hypoxic conditions.

### 2.5.3. Intermittent hypoxic exposure

Flies were kept in tubes with standard food. Tubes were transferred from standard 25 °C conditions to a 1 % O<sub>2</sub> (hypoxic) environment. After 5 minutes, tubes were removed from the hypoxic environment to ambient normoxic conditions. After 10 minutes, tubes were transferred back into the hypoxic environment. This 15 minute cycle of 5 minutes in hypoxic and 10 minutes in ambient normoxic conditions was repeated 10 times before transferring tubes back to standard 25 °C conditions.

### 2.5.4. Continuous hypoxic exposure

Flies were kept in tubes with standard food. Tubes were transferred from standard 25 °C conditions to a 5 % O<sub>2</sub> (hypoxic) environment. After 24 hour incubation in hypoxic conditions, tubes were either immediately transferred back to standard 25 °C conditions or flies were processed for biochemical experiments.

## **2.6. Immunohistochemistry (IHC)**

### **2.6.1. Salivary gland dissection**

3<sup>rd</sup> instar larvae were collected and placed in cold PBS (137 mM NaCl, 2.7 mM KCl, 10mM Na<sub>2</sub>HPO<sub>4</sub>, 1.8 mM KH<sub>2</sub>PO<sub>4</sub>) on a sylgard-coated (Silicone elastomere kit, DowCorning, USA) plate and dissected using dissecting forceps (DUMONT, 0208-5SPSF-PO), under a Stemi 305 light microscope . Larval salivary glands were fixed in 3.7 % formaldehyde (FA) in PBS for 7 minutes before washing in PBS. Fixed salivary glands were either processed further by antigen retrieval and antibody staining or immediately mounted on microscope slides in VECTASHIELD Antifade mounting medium (Vector Laboratories, H-1000-10) under coverslips.

Antigen retrieval was performed by immersing fixed salivary glands in sodium citrate buffer (10 mM Trisodium citrate, 0.05 % Tween 20, pH 6.0) in a 1.5 ml tube and boiling at 98 °C for 20 minutes and cooling at room temperature for 20 minutes. This was repeated 3 times in total before removing sodium citrate buffer and washing 3 times in 0.5 % PBS-T (Triton X-100), before moving on to antibody staining.

In a 1.5 ml tube, salivary glands were immersed in primary antibody (Table 2.3) in 0.5 % PBS-T at 4 °C and rotating overnight. Primary antibody was removed, and salivary glands rinsed 3 times in 0.5 % PBS-T before immersing in TwoPro3 (AAT Bioquest, 17572, 1:50,000 in 0.5 % PBS-T) at room temperature and rotating for 15 minutes. TwoPro3 solution was removed, and salivary glands rinsed 3 times in 0.5 % PBS-T before immersing in secondary antibody (Table 2.3) in 0.5 % PBS-T at room temperature and rotating for 1 hour. Secondary antibody was removed, and salivary glands were rinsed 3 times before mounting on microscope slides as described above.

Mounted salivary glands were imaged with a 10x objective, in 1 µm slices, using an EVOS M5000 fluorescence microscope (ThermoFisher). Microscope settings were kept constant between samples and conditions.

Z-projection images were generated from maximum intensity of slice images. Quantification was performed in ImageJ. In brief, fluorescence of the nuclear dye TwoPro3 was used to identify nuclei and manually create nuclear regions of interest (ROI). Nuclei in the fat body were excluded from analysis and nuclear ROI were then used to measure nuclear fluorescence in the target channel (Fig. 2.5). Nuclear/Cytoplasmic fluorescence was calculated from corrected total nuclear fluorescence (CTNF) and corrected total cytoplasmic fluorescence (CTCF):

$CTNF = \text{Integrated density}_{(nuclear)} - (\text{Measured area}_{(nuclear)} \times \text{Mean background fluorescence})$

$\text{Integrated density}_{(cytoplasmic)} = \text{Integrated density}_{(salivary gland)} - \text{Integrated density}_{(nuclear)}$

$\text{Measured area}_{(cytoplasmic)} = \text{Measured area}_{(salivary gland)} - \text{Measured area}_{(nuclear)}$

$CTCF = \text{Integrated density}_{(cytoplasmic)} - (\text{Measured area}_{(cytoplasmic)} \times \text{Mean background fluorescence})$

$\text{Nuclear/Cytoplasmic fluorescence} = CTNF/CTCF$

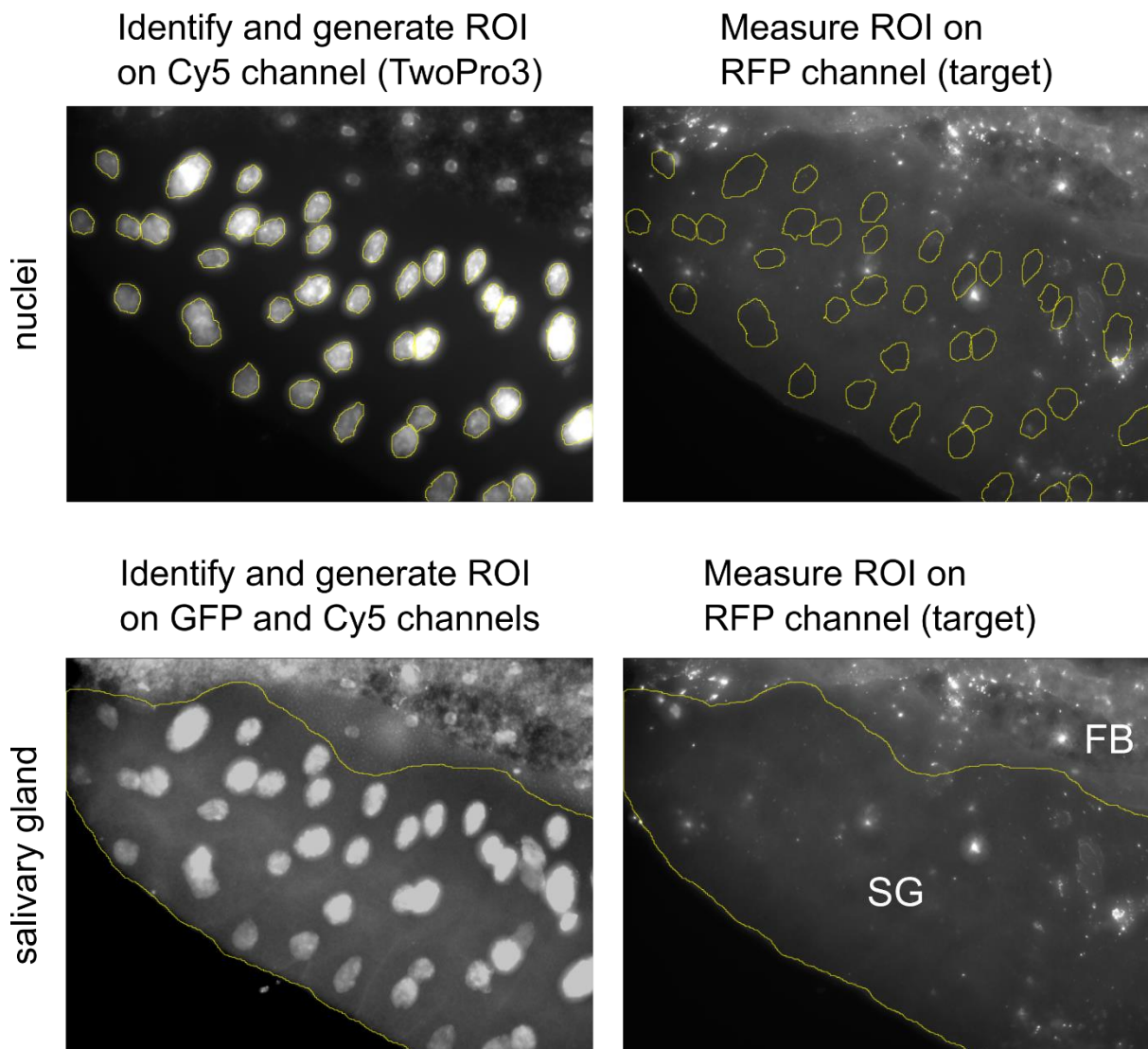


**Figure 2.5 Nuclear/Cytoplasmic fluorescence analysis.** Images were analysed in ImageJ to measure nuclear and cytoplasmic RFP (target) fluorescence intensity in salivary gland cells. Nuclear ROI were generated based on the nuclear fluorescence of TwoPro3 and subsequently measured in the RFP channel. A whole salivary gland (SG) ROI, excluding the fat body (FB), was generated from the GFP (mCD8-EGFP or GR1000-EGFP) and TwoPro3 fluorescence and measured in the RFP channel. Obtained measurements were used to calculate Nuclear/Cytoplasmic fluorescence.

### **2.6.2. Adult brain dissections**

Flies were anaesthetised and dissected individually in cold PBS on a sylgard-coated plate using dissection forceps. Flies from all experiments were CO<sub>2</sub> anaesthetised before dissection, except flies from experiments involving hypoxic exposure which were cold anaesthetised instead to avoid CO<sub>2</sub>-induced hypoxia. Dissected brains were fixed in 3.7 % FA in PBS at room temperature for 1 hour. Fixed brains were kept in PBS at 4 °C for further processing.

### **2.6.3. TUNEL Assay**

Terminal deoxynucleotidyl transferase-dUTP nick end labelling (TUNEL) assay was performed using Click-iT™ Plus TUNEL Alexa Fluor™ 594 Assay kit (Invitrogen, C10618) and adapted from manufacturer's protocol. In brief, fixed fly brains were permeabilised in Proteinase K solution at 37 °C for 15 minutes. permeabilised brains were washed in 0.5 % PBS-T, followed by PBS and then dH<sub>2</sub>O. Brains were incubated in 50 µl TdT Reaction Buffer at 37 °C for 10 minutes. TdT reaction buffer was removed and 50 µl TdT reaction mixture (TdT reaction buffer, EdUTP nucleotide mixture and TdT enzyme) was added before incubating at 37 °C for 60 minutes. TdT reaction mixture was removed, and brains were washed in dH<sub>2</sub>O followed by 3 % BSA in PBS, then 0.1 % PBS-T (Tween 20) then PBS. Brains were incubated in 50 µl Click-iT™ Plus TUNEL reaction cocktail (Click-iT™ Plus TUNEL reaction buffer, copper protectant, Alexa Fluor™ 594 picolyl azide and Click-iT™ Plus TUNEL reaction buffer additive) at 37 °C for 30 minutes in darkness. Reaction cocktail was removed, and brains were washed in 3 % BSA in PBS for 5 minutes then PBS. After washing, brains were mounted as described above.

Brains were imaged with a 20x objective, in 0.5 µm slices, using an EVOS M5000 fluorescence microscope (ThermoFisher). Microscope settings were kept constant between samples and conditions.

Quantification was performed in ImageJ. Z-projection images were generated from maximum intensity of slice images. TUNEL signal was quantified as corrected total brain fluorescence (CTBF) from Z-projection images.

CTBF = Integrated density – (Measured area of brain x Mean background fluorescence)

## 2.6.4. Imaging apparatus

**Table 2.2. Filter cubes used in this study.**

Filter cube	Excitation; Emission	Dyes used in this study
DAPI	357/44nm; 447/60nm	DAPI
GFP	482/25nm; 524/24nm	EGFP
RFP	531/40nm; 593/40nm	Cy3
Texas Red	585/29nm; 628/32nm	Alexa Fluor™ 594
Cy5	628/40nm; 692/40nm	Cy5, Alexa Fluor™ 647, TwoPro3

## 2.7. Biochemistry

### 2.7.1. Protein extraction

A minimum of 500 flies (for co-immunoprecipitation) or 20 flies (for Western blotting) per genotype were collected and flash frozen in 15 ml centrifuge tubes on dry ice, before vortexing for 30s to remove heads from flies. Heads were isolated by passing the vortexed flies sequentially through pre-chilled 710 and 425 µm sieves. Heads were transferred to 1.5 ml tubes on dry ice before being homogenised thoroughly using pre-chilled pestles. Tubes were placed on ice and 2 µl of RIPA lysis buffer (10 mM Tris-Cl pH 8.0, 1 mM EDTA, 0.5 mM EGTA, 1 % Triton X-100, 0.1 % sodium deoxycholate, 0.1 % SDS, 140 mM NaCl) were added per head. Samples were vortexed to suspend homogenate in RIPA and incubated on ice for 30 minutes, vortexing periodically. Debris was pelleted by centrifuging for 15 minutes at 14,000 rpm at 4 °C, and supernatant was transferred to a fresh 1.5 ml tube.

### **2.7.2. Protein quantification**

Resulting protein concentration was quantified using the Pierce BCA Protein assay kit (Thermo Scientific, 23225). In a 96-well plate, an 8 point, 2-fold standard curve of bovine serum albumin (BSA) was produced by serial dilution in RIPA. Protein samples were loaded as 1:10 and 1:20 dilutions in RIPA. 200 µl of BCA reagent was added to each well before incubating at 37 °C for 60 minutes. Absorbance at 562 nm was measured using a Pherastar platereader (BMG Labtech, Germany). Measurements were used to determine sample protein concentration.

### **2.7.3. Western blotting**

Protein samples were diluted in RIPA buffer and 5x Laemmli (300mM Tris-Cl pH 6.8, 50 % Glycerol, 10 % SDS, 0.05 % bromophenol blue) buffer to a final concentration of 2 µg/µl protein and 1x Laemmli. Diluted protein samples were boiled at 95 °C for 10 minutes before storing at -80 °C for later use.

SDS-PAGE gels were hand-cast at 1 mm thickness as 12 % resolving (12 % acrylamide/bis, 375 mM Tris-Cl pH 8.8, 0.001 % SDS, 0.0005 % TEMED, 0.0005 % APS) and 4 % stacking (4 % acrylamide/bis, 126 mM Tris-Cl pH 6.8, 0.001 % SDS, 0.001 % TEMED, 0.0005 % APS) gels and a 10-well comb. Individual wells were loaded with 10 µl PageRuler™ Plus Prestained Protein Ladder (Thermo Scientific, 26619) or 20 µl (40 µg) prepared protein sample. Gels were run using a Mini-PROTEAN Tetra Vertical Electrophoresis Cell (Bio-Rad) with running buffer (25 mM Tris, 192 mM glycine, 0.1 % SDS) at 80 V through the stacking gel and 200 V through the resolving gel for approximately 1 hour, until the loading front reached the very bottom of the gel.

Proteins in the gel matrix were blotted onto Immobilon-FL PVDF membrane (Millipore, IPFL00010), pre-activated in methanol for 60 seconds, by running in transfer buffer (25 mM Tris, 192 mM glycine, 20 % methanol) at 100 V for 1 hour using a Mini-PROTEAN Trans-Blot module (Bio-Rad, USA). Blotted membranes were air-dried briefly before blocking in 5 % milk in TBS-T (20 mM Tris, 150 mM NaCl, 0.1 % Tween 20, pH 7.6), rolling for 1 hour at room temperature. Blocked membranes were rinsed 3 times in TBS-T, rolling for 5 minutes at room temperature before incubating in primary antibody (Table 2.3) in TBS-T, rolling overnight at 4 °C. Membranes were subsequently rinsed 3 times in TBS-T, rolling for 5 minutes at room temperature before incubating in secondary antibody (Table 2.3) in TBS-T, rolling for 1 hour at room temperature. Membranes were then rinsed 3 times in TBS-T, rolling

for 5 minutes before imaging using an Odyssey XF Imager (LI-COR, USA). Membranes were stained and imaged sequentially for individual target proteins.

Images were analysed in ImageJ using the Analyse Gel function. Target band intensity was normalised to at least one of the following loading controls, depending on the experiment:  $\alpha$ -tubulin,  $\beta$ -actin, histone H3 or LaminC.

#### **2.7.4. Co-immunoprecipitation and sample preparation for tandem mass spectrometry**

Co-immunoprecipitation (co-IP) for tandem mass spectrometry (MS/MS) was performed on protein lysates, generated as described above, using the ChromoTek iST GFP-Trap Kit for AP-MS sample preparation of GFP-fusion proteins (Chromotek, gtak-iST) following the manufacturer's instructions, with some modification. Briefly, beads were mixed thoroughly by pipetting and 25  $\mu$ l of beads added to a clean 1.5 ml tube. Beads were washed with 500  $\mu$ l RIPA, centrifuged at 2,500 rcf for 2 min at 4 °C and the supernatant discarded. Beads were washed again with 500  $\mu$ l PBS, centrifuged at 2,500 rcf for 2 min at 4 °C and the supernatant discarded. Protein lysates were diluted to 1 mg/ml and 50  $\mu$ l removed and stored as 'input'. 1 ml of 1 mg/ml protein sample was added to the beads and left rotating at 4 °C overnight. The following day samples were centrifuged at 2,500 rcf for 2 min at 4 °C and the supernatant removed and stored as 'flow-through'. Beads were washed with 500  $\mu$ l RIPA, centrifuged at 2,500 rcf for 2 min at 4°C and the supernatant removed and stored as 'wash'. Following the co-immunoprecipitation steps an "on-bead" digestion was performed following manufacturer's instructions for the the ChromoTek iST GFP-Trap Kit. Briefly 50  $\mu$ L of the ChromoTek iST GFP-Trap Kit "LYSE" reagent was added to the washed beads samples placed in a pre-heated heating block (60 °C; 1,000 rpm; 10 min) to denature, reduce and alkylate proteins. The ChromoTek iST GFP-Trap Kit "DIGEST" Trypsin-mix reagent was prepared as described in the manufacturer's instructions, 50  $\mu$ L added to the beads and incubated at 37 °C with 500 rpm mixing for 2 hours. 100  $\mu$ L of "STOP" reagent was added to the bead-digestion and samples mixed at room temperature (500 rpm) for 1 min. Beads were centrifuged (2,500 rcf, 2 min, room temperature) and the supernatant added to the ChromoTek iST GFP-Trap Kit purification cartridge, which was centrifuged at 3,800 rcf for 3 min at room temperature. The cartridge was washed twice using the kit's wash buffers, as described in the manufacturer's instructions. The cartridge was placed in a new collection tube and the peptides eluted from the cartridge using the kit "ELUTE" buffer. The sample in the collection tube was then placed in a speed vac at 45 °C until completely dry before resuspending at a concentration of 1 g/L using the kits "LC-LOAD" buffer (room temperature,

500 rpm, 5 min). Following sample quality control samples were analysed through GeLC-MS/MS using an Orbitrap Elite (ThermoFisher Scientific) mass spectrometer.

#### **2.7.5. Protein identification**

Charge state deconvolution and deisotoping were not performed. All MS/MS samples were analysed using Mascot (Matrix Science, London, UK; version 2.5.1). Mascot was set up to search the SwissProt\_2018\_01 database (selected for *Drosophila*, 293679 entries) assuming the digestion enzyme trypsin. Mascot was searched with a fragment ion mass tolerance of 0.015 Da and a parent ion tolerance of 8.0 PPM. Carbamidomethyl of cysteine was specified in Mascot as a fixed modification. Oxidation of methionine was specified in Mascot as a variable modification.

Scaffold (version Scaffold\_5.2.0, Proteome Software Inc., Portland, OR) was used to validate MS/MS based peptide and protein identifications. Peptide identifications were accepted if they could be established at greater than 50.0% probability by the Peptide Prophet algorithm (Keller *et al.*, 2002) with Scaffold delta-mass correction. Protein identifications were accepted if they could be established at greater than 95.0% probability and contained at least 2 identified peptides. Protein probabilities were assigned by the Protein Prophet algorithm (Nesvizhskii *et al.*, 2003). Proteins that contained similar peptides and could not be differentiated based on MS/MS analysis alone were grouped to satisfy the principles of parsimony. Proteins were classed as present in a condition if they were identified in at least one of the biological replicates of that condition.

Statistical testing was performed in Scaffold. Fisher's exact t-test with Benjamini-Hochberg correction was performed to identify proteins present at significantly different ( $p < 0.05$ ) levels between conditions.

#### **2.7.6. Protein Ontology**

For DPR-interacting proteins identified in *Drosophila* species other than *Drosophila melanogaster*, *D. melanogaster* orthologs were identified using OrthoDB v11 (Kuznetsov *et al.*, 2023). Protein ontology of DPR-interacting *D. melanogaster* proteins was performed using ShinyGO v0.80 (Ge *et al.*, 2020). The following settings were used for analysis: FDR cutoff = 0.05; minimum pathway size = 2; maximum = 2000; remove redundancy ON; background = all protein coding genes; select by FDR, sort by Fold Enrichment.

### **2.7.7. Trizol extraction of RNA**

RNA was collected using TRIzol reagent (Invitrogen, 15596026) and a protocol adapted from the manufacturer's. Briefly, 20-40 flies per condition were flash frozen on dry ice. Frozen flies were vortexed for 30 seconds to remove their heads. Heads were separated from bodies, wings and legs using 710 and 425  $\mu\text{m}$  sieves and collected in 1.5 ml tubes. Heads were mechanically homogenised using a pestle. 200  $\mu\text{l}$  TRI Reagent was added and the mixture was vortexed before incubation at room temperature for 5 minutes. 40  $\mu\text{l}$  chloroform was added and the mixture shaken vigorously for 15 seconds before incubation at room temperature for 5 minutes. The mixture was separated into phases by centrifuging for 15 minutes at 12,000 xg at 4 °C. 100  $\mu\text{l}$  of aqueous phase was transferred to a new 1.5 ml tube without disturbing the lower phases. 50  $\mu\text{l}$  of TRI Reagent was added and mixed by shaking. 30  $\mu\text{l}$  chloroform was added and shaken vigorously for 15 seconds before incubating for 5 minutes at room temperature. The mixture was separated into phases by centrifuging for 5 minutes at 12,000 xg at 4 °C. 100  $\mu\text{l}$  of aqueous phase was transferred to a new 1.5 ml tube and 100  $\mu\text{l}$  of chloroform was added before shaking to mix. The mixture was allowed to separate out for 30 seconds before 80  $\mu\text{l}$  of aqueous phase was transferred to a new tube. RNA was precipitated from the aqueous phase by adding 240  $\mu\text{l}$  cold ethanol and incubating at -20 °C overnight. Precipitated RNA was pelleted by centrifuging for 30 minutes at 14,000 rpm at 4 °C. The supernatant was removed, and the pellet washed by pipetting and vortexing in 70 % ethanol (in DEPC-treated dH<sub>2</sub>O). Washed RNA was pelleted by centrifuging at for 10 minutes at 14,000 rpm at 4 °C. Supernatant was removed without disturbing the RNA pellet, before air drying for 15 minutes. RNA pellets were resuspended in 20  $\mu\text{l}$  RNase-free dH<sub>2</sub>O pre-warmed to 55 °C. RNA was immediately analysed using an NP60/50 NanoPhotometer® (Implen GmbH, Germany). Only samples of at least 100 ng/ $\mu\text{l}$ , A260/280 > 1.9 and A260/230 > 1.5 were used for RT-qPCR. RNA was stored at -80 °C for further use.

### **2.7.8. DNase treatment and reverse transcription**

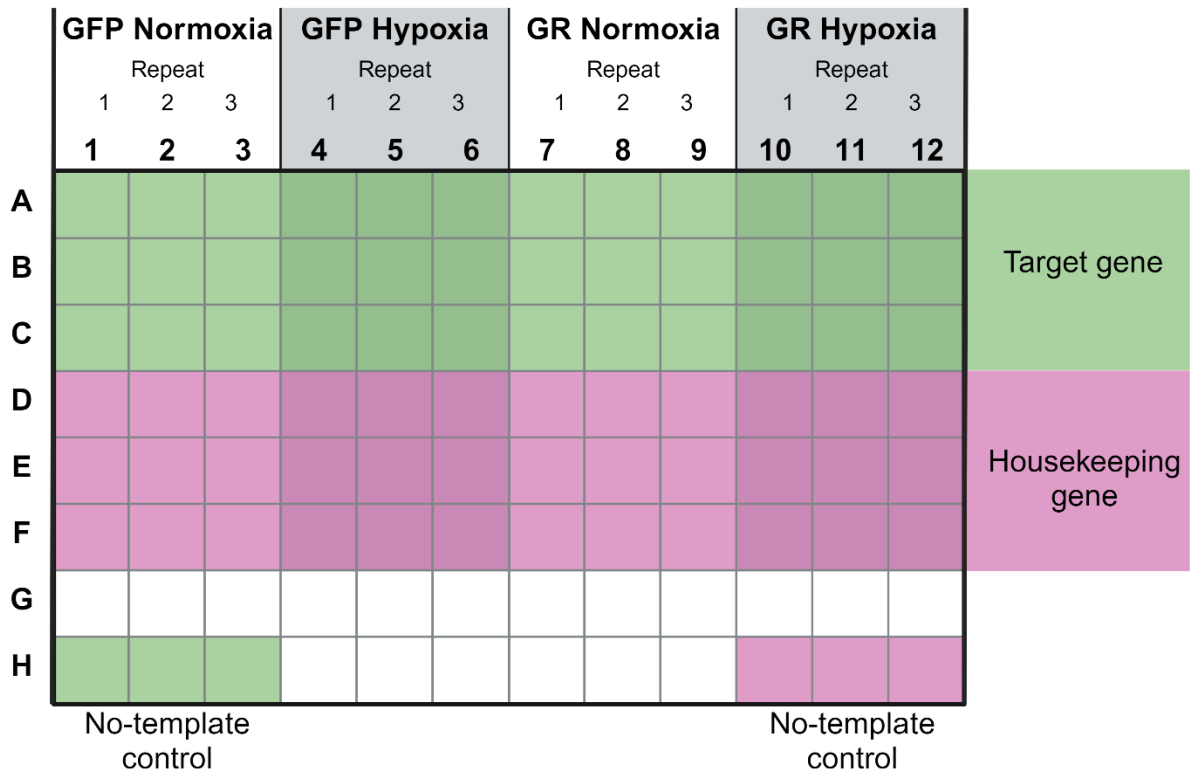
RNA was DNase treated to remove any genomic DNA contamination. DNase treatment was performed using DNase I recombinant, RNase-free (Roche, 4716728001). 2  $\mu\text{g}$  RNA was added to a tube with 2.5 U DNase I, 5  $\mu\text{l}$  10x incubation buffer and dH<sub>2</sub>O in 50  $\mu\text{l}$  total reaction volume. Reactions were incubated at 37 °C for 20 minutes, then 75 °C for 10 minutes to deactivate DNase. DNase-treated RNA was subsequently used for reverse transcription with M-MLV reverse transcriptase (Invitrogen, 28025013). Briefly, 50  $\mu\text{l}$  DNase treatment reaction was added to a tube with 4  $\mu\text{l}$  50  $\mu\text{M}$  random hexamers (Invitrogen, N8080127) and 5  $\mu\text{l}$  10 mM dNTPs (Meridian Bioscience, BIO39044) and incubated at 65 °C

for 5 minutes. Following incubation, tubes were immediately chilled on ice and 20 µl 5x First-Strand buffer, 10 µl 100 mM DTT and 6 µl DEPC-treated dH<sub>2</sub>O were added before incubating at 37 °C for 2 minutes. 5 µl M-MLV RT was added to tubes and cDNA synthesis performed in a thermocycler running at 25 °C for 10 minutes, then 37 °C for 50 minutes and 70 °C for 15 minutes. cDNA was stored at -20 °C for later use.

### **2.7.9. RT-qPCR**

Reactions consisting of 1 µl 1/4 cDNA dilution, 1 µl diluted primer mix, 3 µl DEPC-treated dH<sub>2</sub>O and 5 µl Brilliant II SYBR® Green qPCR Master Mix (Agilent, 600828) were set up in individual wells of a 96-well qPCR plates (Bio-Rad, MLL9651) with optical lids (Bio-Rad, TCS0803). Plates were set up with 3 independent replicates per condition (GFP normoxia, GFP hypoxia, GR normoxia, GR hypoxia), with triplicates for each reaction for both target and housekeeping gene (Fig. 2.6). Two plates per age were run, for a total of 6 independent replicates per condition and age. Triplicate reactions of no-template control, in which cDNA was replaced with DEPC-treated dH<sub>2</sub>O, were also included for target and housekeeping gene.

Plates were run in a C1000 Touch™ thermal cycler (CFX96™ Real-Time System, Bio-Rad). Plates for all target genes, except Pvf1, were run on protocol 1. Protocol 2 was used for Pvf1 plates, since primers for Pvf1 had been previously optimised on protocol 2. Protocols 1 and 2 are outlined in Figure 2.6.



#### Protocol 1

95 °C for 10 minutes  
 95 °C for 30 seconds  
 60 °C for 30 seconds  
 Plate read  
 72 °C for 1 minute  
 95 °C for 1 minutes  
 60 °C for 31 seconds  
 60 °C for 5 seconds  
 (+0.5 °C per cycle)  
 Plate read

45x

70x

#### Protocol 2

95 °C for 3 minutes  
 95 °C for 5 seconds  
 60 °C for 10 seconds  
 Plate read  
 72 °C for 30 minute  
 95 °C for 1 minutes  
 60 °C for 31 seconds  
 60 °C for 5 seconds  
 (+0.5 °C per cycle)  
 Plate read

45x

70x

**Figure 2.6 RT-qPCR experimental conditions.** Schematic of plate layout for RT-qPCR experiments: three technical replicates are run per condition per plate, and all reactions are run in triplicate. Plates for all targets were run using protocol 1, except Pvf1 which was run using protocol 2.

### 2.7.10 RT-qPCR primers

RT-qPCR primers were purchased from Sigma in solution (H<sub>2</sub>O) and desalted, at a concentration of 100 µM and synthesis scale of 25 nmol.

**Table 2.4. RT-qPCR primers used in this study.** Primers were initially selected based upon published use or computational design by Fly Primer Bank. All primers were optimised and validated for use in this study.

Target Gene	Primer Sequences (5'-3')	Dilution factor	Source
Sima	F: AGCCCAATCTGCCGCCAACC R: TCGGACACCTTCGAGCTCCAGAA	1/20	Bandarra <i>et al.</i> , 2014
dLdh	F: CAGTTCGCAACGAACGCGCA R: CAGCTCGCCCTGCAGCTTGT	1/10	Bandarra <i>et al.</i> , 2014
Pvf1	F: AATCAACCGTGAGGAATGCAA R: GCACGCGGGCATATAGTAGT	1/10	Fly Primer Bank (PP26981)
Dorsal	F: TGTTCAAATCGCGGGCGTCGA R: TCGGACACCTTCGAGCTCCAGAA	1/40	Bandarra <i>et al.</i> , 2014
Dif	F: CGGACGTGAAGCGCCGACTTG R: CAGCCGCCTGTTTAGAGCGG	1/40	Bandarra <i>et al.</i> , 2014
Relish	F: TGGATACCATCAAATGGCCTG R: CTTGTACCGAAAGCGGAACTT	1/10	Fly Primer Bank (PP2664)
dCYLD	F: ATCGAGGTAGAAGACGAATCCA R: GCATCTGTTGGCTGGTACAAAA	1/40	Bandarra <i>et al.</i> , 2014
Diptericin	F: ACCGCAGTACCCACTCAATC R: ACTTTCCAGCTCGGTTCTGA	1/40	Bandarra <i>et al.</i> , 2014
Drosomycin	F: GTTCGCCCTCTTCGCTGTCCTGA R: CCTCCTCCTTGACACACGACG	1/40	Bandarra <i>et al.</i> , 2014
Attacin A	F: AGGTTCCCTTAACCTCCAATC R: CATGACCAGCATTGTTGTAG	1/40	Bandarra <i>et al.</i> , 2014

### 2.7.11 Primer optimisation

RT-qPCR primers must be properly optimised to minimise the presence of primer dimers and off-target binding, in order to accurately quantify target cDNA. Optimisation was performed with cDNA generated from RNA collected from wildtype flies.

Each primer pair was tested at three dilutions of the 100  $\mu$ M stock: 1/10, 1/20 and 1/40. Triplicate qPCR reactions were run for each primer concentration, for both cDNA and no-template control conditions. qPCR reactions were set up and run according to the protocol described above. Using CFX Maestro software (Bio-Rad), optimal primer concentrations were selected based on the presence of a single peak in the melt curve in cDNA reactions and a Ct value  $>38$  in no-template reactions. 2  $\mu$ l 6x Blue/Orange loading dye (Promega, G1881) was added to no-template and cDNA reactions containing optimal primer concentration and reactions were run on 1 % agarose gels containing ethidium bromide in TAE at 100 V for 1 hour. Gels were imaged using the Syngene G:Box (Syngene, UK). Gel images were used to confirm the presence of a single qPCR product in cDNA reactions, which is absent in no-template reactions.

Primer pairs were tested further, at their optimal concentration, to determine primer efficiency. Primer efficiency should be comparable between the target gene and housekeeping gene, as this is an assumption made in the final analysis (Double-delta), and as close to 100 % as possible to ensure that resulting Ct values are proportional to the concentration of target cDNA. Optimal primer concentrations were tested with a standard curve of cDNA concentrations, set up and run in duplicate qPCR reactions according to the protocol described above. Mean Ct values were plotted against log cDNA concentration to determine the  $R^2$  value for each primer pair. A minimum  $R^2$  value  $>0.99$  was required for a primer pair to be used in final qPCR experiments.

### 2.7.12 Analysis

CFX Maestro software was used to extract raw Ct data and check melt curves of individual wells, to identify any aberrant reactions to be discounted from further analysis. Ct values were used to calculate relative expression by the double-delta method. Analysis of individual plates was performed separately, by calculating  $\Delta Ct_{(\text{control})}$  (baseline) from the mean Ct values of all 3 technical replicates of the control (GFP Normoxia) condition on each plate. Individual GFP Normoxia replicates were compared against this baseline to demonstrate inter-repeat variability and permit statistical analysis.

Double delta analysis:

$$\Delta Ct_{(\text{control})} = \text{Mean target } Ct_{(\text{control})} - \text{Mean housekeeping } Ct_{(\text{control})}$$

$$\Delta Ct_{(\text{experimental})} = \text{Mean target } Ct_{(\text{experimental})} - \text{Mean housekeeping } Ct_{(\text{experimental})}$$

$$\Delta\Delta Ct = \Delta Ct_{(\text{experimental})} - \Delta Ct_{(\text{control})}$$

$$\text{Relative expression} = 2^{-\Delta\Delta Ct}$$

### 2.7.13 Amplex Red H<sub>2</sub>O<sub>2</sub> assay

Amplex Red H<sub>2</sub>O<sub>2</sub> assay was performed using the Amplex<sup>TM</sup> Red Hydrogen Peroxide/Peroxidase Assay kit (Invitrogen, A22188) and adapted from manufacturer's protocol. In brief, male flies were cold anaesthetised in sealed tubes under their treatment conditions. Fly brains were isolated by dissection in cold HL3 (70 mM NaCl, 5 mM KCl, 20 mM MgCl<sub>2</sub>, 10 mM NaHCO<sub>3</sub>, 115 mM sucrose, 5 mM trehalose, 5 mM HEPES, 0.2 mM CaCl<sub>2</sub>) on a sylgard-coated plate. 3 brains per condition were placed in 25 µl of cold HL3 in a 96-well plate, kept on ice until all conditions were prepared. On the same plate, a standard curve of H<sub>2</sub>O<sub>2</sub> was prepared by 2-fold serial dilution of 5 µM H<sub>2</sub>O<sub>2</sub> in HL3. 25 µl of 100 µM Amplex Red and 0.2 U/ml HRP in HL3 was added to each well of brains and standard curve. The plate was wrapped in foil to protect the dye from light and incubated at 29 °C for 5 hours. Fluorescence (544/600 Ex/Em) was measured every hour using FLUOstar OMEGA platereader (BMG Labtech).

### 2.8. Generation of graphics, statistics and figures

Graphs were generated and corresponding statistical tests were performed in GraphPad Prism 10 software. Microscopy images were processed in ImageJ. Graphics were generated using BioRender and Inkscape. Figures were compiled using Inkscape.

## 2.9. Antibodies

**Table 2.5. Antibodies used in this study**

Antibody	Species	Concentration used	Source
<b>Primary</b>			
Anti-CRM1	Rabbit	WB: 1:5000 IHC: 1:250	Proteintech (27917-1-AP)
Anti-YAN	Mouse	IHC: 1:500	DSHB (8B12H9)
Anti-exd	Mouse	IHC: 1:5	DSHB (B11M)
Anti-sima	Rabbit	WB: 1:5000 IHC: 1:100	Gift from Dr. Pablo Wappner
Anti-Alpha tubulin	Mouse	WB: 1:50,000 IHC: 1:5000	Proteintech (66031-1-Ig)
Anti-Histone H3	Rabbit	WB: 1:5000	Proteintech (17168-1-AP)
Anti-Beta actin	Mouse	WB: 1:100,000	Proteintech (60008-1-Ig)
Anti-Beta-galactosidase	Mouse	WB: 1:5000	Promega (Z378A)
Anti-LaminC	Mouse	WB: 1:1000 IHC: 1:20	DSHB (LC28.26)
<b>Secondary</b>			
Anti-rabbit 700	Goat	WB: 1:5000	LI-COR (926-68071)
Anti-rabbit 800	Goat	WB: 1:5000	LI-COR (926-32211)
Anti-mouse 700	Goat	WB: 1:5000	LI-COR (926-68070)
Anti-mouse 800	Goat	WB: 1:5000	LI-COR (926-32210)
Anti-rabbit Cy3		IHC: 1:250	Jackson ImmunoResearch (111-165-003)
Anti-mouse Cy3	Goat	IHC: 1:250	Jackson ImmunoResearch (115-165-003)
Anti-mouse Cy5	Goat	IHC: 1:250	Jackson ImmunoResearch (115-175-146)
<b>Nanobodies</b>			
Anti-GFP ATTO488	Alpaca	IHC: 1:250	Chromotek (gba488-100)

### 3. Identification of DPR interacting proteins using 1000-repeat DPR models

#### 3.1. Introduction

Since the discovery that RAN translation of the G<sub>4</sub>C<sub>2</sub> repeat expansion in *C9orf72* produces DPRs, research has provided evidence pointing to DPRs as the primary driver of C9-mediated neurodegeneration and disease (Mizielinska *et al.*, 2014; Wen *et al.*, 2014; Tran *et al.*, 2015; Moens *et al.*, 2018; Solomon *et al.*, 2018). However, there is conflicting evidence with regards to the degree of toxicity of each of the DPRs and the underlying cellular and molecular mechanisms of their toxicity. This is believed to be, at least in part, due to the disparity in DPR repeat lengths used between studies (Morón-Oset *et al.*, 2019; Radwan *et al.*, 2020; Kriachkov *et al.*, 2023). While the majority of studies were limited to DPRs of <100 repeats, recent studies modelled DPRs of a physiologically-relevant 1000 repeats in HeLa cells, zebrafish and *Drosophila* (Callister *et al.*, 2016; Swaminathan *et al.*, 2018; West *et al.*, 2020). These 1000-repeat DPRs demonstrated patterns of DPR toxicity, morphology and localisation of DPR inclusions that were different to shorter repeat models, but more similar to what is seen in patient-derived tissue. However, study of cellular and molecular mechanisms of 1000-repeat DPR toxicity has been somewhat limited (Ryan *et al.*, 2022; Bennett *et al.*, 2023). Given the observed differences between short- and long-repeat DPRs, it is possible that mechanisms of DPR toxicity also differ between short- and long-repeat DPRs. Therefore, we believe that using 1000-repeat DPR models is important for elucidating mechanisms of toxicity associated with the longer repeat DPRs produced in disease.

One key feature of DPRs is their propensity to aggregate into inclusions, as seen in patient post-mortem tissue (Mori, Weng, *et al.*, 2013). Aberrant protein aggregation is seen across a range of neurodegenerative disease including Alzheimer's disease, Parkinson's disease and FTD/ALS (Masters *et al.*, 1985; Spillantini *et al.*, 1997; Neumann *et al.*, 2006b). These aggregated proteins can sequester physiological proteins, disrupting their function and leading to impairments in the biological processes in which they are involved (Olzscha *et al.*, 2011). This can lead to negative effects on cell function and survival, thus causing disease. DPRs have been shown to interact with and sequester other proteins to mediate DPR toxicity (May *et al.*, 2014). However, DPR-protein interactions have not been examined in 1000-repeat DPRs. Given the mechanistic role of protein sequestration in other neurodegenerative diseases, and evidence from short-repeat models, protein sequestration by DPRs is a likely mechanism of DPR toxicity. DPR-protein interactions provide the basis of protein sequestration to DPR inclusions.

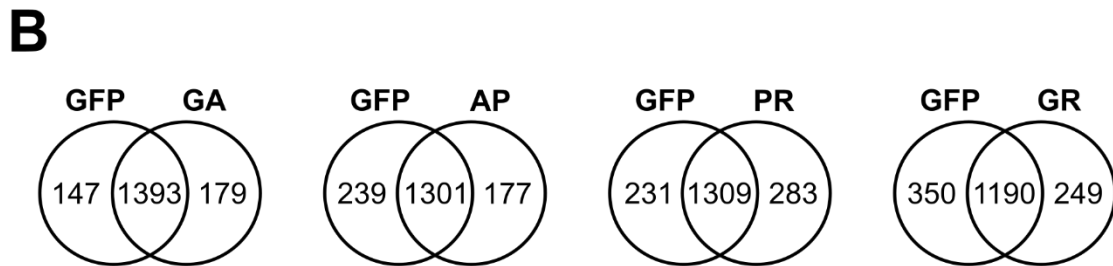
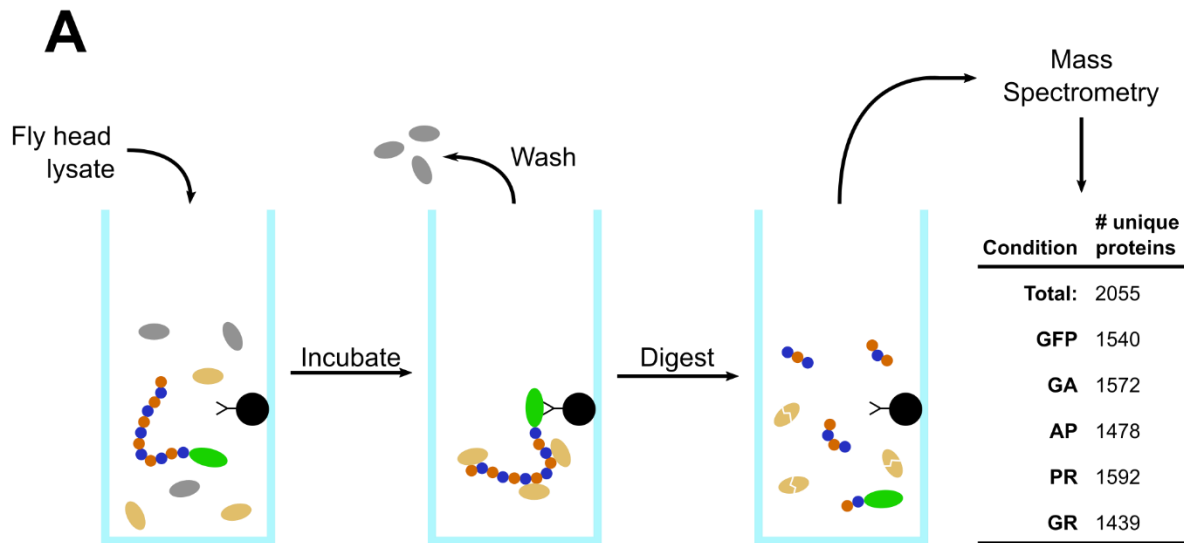
Therefore, the aims of this chapter are:

1. Identify proteins that interact with 1000-repeat DPR species
2. Identify biological processes likely affected by DPR-protein interactions
3. Identify modifiers of GR toxicity from GR-interacting proteins

## **3.2. Results**

### **3.2.1. 1000-repeat DPR-interacting proteins are identified by tandem mass spectrometry following co-immunoprecipitation**

DPR-interacting proteins were identified using tandem mass spectrometry (MS/MS) following co-immunoprecipitation (co-IP) of individual 1000-repeat DPRs from the heads of flies pan-neuronally expressing (nSyb-Gal4 (III)) individual DPRs (Fig. 3.1). Briefly, heads from flies pan-neuronally expressing single GFP-tagged DPRs (UAS-DPR1000-EGFP), or a GFP control (UAS-mCD8-GFP), were lysed and lysates used for co-immunoprecipitation using chromotek GFP-Trap® magnetic beads, as described in the methods (2.7.1-2.7.5). Following co-immunoprecipitation and on-bead digestion was performed prior to identification of DPR-interacting proteins using MS/MS (see methods 2.7.6). Bioinformatic analysis of MS/MS data was performed using Scaffold and ShinyGO (see Methods 2.7.7). Sample preparation, Scaffold analysis, and protein ontology were performed by Duncan Garner. MS/MS and Mascot analysis were performed by University of Sheffield Faculty of Science Mass Spectrometry Centre (University of Sheffield, UK).



**C**

	GA	AP	PR	GR
<b>Significant DPR-interacting proteins (<math>p &lt; 0.05</math>)</b>	12	20	37	93
<b>Non-significant interacting proteins (<math>p &gt; 0.05</math>)</b>	2039	2016	2002	1912
<b>Significant GFP-interacting proteins (<math>p &lt; 0.05</math>)</b>	4	19	16	50

**Figure 3.1. Isolation and identification of DPR-interacting proteins.** A) Schematic of co-immunoprecipitation (co-IP) of DPR1000-interacting proteins using DPR1000-EGFP as bait protein. Black circle = GFP-trap® magnetic bead, Yellow oval = DPR-interacting protein, Grey oval = non-interacting protein, Orange/blue circles = DPR1000 with EGFP tag (green oval). B) Venn diagrams illustrating the number of unique proteins identified in each DPR and their presence in the GFP condition. C) Table of number of unique proteins output by Fisher's Exact t-test with Benjamini-Hochberg correction ( $p < 0.05$ ) of each DPR against GFP. Proteins used in this study are highlighted in red.

A total of 2055 unique proteins were identified across all five conditions, with 1400-600 being identified in each condition individually (Fig. 3.1A). The majority of proteins identified in each of the DPR conditions were also identified in the GFP condition (Fig. 3.1B), indicating that these proteins likely interact with the GFP tag rather than or in addition to the DPRs themselves. Due to this overlap, two strands of analysis are required to identify DPR-interacting proteins. First, proteins which interact solely with the DPR and not the GFP tag were identified by their presence in DPR but not GFP conditions. PR interacted with the most non-GFP interacting proteins followed by GR, GA then AP with 283, 249, 179 and 177 proteins respectively (Fig. 3.1B, Appendix). These will be referred to as “DPR+ GFP-proteins”.

Secondly, proteins which were detected at significantly higher levels in DPR compared to GFP conditions were identified (Fig. 3.1C, Appendix; Fisher’s Exact t-test with Benjamini-Hochberg correction,  $p < 0.05$ ). In addition to selecting only significant results from the previous group, this also identified two other groups of proteins: those which interact with the GFP tag, for which the interaction is enhanced by the DPR; and those which bind to both the GFP tag and the DPR, with a higher affinity for the DPR. GR had the most significant protein interactions, followed by PR, AP then GA with 93, 37, 20 and 12 proteins respectively (Appendix). These will be referred to as “significant DPR-interacting proteins”. While there was overlap between the proteins produced by each analysis, many proteins were exclusive to one or the other.

Results from both strands of analysis demonstrated increased levels of protein interaction between the arginine-containing DPRs, PR and GR, compared to the alanine-containing DPRs, GA and AP. While the arginine-containing DPRs exhibited similar levels of protein interaction in the first strand of analysis, the number of significant PR-protein interactions was markedly reduced compared to that of GR. The alanine containing DPRs exhibited similar levels of protein interaction across both strands of analysis.

### **3.2.2. 1000-repeat DPRs interactomes are enriched in distinct profiles of biological processes**

Following identification of DPR-interacting proteins, we sought to identify biological processes enriched for DPR-interacting proteins, as those are likely most affected by DPR-protein interactions. Protein ontology was performed on DPR-interacting proteins from both strands of analysis to identify biological process enriched for DPR-interacting proteins. For each DPR individually, DPR-interacting proteins were compared against the GOBiologicalProcesses database to identify all processes significantly enriched for DPR-

interacting proteins. The 20 most significantly enriched processes were examined further through network analysis to identify shared genes between processes.

For the 179 GA+ GFP- proteins, a total of 63 biological processes were found to be significantly enriched. Among the 20 most significantly enriched processes there were a high number of overlapping organic metabolic processes, especially amino acid metabolism with “cellular amino acid catabolic process”, “alpha amino acid metabolic process”, and “cellular amino acid metabolic process” being 9.1-, 8.5- and 5.5-fold enriched respectively (Fig. 3.2A, B). A separate cluster of enriched processes were found in RNA processing and metabolism, with “ncRNA processing”, “ncRNA metabolic process” and “RNA processing” being 3.4-, 3.4- and 2.6-fold enriched respectively (Fig. 3.2A, B). From the 12 significant GA-interacting proteins, 105 biological processes were significantly enriched. There was a high degree of overlap between the 20 most significantly enriched processes, but processes predominantly fell into two categories: polysaccharide metabolism or cytoskeletal organisation (Fig. 3.2C, D). Apart from cytoskeletal processes, significantly enriched processes were predominantly driven by two GA-interacting proteins: jaguar (jar) and shaggy (sgg).

177 AP+ GFP- proteins were identified and a total of 128 biological processes were enriched among them. One distinct cluster among the 20 most significant processes was in lipid modification, with 20.9- and 7-fold enrichment in “phosphatidylinositol dephosphorylation” and “lipid modification” respectively (Fig. 3.3A, B). Multiple signalling processes were also among the most significantly enriched, especially the MAPK cascade which represented 6 of the 20 most significantly enriched processes (Fig. 3.3A). 20 significant interacting proteins were identified in AP and among these were multiple isoforms of two proteins, CLIP-190 and Myosin heavy chain, which constituted 7 of the 20 proteins. Protein ontology of the 13 unique significant AP-interacting proteins revealed significant enrichment in 21 biological processes. 12 of the 20 most significantly enriched processes were cytoskeletal organisation and transport processes (Fig. 3.3C). Cytoskeletal transport processes primarily involved organelle transport, particularly vesicle and mitochondrial transport which were enriched up to 181- and 153-fold respectively (Fig. 3.3C). “Myofibril assembly” and “striated-/muscle cell development” formed an overlapping cluster with cytoskeletal processes.

Analysis of the 283 PR+ GFP- proteins revealed 199 significantly enriched biological processes. The most significant processes predominantly involved molecular transport within the cell, including 2.3- and 2.6-fold enrichment in broad processes such as “macromolecule localisation” and “intracellular transport” (Fig. 3.4A). Two main subgroups were present within these transport processes: protein transport and localisation, and exocytosis and secretion pathways (Fig. 3.4B). Statistical testing revealed 37 significant PR-interacting

proteins, enriched in 97 biological processes. These processes fell into relatively distinct clusters with more limited overlap than in GA and AP (Fig. 3.4D). A central cluster of transport and localisation processes overlapped separately with two clusters of biosynthetic processes and membrane budding and fission processes, the latter of which demonstrated 252-fold enrichment. This high enrichment is driven by the fact that 2 out of the 3 proteins in those pathways are significant proteins in PR.

249 proteins were identified as GR+ GFP- and were found to be enriched in 201 biological processes. 17 of the 20 most significantly enriched processes were transport or localisation processes, with the broad processes “macromolecule localisation”, “intracellular transport” and “establishment of localisation within cell” being 2.3-, 2.8- and 2.8-fold enriched respectively (Fig. 3.5A). Among these, Golgi-related processes were the most significantly enriched, up to 17.6-fold (Fig. 5A). Also of note was a cluster of 4 broad exocytosis and secretion processes which were 4.8-7.7-fold enriched (Fig. 3.5A, B). 93 significant interacting proteins were identified in GR, associated with significant enrichment in 251 biological processes. The general theme of transport and localisation processes was also enriched among significant GR-interacting proteins, although multiple ion transport processes emerged in this group with up to 11-fold enrichment (Fig. 3.5C). Among other synaptic processes, a 5.1-fold enrichment in “synaptic signalling” and 5.3-fold enrichment in “chemical synaptic transmission” were observed. Together with vesicle processes, such as “synaptic vesicle cycle”, these formed a relatively distinct cluster of enriched processes in GR (Fig. 3.5.D). Another distinct cluster included, among other related processes, 3.1-fold enrichment in “small molecule metabolic processes” and 8.4-fold enrichment in “fatty acid metabolic processes” (Fig. 3.5C, D).

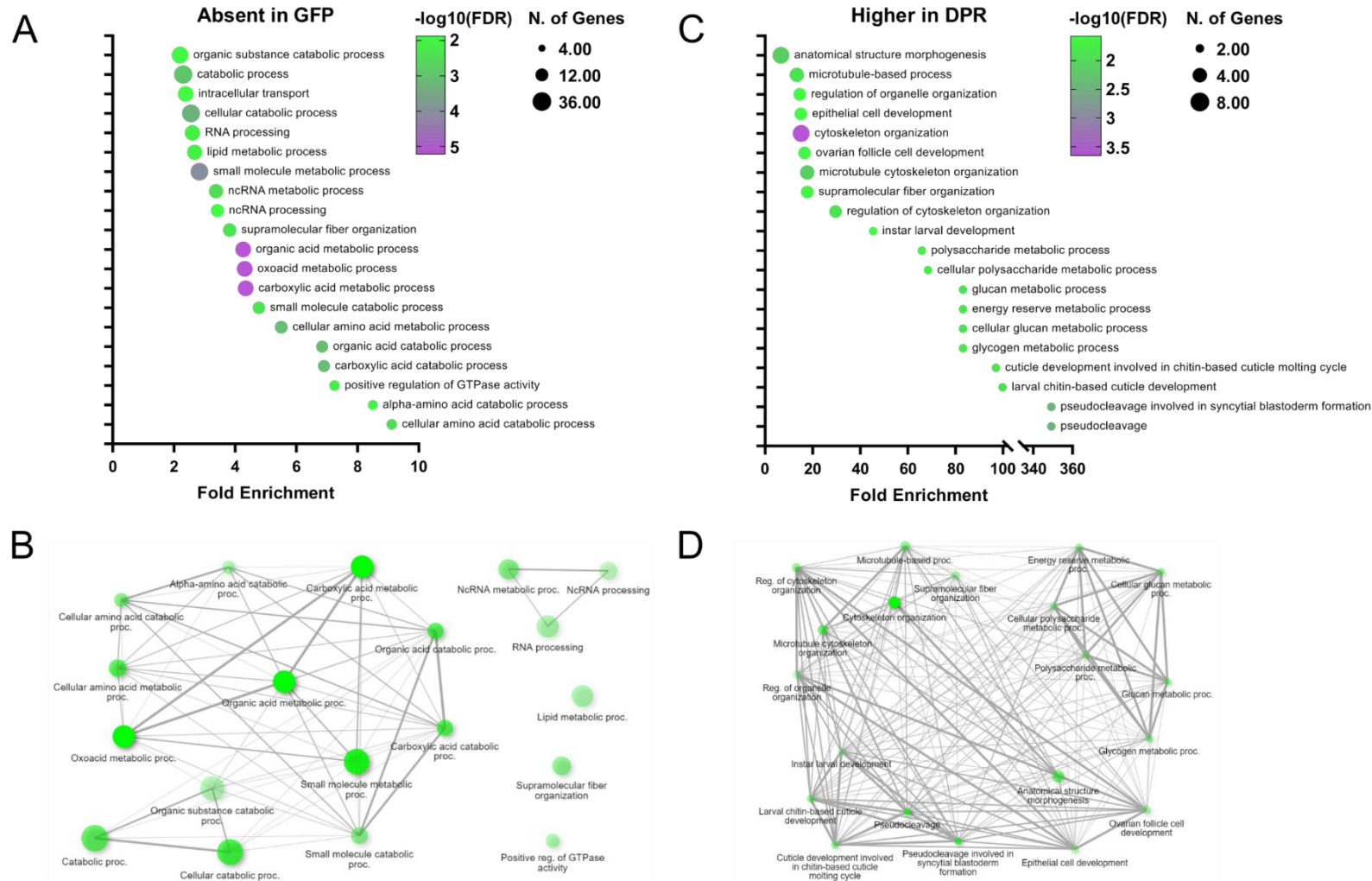


**Figure 3.2. The GA1000 interactome is significantly enriched in cytoskeletal, metabolic and RNA processes.** A, C) 20 most significantly enriched GO biological processes from GA-interacting proteins. False discovery rate (FDR) <0.05, hypergeometric test) B, D) Networks of processes from A, C representing proteins shared between processes. Processes are connected if they share  $\geq 20\%$  of proteins. Thicker lines represent increased number of shared proteins. Bigger circles represent increased number of proteins. Darker circles represent more significantly enriched processes.

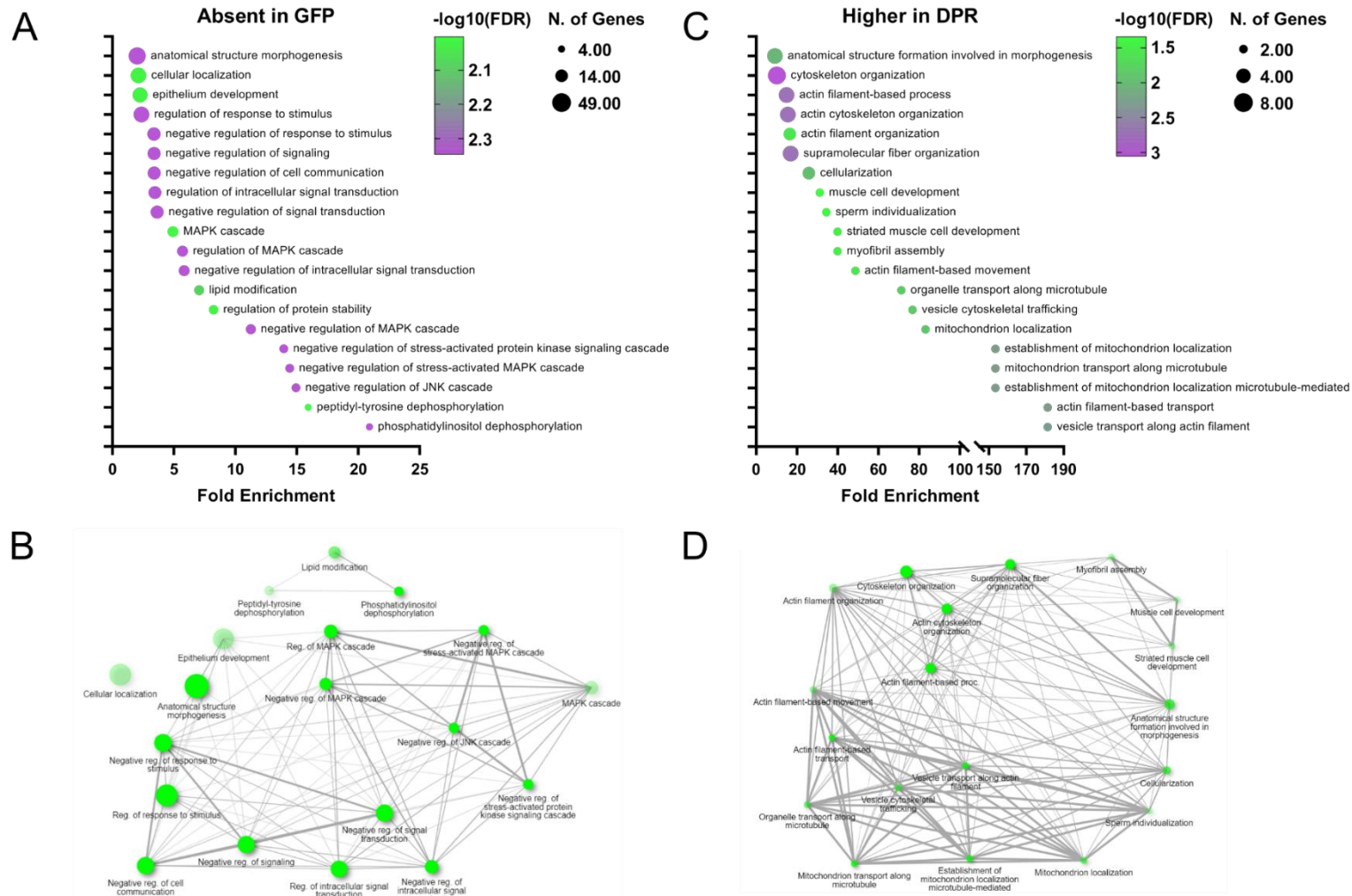


**Figure 3.3. The AP1000 interactome is significantly enriched in cytoskeletal and signalling processes.** A, C) 20 most significantly enriched GO biological processes from AP-interacting proteins. False discovery rate (FDR) <0.05, hypergeometric test) B, D) Networks of processes from A, C representing proteins shared between processes. Processes are connected if they share  $\geq 20\%$  of proteins. Thicker lines represent increased number of shared proteins. Bigger circles represent increased number of proteins. Darker circles represent more significantly enriched processes.

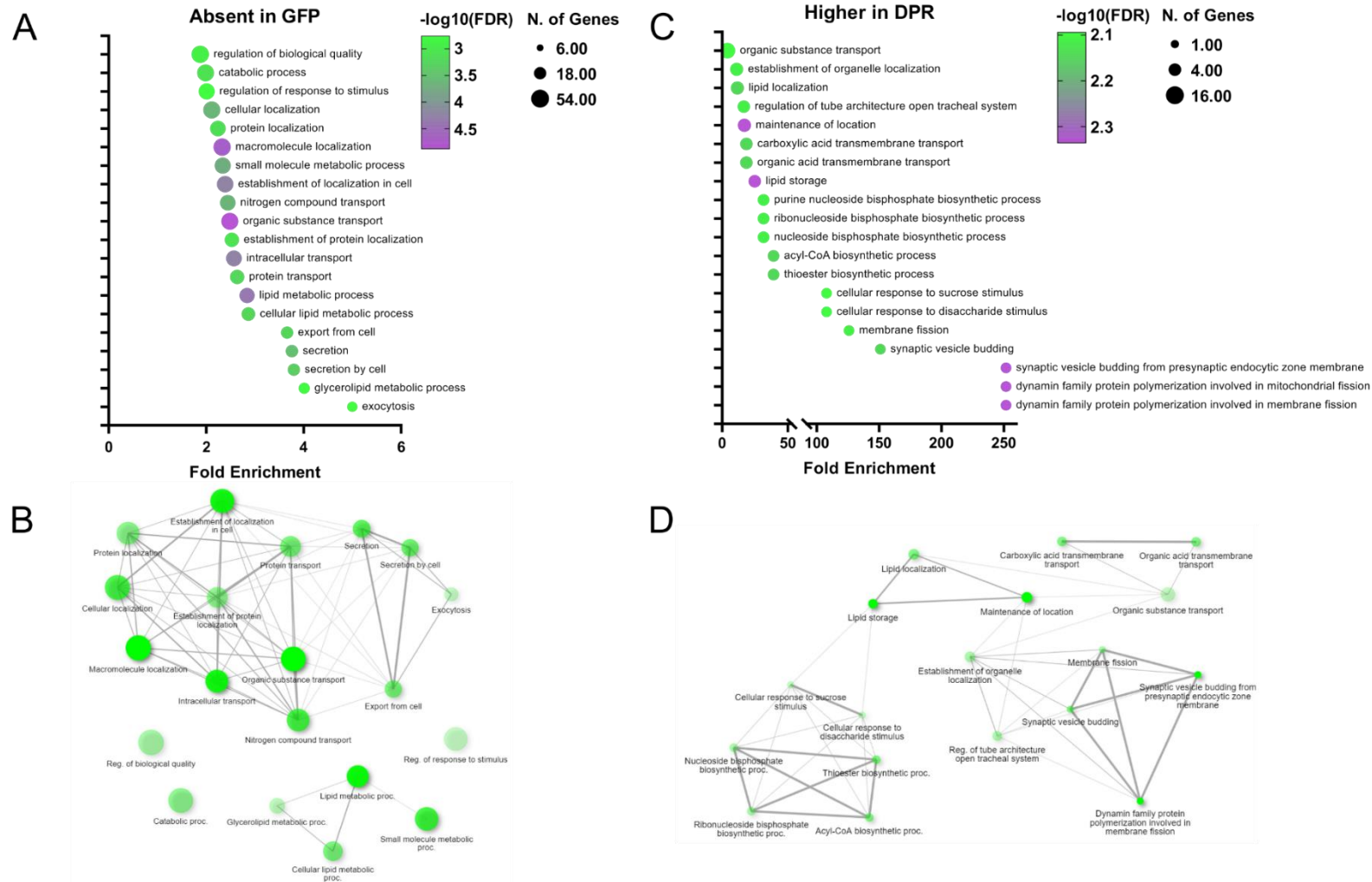


**Figure 3.4. The PR1000 interactome is significantly enriched in multiple transport and localisation processes.** A, C) 20 most significantly enriched GO biological processes from PR-interacting proteins. False discovery rate (FDR) <0.05, hypergeometric test) B, D) Networks of processes from A, C representing proteins shared between processes. Processes are connected if they share  $\geq 20\%$  of proteins. Thicker lines represent increased number of shared proteins. Bigger circles represent increased number of proteins. Darker circles represent more significantly enriched processes.

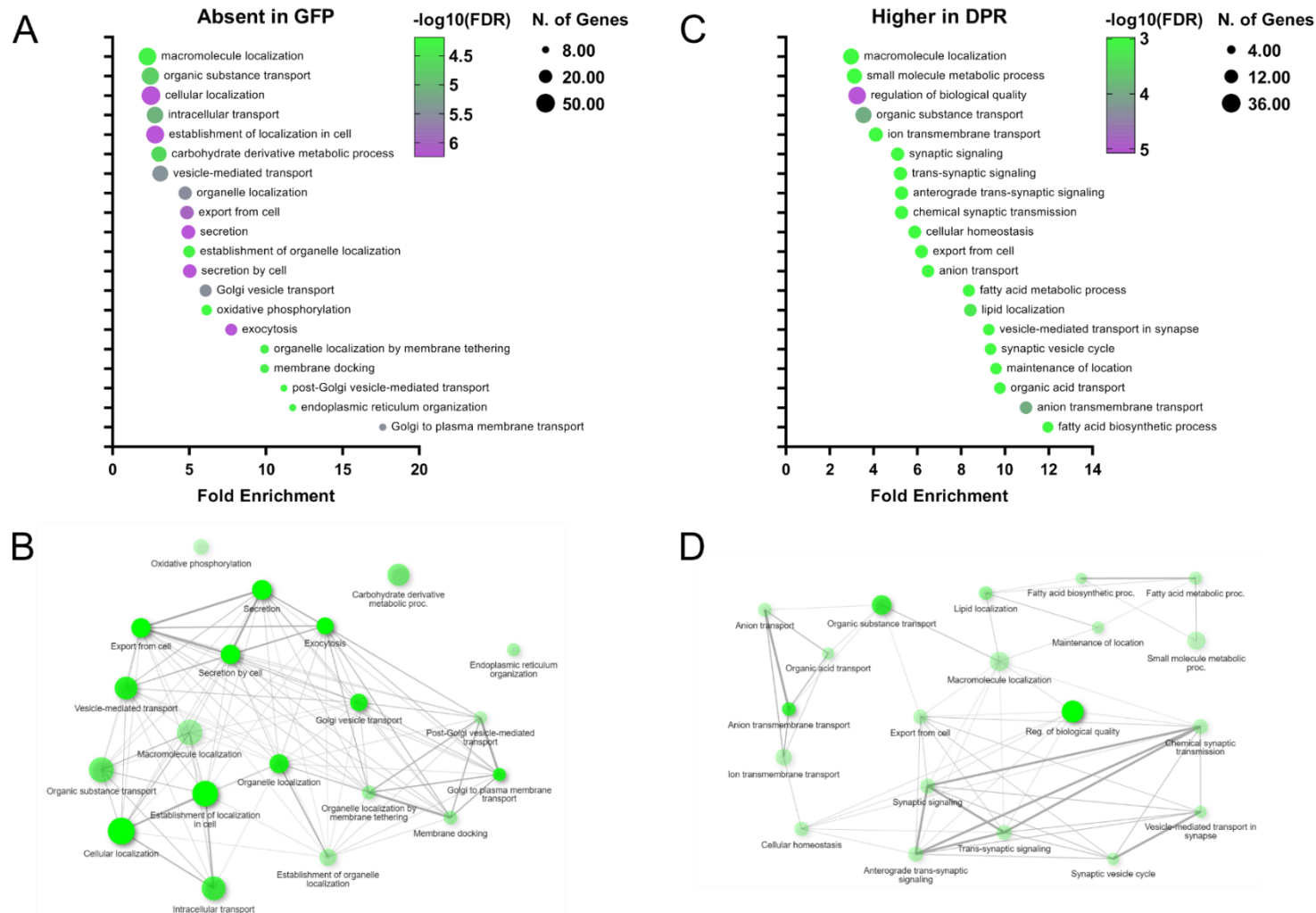


**Figure 3.5. The GR1000 interactome is significantly enriched in multiple transport and localisation processes.** A, C) 20 most significantly enriched GO biological processes from GR-interacting proteins. False discovery rate (FDR) <0.05, hypergeometric test) B, D) Networks of processes from A, C representing proteins shared between processes. Processes are connected if they share  $\geq 20\%$  of proteins. Thicker lines represent increased number of shared proteins. Bigger circles represent increased number of proteins. Darker circles represent more significantly enriched processes.

### 3.2.3. XPO1 and CNOT1 are potential modifiers of GR1000 toxicity

In an effort to study the mechanistic role of DPR-protein interactions and their related biological processes in further depth, we sought to narrow the breadth of our investigation. GR is the only DPR that has been correlated with neurodegeneration and clinical severity in patients (Saber *et al.*, 2018; Sakae *et al.*, 2018; Quaegebeur *et al.*, 2020). GR also appears to be the most toxic DPR in most DPR models, including the 1000-repeat DPR fly models which demonstrate a severe reduction in fly lifespan and age-related decline in motor function (West *et al.*, 2020). In this model GR is also the only DPR to cause significant TDP-43 mislocalisation (West *et al.*, 2020). Therefore, we focussed on GR-protein interactions and their related biological processes in our investigation of the mechanisms of DPR toxicity.

To further focus our investigation, GR-interacting proteins were shortlisted for modifier screening. 6 proteins (Table 3.1) were selected based upon their representation of identified processes; disease relevance; homology in humans; novelty; interest; and availability of reagents (e.g. antibodies, fly lines).

One of the most interesting processes enriched in GR was synaptic vesicle processes, which are extremely important in neuronal function and neurodegenerative disease. In fact, impairments in synaptic vesicle dynamics have been widely observed in C9 models (Freibaum *et al.*, 2015; Zhang *et al.*, 2015; Perkins *et al.*, 2021). As such, two proteins were selected to represent synaptic vesicle processes.

Shi (DNM1 in humans) was predominantly selected to represent the synaptic vesicle processes identified from. DNM1 was also found to be present in 8 of the 20 most significantly enriched processes from significant GR-interacting proteins. DNM1 has a key role in endocytosis, an important process in vesicle recycling and, therefore, synaptic transmission. It is therefore unsurprising that functional impairment of DNM1 is associated with paralysis phenotypes in *Drosophila* and has been studied extensively in relation these phenotypes. With regards to ALS, DNM1 expression (Lee *et al.*, 2023) and localisation (Gershoni-Emek *et al.*, 2016) has been demonstrated to be perturbed in ALS. DNM1 has also been identified as a mediator of TDP-43 toxicity (Bharathi, Girdhar and Patel, 2021).

Nsf2 (NSF in humans) was also selected to represent synaptic vesicle processes. NSF was found to be present in 10 of the 20 most significantly enriched processes from significant GR-interacting proteins, so is also likely to represent other enriched processes. NSF functions in SNARE recycling, thus playing a key role in synaptic neurotransmitter release and synaptic transmission. NSF is not widely implicated in ALS but has been shown to be differentially methylated and its expression downregulated in sALS (Lederer *et al.*, 2007; Morahan *et al.*, 2009).

GCS2 $\alpha$  (GANAB in humans) was selected to represent regulation of biological quality. GANAB is the catalytic  $\alpha$  subunit of the Glucosidase 2 protein and functions in protein quality control. Interestingly, the  $\beta$  subunit was also identified as a significant GR-interacting protein, however we were unable to study this due to poor survival of relevant fly lines. Loss of GANAB function is associated with impairment of the unfolded protein response (UPR) and subsequent ER stress, both of which have been identified in sALS (Ilieva *et al.*, 2007; Masi and Orlando, 2022).

Not1 (CNOT1 in humans) functions, as part of the CCR4-NOT complex, in regulating gene expression through mRNA deadenylation and translation repression. While CNOT1 was included under regulation of biological quality, it was predominantly selected based on its RNA processing function. RNA processing has been widely implicated in previous studies of PR/GR interactions and toxicity but not here (Liu *et al.*, 2022). Therefore, CNOT1 also represents previously identified RNA processes. Loss CNOT1 function has also been linked to neurodevelopmental delay (Vissers *et al.*, 2020), indicating its importance in the nervous system.

c11.1 (mROH1 in humans) is a protein that has not been studied extensively, so its function has not been fully elucidated. However, it has been observed to be recruited to the late endosome/early lysosome and accumulates at lysosomal membranes (Gillingham *et al.*, 2014). Additionally, mutations in mROH1 lead to delayed exocytosis of post-lysosomes (Thomason, King and Insall, 2017). Altogether, these findings point to a role for mROH1 in autophagy and endolysosomal pathways. While these processes were not enriched in GR-interacting proteins, their dysfunction has been associated with multiple forms of ALS, including C9 ALS (Otomo, Pan and Hadano, 2012; Beckers *et al.*, 2023). Therefore, we believe that the mROH1-GR interaction was worth studying.

Emb (XPO1 in humans) is a key nuclear export protein, responsible for the export of a range of protein and RNA targets from the nucleus into the cytoplasm. While XPO1 was included under the enriched localisation and transport processes, the processes are extremely broad and XPO1 cannot truly represent them in their entirety. However, XPO1 was primarily selected based on previous studies implicating nucleocytoplasmic transport defects in C9 disease (Freibaum *et al.*, 2015; Jovičić *et al.*, 2015; Zhang *et al.*, 2015). It is highly contended whether there is a role of XPO1 in GR and PR toxicity, with numerous studies presenting evidence either way (Freibaum *et al.*, 2015; Vanneste *et al.*, 2019; Hutten *et al.*, 2020; Ramic *et al.*, 2021; Jafarinia, Van der Giessen and Onck, 2022). Therefore, XPO1 is a particularly interesting target for us to study in relation to GR1000 toxicity.

**Table 3.1. GR-interacting proteins shortlisted for genetic modifier screening.** *Drosophila* gene and the estimated human orthologue are shown. DIOPT v9.1 homology score indicates degree of homology between *Drosophila* and human genes using data from multiple homology tools to generate a weighted homology score (Hu *et al.*, 2011). A higher score indicates greater homology.

<b><i>Drosophila</i> gene</b>	<b>Human orthologue</b>	<b>DIOPT homology score (/14)</b>	<b>Function</b>
Shibire (Shi)	Dynamin 1 (DNM1)	13	Vesicle recycling
Glucosidase 2 $\alpha$ subunit (GCS2 $\alpha$ )	Glucosidase II $\alpha$ subunit (GANAB)	13	Protein folding and quality control
N-ethylmaleimide sensitive factor 2 (Nsf2)	N-ethylmaleimide sensitive factor (NSF)	14	SNARE recycling
c11.1	Maestro heat like repeat family member 1 (mROH1)	12	Lysosomal regulation
CCR4-NOT transcription complex subunit 1 (Not1)	CCR4-NOT transcription complex subunit 1 (CNOT)	14	mRNA degradation, translation inhibition
Embargoed (emb)	Exportin 1 (XPO1)	14	Nuclear export

Not all GR-protein interactions and related processes will mediate toxicity and therefore be relevant to disease. It is therefore important to confirm that the identified GR-protein interactions mediate GR toxicity, by genetic screening of interacting proteins for modifiers of GR toxicity. Here, the *Drosophila* eye provides an excellent platform for toxicity modifier screening and has been used extensively in such experiments (Freibaum *et al.*, 2015; Zhang *et al.*, 2015; Boeynaems *et al.*, 2016; West *et al.*, 2020). The genetic tractability of *Drosophila*, combined with the commercially available libraries of RNAi lines for *Drosophila* genes, provide the necessary tools for robust screening experiments. The uniform, compound structure of the fly eye is disrupted by cytotoxicity to produce morphological defects which can be easily visualised. Commonly observed eye phenotypes include pigmentation defects, melanised patches, and disorganisation of the ommatidial array and interommatidial bristles. The presence of these phenotypes was scored based upon a strict 9-point scoring system (Pandey *et al.*, 2007; Ritson *et al.*, 2010; He *et al.*, 2014; West *et al.*,

2020), allowing quantification of eye phenotype severity. Using the Glass Multimer Reporter (*GMR*)-*Gal4* driver, specific expression of *UAS* constructs can be driven in the fly eye. *GMR-Gal4* was used to drive expression of GR1000 alongside *UAS* constructs to knockdown, via RNAi, or overexpress shortlisted proteins. When introducing multiple *UAS* elements to flies, it is important to use appropriate controls with the same number of *UAS* elements to control for titration of Gal4. *UAS-mCherry-RNAi* was used as a control for RNAi lines, while *UAS-mCD8-EGFP* was used as a control for overexpression lines. Eye screening was performed at 29 °C to enhance activity of the Gal4/*UAS* system, increasing GR1000 expression and eye phenotype severity.

GR1000 expression was mildly toxic alongside control RNAi and was enhanced slightly by simultaneous GFP expression (Fig. 3.6A, B). GFP expression with control RNAi also conferred very mild toxicity, but less than was seen in GR1000 counterparts. Knockdown of DNM1 caused similar, significant ( $p < 0.0001$ ) levels of lethality both GFP and GR1000 expressing flies, with 61 % of flies not surviving to adulthood (Fig. 3.6A, B). Those that did survive demonstrated relatively severe eye phenotypes which were more severe in GR1000-expressing flies than their GFP counterparts (Fig. 3.6A, B). Significant ( $p < 0.0001$ ) lethality was also seen with knockdown of NSF in GFP and GR1000 flies, with 94 and 88 % of flies dying before adulthood respectively (Fig. 3.6A, B). While the degree of lethality was slightly reduced in GR1000 compared to GFP flies, the eye phenotype of surviving flies was similar across both genotypes. Knockdown of mROH cause a significant ( $p < 0.0001$ ) reduction in eye phenotype severity of GR1000 flies, with nearly 85 % flies demonstrating no eye phenotype (Fig. 3.6A, B). However, the same significant ( $p < 0.0001$ ) effect was also seen in GFP where 98 % of flies showed no eye phenotype. GANAB knockdown had no significant effect on eye phenotypes of GFP or GR flies ( $p = 0.71$  and  $> 0.9999$ , respectively).

Knockdown and overexpression lines were available for two of the shortlisted proteins: CNOT1 and XPO1. The overexpression line for CNOT1 carried *UAS*-driven human CNOT1, rather than the *Drosophila* gene Not1. RNAi knockdown of CNOT1 significantly exacerbated eye phenotypes in GFP ( $p = 0.0119$ ) but not GR1000 ( $p > 0.9999$ ) flies (Fig. 3.6A, B). Overexpression of human CNOT1 significantly reduced the severity of eye phenotypes in GFP flies ( $p < 0.0001$ ) but had no significant effect in GR1000 flies ( $p = 0.6434$ ), compared to GR1000 flies overexpressing GFP as a control (Fig. 3.6A, B). The line for overexpression of XPO1 was *UAS-Vc-emb*, whereby expression of *emb* (the *Drosophila* orthologue of XPO1) tagged with the C-terminal half of the fluorescent protein Venus is *UAS*-driven. Due to major differences in reported knockdown efficacy, two lines for RNAi knockdown of XPO1 were tested: BDSC:34021 and BDSC:31353, denoted here as XPO1<sup>(1)</sup> and XPO1<sup>(2)</sup> respectively. XPO1<sup>(1)</sup> has a reported knockdown efficiency of 85 %, while XPO1<sup>(2)</sup> is reported

at 40 % (Okazaki, Yamazoe and Inoue, 2020). Knockdown of XPO1 caused a significant ( $p < 0.0001$ ) reduction in GR1000-associated eye phenotype severity which appeared stronger in the stronger knockdown line XPO1<sup>(1)</sup>, compared to XPO1<sup>(2)</sup>. However, a similar significant effect was seen in GFP flies (XPO1<sup>(1)</sup>:  $p < 0.0001$ , XPO1<sup>(2)</sup>:  $p = 0.0002$ ). Overexpression of XPO1 was 100 % lethal alongside expression of GR1000. While overexpression of XPO1 also caused lethality in 76 % of GFP flies, the surviving flies demonstrated the most severe eye phenotypes (Fig. 3.6A, B).

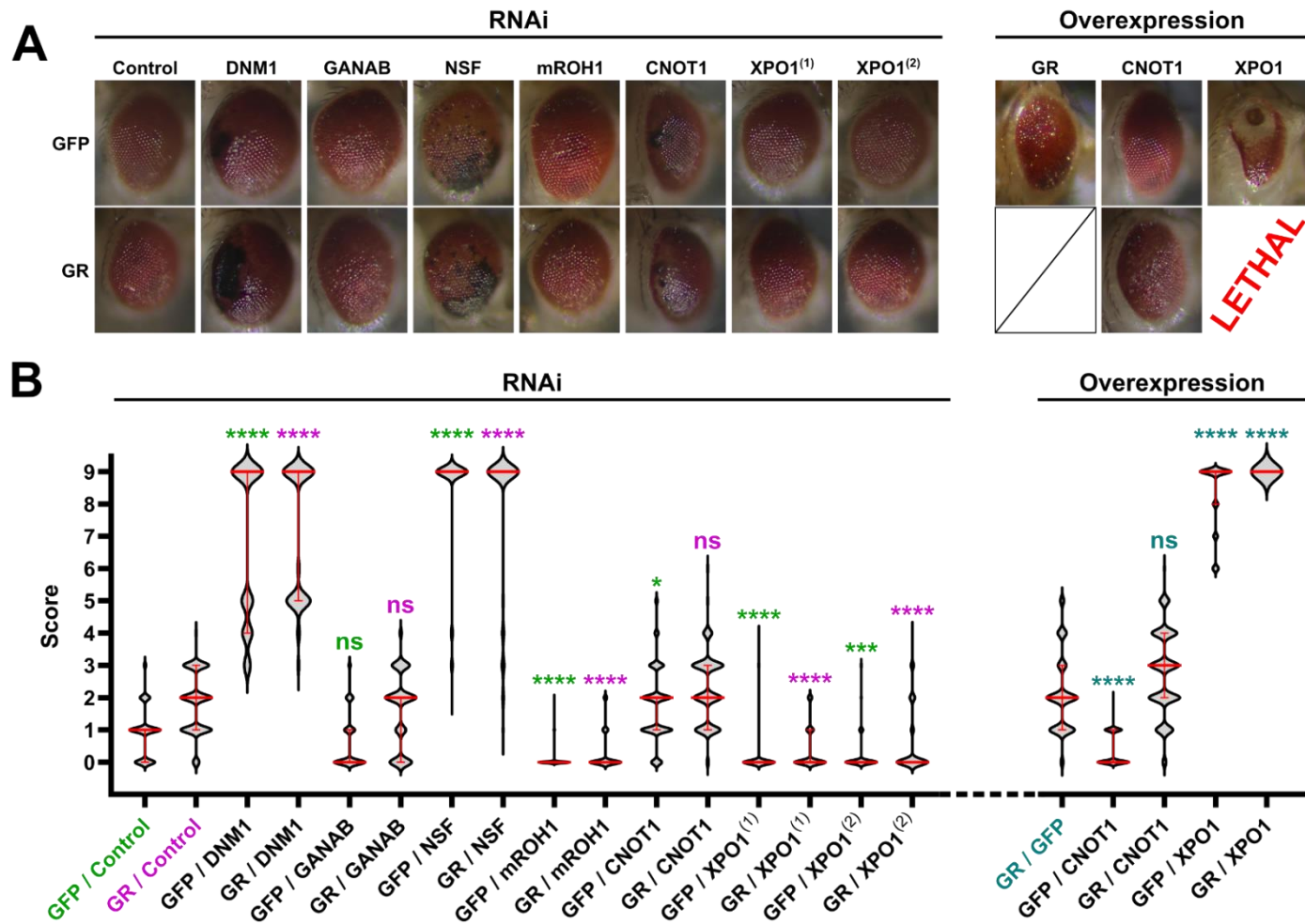


**Figure 3.6. Genetic manipulation of shortlisted genes modifies GFP- and GR1000-induced phenotypes in the *Drosophila* eye.** A) Representative images of *Drosophila* eyes co-expressing GFP or GR1000 with RNAi or overexpression of denoted proteins. B) Quantification of eye phenotype scores awarded based on 9-point scoring system, in which lethality scores 9 points. Lines represent median, error bars represent interquartile range. Stats are Kruskal-Wallis test with Dunn's multiple comparisons test of preselected pairs, with genotypes compared to their respective GFP (green), GR (magenta) or overexpression (blue) control. \*  $p < 0.05$ , \*\*  $p < 0.01$ , \*\*\*  $p < 0.001$ , \*\*\*\*  $p < 0.0001$ .

### 3.3. Discussion

#### 3.3.1. Identification of physiologically-relevant DPR-proteins interactions

This chapter begins with the first identification of DPR-interacting proteins in a 1000-repeat DPR model. While DPR-interacting proteins have previously been identified by various methods, as summarised in Table 3.2, these studies have been limited to repeat lengths <175 (May *et al.*, 2014; Hartmann *et al.*, 2018; Moens *et al.*, 2019; Radwan *et al.*, 2020; Bozič *et al.*, 2022; Pu *et al.*, 2022). Given the length-dependent effects on toxicity, morphology and localisation demonstrated in DPR models, this study provides the first investigation of DPR-protein interactions using repeat models of a length comparable to the longer repeat lengths observed in patients. However, it is important to note the caveats to this experiment conferred by the experimental setup. Firstly, performing co-IP on whole *Drosophila* head lysates exposes the bait DPRs to proteins from all cell types in the fly head, despite only being expressed in neurons. This may result in protein interactions occurring *in vitro* which, while possible, would not occur *in vivo* due to DPRs never being present in those cell types. Secondly, our co-IP setup captures proteins which interact with DPRs under the conditions of the lysis buffer, RIPA, which may not represent the *in vivo* conditions under which DPRs are found. The use of a stringent lysis buffer (RIPA) is necessary given the insoluble nature of the long DPRs, however may result in a loss of weak DPR-protein interactions. To counteract these drawbacks, Bozič *et al.* (2022) used BioID proximity labelling to label only those proteins interacting with DPRs *in vivo*, in the cells in which they are expressed. While this method does have advantages, it would require the additional step of ligating the BioID biotin ligase to each of the DPR1000 constructs. Given the challenges faced in the production and cloning of the DPR1000 constructs, there was no scope for BioID proximity labelling in this project. A more feasible alternative for future work would be the use of a GFP-binding BioID, pioneered in zebrafish by Xiong *et al.* (2021), to target BioID to EGFP-tagged DPR1000 without the need for cloning of the DPR1000 constructs.

#### 3.3.2. Distinct protein interaction profiles between DPRs

Previous studies have identified the arginine-containing DPRs as the most promiscuous in terms of protein interactions. Our data demonstrate marginally increased interaction promiscuity of GR and PR, compared to AP and GA, in both DPR+ GFP- and significant DPR-interacting proteins (Radwan *et al.*, 2020; Bozič *et al.*, 2022). This increased protein binding is likely facilitated by the positive charge conferred by the arginine content of these DPRs. The high toxicity of GR and PR in models (Mizielinska *et al.*, 2014; Wen *et al.*, 2014; Freibaum *et al.*, 2015; Tao *et al.*, 2015; Lee *et al.*, 2016), combined with their promiscuity

shown here and previously, supports the hypothesis of protein sequestration by DPRs as a potential mechanism of toxicity. Interestingly, studies have shown a substantially increased number of PR-interacting proteins compared to GR (Hartmann *et al.*, 2018; Moens *et al.*, 2019; Radwan *et al.*, 2020). Here PR interacted with more proteins that were absent in GFP, but GR had notably more proteins which were significantly higher in GR than GFP. The difference between our findings and those of previous studies may be explained by the disparity in repeat length between our models and those used in said studies. At shorter repeats PR has been shown to be more toxic than GR (Wen *et al.*, 2014; Jovičić *et al.*, 2015; Lee *et al.*, 2016), but at 1000 repeats GR appears substantially more toxic than PR (West *et al.*, 2020), in accordance with interactome findings.

Previous studies have shown distinct DPR interactomes and enriched processes, with a partial overlap between DPRs that varies between studies. We show a similar effect here, by examining protein ontology of DPR-interacting proteins. The most significantly enriched processes demonstrate very little overlap between DPRs. This effect is strongest when looking at the protein ontology of significant DPR-interacting proteins, with a higher degree of overlap between protein ontology of DPR+ GFP- interacting proteins, likely due to increased number of proteins included.

**Table 3.2. Summary of DPR interactome studies and their findings.** Interactome findings are summarised for each DPR studied. Interactome includes biological processes enriched for interacting proteins where such analysis was performed.

<b>Study</b>	<b>Model system</b>	<b>Method of protein identification</b>	<b>DPRs studied</b>	<b>Interactome</b>
May <i>et al.</i> (2014)	Primary rat cortical neurons	MS following co-IP with DPR as bait	GA149	Ubiquitin-proteasome system Cytoskeleton
Kanekura <i>et al.</i> (2016)	NSC34 cells	MS following co-IP with DPR as bait	PR20	Translation Ribosome assembly mRNA splicing
Hartmann <i>et al.</i> (2018)	Primary rat cortical neurons HEK293 cells	MS following co-IP with DPR as bait	PR175	Ribosome Stress granules RBPs Histones Nucleolus

				Splicing
			GR149	Ribosome Stress granules RBPs Histones Nucleolus Methylosome
Moens <i>et al.</i> (2019)	Drosophila heads	MS following tandem affinity purification with DPR as bait	PR100	Ribosome Translation
			GR100	Translation
Radwan <i>et al.</i> (2020)	N2A cells	MS following co-IP with DPR as bait	GA101	Endoplasmic reticulum Ubiquitin-proteasome system
			AP101	Cytoskeleton
			PR101	Translation Ribosome biogenesis Cytoskeleton Mitochondria Chromatin Splicing
			GR101	Translation Ribosome biogenesis Cytoskeleton Methylosome Chromatin Splicing

Božič <i>et al.</i> (2022)	HEK293 cells	BioID2 proximity labelling	GA125	Translation Mitotic cell cycle Proteasome
			AP125	Translation
			PR125	Translation RNA processing Viral replication
			GR125	Translation Cell-cell adhesion Viral replication
Pu <i>et al.</i> (2022)	HEK293 cells	MS following co-IP with DPR as bait	GA150	Protein synthesis Chaperones Ubiquitin-proteasome system
Liu <i>et al.</i> , (2022)	HEK293 cells	BioID proximity labelling	GA100	Ubiquitin-proteasome system Unfolded-protein response
			GR100	rRNA processes Ribosome biogenesis RNA processing
			PR100	rRNA processes Ribosome biogenesis RNA processing

### 3.3.3. Localisation of DPR interactomes aligns with DPR localisation

As noted above, one limitation of our experimental protocol is that the bait DPRs are exposed to complete head lysates, which may lead to *in vitro* protein interactions that do not occur *in vivo*. One artifact that may arise from this is the identification of DPR-interacting proteins and processes from not just cell types, but also cellular compartments that would not contain DPRs *in vivo*. Therefore, it is important to consider the proteins and processes identified by our MS/MS experiments in the context of our knowledge of DPR localisation. By doing this we can consider the likelihood of these DPR-protein interactions occurring *in vivo*.

In *Drosophila* neurons, AP1000 was observed with diffuse granular cytoplasmic localisation and as perinuclear cytoplasmic aggregates (West *et al.*, 2020). The ER was one of the most well represented cellular compartments among proteins present in AP but absent in GFP. While ER localisation has not been described, perhaps the observed perinuclear cytoplasmic AP aggregates are in fact localised to the ER. The other well represented cellular compartments in the present in AP, absent in GFP group were non-membrane-bound organelles, mitochondria, cytosol, nuclear lumen and vesicles. Nuclear localisation has not been previously described, so it is likely that these DPR-protein interactions are artifacts of the experimental protocol. Diffuse granular cytoplasmic localisation could well be representative of the presence of AP1000 in the other cellular compartments identified from AP1000-protein interactions, therefore increasing our confidence in the accuracy of our data. Additionally, AP1000 was observed to colocalise with the cytoskeleton and cell membrane in HeLa cells (Callister *et al.*, 2016). This aligns with the cytoskeleton and membrane being the most well represented cellular compartments among proteins significantly higher in AP and present in AP but absent in GFP, respectively.

In both HeLa cells and *Drosophila* neurons, GA1000 was observed as axonal, cytoplasmic and perinuclear cytoplasmic aggregates (Callister *et al.*, 2016; West *et al.*, 2020). Axonal aggregation aligns with almost all of the significant GA1000-interacting proteins being cytoskeletal. A wider range of cellular compartments were identified among the proteins present in GA but absent in GFP, including non-membrane-bound organelles, mitochondria, cytosol, nucleus and vesicles. Cytosolic and non-membrane-bound organelle proteins are highly likely to be exposed to GA1000 aggregates, based upon their observed localisation. Mitochondrial, vesicular and nuclear GA1000 have not been described, indicating that these DPR-protein interactions may not be occurring *in vivo*. However, it is possible that large GA1000 aggregates observed in the cytoplasm also interact with mitochondria and vesicles.

PR1000 was observed with almost entirely nucleolar presence in HeLa cells (Callister *et al.*, 2016), whereas West *et al.* (2020) observed nuclear and cytoplasmic localisation of PR1000

in *Drosophila* neurons. However, nuclear and nucleolar proteins were not identified in either sets of PR1000-interacting proteins. While the lack of nucleolar proteins comes as no surprise, given that this study was performed in *Drosophila* rather than HeLa cells, the lack of nuclear proteins is somewhat unexpected. It may, therefore, be the case that PR1000 does not interact with nuclear proteins, despite being present in the nucleus. In line with West *et al.*'s observation of mostly cytoplasmic PR1000, cytosol was one of the cellular compartments represented by proteins present in PR but absent in GFP. However, the compartment most well represented between both sets of PR1000-interacting proteins was the plasma membrane. While localisation specifically to the plasma membrane has not been described, plasma membrane proteins would likely be exposed to cytoplasmic PR1000, leading us to believe that these interactions are likely to occur *in vivo*. Interestingly, a number of synaptic proteins were also identified as PR1000-interactors. Observed cytoplasmic localisation of PR1000 into the neurites may well extend into the synapse (West *et al.*, 2020), but synaptic localisation specifically has not been described. The other predominant cellular compartments represented among PR1000-interacting proteins were ER and mitochondrion. While localisation of PR1000 to these organelles has not been observed, it may well be the case that PR1000 is present in these organelles at the similar levels to the cytosol, leading to a diffuse appearance throughout the cytoplasm.

In HeLa cells, GR1000 was observed to have a predominantly diffuse cytoplasmic localisation, although some nucleolar presence was also observed (Callister *et al.*, 2016). Despite this, and West *et al.*'s (2020) observation of nuclear GR1000 in *Drosophila* neurons, neither nucleolar nor nuclear proteins were identified in either set of GR-interacting proteins. Therefore, it may be the case that GR1000 does not interact with and sequester proteins when present in the nucleus. Diffuse cytoplasmic GR1000 was observed in both HeLa cells and *Drosophila* neurons (Callister *et al.*, 2016; West *et al.*, 2020), but cytosol was not identified as one of the cellular compartments enriched for GR1000-interacting proteins. However, as in PR1000, most GR1000-interacting proteins belonged to plasma membrane and synapse compartments. Proteins in either of these compartments would be exposed to cytoplasmic GR1000, leading us to believe that these interactions are likely to occur *in vivo* but not as part of GR1000 localisation or aggregation in these compartments specifically. Similar to PR1000, a number of ER, mitochondrial and vesicular proteins were identified as GR1000-interactors. While specific localisation to these organelles has not been described, it is possible that the presence of diffuse GR1000 in these compartments would be indistinguishable amongst diffuse cytoplasmic GR1000.

Altogether, the DPR-interacting proteins identified in this study largely belong to cellular compartments in which 1000-repeat DPRs have been observed to be present. However,

there are some notable exceptions to this. The identification of AP1000 interactions with nuclear proteins, despite there being no reports of nuclear AP1000, is likely an artifact of our experimental protocol. On the other hand, it appears that the arginine-containing DPRs do not interact with nuclear proteins, despite observed nuclear/nucleolar localisation of these DPRs. It is also worth noting that localisation of most of the 1000-repeat DPRs has been observed as diffuse cytoplasmic but has not examined localisation to cellular compartments contained within the cytoplasm, perhaps due to insufficient resolution. Therefore, it is difficult for us to comment on the validity of our data with regards to DPR1000 interactions with proteins in cellular compartments such as mitochondria, vesicles, plasma membrane and synapse.

### **3.3.4. GA exhibits a length dependent interactome**

As the DPR found most commonly in patient tissue (Mackenzie *et al.*, 2015), GA has been studied extensively in relation to DPR-protein interactions. Additionally, the propensity of GA to aggregate makes it particularly relevant in the hypothesis of protein sequestration as a mechanism of DPR toxicity. Multiple studies of the short repeat GA interactome have identified enrichment in the ubiquitin-proteasome system (UPS) (May *et al.*, 2014; Radwan *et al.*, 2020; Božič *et al.*, 2022; Liu *et al.*, 2022; Pu *et al.*, 2022). While there were no UPS or related processes among the 20 most significantly enriched processes, “protein modification by small protein removal” was significantly enriched ( $p = 0.04$ ) among GA+ GFP- proteins. This enrichment was driven by the deubiquitinases and regulator proteins Usp47, Uaf1 and puf. This was also one of the significantly enriched processes identified by (Liu *et al.*, 2022), driving the UPS enrichment in GA<sub>100</sub>-interacting proteins. Pu *et al.* (2022) identified a direct interaction between GA and the proteasome via PSMD2, but the fly homolog Rpn1 was not identified as a GA-interacting protein in our study. Given the absence of previously identified key GA-proteasome interactions and lack of enrichment in UPS processes, it appears that 1000-repeat GA may not interact with the UPS in the same way as shorter repeats do. A number of other GA-protein interactions identified in shorter repeat models are not replicated in our study: the fly homologs of RAD23 (May *et al.*, 2014; Zhang *et al.*, 2016), Unc119 (May *et al.*, 2014), Agrin (Tu *et al.*, 2023), SV2 (Jensen *et al.*, 2020), hnRNPA3 and ATM (Nihei *et al.*, 2020) were not identified as GA-interacting proteins here. In fact, the majority of processes significantly enriched for significant GA-interacting proteins have not been identified in previous studies of GA-protein interactions. Enrichment in these processes is predominantly driven by the GA interaction with shaggy (*sgg*) (Glycogen Synthase Kinase-3 $\beta$  (GSK-3 $\beta$ ) in humans). GSK-3 $\beta$  is a ubiquitously expressed, constitutively active, proline-directed serine/threonine kinase implicated in fundamental processes including immune regulation, metabolism, microtubule stability and gene transcription. GSK-3 $\beta$  hyperactivity

has been implicated in Tau hyperphosphorylation, increased beta-amyloid accumulation, neuroinflammation and TDP-43 toxicity, all hallmarks of FTD as well as dementia more widely. Indeed, *Drosophila* sgg has been shown to mediate age-dependent TDP-43 toxicity (Sreedharan *et al.*, 2015). Furthermore, perturbation of GSK-3 $\beta$  has also been shown to disrupt neuronal structure and signalling (Owen and Gordon-Weeks, 2003; Kim *et al.*, 2006; Gobrecht *et al.*, 2014; Liz *et al.*, 2014). As such, GSK-3 $\beta$  has long been considered a promising therapeutic target for dementia and other neurodegenerative diseases.

Cytoskeletal processes were notably enriched among significant GA-interacting proteins, driven by multiple protein interactions. While cytoskeletal proteins and processes have previously been associated with GA (May *et al.*, 2014), they are more commonly associated with the arginine-containing DPRs (Radwan *et al.*, 2020; Shiota *et al.*, 2022). Given our findings that cytoskeletal processes are heavily associated with GA and AP, but not PR and GR, we provide evidence towards a role of the alanine-containing DPRs in the cytoskeletal disruption that is seen in C9ALS motor neurons (Sato *et al.*, 2014). This may suggest that all DPRs are capable of perturbing cytoskeletal organisation, potentially via distinct mechanisms. Whether these pathways converge remains unclear and may be dependent on whether each DPR species is present in the same cell type. Further, previous evidence suggests that DPRs may interact with each other and that this can alter their physical properties, which may lead to further differences in protein-interactions (Darling *et al.*, 2019; West *et al.*, 2020). Similarly, the existence of chimeric DPR species may also result in distinct DPR-protein interactions (McEachin *et al.*, 2020; Latallo *et al.*, 2023).

### **3.3.5. AP1000 exhibits a small but novel interactome**

As the least prevalent and toxic DPR, AP is relatively understudied in general and in terms of DPR-protein interactions. Those studies that have included AP have identified very few AP-protein interactions (Radwan *et al.*, 2020; Božič *et al.*, 2022), which is replicated in our study. While this may be unsurprising given the apparent lack of AP toxicity in short repeat models (Mizielinska *et al.*, 2014; Wen *et al.*, 2014; Boeynaems *et al.*, 2016; Xu and Xu, 2018), it does not explain the electrophysiological defects, neurodegeneration, and early-onset motor deficits in *Drosophila* expressing AP1000 (West *et al.*, 2020). Despite the reduced number of significant AP-interacting proteins in our study, clear trends did appear among interacting proteins. Cytoskeletal organisation and transport processes made up 12 of the 20 most significantly enriched processes. The broadest process, “cytoskeleton organisation”, included 7 of the 13 unique significant AP-interacting proteins. Radwan *et al.* (2020) also identified cytoskeletal proteins as AP-interacting proteins in N2A cells, however they did not

observe enrichment in cytoskeletal processes. These data provide a strong basis for a role AP in the disruption of cytoskeletal proteins and processes. Given that cytoskeletal disruption and transport defects have been observed in C9 and sporadic ALS motor neurons (Sasaki *et al.*, 1990; Satoh *et al.*, 2014), this may suggest a key role of AP in C9 disease.

The other cluster of significantly enriched processes that emerged in AP, in AP+ GFP-interacting proteins, was the regulation of the MAPK/JNK signalling cascade. MAPK/JNK signalling occurs in response to a number of cellular stressors (Vlahopoulos and Zoumpourlis, 2004) and has been shown to be hyperactivated in multiple forms of ALS, including C9 ALS (Sahana and Zhang, 2021). Interestingly, Wang *et al.* (2019) demonstrated PR-mediated activation of JNK signalling and a key role of JNK in PR-induced neurodegeneration. However, this study did not include AP. Our findings provide a link between AP and JNK signalling, highlighting the need for further study of a potential role of JNK signalling in AP toxicity, especially since JNK signalling has been previously implicated in PR toxicity.

Some muscle cell processes were also significantly enriched among significant AP-interacting proteins. While this does not indicate the presence of AP in muscle tissues, due to the previously mentioned drawbacks of our experimental method, it does have interesting implications for disease. The identification of GA in the skeletal muscle of C9 ALS patients demonstrated the potential for DPRs to be present and act in non-neural cells (Cykowski *et al.*, 2019). If there is potential for the presence of AP in muscle tissue, then our data provides a mechanism through which AP could disrupt muscle processes, providing a novel mechanism of disease. Importantly, enrichment in muscle cell process was driven by interactions with Myosin Heavy Chain (Mhc) which is expressed in a variety of cell types, including muscle cells and neurons (Li *et al.*, 2022). In neurons, myosin functions in cytoskeletal dynamics and membrane transport (Kneussel and Wagner, 2013). Therefore, these processes may also be implicated in AP1000 toxicity by the interaction with Mhc.

### **3.3.6. PR exhibits a length dependent interactome**

Studies of short repeat PR toxicity have identified a number of nuclear and nucleolar processes disrupted by PR to contribute to a general nucleolar dysfunction (Mizielinska *et al.*, 2017; White *et al.*, 2019). In line with this, short repeat PR has been shown to interact with ribosome biogenesis, chromatin, histone and other nucleolar proteins (Hartmann *et al.*, 2018; Radwan *et al.*, 2020; Liu *et al.*, 2022). However, this nucleolar enrichment was not seen in our PR1000 data. Instead, we show enrichment of PR1000-interacting proteins in transport and localisation processes. These processes are very broad and enriched in PR-

interacting proteins involved in the transport of ions, proteins, amino acids and lipids, among other molecules. Genes in ion and protein transport have been shown to be upregulated in C9 ALS motor neurons (Selvaraj *et al.*, 2018), but effects on amino acid and lipid transport have not been described. Although, disruptions in lipid metabolism have been reported in C9 patient tissue and models. By interacting with and potentially disrupting lipid transport proteins, PR1000 may cause disruption in wider lipid metabolism as others have observed in C9 patient tissue and models (Le *et al.*, 2023; Giblin *et al.*, 2024). This disruption was demonstrated as detrimental in these studies, highlighting the potential of PR1000-mediated disruption in the pathways as a mechanism of toxicity.

A number of exocytic and synaptic vesicle processes were also enriched among PR-interacting proteins. Synaptic dysfunction in various forms has been implicated in C9 FTD/ALS, including perturbed synaptic proteome, impaired synaptic vesicle dynamics and reduced active zones (Freibaum *et al.*, 2015; Zhang *et al.*, 2015; Jensen *et al.*, 2020; Perkins *et al.*, 2021; Laszlo *et al.*, 2022). These effects have been linked to DPRs previously, for example GA149 was shown to impair synaptic vesicle dynamics (Jensen *et al.*, 2020). Our findings link PR to synaptic dysfunction, through interaction with proteins functioning in synaptic vesicle processes. If the interaction with PR is disruptive to protein function, then PR may impair synaptic vesicle dynamics. This may lead to perturbed synaptic and neuronal activity, excitability, plasticity, and ultimately neurodegeneration.

Previous studies have identified strong PR interactions with ribosomal proteins and enrichment in translation processes and ribosome biogenesis pathways, in line with the nucleolar localisation of short repeat PR (Hartmann *et al.*, 2018; Moens *et al.*, 2019; Radwan *et al.*, 2020; Božič *et al.*, 2022; Liu *et al.*, 2022). In fact, Moens *et al.* (2019) identified 64 ribosomal proteins as PR interactors. PR and GR have also been shown to bind the polypeptide tunnel of ribosomes (Loveland *et al.*, 2022) and cause ribosome stalling during their own translation (Kriachkov *et al.*, 2023). However, our study with PR1000 has only identified one PR-interacting ribosomal protein, Rpl37A, although this interaction was not significant. 3 proteins functioning in ribosome biogenesis pathways were also identified as PR-interactors, but ribosome biogenesis processes were not among the most significantly enriched processes in PR. While our data do support an interaction between PR, ribosomes and their biogenesis, it appears that this interaction may be weaker than initially suggested by short repeat studies, especially with regards to the direct interaction of PR with ribosomal proteins. This is in line with PR1000 not demonstrating the same nucleolar localisation, rather nuclear and cytoplasmic, shown by shorter repeat models (West *et al.*, 2020).

### 3.3.7. GR1000 exhibits many, novel protein interactions

Our data show that GR has the most significant DPR-protein interactions and the second most protein interactions that are absent in GFP. This high level of protein interaction, combined with GR's high levels of toxicity, make it particularly attractive in the study of DPR-protein interactions as a mechanism of DPR toxicity. While GR's prolific protein interaction has been observed in many studies previously, Moens *et al.* (2019) identified only 12 proteins as interactors of GR<sub>100</sub> in *Drosophila*, none of which were identified in our study. Therefore, our study not only demonstrates that GR1000 carries the same widespread protein interactions as in most shorter models, but also that this can be seen in *Drosophila* where it had not been previously.

For the most part, previous studies of DPR-protein interactions have shown a high degree of overlap between GR and PR. However, we show distinct interactome profiles between the two DPRs, with some common proteins and processes between them. As with PR, studies of short repeat GR identified ribosomal and translation processes, and histones, chromatin and ribosome biogenesis proteins in the nucleolus (Hartmann *et al.*, 2018; Moens *et al.*, 2019; Radwan *et al.*, 2020; Božič *et al.*, 2022; Liu *et al.*, 2022). GR1000 did interact with the ribosomal proteins RpL37A and RpS12, although these interactions were not significant and neither ribosomal nor ribosome biogenesis processes were significantly enriched in GR.

While GR1000 interactome-enriched processes overlapped with PR1000 with regards to transport and localisation processes, enrichment in other processes contributed to a more distinct GR1000 interactome profile. Golgi and synaptic vesicle processes formed a notable group enriched with GR-interacting proteins, such as Syt7 which, alongside other related proteins, has been shown to interact with GR149 (Hartmann *et al.*, 2018). In combination with synaptic vesicle processes, enrichment in ion transport provides a strong basis for a role of GR in synaptic dysfunction. As described above (3.3.5), synaptic dysfunction and impaired synaptic vesicle dynamics have been widely implicated in FTD/ALS. Our findings provide a link between GR and impairments in synaptic vesicle dynamics seen in C9 models (Freibaum *et al.*, 2015; Zhang *et al.*, 2015; Perkins *et al.*, 2021). The interaction of GR1000 with ion transport proteins implicates another mechanism of synaptic and neuronal dysfunction in DPR toxicity. Neuronal hyperexcitability is a hallmark feature of ALS (Wainger and Cudkowicz, 2015), including C9 ALS (Geevasinga *et al.*, 2015), and has been shown to be caused by the C9 mutation (Selvaraj *et al.*, 2018). Hyperexcitability and resulting excitotoxicity occurs through ion channel perturbations (Selvaraj *et al.*, 2018), which have also been shown to be caused by PR (Jo *et al.*, 2022). The interaction of GR1000 with ion

transport proteins may sequester them away from the neuronal membrane, leading to perturbed neuronal excitability and potential neurotoxicity.

Oxidative phosphorylation is the mitochondrial process through which the majority of ATP is produced and is particularly important in energy-demanding neurons. Oxidative phosphorylation was also enriched for GR+ GFP- interacting proteins. Oxidative phosphorylation has been shown to be impaired in patient fibroblast from both sALS and fALS, including C9 ALS (Debska-Vielhaber *et al.*, 2021), with mitochondrial dysfunction and bioenergetic defects also being identified in C9 patient fibroblasts (Onesto *et al.*, 2016; Alvarez-Mora *et al.*, 2022). Interestingly, mitochondrial and bioenergetic defects have also been shown to cause dysfunctional motor neuron axonal homeostasis in C9 ALS (Mehta *et al.*, 2021). While GR-mediated disruption of oxidative phosphorylation has not been described previously, GR has been shown to bind mitochondrial proteins, such as Atp5a1, and cause disruption in mitochondria, the sites of oxidative phosphorylation (Lopez-Gonzalez *et al.*, 2016; Choi *et al.*, 2019). Our data also demonstrate an interaction of GR1000 with oxidative phosphorylation proteins, with potential to cause disruption of mitochondrial function and downstream motor neuron dysfunction.

### **3.3.8. DNM1 and NSF are key proteins but do not modify GR1000 toxicity**

One of the characteristic processes enriched in GR was Golgi and synaptic vesicle processes, which are extremely important to neuronal function and relevant to neurodegenerative disease. Two of the GR-interacting proteins involved in these processes, Dnm1 (DNM1 in human) and Nsf2 (NSF in human), were therefore shortlisted for further study. DNM1 and NSF demonstrated particular relevance among significant GR-interacting proteins, being present in 8 and 10 of the 20 most significantly enriched processes respectively. In addition to their key role in synaptic processes, both DNM1 and NSF have been linked to ALS. NSF has been shown to be differentially methylated and its expression downregulated in sALS (Lederer *et al.*, 2007; Morahan *et al.*, 2009). DNM1 expression has also been shown to be reduced in the motor cortex of ALS patients (Lee *et al.*, 2023). DNM1 has also been identified as a mediator of TDP-43 toxicity (Bharathi, Girdhar and Patel, 2021) and has been observed to be mislocalised away from the synapse in SOD1 ALS (Gershoni-Emek *et al.*, 2016).

In the toxicity modifier screen, knockdown of either protein caused substantial toxicity and lethality in both GFP control and GR1000-expressing flies. The % of flies surviving to adulthood was consistent between GFP and GR1000-expressing flies for knockdown of both proteins, suggesting that neither protein is a potent modifier of GR1000 toxicity. To validate

this further, future investigation should look to examine whether overexpression of either of these genes has an impact of GR1000 phenotypes. However, these overexpression lines do not currently exist. Whilst the *Drosophila* eye is a powerful system for performing fast and simple modifier screens this system can be limited by a lack of an ageing component to the phenotypes seen. Much of the perturbation seen in the eye may be driven during developmental stages and does not change with ageing. As such, further examination could look to assess the effect of knockdown/overexpression on phenotypes other than those seen in eye-screens, for example the age related motor-dysfunction and neurodegeneration phenotypes previously described. Despite this, the observation of severe phenotypes with knockdown of these two proteins highlights that vesicle processes are key biological processes. While this does support the further study of the GR-DNM1/NSF interaction, the severity of these phenotypes could provide major challenges in such study.

### **3.3.9. mROH1 and GANAB represent novel GR interactors but do not modify GR1000 toxicity**

mROH1, the human orthologue of c11.1 in *Drosophila*, is a relatively understudied protein. It has been shown to bind Rab7 *in vitro*, implicating recruitment to the late endosome/lysosome (Gillingham *et al.*, 2014). In fact, mROH1 was found to accumulate at lysosomal membranes and mROH1 mutants exhibited delayed exocytosis of post-lysosomes (Thomason, King and Insall, 2017). Autophagy and endolysosomal dysfunction have previously been implicated in multiple forms of ALS, including C9 ALS (Otomo, Pan and Hadano, 2012; Beckers *et al.*, 2023). While endolysosomal processes were not enriched in GR1000-interacting proteins, the GR-mROH1 interaction may prove sufficient for disruption of said processes. In our eye screen, knockdown of mROH1 appeared to alleviate GR1000-induced eye phenotypes. However, knockdown of mROH1 also reduced the mild rough-eye phenotype observed in GFP-expressing flies.

GCS2 $\alpha$ , the *Drosophila* orthologue of GANAB, was identified as significant GR1000-interacting protein that was absent in GFP. GANAB is the catalytic  $\alpha$  subunit of the Glucosidase 2 protein in the ER, functioning in the maturation of glycoproteins and protein chaperoning (Masi and Orlando, 2022). Interestingly, the  $\beta$  subunit of Glucosidase 2, PRKCSH, was also a significant GR1000-interacting protein that was absent in GFP, but the relevant fly lines did not survive for us to study them. Hartmann *et al.* (2018) showed that GANAB interacts with PR149, but not GR149, while our data shows GANAB as both a PR- and GR-interacting protein. Mutations in GANAB are predominantly associated with polycystic liver disease (Porath *et al.*, 2016), but differential GANAB expression has been

associated with multiple sclerosis and schizophrenia (Masi and Orlando, 2022; Xue *et al.*, 2023). In the ER, GANAB forms part of the UPR. Loss of GANAB function is associated with UPR impairment and subsequent ER stress, both of which are associated with sALS (Ilieva *et al.*, 2007; Masi and Orlando, 2022). In this manner, DPR-mediated sequestration of GANAB may cause loss of function, leading to UPR impairment and ER stress downstream toxicity.

Knockdown of GANAB caused a slight reduction in eye phenotype severity in both GFP- and GR1000-expressing flies. This was the smallest change in eye phenotype severity observed in the toxicity modifier screen. This indicates that not only is GANAB unlikely to be a modifier of GR1000 toxicity, but manipulation of its expression may also not be linked to toxicity in *Drosophila*.

### **3.3.10. CNOT1 is a potential modifier of GR1000 toxicity**

Not1, the *Drosophila* orthologue of CNOT1, was identified as a significant GR-interacting protein that was absent in GFP. CNOT1 was also identified in the biological process “regulation of biological quality”, but, unlike other proteins in this process, was not identified elsewhere. CNOT1 forms part of the CCR4-NOT complex, which functions in mRNA deadenylation and translational repression (Ito *et al.*, 2011). While RNA processing has previously been shown to be enriched in the GR and PR interactome (Liu *et al.*, 2022), our data do not replicate these findings. However, CNOT1 may represent a link between GR1000 and RNA processing. Depletion of CNOT1 was found to cause ER-stress-mediated apoptosis (Ito *et al.*, 2011) and loss-of-function mutations in CNOT1 have been shown to cause neurodevelopmental delay (Vissers *et al.*, 2020). Therefore, CNOT1 was shortlisted for screening.

In the screen for modifiers of GR1000 toxicity, CNOT1 was identified as a potential modifier of toxicity although the results were not clear. Knockdown of CNOT1 exacerbated eye phenotypes in GR1000-expressing flies, although a similar, if not stronger, effect was seen in GFP control flies. Overexpression of human CNOT1 caused almost no eye phenotype in GFP-expressing flies but caused a slight increase in eye phenotype severity in GR1000-expressing flies. While these overexpression results potentially implicate CNOT1 as a modifier of GR1000 toxicity, the effects are unclear and not as strong as other shortlisted proteins, such as XPO1.

### 3.3.11. XPO1 is relevant to C9 disease and a potential modifier of GR1000 toxicity

In 2015, three groups independently implicated nucleocytoplasmic transport dysfunction in C9 disease (Freibaum *et al.*, 2015; Jovičić *et al.*, 2015; Zhang *et al.*, 2015). In 30- and 58-repeat pure repeat *Drosophila* models, nucleocytoplasmic transport genes, including XPO1, were identified as modifiers of G<sub>4</sub>C<sub>2</sub> toxicity (Freibaum *et al.*, 2015; Zhang *et al.*, 2015). GR was identified as the most toxic species in these models, but since they are both pure repeat models, toxicity may also arise from RNA foci and other DPRs. Screening in yeast also identified nucleocytoplasmic transport genes as modifiers of PR50 toxicity, but nuclear export genes such as XPO1 were not among them (Jovičić *et al.*, 2015). Nucleocytoplasmic transport encompasses a collection of processes involved in the bi-directional movement of proteins and RNA between the nucleus and the cytoplasm. The proteins involved in these processes can be broadly categorised as nuclear import factors; nuclear export factors; nuclear pore complex (NPC) factors; and Ran-GTPase active transport factors. While C9-mediated disruption of nucleocytoplasmic transport is clear, how each of these categories is affected remains unclear. Initial studies identified modifiers of G<sub>4</sub>C<sub>2</sub> toxicity in all 4 categories, with particular enrichment in nuclear import factors (Freibaum *et al.*, 2015; Zhang *et al.*, 2015). Since then, research has shown that the arginine rich DPRs interact with nuclear import factors to disrupt nuclear import (Hayes *et al.*, 2020; Hutten *et al.*, 2020; Jafarinia, Van der Giessen and Onck, 2022). However, our DPR-protein interaction data does not show any interactions between 1000-repeat DPRs and nuclear import factors.

The most notable nucleocytoplasmic transport protein identified in our data is the interaction of emb, the *Drosophila* orthologue of the nuclear export factor Exportin 1 (XPO1), with GR and PR. XPO1 is a major transport protein which mediates the nuclear export of >200 proteins and RNA species (Thomas and Kutay, 2003; Xu, Grishin and Chook, 2012; Fu *et al.*, 2013), although some studies estimate XPO1 to export >1000 proteins (Kırlı *et al.*, 2015). XPO1 recognises cargo proteins through nuclear export signals (NESs), including the leucine-rich (classical) NES (Fornerod *et al.*, 1997). Ran GTPase binds XPO1 alongside cargo proteins, providing the energy required for nuclear export through hydrolysis of GTP (Kehlenbach *et al.*, 2001). Importantly, XPO1 is highly conserved, with 71 % sequence identity between human and *Drosophila* XPO1 (Collier *et al.*, 2000).

The XPO1 interaction is particularly interesting, given that GR and PR50 has been shown to disrupt XPO1-mediated nuclear export (Ramic *et al.*, 2021) and XPO1 has been identified as a modifier of (GR-driven) (G<sub>4</sub>C<sub>2</sub>)<sub>58</sub> toxicity (Freibaum *et al.*, 2015). However, Vanneste *et al.* (2019) found that GR and PR20 do not interfere with XPO1-mediated nuclear export. This may be explained by the finding that short repeat GR and PR showed little to no DPR-XPO1

interaction (Hutten *et al.*, 2020; Jafarinia, Van der Giessen and Onck, 2022). However, it is important to note Hutten *et al.*'s (2020) observation that XPO1 levels in their model system may have been too low to detect an interaction with GR25, and that Jafarinia, Van der Giessen and Onck (2022) observed an increasing binding probability of XPO1 with PR with increasing repeat length. These observations may explain why we observe an XPO1-DPR interaction where, previously, others have not.

XPO1 was primarily shortlisted on the basis of its strong interaction with GR, absent in GFP and significantly higher in GR, and its relevance to mechanisms of disease. In our GR toxicity modifier screen, XPO1 shows a potential toxicity modifying effect, although the results are unclear. Knockdown of XPO1 alleviated most GR1000 toxicity, but a similar effect was also seen in GFP control flies. XPO1 overexpression caused 100 % lethality in GR1000-expressing flies, a notably strong phenotype in a *Drosophila* eye screen. However, lethality was also observed in GFP control flies, although to a lesser extent. These data point towards a toxicity-modifying effect of XPO1 on GR1000, although this effect may not be specific to GR1000, given the effects observed in GFP controls. While this does not align with the observation of a GR1000-XPO1 interaction that is not present in GFP controls, it does not rule out the mechanistic potential of XPO1 in GR1000 toxicity.

By interacting with GR1000, XPO1 may be sequestered to GR1000 inclusions, preventing XPO1 transport between the nucleus and cytoplasm. This would impair XPO1 function as a nuclear export protein, leading to nuclear accumulation of XPO1 cargo proteins and RNA. Given the high number of XPO1 cargoes, this could lead to toxicity through widespread disruption in downstream processes.

### 3.4. Conclusions

In this chapter, we sought to identify proteins that interact with 1000-repeat DPR species, in an effort to uncover potential mechanisms of DPR toxicity. Previous studies have demonstrated that 1000-repeat DPRs possess different toxicity, morphology and localisation to shorter repeat DPRs. Our data demonstrate that these differences are also observed in the interactomes of 1000-repeat DPRs, both in terms of which proteins they interact with and the promiscuity of their protein interaction. Our findings highlight, as in previous studies, that individual DPRs species possess unique protein interactomes and biological processes enriched with these interactomes. Despite these unique DPR profiles, there is some overlap between DPRs, especially within the alanine-containing and arginine-containing DPRs. Many of the biological processes enriched within the DPR interactomes are relevant to neurodegenerative disease, including C9 FTD/ALS. In line with previous studies, we demonstrate elevated protein interaction of the arginine-containing DPRs, perhaps relating to their high toxicity. To identify GR1000-interacting proteins with a mechanistic role in GR1000 toxicity, we shortlisted 6 proteins identified by MS/MS. These shortlisted proteins were screened for modifiers GR1000 toxicity in a genetic interactions screen, performed in the *Drosophila* eye. We demonstrated that 2 of these proteins, CNOT1 and XPO1, are potential modifiers of GR1000 toxicity and therefore may have a mechanistic role in GR1000 toxicity. XPO1 in particular warrants further study, due to its previous implication in toxicity in models of C9 FTD/ALS.

## 4. Characterisation of XPO1 as a GR1000-interacting protein

### 4.1. Introduction

Having identified XPO1 as a potential modifier of GR1000 toxicity, we wanted to further characterise the nature of the XPO1-GR1000 interaction and its role in GR1000 toxicity. While CNOT1 was also identified as a potential modifier of GR1000 toxicity, we chose to focus our research on XPO1 given the evidence towards its particular relevance to C9 disease. NCT disruption has been identified across multiple forms of ALS (Kinoshita *et al.*, 2009; Nagara *et al.*, 2013; Shang *et al.*, 2017; Chou *et al.*, 2018; Aizawa *et al.*, 2019), including C9 disease (Freibaum *et al.*, 2015; Jovičić *et al.*, 2015; Zhang *et al.*, 2015; Lee *et al.*, 2016; Chou *et al.*, 2018; Solomon *et al.*, 2018). XPO1 has been implicated in ALS-related NCT defects, although evidence is conflicting. Additionally, modulation of XPO1 expression and activity has been shown to modulate ALS phenotypes and/or DPR toxicity (Freibaum *et al.*, 2015; Zhang *et al.*, 2015; Boeynaems *et al.*, 2016; Archbold *et al.*, 2018; Chou *et al.*, 2018; Steyaert *et al.*, 2018). With regards to XPO1 and DPRs, some studies have shown that XPO1 does not appear to physically interact with DPRs (Hutten *et al.*, 2020; Jafarinia, Van der Giessen and Onck, 2022) and that DPRs do not impair XPO1-mediated nuclear export (Vanneste *et al.*, 2019). However, Ramic *et al.* (2021) demonstrated that arginine-containing DPRs do disrupt XPO1-mediated nuclear export, while our own data (Chapter 3) reveals potential XPO1 interactions with the arginine-containing DPRs.

Data from our toxicity modifier screen reveals that genetic manipulation of XPO1 expression modifies GR1000 toxicity when XPO1 RNAi lines are co-expressed with GR1000 in the fly eye. While the *Drosophila* eye is an excellent system for screening modifiers of cytotoxicity, it does not permit the study of modifiers of more nuanced phenotypes caused by disruption of cellular processes without outright cytotoxicity. Eye phenotypes are also often driven largely during development and, as such, do not show age related changes. It is therefore important to study XPO1 in relation to other phenotypes associated with GR1000 expression. From published (West *et al.*, 2020) and unpublished data from our group, we have demonstrated that pan-neuronal expression of GR1000 causes reduced lifespan; brain vacuolisation; age-related motor decline; and reduced activity. These complex phenotypes likely occur as the culmination of GR1000-mediated disruption in multiple cellular and molecular processes, perhaps including NCT.

In order to develop our understanding of the mechanistic role of XPO1 in GR1000 toxicity, it is also important to investigate the nature of the GR1000-XPO1 interaction *in vivo*. By studying this interaction, we hope to characterise how the physiological function of XPO1 is affected by its interaction with GR1000. With this knowledge, we can begin to understand

the effects of GR1000 expression on nuclear export and downstream processes. This would provide further insight into molecular mechanisms of GR1000 toxicity.

Therefore, in this chapter we aim to:

1. Establish whether XPO1 is a modifier of GR1000-mediated phenotypes
2. Characterise how XPO1 is affected by the GR1000-XPO1 interaction

## 4.2. Results

### 4.2.1. Knockdown of XPO1 modifies age-related GR1000 motor deficits

One of the most ALS-relevant phenotypes observed in flies pan-neuronally expressing GR1000 is an age-related decline in motor function. West *et al.* (2020) showed previously that flies pan-neuronally expressing GR1000 exhibit a significant age-related decline in climbing ability starting at 14 days post eclosion (dpe). We replicate these findings here in flies pan-neuronally (nSyb-Gal4 (II)) expressing GR1000 alongside an RNAi control (UAS-mCherry RNAi) (Fig. 4.1). By 28 dpe, almost all GR1000-expressing flies are unable to climb at all. While control flies pan-neuronally expressing UAS-mCD8-GFP (GFP) also exhibit an age-related decrease in climbing ability, it is not as severe as in GR1000 flies (Fig 4.1A, C, D).

Two independent XPO1-RNAi lines, XPO1<sup>(1)</sup>-RNAi (RRID:BDSC\_34021) and XPO1<sup>(2)</sup>-RNAi (RRID:BDSC\_31353) were used to examine the effect of pan-neuronal XPO1 knockdown on GR1000 toxicity. Pan-neuronal (nSyb-Gal4 (II)) RNAi knockdown of XPO1 had mixed effects on motor function. Knockdown using the XPO1<sup>(1)</sup> RNAi line, which has previously been reported as showing ~85% knockdown efficiency, caused a significant and near ablation of climbing in GFP control flies from 7 dpe onwards, causing lethality by 28 dpe (Fig. 4.1A,B, E). Flies pan-neuronally co-expressing GR1000 with XPO1<sup>(1)</sup>-RNAi demonstrated significantly increased climbing ability compared to XPO1<sup>(1)</sup>-RNAi in a GFP control background at 7 dpe but not at later timepoints (Fig 4.1A, B). Despite this, the climbing ability of flies co-expressing GR1000 with XPO1<sup>(1)</sup>-RNAi was significantly reduced compared to those co-expressing GR1000 with an RNAi Control (mCherry-RNAi) at 7 dpe (Fig. 4.1B). XPO1<sup>(2)</sup>-RNAi, previously reported to show ~40 % knockdown efficiency, alongside expression of GR1000 caused a significant increase in climbing ability at 7 dpe compared to flies co-expressing GR1000 with an RNAi Control (Fig. 4.1B). XPO1<sup>(2)</sup>-RNAi also delayed the age-related decline in climbing ability of GR1000 flies compared to GFP controls (Fig. 4.1A, C, D). Flies pan-neuronally co-expressing GR1000 with XPO1<sup>(2)</sup>-RNAi demonstrated significantly reduced climbing ability compared to flies co-expressing XPO1<sup>(2)</sup>-RNAi in a GFP

control background at 21 and 28 dpe (Fig. 4.1D, E), where a significant reduction was seen from 14 dpe onwards in their RNAi control counterparts (Fig. 4.1C).

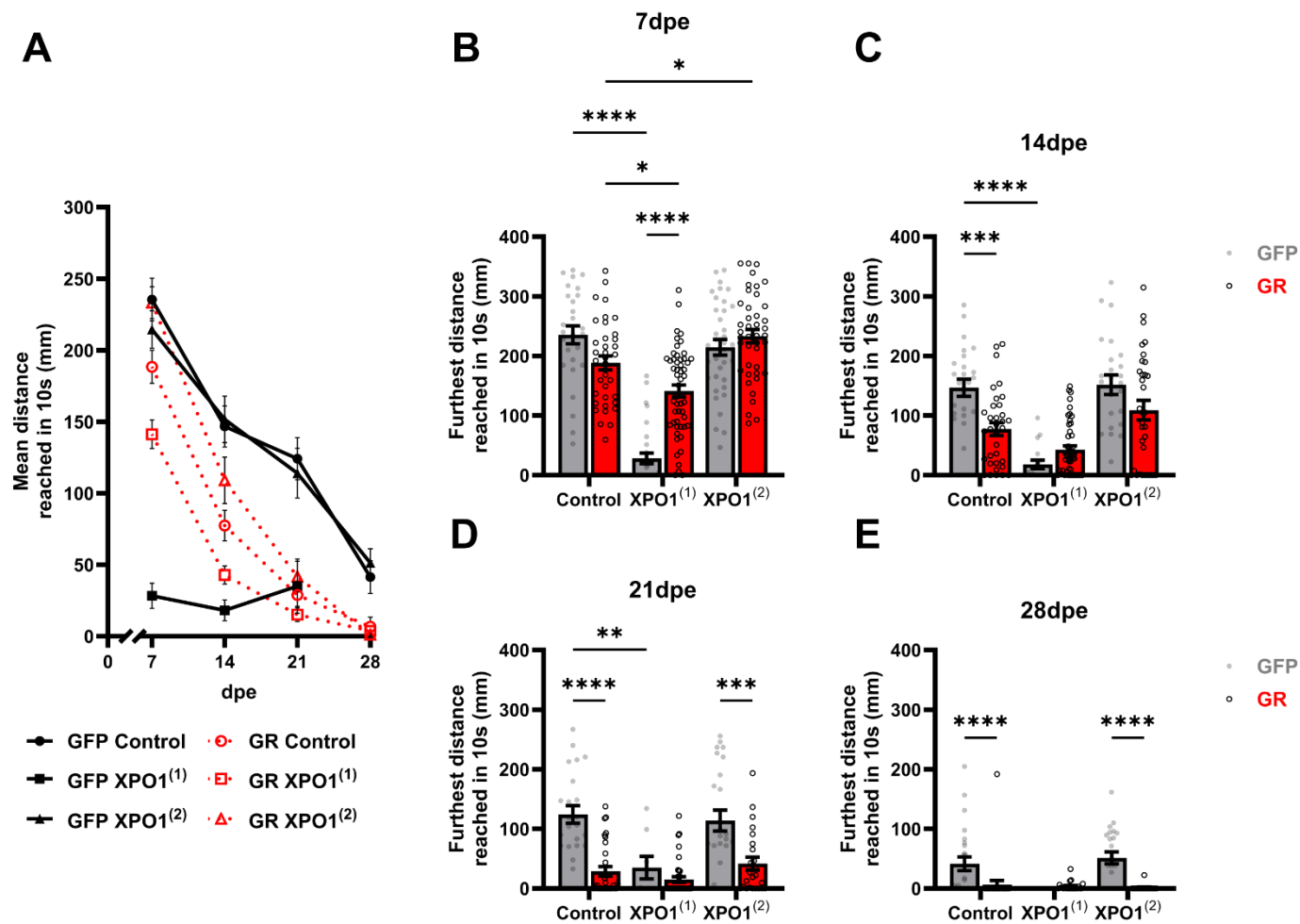


**Figure 4.1. Knockdown of XPO1 delays age-related motor decline in flies pan-neuronally expressing GR1000.** A) Quantification of fly climbing ability throughout the fly lifetime. Climbing ability was measured as the furthest distance reached in 10 seconds in SING assay at B) 7, C) 14, D) 21 and E) 28 days post eclosion (dpe). Flies pan-neuronally (nSyb-Gal4 (II)) expressing GFP or GR1000, alongside mCherry RNAi (control) or XPO1 RNAi were used. Points represent individual flies; bars represent mean and error bars show SEM. Stats are two-way ANOVA with Šídák's multiple comparisons test of preselected pairs. \*  $p < 0.05$ , \*\*  $p < 0.01$ , \*\*\*  $p < 0.001$ , \*\*\*\*  $p < 0.0001$ . N = 3.

#### **4.2.2. GR1000 motor activity deficits are not modified by knockdown of XPO1**

Another motor phenotype associated with pan-neuronal expression of GR1000 is a reduction in motor activity. Fly motor activity can be measured using *Drosophila* activity monitors (DAM), whereby individual flies are housed in sealed tubes with infrared beams passing across the tube at points along the length of the tube. When a fly breaks a beam, it is recorded as a count. Total counts are recorded across a 24 hour period as a measure of motor activity.

We have previously observed that pan-neuronal expression of GR1000 causes a significant decrease in activity compared to controls expressing GFP at all timepoints. These observations are replicated here in flies pan-neuronally (nSyb-Gal4 (II)) expressing GR1000 alongside an RNAi control (Fig. 4.2).

At earlier timepoints, pan-neuronal expression of XPO1<sup>(1)</sup>-RNAi caused a significant reduction in activity in both GFP and GR1000 flies, compared to their control counterparts (Fig. 4.2). There was no significant difference in activity between flies co-expressing XPO1<sup>(1)</sup>-RNAi and GFP and those expressing XPO1<sup>(1)</sup>-RNAi and GR1000. XPO1<sup>(2)</sup>-RNAi did not rescue the activity deficits in GR1000 flies compared to GFP flies, despite increasing the activity of GFP flies at 8dpe (Fig. 4.2A).

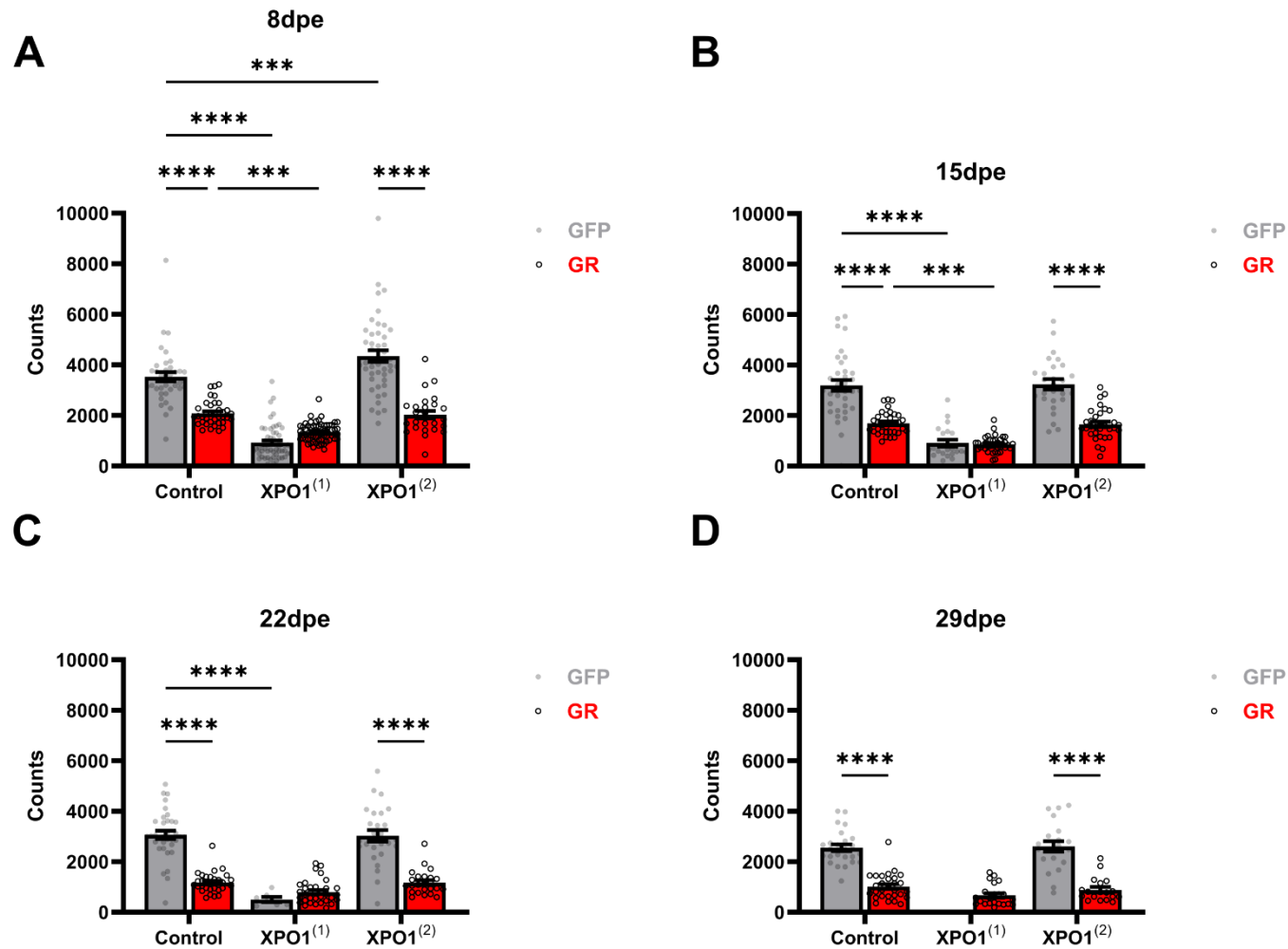


**Figure 4.2. Knockdown of XPO1 does not modify activity deficits in flies pan-neuronally expressing GR1000.** Activity was measured as total counts in a 24 hour period at A) 8, B) 15, C) 22 and D) 29 dpe. Flies pan-neuronally (*nSyb-Gal4 (II)*) expressing GFP or GR1000, alongside *mCherry RNAi* (control) or XPO1 RNAi were used. Points represent individual flies; bars represent mean and error bars show SEM. Stats are two-way ANOVA with Šídák's multiple comparisons test of preselected pairs. \*  $p < 0.05$ , \*\*  $p < 0.01$ , \*\*\*  $p < 0.001$ , \*\*\*\*  $p < 0.0001$ .  $N = 3$ .

### 4.2.3. XPO1 is a modifier of GR1000 sleep phenotypes

Sleep disturbances have been reported in 30-75 % of FTD patients and over 70 % of ALS patients (Srikanth, Nagaraja and Ratnavalli, 2005; Fernández Martínez *et al.*, 2008; Guarnieri *et al.*, 2012; Devenney *et al.*, 2021) but are often overlooked in studies of both diseases. DPRs have been identified in circadian and sleep associated cells in C9 FTD and ALS patients, perhaps mediating sleep disturbances in these cases (Dedeene *et al.*, 2019). Sleep phenotypes have also been observed and associated with DPRs in *Drosophila* models of FTD/ALS (Godfrey *et al.*, 2023; Uy *et al.*, 2024). Having observed reduced activity in flies pan-neuronally expressing GR1000, we sought to investigate whether this could also be associated with sleep disturbances and whether they are modified by knockdown of XPO1. In *Drosophila*, sleep is defined as a period of inactivity lasting 5 minutes or longer (Cirelli and Bushey, 2008). As such, sleep can be measured in flies using DAM data from activity experiments.

Pan-neuronal co-expression of an RNAi control with GR1000 caused a significant increase in total sleep compared to flies co-expressing the RNAi control with GFP at 8, 15 and 29 dpe (Fig. 4.3A, B, D). Pan-neuronal co-expression of GR1000 with RNAi control also caused an age-related increase in dark sleep bout duration compared to flies co-expressing GFP with RNAi control (Fig. 4.4B, C, D). Light sleep bout duration remained relatively unaffected by GR1000 expression (Fig. 4.4). Flies pan-neuronally co-expressing GFP or GR1000 with XPO1<sup>(1)</sup>-RNAi both demonstrated significantly increased total sleep compared to their RNAi control counterparts, although this effect was lost at 22 and 15 dpe respectively (Fig. 4.3B, C). However, the age-related increase in total sleep observed between GR1000 and GFP flies in an RNAi control background was completely ablated by severe knockdown of XPO1 using XPO1<sup>(1)</sup> RNAi (Fig. 4.3A, B, C). Increased total sleep in GR1000 flies was also observed alongside XPO1<sup>(2)</sup>-RNAi expression, although this was only significant at 8 and 29 dpe (Fig. 4.3A, D). Interestingly, the GR1000-mediated age-related increase in dark sleep bout duration was delayed by XPO1<sup>(2)</sup>-RNAi expression and was associated with a similar increase in light sleep bout duration (Fig 4.4C, D).

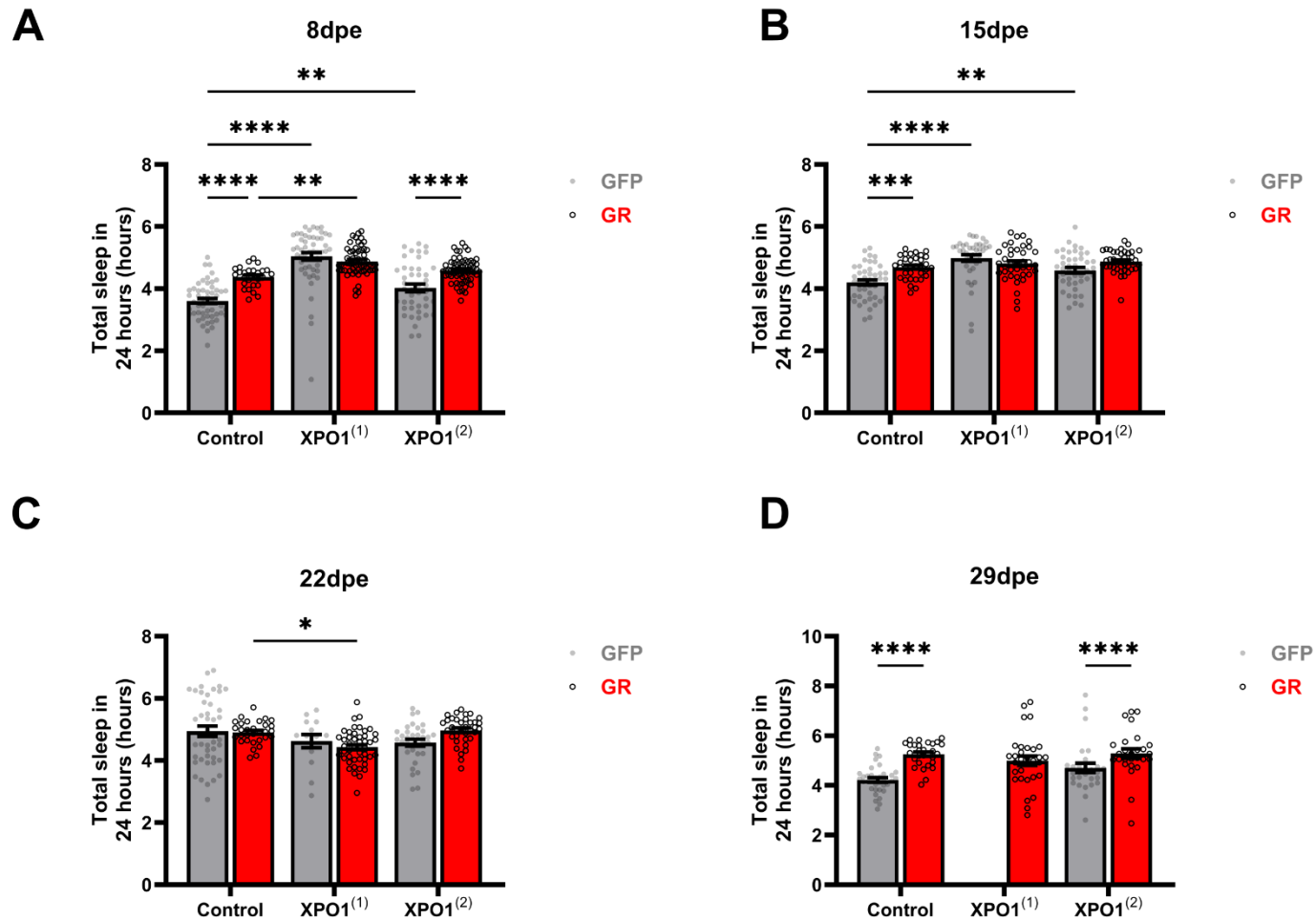


**Figure 4.3. Total sleep is increased in flies pan-neuronally expressing GR1000.** Total sleep was measured in a 24 hour period at A) 8, B) 15, C) 22 and D) 29 dpe. Flies pan-neuronally (nSyb-Gal4 (II)) expressing GFP or GR1000, alongside mCherry RNAi (control) or XPO1 RNAi were used. Points represent individual flies; bars represent mean and error bars show SEM. Stats shown are two-way ANOVA with Šídák's multiple comparisons test of preselected pairs. \*  $p < 0.05$ , \*\*  $p < 0.01$ , \*\*\*  $p < 0.001$ , \*\*\*\*  $p < 0.0001$ . N = 3.

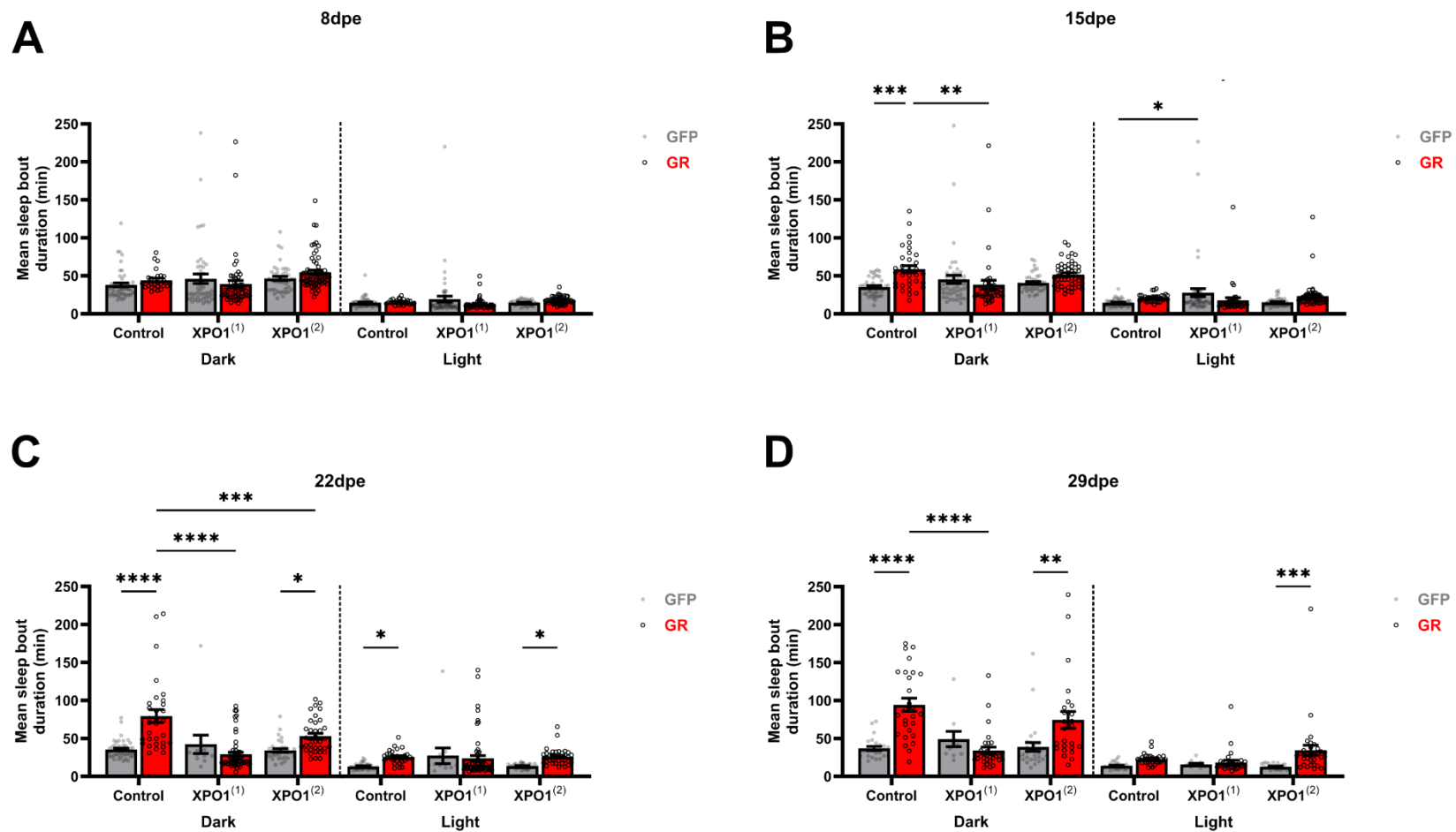


**Figure 4.4. Pan-neuronal expression of GR1000 causes changes in sleep bout duration that are modified by knockdown of XPO1.** Sleep bout duration was measured across light and dark phases in a 24 hour period. Flies pan-neuronally (nSyb-Gal4 (II)) expressing GFP or GR1000, alongside mCherry RNAi (control) or XPO1 RNAi were used. Flies were assayed at 8, 15, 22 and 29 dpe. Points represent individual flies; bars represent mean and error bars show SEM. Stats shown are two-way ANOVA with Šídák's multiple comparisons test of preselected pairs. \*  $p < 0.05$ , \*\*  $p < 0.01$ , \*\*\*  $p < 0.001$ , \*\*\*\*  $p < 0.0001$ . N = 3.

#### 4.2.4. Interaction with GR1000 does not disrupt XPO1 localisation or function

Under the hypothesis of DPR toxicity via protein sequestration, said sequestration leads to altered protein function which causes toxicity. To understand how the GR1000-XPO1 interaction contributes to GR1000-mediated toxicity and phenotypes, it is important for us to understand how XPO1 function is affected by this interaction. As a nuclear export protein, XPO1 constantly shuttles between the nucleus and the cytoplasm in its transport of cargo, making XPO1 localisation key to its function (Stade *et al.*, 1997). By interacting with GR1000, XPO1 localisation is likely to be disrupted, therefore severely impairing XPO1 function. GR1000 localises predominantly in the cytoplasm, with some nuclear presence (Mackenzie *et al.*, 2015; Callister *et al.*, 2016; West *et al.*, 2020). Therefore, we hypothesised that GR1000 would cause a more cytoplasmic localisation of XPO1. We sought to investigate this hypothesis via antibody-based approaches, such as immunocytochemistry and Western blotting.

To our knowledge only one antibody has been generated against *Drosophila* XPO1 (Roth *et al.*, 2003), however this antibody was unavailable to us. XPO1 is a highly conserved protein with *Drosophila* XPO1 sharing 71 % sequence identity with human XPO1 (Collier *et al.*, 2000). Therefore, we were able to identify an antibody against human XPO1 ( $\alpha$ -XPO1, 27917-1-AP, Proteintech) that had the potential to bind *Drosophila* XPO1, as it was raised against an epitope with high sequence homology. Other groups have successfully used antibodies raised against human XPO1 to identify *Drosophila* XPO1 previously (Fasken *et al.*, 2000). Given that this antibody has not been used in *Drosophila* before, it was important for us to validate its recognition of *Drosophila* XPO1. Validation was performed by Western blotting of protein lysates extracted from the heads of flies pan-neuronally expressing XPO1<sup>(1)</sup>-RNAi, XPO1<sup>(2)</sup>-RNAi or UAS-XPO1 and comparing XPO1 levels to protein extracted from wild-type (wt) flies. Anti-XPO1 staining revealed a pattern of multiple bands that was consistent between conditions (Appendix Fig. 7.1). Among these was a band at roughly 120 kDa (Fig. 4.5A), the previously reported molecular weight of XPO1 in *Drosophila* (Fasken *et al.*, 2000). Quantification of this band revealed a 47 % reduction of band intensity by XPO1<sup>(1)</sup> but a 16 % increase by XPO1<sup>(2)</sup> relative to wild-type (Fig. 4.5B). We expected to observe a ~130 kDa band in the UAS-XPO1 condition, corresponding to the XPO1 tagged with the C-terminus of Venus which is overexpressed in this line. A band at ~130 kDa was observed but it was observed in all conditions, indicating that it was unlikely to be tagged XPO1 (Fig. 4.5A). 120 kDa band intensity in the UAS-XPO1 overexpression line were equal to wild-type (Fig. 4.5B). Interestingly, a band at roughly 105 kDa was present in both RNAi conditions but in neither wild-type nor overexpression conditions (Appendix Fig. 7.1).

Despite confusing results in the antibody validation, we wanted to investigate the effects of GR1000 expression on the localisation of the 120 kDa protein, which is the most likely to be XPO1, identified by anti-XPO1. To examine localisation by Western blotting we performed nuclear/cytoplasmic fractionation of protein from the heads of flies pan-neuronally (nSyb-Gal4 (III) expressing either GFP or GR1000. If the GR1000-XPO1 interaction disrupts XPO1 localisation then we would expect to see a GR1000-associated shift in XPO1 levels between the cytoplasm and nucleus. Western blotting revealed a 120 kDa band in the cytoplasmic fraction of both GFP and GR1000 flies (Fig. 4.5C), however no band was present in the nuclear fraction of either (Appendix Fig. 7.2). The absence of a nuclear band is likely due to low total protein concentrations obtained by nuclear fractionation, especially given the low intensity of the band in the cytoplasmic fraction of reasonable total protein concentration. Despite not detecting the 120 kDa protein in nuclear fractions, we sought to assess nuclear/cytoplasmic localisation of the protein by quantifying the cytoplasmic fraction alone. Quantification revealed no significant difference in the intensity of the 120 kDa band between cytoplasmic fractions from GFP and GR1000 flies (Ratio paired t-test,  $p = 0.55$ ) (Fig. 4.5D).

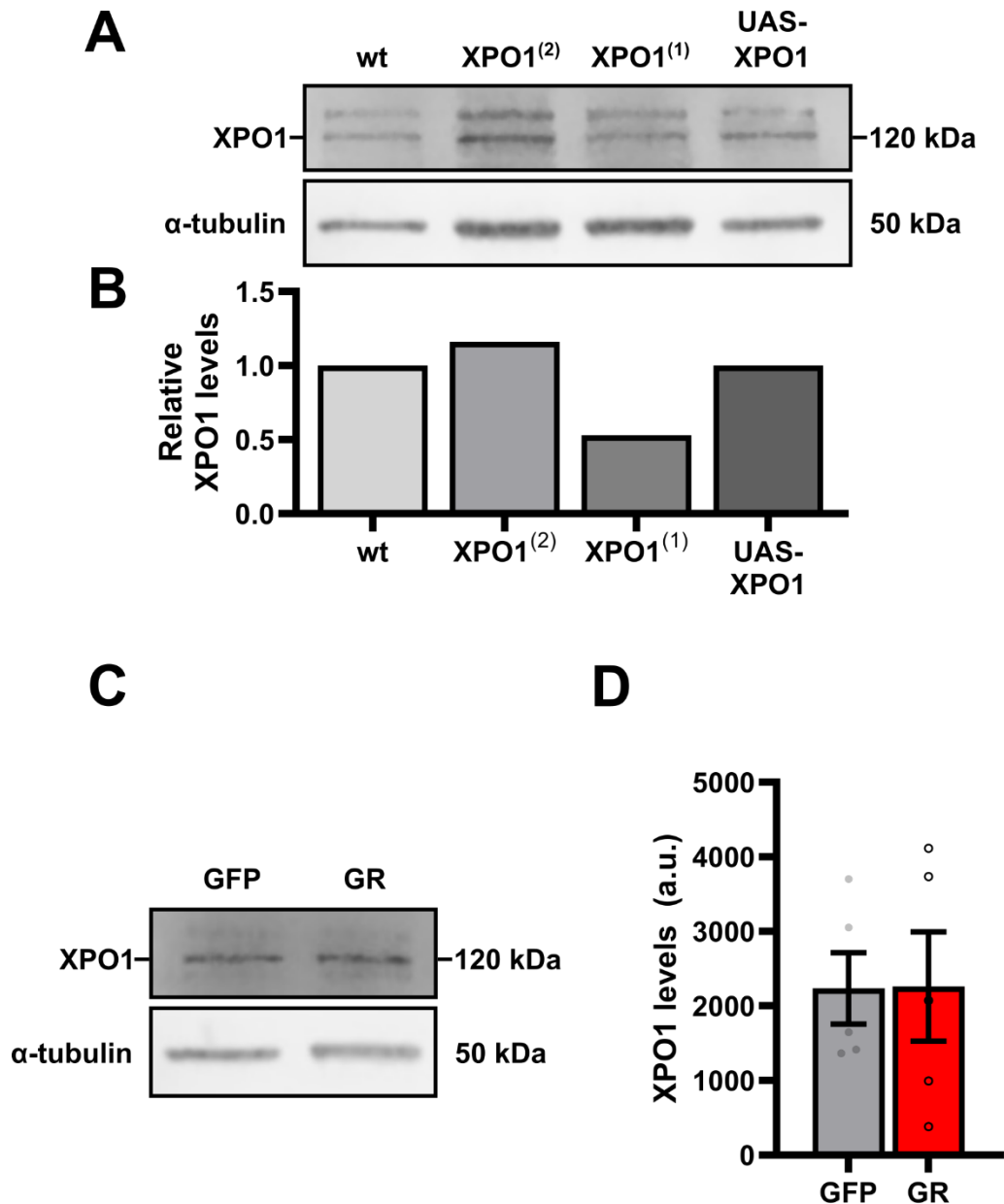


**Figure 4.5. Cytoplasmic 120 kDa band intensity does not change with GR1000 expression.** A) Western blot of head protein from wt (CantonS crossed to OregonR) flies or flies pan-neuronally (nSyb-Gal4 (III)) expressing noted constructs.  $\alpha$ -tubulin was used as a loading control. B) Quantification of 120 kDa band from A, normalised to  $\alpha$ -tubulin band intensity. Quantification is shown as relative to wild-type. C) Representative Western blot of head cytoplasmic protein fraction from flies pan-neuronally (nSyb-Gal4 (III)) expressing GFP or GR1000. D) Quantification of Western blots represented in C. Individual points represent biological replicates; bars represent mean and error bars show SEM.

Next, we sought to study XPO1 localisation by immunohistochemical analysis. While this facilitates better visualisation of changes in XPO1 localisation, it does not permit the same quantification as Western blotting. We began with immunohistochemical analysis of the salivary glands of *Drosophila* larvae expressing either GFP or GR1000 under the control of *OK6-Gal4*, which drives expression in larval salivary glands, among other tissues. While larval salivary glands are not a neuronal tissue and therefore bear little disease relevance, previous studies have demonstrated that their large cellular and nuclear size facilitates easy visualisation of nuclear and cytoplasmic localisation of proteins (Solomon *et al.*, 2018; West *et al.*, 2020). Anti-XPO1 staining revealed no clear localisation pattern in GFP or GR1000 expressing flies (Fig. 4.6A). Quantification of anti-XPO1 signal identified no significant difference in nuclear/cytoplasmic signal between GFP and GR1000 (Fig. 4.6B). It must be noted that validation of the anti-XPO1 antibody for IHC, using XPO1 RNAi and overexpression lines, was not performed as it was for Western blotting. Therefore, we are unable to confirm that anti-XPO1 is recognising *Drosophila* XPO1 via IHC. In an effort to assess GR1000-mediated effects on XPO1 function, we also stained for two proteins which are exported from the nucleus by XPO1: YAN and exd (Abu-Shaar, Ryoo and Mann, 1999; Tootle, Lee and Rebay, 2003). Staining revealed nuclear and cytoplasmic localisation of both proteins in both GFP and GR1000, although nuclear signal was more readily visible than with anti-XPO1 (Fig. 4.6A). Quantification revealed a trend towards increased nuclear signal of both proteins in GR1000 flies, although this effect was not significant (Fig. 4.6B). We sought to quantify this increase more accurately by Western blotting for both YAN and exd in nuclear/cytoplasmic fractionation blots. However, the antibodies for both proteins were not suitable for Western blotting.

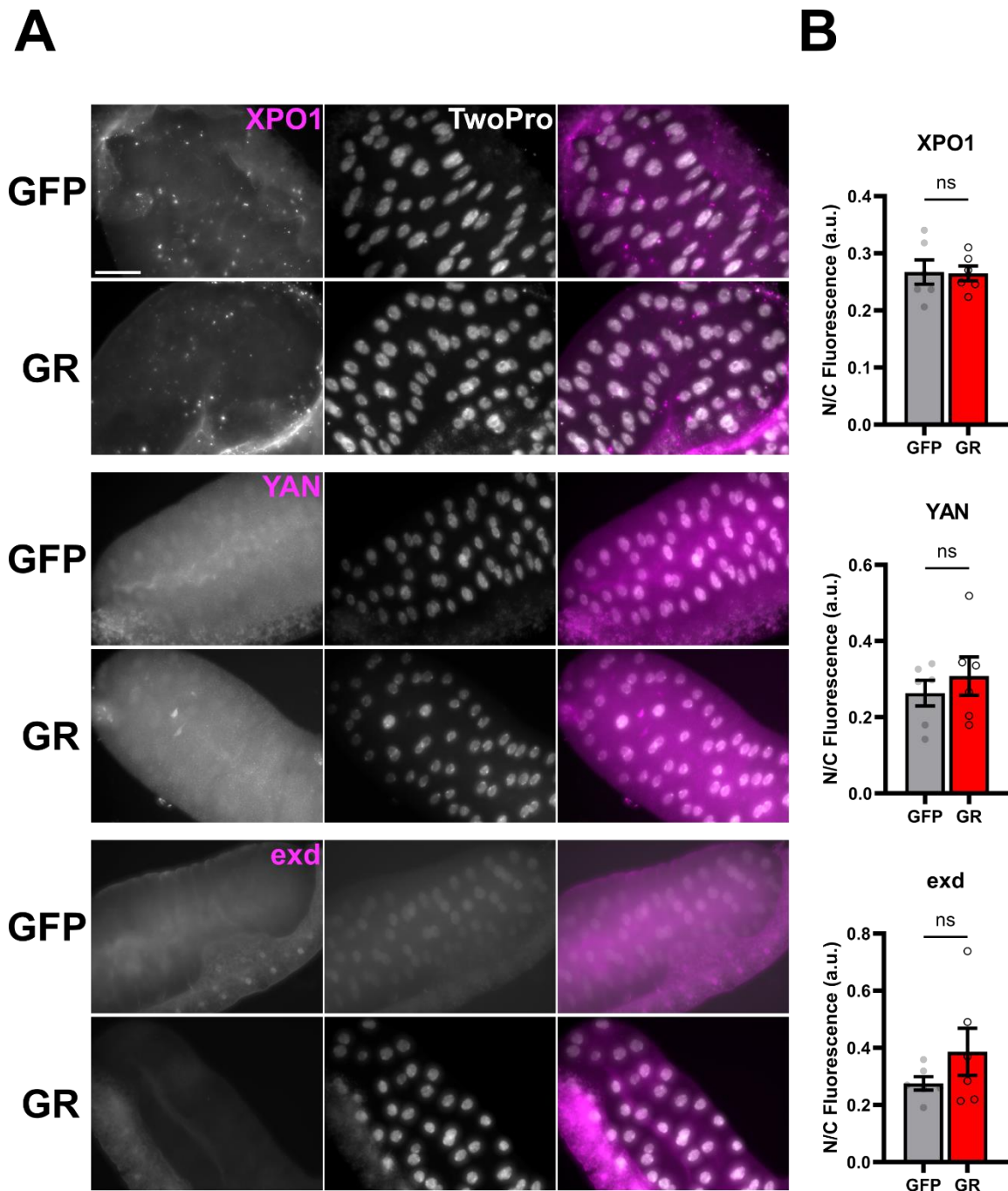


**Figure 4.6. Localisation of anti-XPO1 signal and its cargoes, exd and YAN, is not significantly affected by GR1000 expression.** A) Representative fluorescence microscopy images of salivary glands from 3<sup>rd</sup> instar larvae expressing (OK6-Gal4) GFP or GR1000 and stained for noted proteins (magenta). TwoPro3 staining was used to identify nuclei. Scale bar is 100  $\mu$ m. B) Quantification of nuclear/cytoplasmic fluorescence in images represented in A. Points represent biological replicates; bars represent mean and error bars show SEM. Stats shown are unpaired t-test with Welch's correction (XPO1:  $p = 0.93$ , YAN:  $p = 0.48$ , exd:  $p = 0.25$ ).

Finally, we sought to examine the localisation of anti-XPO1 signal in neurons using immunocytochemistry. Briefly, *Drosophila* primary neurons were cultured, from embryos pan-neuronally (nSyb-Gal4 (III)) expressing GFP or GR1000, *in vitro* before staining with anti-XPO1. In both GFP and GR1000 expressing neurons, anti-XPO1 signal was predominantly observed in the cell body with some axonal presence. Due to a limited number of fluorescent channels, we were unable to stain for nuclei and thus cannot determine whether anti-XPO1 signal in the cell body is nuclear, cytoplasmic or both (Fig. 4.7). Repeated contamination in primary cultures prevented us from obtaining more than one biological replicate and, therefore, quantification of anti-XPO1 signal localisation.

In their study of NCT impairments in a *Drosophila* model of C9 disease, Freibaum *et al.* (2015) identified nuclear envelope abnormalities in larval salivary glands expressing (G<sub>4</sub>C<sub>2</sub>)<sub>58</sub>. Given previous evidence for the arginine-containing DPRs disrupting wider nuclear processes (Mizielinska *et al.*, 2017), we sought to investigate such disruption in GR1000-expressing flies. The nuclear envelope was visualised using the RFP-Nup107 line, in which the nuclear envelope protein Nup107 has been endogenously tagged with RFP (Katsani *et al.*, 2008). In their model, Freibaum *et al.* (2015) observed a wrinkled appearance of the nuclear envelope and nuclear inclusions of RFP-Nup107. In larval salivary glands expressing GFP or GR1000 we observed nuclei with a wrinkled nuclear envelope and delamination of the nuclear envelope (Fig. 4.8A, inset). Quantification of the proportion of abnormal nuclei in each condition revealed a trend towards increased nuclear abnormalities in GR1000, although this effect was not significant (Fig. 4.8B).

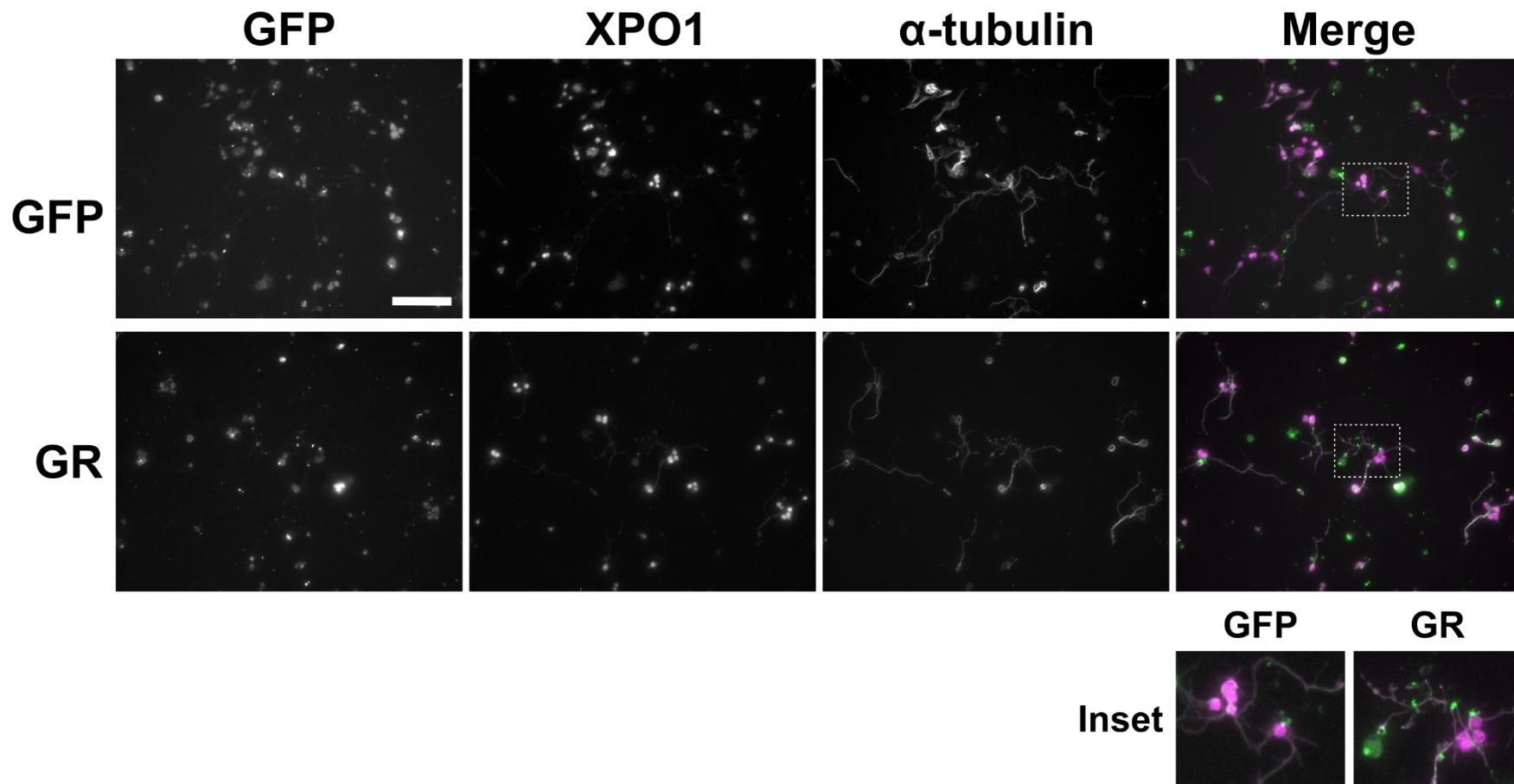


**Figure 4.7. Anti-XPO1 signal localises predominantly to the neuronal cell body in *in vitro* *Drosophila* primary neurons.** Representative fluorescence microscopy images of *Drosophila* primary neurons expressing (nSyb-Gal4 (III)) either GFP or GR1000. Scale bar is 50µm.

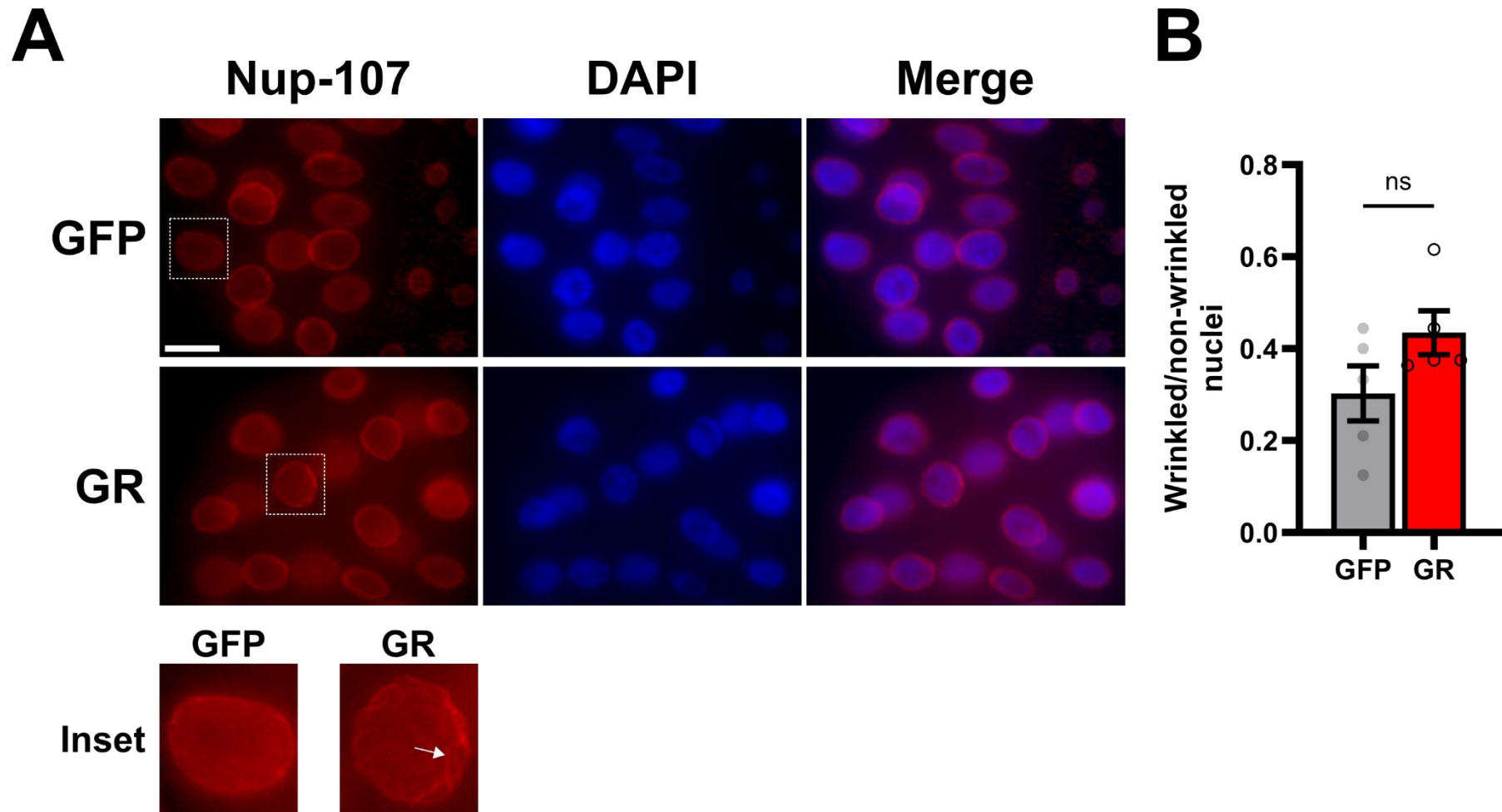


**Figure 4.8. Nuclear envelope abnormalities are not significantly more common in flies expressing GR1000.** A) Representative images of salivary glands from 3<sup>rd</sup> instar larvae expressing (OK6-Gal4) GFP or GR1000 alongside RFP-Nup107. White arrow illustrates wrinkling and delamination of the nuclear envelope for quantification. Scale bar is 50  $\mu$ m. DAPI was used to visualise nuclei. B) Quantification of the ratio of nuclei with/without nuclear delamination. Points represent biological replicates; bars represent mean and error bars show SEM. Stats shown are unpaired t-test with Welch's correction ( $p = 0.122$ ).

### 4.3. Discussion

#### 4.3.1. Severe knockdown of XPO1 is detrimental

The XPO1<sup>(1)</sup>-RNAi line has previously been shown to cause an 85 % reduction in XPO1 mRNA. Our Western blot data show that this mRNA reduction is associated with a 50 % reduction in the intensity of the 120 kDa band revealed by anti-XPO1 (Fig. 4.5B), although this data should be interpreted carefully as only one biological replicate was used; the antibody used was not fully validated; and the 120 kDa band was not confirmed as XPO1. Despite these caveats, there appears to be a consensus among our and previous data that XPO1<sup>(1)</sup>-RNAi induces more severe knockdown of XPO1 compared to XPO1<sup>(2)</sup>-RNAi.

XPO1<sup>(1)</sup>-RNAi caused a significant reduction in the climbing ability and activity of flies pan-neuronally (nSyb-Gal4 (II)) expressing GFP, with a near ablation of climbing even in young flies. XPO1<sup>(1)</sup>-RNAi significantly reduced the climbing and activity of young flies pan-neuronally expressing GR1000, although this reduction was not as severe as in GFP flies. XPO1<sup>(1)</sup>-RNAi also caused an increase in total sleep in young GFP flies. While a similar effect was observed in 8 dpe flies co-expressing GR1000 and XPO1<sup>(1)</sup>-RNAi, it was reversed by 22 dpe. The negative effects of XPO1<sup>(1)</sup>-RNAi on GFP control flies compared to their GR1000 counterparts is exemplified by the observation that no flies co-expressing GFP and XPO1<sup>(1)</sup>-RNAi survived to 28 dpe.

Altogether, our data suggest that severe knockdown of XPO1 is harmful in *Drosophila*, causing severe impairments in GFP flies. While this knockdown also exacerbated GR1000-mediated phenotypes, GR1000 flies were not as drastically affected as their GFP counterparts. Given that XPO1 loss of function has been shown to be lethal in *Drosophila* (Collier *et al.*, 2000), it is unsurprising that severe knockdown is also deleterious. If GR1000 toxicity is mediated by XPO1 sequestration and functional impairment, it is understandable that XPO1 knockdown and further functional impairment would exacerbate GR1000-mediated phenotypes. However, the disparity in phenotypic severity between flies co-expressing GFP and XPO1<sup>(1)</sup>-RNAi and those co-expressing GR1000 and XPO1<sup>(1)</sup>-RNAi is an unexpected and intriguing observation. We propose two hypotheses for this disparity. The first is that GR1000 causes maximal disruption to XPO1 function, such that severe XPO1 knockdown in GR1000 flies cannot cause much more impairment as it can in GFP flies. The other hypothesis is that cells expressing GR1000 circumvent impairments in XPO1 function by upregulating other nuclear export pathways. Therefore, severe knockdown of XPO1 does not affect GR1000 flies as much as GFP flies because GR1000 are already compensating for XPO1 functional impairments. This hypothesis is built upon the observed redundancy among NCT pathways (Baade and Kehlenbach, 2019).

### 4.3.2. Partial knockdown of XPO1 delays the onset of age-related GR1000 phenotypes

Behavioural experiments revealed the potential of XPO1<sup>(2)</sup>-RNAi to modify, by delaying or slowing the onset of, age-related GR1000 phenotypes. Compared to RNAi control, XPO1<sup>(2)</sup>-RNAi significantly increased the climbing ability of flies pan-neuronally (nSyb-Gal4 (II)) expressing GR1000 (Fig. 4.1). This increase at 7 dpe was associated with a 7 day delay in the onset of significant climbing deficits of GR1000-expressing flies relative to GFP controls. Age-related motor deficits are the characteristic symptoms of ALS, so the observation that partial knockdown can delay their onset in a *Drosophila* model of the disease is extremely interesting from an ALS perspective. A similar effect is seen in the age-related increase in dark sleep bout duration (Fig. 4.4). Interestingly, partial knockdown does not cause an amelioration of GR1000-mediated activity deficits. However, we have previously shown in the lab that these deficits are not age-related and are present from eclosion. Thus activity, sleep and motor dysfunction in GR1000 expressing flies may be underpinned by perturbations to distinct molecular mechanisms, not all of which can be alleviated by knockdown of XPO1.

A potential caveat to these findings is that our validation data indicates that XPO1<sup>(2)</sup>-RNAi partially increases, rather than partially decreasing, the intensity of the 120 kDa band revealed by anti-XPO1 staining (Fig. 4.5A). However, this validation data also comes with its own aforementioned caveats and XPO1<sup>(2)</sup>-RNAi has previously been validated and used extensively (Sowa *et al.*, 2018; Cunningham *et al.*, 2020; Okazaki, Yamazoe and Inoue, 2020; Rossi *et al.*, 2021). Therefore, we are inclined to believe that XPO1<sup>(2)</sup>-RNAi is causing a partial knockdown of XPO1 in our model and the limitations lie within the availability of antibodies for quantification of protein abundance.

The ability of partial knockdown to slow the onset of age-related phenotypes, but not ameliorate basal deficits, provides insight into the potential role of XPO1 in mediating these phenotypes. Their age-related nature suggests that these phenotypes are caused by the accumulation of some biological damage or toxicity at the cellular and/or molecular level. In the case of XPO1, the most obvious hypothesis would be that the GR1000-XPO1 interaction leads to the toxic nuclear accumulation of XPO1 cargo. This could explain the observed increase in nucleolar volume associated with GR inclusions in neurons of C9 patients and in GR100 expressing *Drosophila* (Mizielinska *et al.*, 2017). While our data do show a trend towards the nuclear accumulation of XPO1 cargoes exd and YAN in GR1000-expressing salivary glands, this effect is not significant ( $p = 0.25$  and  $0.48$  respectively) (Fig. 4.6B). However, it is important to note that the broad confidence intervals seen in the quantification

of XPO1 targets YAN and exd in GR1000 expressing flies, compared to controls, raise the possibility that the sample size is insufficient to draw definitive conclusions (YAN: GFP; 95% CI[0.18,0.35], GR; 95% CI[0.18,0.44], exd: GFP; 95% CI[0.22,0.34], GR; 95% CI[0.17,0.60]). It is worth considering that the accumulation of cargo could very well require time provided by aging, which cannot be achieved in larval tissues. To account for this, future experiments should look to characterise the localisation and potential nuclear accumulation of XPO1 cargoes in the nervous system of GR1000 models throughout the adult lifespan. To improve the resolution of these experiments and/or to perform them in specific neurons would require the generation of new tagged lines, which was beyond the scope of this thesis. Our data is consistent with the finding that GR20 does not obstruct XPO1-mediated nuclear export (Vanneste *et al.*, 2019). Two studies observed neuroprotective effects of pharmacological inhibitors of XPO1 in model of ALS (Zhang *et al.*, 2015; Chou *et al.*, 2018). However, neuroprotective effects were only observed at low pharmacological doses, with higher doses resulting in neurotoxicity. Interestingly, Archbold *et al.* (2018) demonstrated that only the higher, not the lower, doses used in these studies actually cause inhibition of XPO1-mediated nuclear export. Therefore, these studies support the hypothesis of toxicity through the nuclear accumulation of XPO1 cargo.

An alternative hypothesis would be that the GR1000-XPO1 interaction leads to the accumulation of toxic species through a gain-of-function mechanism. This is supported by our finding that partial knockdown of XPO1 by XPO1<sup>(2)</sup>-RNAi delays the onset of GR1000 phenotypes. One possible gain-of-function mechanism would be the sequestration of XPO1 cargo to GR inclusions, through the interaction of sequestered XPO1 with the nuclear export signal (NES) of its cargo. XPO1, along with other NCT proteins, has already been shown to be recruited to TDP-43 inclusions by its interaction with the TDP-43 NES (Chou *et al.*, 2018). Since XPO1 cargo proteins have been identified in a plethora of cellular and molecular processes (Baade and Kehlenbach, 2019), their sequestration could lead to a range of aberrant effects. However, we did not observe inclusions of XPO1 or its cargoes in GR1000-expressing cells. Although, it is worth noting that our study was limited by suitability of antibodies against XPO1 and its cargoes.

#### **4.3.3. XPO1 localisation and function may be unaffected by the GR1000-XPO1 interaction**

Here, we attempted to study the effects of the GR1000-XPO1 interaction on XPO1 localisation and, therefore, function using antibody-based approaches. Due to a lack of antibodies targeting *Drosophila* XPO1, we opted to use an antibody raised against a human

XPO1 epitope with high sequence homology to *Drosophila* XPO1. We attempted to validate this anti-XPO1 for use in Western blotting, but not IHC, of *Drosophila* XPO1 using XPO1 RNAi and overexpression lines. Anti-XPO1 did recognise a protein at 120 kDa, the previously reported molecular weight of *Drosophila* XPO1, but our validation data indicated that this was unlikely to be XPO1. Our validation data indicated that either anti-XPO1 does not recognise *Drosophila* XPO1, or XPO1 RNAi and overexpression lines were not working as intended. Given that the expression lines had been previously used, validated, and had demonstrated expected effects in behavioural experiments, we believe that the unclear data likely arises from anti-XPO1 not recognising *Drosophila* XPO1 in Western blotting. Regardless, cytoplasmic levels of the 120 kDa protein were observed to be equal between GFP and GR1000.

While our data do not support the use of anti-XPO1 in Western blotting of *Drosophila* samples, we did not perform validation of the antibody for use in IHC of *Drosophila* tissue. Therefore, we cannot confirm that the antibody is unsuitable for use in IHC experiments. However, we must also be cautious about drawing conclusions from these experiments. Localisation of anti-XPO1 signal did not appear to be altered by expression of GR1000 in *Drosophila* primary neurons or larval salivary glands, indicating that XPO1 localisation may be unaffected by GR1000. This indicates that XPO1 may not be sequestered into GR1000 inclusions, despite MS/MS data demonstrating their potential interaction. Difficulties visualising GR1000 inclusions by fluorescence microscopy added further challenge to determining whether XPO1 does co-localise with GR1000 inclusions. This is supported by our findings that XPO1 function is not significantly affected by GR1000, as measured by the nuclear/cytoplasmic localisation of XPO1 targets YAN and exd. However, these two proteins both demonstrated trends towards increased nuclear localisation in GR1000 flies, hinting at GR1000-mediated reductions in XPO1 function. Unsuitable antibodies prevented us from quantifying this increase more accurately via Western blot.

Altogether, the unsuitability of anti-XPO1 for us in *Drosophila* makes it difficult to make conclusions about the effects of GR1000 on XPO1 localisation. However, our functional data indicate that there are insignificant trends towards GR1000-mediated disruptions in XPO1 function.

TDP-43 pathology, a key pathological feature of FTD/ALS, is often associated with NCT defects (Chou *et al.*, 2018). While we do not show defects in XPO1-mediated nuclear export here, the potential for GR1000-associated NCT defects and the importance of TDP-43 in C9 disease prompted us to consider the implications of GR1000 on TDP-43 localisation. GR has been linked to the mislocalisation of *Drosophila* TDP-43 (TBPH) (Solomon *et al.*, 2018) and

GR1000 has been shown to cause significant mislocalisation of TBPH in larval salivary glands (West *et al.*, 2020). We sought to examine this phenotype in relation to our study of GR1000, XPO1 and NCT but were prevented from doing so by a lack of publicly available TDP-43/TBPH antibodies that worked in our hands. To overcome these limitations, future experiments could look to utilise the recent hTDP-43 *Drosophila* lines generated by Chang and Morton (2017) in which endogenous *Drosophila* TBPH has been replaced with human TDP-43 via CRISPR/Cas9 genome editing. Crossing these lines into a GR1000 or control background would allow us to monitor TDP-43 using a number of established anti-hTDP-43 antibodies.

#### **4.3.4. Study of the GR1000-XPO1 interaction is hampered by the lack of appropriate tools in *Drosophila***

While our XPO1 localisation and function data is consistent across experiments, they all have the caveat that the anti-XPO1 antibody is not fully validated in *Drosophila*. While we attempted to validate this antibody, we were unable to confirm its recognition of *Drosophila* XPO1. The consistent presence of multiple bands on Western blots indicates that this antibody recognises multiple proteins. The band at roughly 120 kDa, the observed molecular weight of XPO1 in *Drosophila* (Fasken *et al.*, 2000), is reduced by XPO1<sup>(1)</sup>-RNAi but increased by XPO1<sup>(2)</sup>-RNAi. While this may occur due to ineffective RNAi knockdown by XPO1<sup>(2)</sup>-RNAi, we believe that this is unlikely since both RNAi lines have been used extensively and previously validated (Sowa *et al.*, 2018; Cunningham *et al.*, 2020; Okazaki, Yamazoe and Inoue, 2020; Rossi *et al.*, 2021). Therefore, we believe it is unlikely that this antibody recognises *Drosophila* XPO1 by Western blot and is unsuitable for further use. Additionally, the antibody revealed the expected, predominantly nuclear, XPO1 localisation pattern in primary neurons but staining in larval salivary glands revealed little to no signal at all. This lack of signal may have occurred due to experimental procedures, but this is unlikely because a clear nuclear signal was observed in the fat bodies of these salivary glands. As discussed above, there are clear caveats to our Western blotting and immunochemistry data. Therefore, it is important that these experiments are repeated with an anti-XPO1 antibody that is properly validated for use in *Drosophila*.

One tool that would be especially useful in antibody validation would be an XPO1 overexpression fly line in which XPO1 is tagged with a commonly used protein tag, such as hemagglutinin (HA). With such a line, anti-XPO1 recognition of *Drosophila* XPO1 could be confirmed using antibodies recognising the protein tag. A tagged XPO1 line would also allow us to validate the GR1000-XPO1 interaction by performing Western blots following co-IP

using XPO1 as bait. We attempted to generate a UAS-XPO1-FLAG-HA fly line by microinjection of *Drosophila* embryos with a premade plasmid construct (DGRC\_1619364). However, no successful transformants were produced. Subsequent attempts at subcloning the construct into our own transgenic expression vectors were slowed by incompatible cloning sites and unsuccessful ligations, among other difficulties. Therefore, generation of this line was not possible within the time constraints of this project.

Here, we measured XPO1 function by assessing the localisation of YAN and exd, two XPO1 cargo proteins. Previous studies have measured XPO1 function more directly, using fluorescent reporters of NCT. These reporters are generated by tagging a fluorescent protein with nuclear localisation and export signals (NLS and NES), so that it is constantly transported between the nucleus and the cytoplasm. While these reporters have been used in *C9orf72* models (Vanneste *et al.*, 2019), including *Drosophila* (Zhang *et al.*, 2015), they all utilise GFP as the fluorescent protein and thus cannot be used alongside our EGFP-tagged 1000-repeat DPR constructs. A fly line expressing a non-GFP NCT reporter would be invaluable to our study, but its generation was outside the scope of this project. Such a reporter would allow us to study GR1000-mediated NCT defects in larval salivary glands and primary neuronal cultures and would facilitate the investigation of multiple timepoints with ease. Studying multiple timepoints would allow us to determine whether the GR1000-XPO1 interaction leads to the accumulation of NCT cargoes throughout the fly lifetime.

Pharmacological inhibitors of XPO1-mediated nuclear export have been widely developed and used in studies (Schmidt *et al.*, 2013), due to the relevance of XPO1 in multiple forms of cancer (Lapalombella *et al.*, 2012; Etchin *et al.*, 2013; Zhang *et al.*, 2013). Some of these have been used in studies of NCT in (C9-) FTD/ALS (Zhang *et al.*, 2015; Archbold *et al.*, 2018; Chou *et al.*, 2018). One compound in particular, KPT-276, has been used in a *Drosophila* model of the disease (Zhang *et al.*, 2015). Although our data do not demonstrate GR1000-mediated impairment of XPO1 function, it would be interesting to feed KPT-276 to wild-type or control flies to determine whether inhibition of XPO1 function can recapitulate GR1000 phenotypes. Additionally, feeding KPT-276 to flies pan-neuronally expressing GR1000 would help us understand the extent of any GR1000-mediated inhibition of XPO1 and if it can be inhibited even further.

#### **4.3.5. GR1000 does not significantly damage the nuclear envelope**

Alongside NCT defects, abnormal nuclear envelope morphology has also been observed in FTD/ALS models and patient tissue (Kinoshita *et al.*, 2009; Nagara *et al.*, 2013; Freibaum *et al.*, 2015; Chou *et al.*, 2018; Sirtori *et al.*, 2024). Morphological abnormalities that have been

observed include wrinkled (Kinoshita *et al.*, 2009; Freibaum *et al.*, 2015), discontinuous (Nagara *et al.*, 2013; Sirtori *et al.*, 2024) and invaginated (Freibaum *et al.*, 2015; Chou *et al.*, 2018) nuclear envelopes. Disruption of nuclear envelope homeostasis has been proposed as a key pathogenic event in C9 disease (Sirtori *et al.*, 2024), with nuclear envelope abnormalities observed in pure repeat models (Freibaum *et al.*, 2015) and patient-derived cells (Sirtori *et al.*, 2024). However, Solomon *et al.* (2018) observed no effect of DPR64 expression on the nuclear envelope in *Drosophila* larval salivary glands.

Here we demonstrate that nuclear envelope abnormalities, similar to those observed in previous studies, are more common in flies expressing GR1000, although this effect is not significant ( $p = 0.122$ ) (Fig. 4.8). This phenotype should be studied further using antibodies against more well characterised nuclear envelope proteins, such as mAB414 and RanGAP (Solomon *et al.*, 2018; Sirtori *et al.*, 2024). This was planned within this project but was prevented by difficulties in obtaining antibodies for use in *Drosophila*. Other proteins that are commonly used to study the nuclear envelope are Lamins (Chou *et al.*, 2018; Saberi *et al.*, 2018). Interestingly, Lamin was identified as a GR1000-interacting protein in our MS/MS data and may be mediating the phenotypes we demonstrate here. Lamin staining was performed in GR1000-expressing larval salivary glands, but we were unable to achieve the required resolution for quantification of phenotypes with our imaging apparatus at the time.

#### 4.4. Conclusions

In this chapter we build upon the finding that XPO1 is a GR1000-interacting protein with potential to modify GR1000 toxicity. We demonstrate that partial knockdown of XPO1 slows the onset of key, disease-relevant GR1000-mediated phenotypes in *Drosophila*. In an effort to understand the mechanisms underlying this effect, we sought to study the GR1000-XPO1 interaction and its effects on XPO1 function. The localisation of XPO1, which is imperative to its function, appears unaffected by GR1000 expression. XPO1 function, as measured by the localisation of XPO1 cargo, trends towards being impaired by GR1000, although not significantly so. While we demonstrate the potential of XPO1 in mediating and modifying GR1000-mediated toxicity and phenotypes, our data do not provide a mechanism for this effect. It must be noted, however, that our study of the GR1000-XPO1 interaction and its downstream effects must be interpreted carefully, given its many caveats. It is clear that to truly understand the mechanistic relevance of XPO1 in GR1000-mediated toxicity, we need better research tools for use in *Drosophila*. With the development of these tools, future work could shed light on the effects of GR1000 expression on XPO1 localisation and function and the implications of this on NCT and downstream processes.

## 5. Investigating the role of hypoxia and HIF1 $\alpha$ in GR1000 toxicity

### 5.1. Introduction

So far in this research, we have demonstrated that XPO1 interacts with GR1000 and modifies GR1000-mediated toxicity and phenotypes. However, XPO1 function appears to be unaffected by its interaction with GR1000. In the absence of XPO1 functional impairment, the underlying mechanism of XPO1-mediated GR1000 toxicity is unclear. Therefore, here we seek to investigate another possible mechanism. We believe that XPO1 and NCT are unlikely to play a direct role in toxicity, but rather act as an intermediate for toxicity arising from other biological processes. As a key nuclear export protein, XPO1 is involved in many biological processes through its various cargoes. We hypothesise that mechanisms of GR1000 toxicity associated with XPO1 likely arise through XPO1 cargo proteins.

One such protein is HIF1 $\alpha$ , the transcription factor that acts as the master regulator of the cellular response to hypoxia (Iyer *et al.*, 1998), a state of limited oxygen availability. In response to hypoxia, HIF1 $\alpha$  relocates from the cytoplasm (Fig. 1.5) to the nucleus and initiates transcription of genes involved in processes such as energy metabolism, angiogenesis and cell survival (Lee *et al.*, 2004). Regulation of such processes, especially under hypoxic conditions, is critical in adapting to hypoxia-induced deficits in ATP production and maintaining cell and tissue health. Given the high energy demands of neurons, the nervous system is particularly vulnerable to the effects of hypoxia on energy metabolism (Hyder, Rothman and Bennett, 2013). Therefore, regulation of the hypoxia response by HIF1 $\alpha$  is especially important in the nervous system. As such, a key role of HIF1 $\alpha$  has been identified in a number of neurodegenerative diseases (Chen *et al.*, 2021; Mitroshina *et al.*, 2021).

With regards to ALS, dysregulation of HIF1 $\alpha$  has been identified in model systems and patient tissues. Perturbed HIF1 $\alpha$  expression has been demonstrated in the affected tissues of ALS patients and mouse models (Sato *et al.*, 2012; Nagara *et al.*, 2013; Nomura *et al.*, 2019). Additionally, the HIF1 $\alpha$ -mediated response to hypoxia is altered in ALS patients and models (Ilieva *et al.*, 2003; Moreau *et al.*, 2011; Sato *et al.*, 2012). In one study, Nagara *et al.* (2013) linked this impaired response to impaired nuclear import of HIF1 $\alpha$ . The impaired HIF1 $\alpha$  response is particularly interesting given that several HIF1 $\alpha$  target genes, especially VEGF, have been shown to regulate motor neuron degeneration (Oosthuysen *et al.*, 2001; Lambrechts *et al.*, 2003; Zheng *et al.*, 2004; Sebastià *et al.*, 2009; Wiesner *et al.*, 2013). Additionally, genetic variation in these genes has been identified in sALS cohorts, although an association was not identified (Cronin *et al.*, 2008).

Vascular and blood flow changes characterise ALS pathogenesis, alongside decreased expression of HIF1 $\alpha$  target genes, erythropoietin (EPO) and VEGF (Miyazaki *et al.*, 2012; Pronto-Laborinho, Pinto and De Carvalho, 2014). As a result, hypoxia is observed in affected tissues, such as the spinal cord, of ALS mice (Sato *et al.*, 2012). Downstream hypoxic stress has also been observed in the spinal cord of ALS patients and closely associated with ALS progression (Yamashita *et al.*, 2021). Treatment of this hypoxic stress improved symptomatic and survival outcomes in ALS mice (Zheng *et al.*, 2004; Tada *et al.*, 2019). While these findings demonstrate hypoxic conditions in ALS-relevant tissues, environmental hypoxia has also been linked to ALS. Intermittent hypoxia was shown to aggravate motor neuron degeneration and ALS phenotypes in a mouse model (Kim *et al.*, 2013). Similarly, occupational exposure to hypoxia, as firefighter for example, has been linked to an increased ALS risk (Vanacore *et al.*, 2010).

The evidence for a role of hypoxia and HIF1 $\alpha$  activity in neurodegeneration and ALS is overwhelming. As such, this highlights the role of HIF1 $\alpha$  as an XPO1 cargo, and downstream hypoxia response pathways, as an important pathway for further investigation in the context of our previous work. However, almost all the research into mechanisms linking hypoxia and HIF1 $\alpha$  to ALS has been performed in *in vivo* models of SOD1 ALS. While studies have linked the two to ALS more widely, the role of hypoxia and hypoxic response pathways in C9 disease remains unclear. This chapter, therefore, examines the role of hypoxia, and impaired hypoxic response pathways, as a novel mechanism in C9 disease, as well as a potential common mechanism among forms of ALS.

Therefore, in this chapter we aim to:

1. Investigate HIF1 $\alpha$  as a modifier of GR1000 toxicity
2. Investigate how GR1000 affects the response to hypoxia
3. Determine how hypoxia and HIF1 $\alpha$  activity contribute to GR1000 toxicity

## **5.2. Results**

### **5.2.1. HIF1 $\alpha$ as a modifier of GR1000 toxicity**

To begin investigating HIF1 $\alpha$  as a modifier of GR1000 toxicity, we performed a genetic modifier screen using the *Drosophila* eye as a model system. Two lines for the genetic manipulation of HIF1 $\alpha$  expression were tested, an RNAi line for knockdown and a UAS line for overexpression. Knockdown of HIF1 $\alpha$  significantly reduced the severity of GR1000-associated eye phenotypes (Fig. 5.1B) ( $p < 0.01$ ). Knockdown of HIF1 $\alpha$  had no significant effect on eye phenotype in GFP-expressing flies ( $p > 0.99$ ). In contrast, overexpression of

HIF1 $\alpha$  caused a significant increase in the severity of eye phenotypes in both GFP and GR1000-expressing flies ( $p < 0.0001$ ). These phenotypes were more severe in GR1000-expressing flies than in their GFP controls.

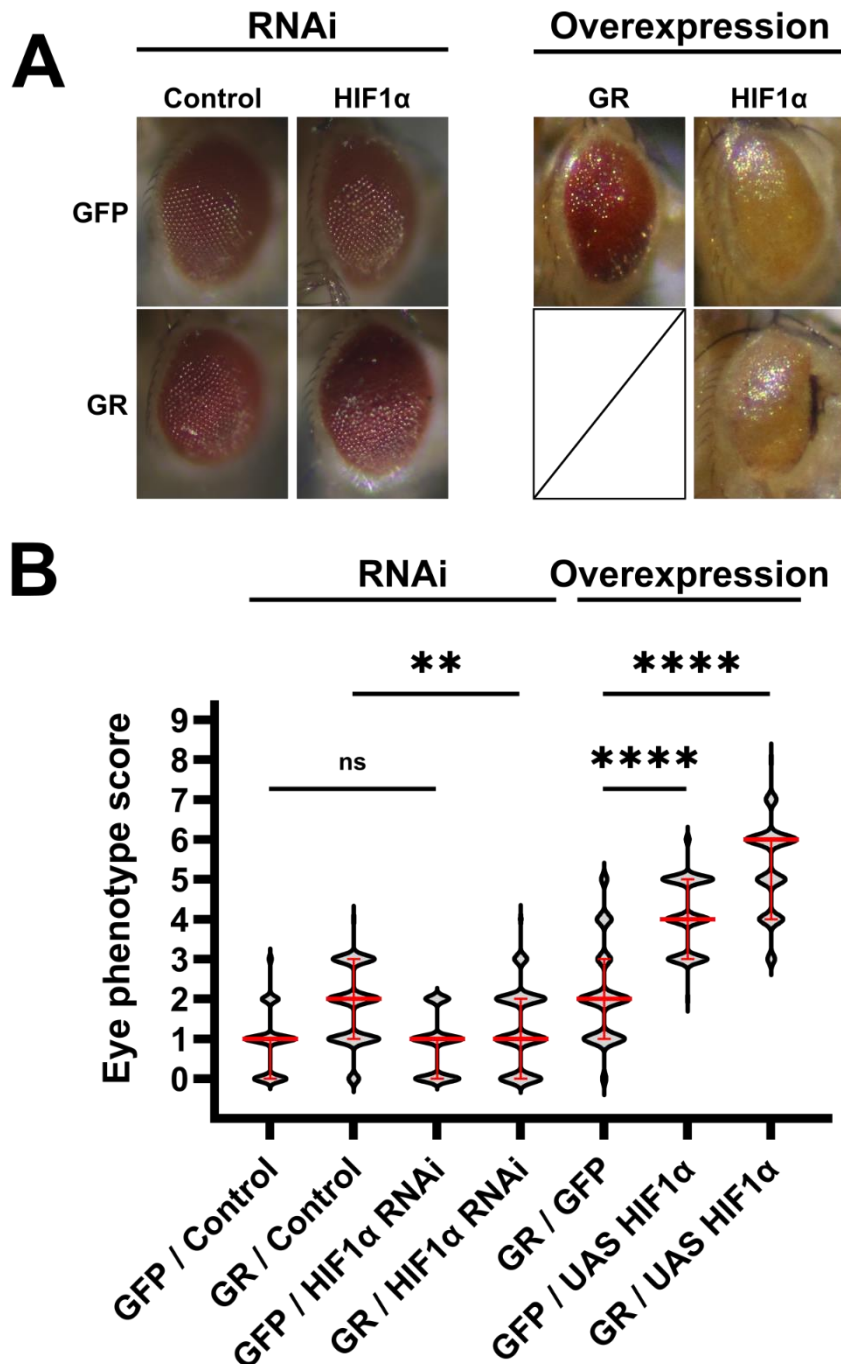


**Figure 5.1. HIF1 $\alpha$  is a modifier of GR1000 toxicity in the *Drosophila* eye.** A) Representative images of *Drosophila* eyes co-expressing (GMR-Gal4) either GFP or GR1000 with RNAi or overexpression of denoted protein. B) Quantification of eye phenotype scores awarded based on 9-point scoring system, in which lethality scores 9. Lines represent median, error bars represent interquartile range. Stats are Kruskal-Wallis test with Dunn's multiple comparisons test of preselected pairs. \*  $p < 0.05$ , \*\*  $p < 0.01$ , \*\*\*  $p < 0.001$ , \*\*\*\*  $p < 0.0001$

Having observed a potential genetic interaction between the *Drosophila* orthologue of HIF1 $\alpha$  (Sima) and GR1000 we asked whether manipulation of HIF1 $\alpha$  had any effect upon previously established neurodegenerative phenotypes in flies pan-neuronally expressing GR1000. Previously we have demonstrated that pan-neuronal expression of GR1000 leads to an age-related decline in motor function when assayed using negative geotaxis “climbing” assays. In contrast to eye screens, these assays allow characterisation of the effect of HIF1 $\alpha$  throughout the lifespan of the fly. GR1000 or GFP control (*UAS-mCD8-GFP*) were pan-neuronally (nSyb-Gal4 (II)) co-expressed with either HIF1 $\alpha$  overexpression (*UAS-HIF1 $\alpha$* ), HIF1 $\alpha$  RNAi (*UAS-HIF1 $\alpha$ -RNAi*) or the control RNAi (*UAS-mCherry-RNAi*) used in previous experiments, which provides a suitable control for the titration of GAL4 in the UAS/GAL4 system and for the expression of an RNAi construct, .

In line with our previous data, flies pan-neuronally expressing GR1000 alongside RNAi control only demonstrated a significant decrease in climbing ability relative to GFP controls at 14 dpe and onwards (14 dpe:  $p = 0.0075$ , 21 dpe:  $p < 0.0001$ , 28 dpe:  $p = 0.0049$ ) (Fig. 5.2A, C, D, E). Both knockdown and overexpression of HIF1 $\alpha$  were associated with significantly decreased climbing ability of flies expressing GR1000 compared to GFP controls at 7 dpe ( $p = 0.0015$  and  $0.0001$  respectively), however this effect was lost past 7 dpe as the climbing ability of GFP controls decreased to roughly equal that of flies expressing GR1000 (Fig. 5.2A, B, C). Relative to co-expression of RNAi control, flies overexpressing HIF1 $\alpha$  RNAi alongside GR1000 exhibited significantly decreased climbing ability at 7 dpe (Fig. 5.2B) ( $p < 0.05$ ). At later ages, the climbing ability of flies co-expressing GR1000 and RNAi control decreased to roughly equal that of flies co-expressing GR1000 and HIF1 $\alpha$ -RNAi (Fig. 5.2A, C, D, E). Where the climbing ability of flies expressing GR1000 and RNAi control decreased from 7 to 14 dpe (Fig. 5.2A, B, C), flies expressing GR1000 alongside UAS-HIF1 $\alpha$  retained their climbing ability, with flies co-expressing GR1000 and UAS-HIF1 $\alpha$  having significantly ( $p = 0.0006$ ) increased climbing ability relative to flies co-expressing GR1000 and RNAi control at 14 dpe (Fig. 5.2C).

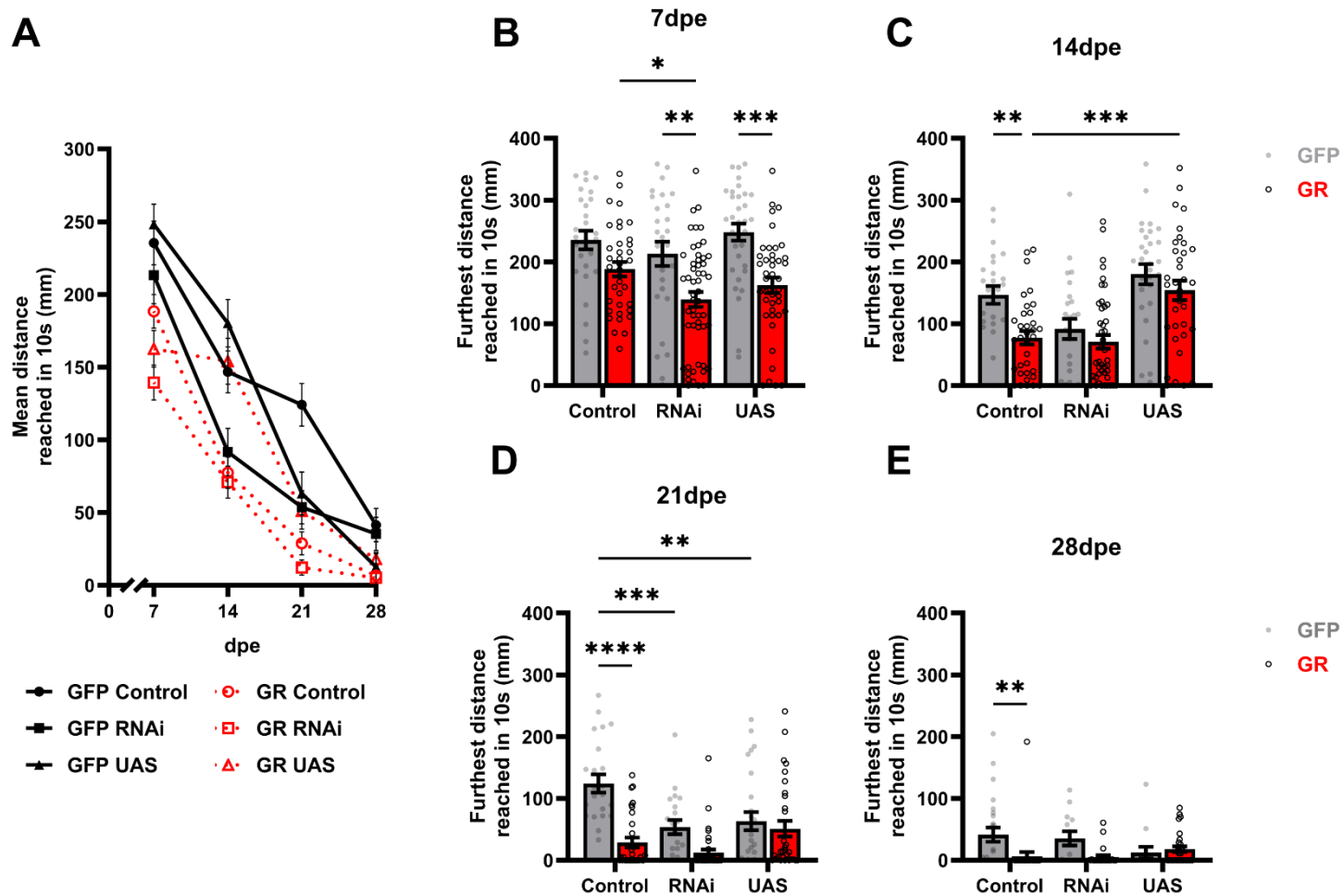


**Figure 5.2. Genetic manipulation of HIF1 $\alpha$  modifies *Drosophila* climbing phenotypes.** A) Quantification of fly climbing ability throughout the fly lifetime. Climbing ability was measured as the furthest distance reached in 10 seconds in SING assay at B) 7, C) 14, D) 21 and E) 28 dpe. Flies pan-neuronally (nSyb-Gal4 (II)) expressing GFP or GR1000, alongside mCherry-RNAi (Control), HIF1 $\alpha$ -RNAi or UAS-HIF1 $\alpha$  were used. Points represent individual flies; bars represent mean and error bars show SEM. Stats are two-way ANOVA with Šídák's multiple comparisons test of preselected pairs. \*  $p < 0.05$ , \*\*  $p < 0.01$ , \*\*\*  $p < 0.001$ , \*\*\*\*  $p < 0.0001$ . N = 3.

Having observed that pan-neuronal co-expression of HIF1 $\alpha$  alleviated GR1000 induced climbing deficits in flies from 14 dpe we asked whether genetic manipulation of HIF $\alpha$  had any effect on the basal motor activity of these flies. Flies expressing GR1000 of all conditions were significantly ( $p < 0.0001$ ) less active than GFP controls across all ages (Fig. 5.3). Overexpression of HIF1 $\alpha$  caused a significant increase in the activity in GFP flies, relative to flies co-expressing GFP and RNAi control, at all ages (8 – 22 dpe:  $p < 0.0001$ , 28 dpe:  $p = 0.0033$ ) (Fig. 5.3). Flies expressing GR1000 alongside overexpression of HIF1 $\alpha$  also demonstrated a slight increase in activity compared to flies co-expressing GR1000 and RNAi control, although this was not significant (8 dpe:  $p = 0.108$ , 15 dpe:  $p = 0.052$ , 22 dpe:  $p = 0.4146$ , 29 dpe:  $p = 0.1773$ ) (Fig. 5.3). All genotypes demonstrated an age-related decline in activity.

Taken together these results suggest that genetic manipulation of HIF1 $\alpha$  expression modifies GR1000 toxicity and motor phenotypes, revealing HIF1 $\alpha$  signalling is relevant to GR1000 toxicity and warrants further study in our model.

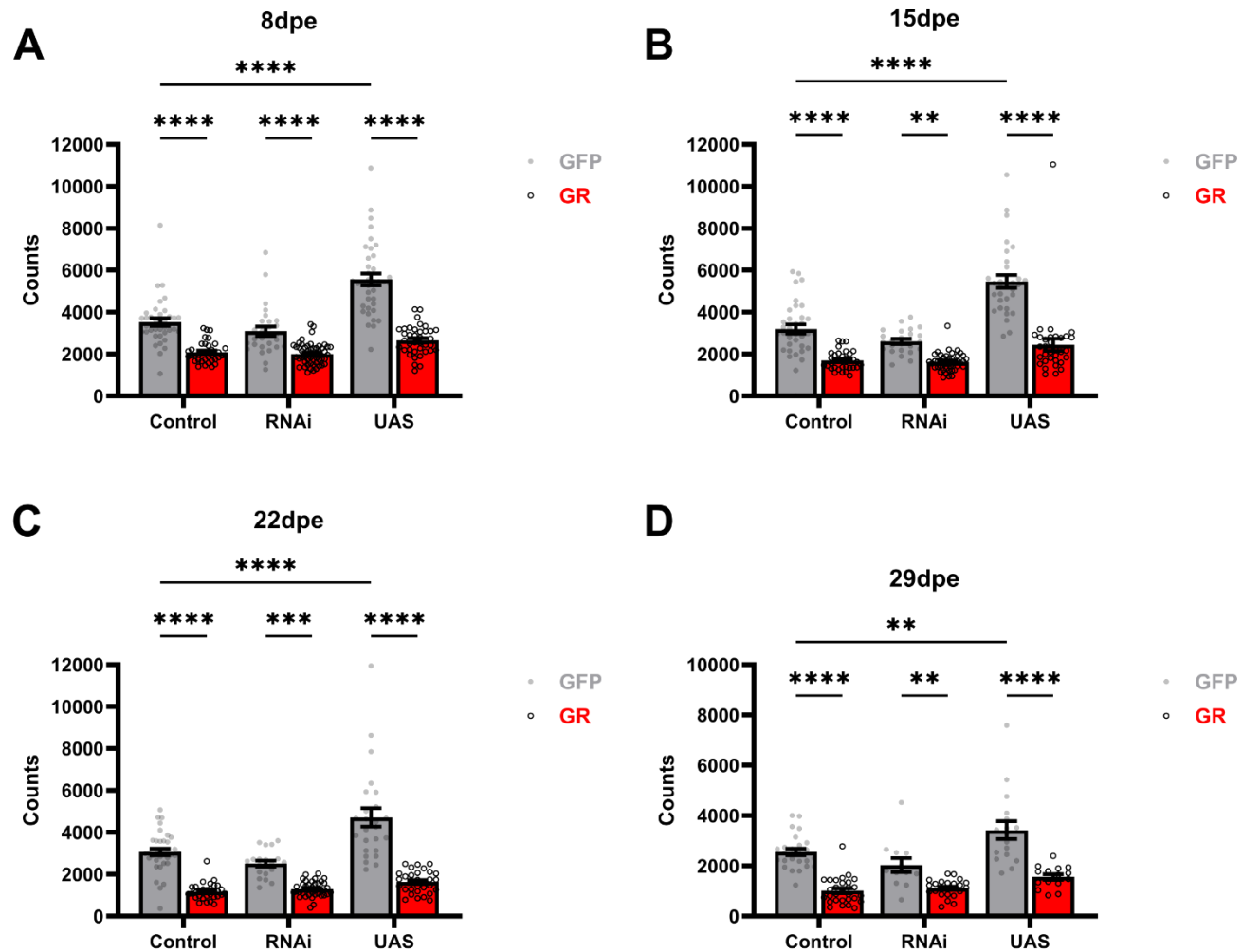


**Figure 5.3. Genetic manipulation of HIF1 $\alpha$  does not modify activity deficits in flies pan-neuronally expressing GR1000.** Activity was measured as total counts in a 24 hour period at A) 8, B) 15, C) 22 and D) 29 dpe. Flies pan-neuronally (nSyb-Gal4 (II)) expressing GFP or GR1000, alongside mCherry-RNAi (Control), HIF1 $\alpha$ -RNAi or UAS-HIF1 $\alpha$  were used. Points represent individual flies; bars represent mean and error bars show SEM. Stats are two-way ANOVA with Šídák's multiple comparisons test of preselected pairs. \*  $p < 0.05$ , \*\*  $p < 0.01$ , \*\*\*  $p < 0.001$ , \*\*\*\*  $p < 0.0001$ . N = 3.

### 5.2.2. Intermittent hypoxia does not cause or exacerbate motor phenotypes

Whilst ALS patients are likely to be exposed to hypoxia as a result of respiratory failure during symptomatic disease, another common theme emerging from studies of ALS is a causative or accelerative role of intermittent hypoxic exposure in genetically susceptible individuals. This is in line with the gene/environment/time hypothesis, whereby disease occurs through the combined effects of genetic susceptibility, environmental risk factors, and aging. Occupational, intermittent exposure to hypoxia is associated with an increased ALS risk (Belli and Vanacore, 2005; Chiò *et al.*, 2005; Vanacore *et al.*, 2010), while intermittent hypoxia has been shown to aggravate motor neuronal loss (Kim *et al.*, 2013). We therefore hypothesised that intermittent hypoxia may cause motor phenotypes in control flies while aggravating GR1000 motor phenotypes.

To study the effects of intermittent hypoxia on GR1000-mediated phenotypes in *Drosophila*, we adapted a regime from Azad *et al.* (2009) (Fig. 5.4A) whereby flies receive a 5 minute exposure to 1 % O<sub>2</sub>, followed by a 10 minute recovery period in 21 % O<sub>2</sub>, repeatedly over a 2 hour period. This is performed once per day for 4 consecutive days from 14 - 17 dpe. This is designed to replicate the brief but intense hypoxic exposure that individuals might receive in professions such as firefighting or sports. Normoxia control flies were maintained at 21 % O<sub>2</sub> for the duration of the intermittent hypoxia. Fly motor phenotypes were assessed by climbing assays immediately after the 2 hour intermittent hypoxia period every day and by activity assays after the 5 day intermittent hypoxia regime.

All genotypes and conditions exhibited an increase in climbing ability from 14 to 15 dpe, although this increase was more marked in flies that received the intermittent hypoxia exposure. This was immediately followed by a decrease back to 14 dpe levels by 16 dpe (Fig. 5.4B). Throughout the intermittent hypoxia regime, GR1000-expressing flies exposed to hypoxia climbed less than GFP controls but exhibited almost identical patterns of climbing ability when compared to normoxic GR1000-expressing flies. In normoxia controls, the climbing ability of GR1000-expressing flies decreased while remaining relatively constant in GFP-expressing flies. This effect is highlighted by the significantly ( $p < 0.0001$ ) decreased climbing ability of GR1000 normoxia flies, relative to their GFP counterparts, at 17 dpe (Fig. 5.4C). At 14 dpe, GR1000-expressing flies that were exposed to intermittent hypoxia had significantly ( $p = 0.0245$ ) reduced climbing ability compared to those exposed to normoxia. A similar trend was observed in GFP flies, although it was not significant ( $p = 0.1475$ ). By 17 dpe, the climbing ability of flies expressing GR1000 was equal between conditions but in flies expressing GFP there was a non-significant ( $p = 0.09$ ) decrease in the climbing ability of those exposed to intermittent hypoxia .

After the 4 day intermittent hypoxia regime, flies were placed into activity monitors at 18 dpe and assayed for 10 days. Both genotypes, regardless of exposure, demonstrated a significant age-related decline in activity (two-way ANOVA with Šídák's multiple comparisons test of preselected pairs. GFP Normoxia:  $p < 0.0001$ , GFP Hypoxia:  $p = 0.0043$ , GR Normoxia:  $p = 0.0207$ , GR Hypoxia:  $p = 0.0037$ ) (Fig. 5.4D). As in previous experiments, flies pan-neuronally expressing GR1000 had significantly reduced activity compared to their GFP counterparts (18 dpe:  $p < 0.0001$ , 28 dpe:  $p = 0.0067$ ). Exposure to intermittent hypoxia had no significant effect on activity in both genotypes (18 dpe: GFP;  $p = 0.2931$ , GR;  $p = 0.9072$ , 28 dpe: GFP;  $p = 0.8656$ , GR;  $p = 0.8889$ ) (Fig. 5.4E).

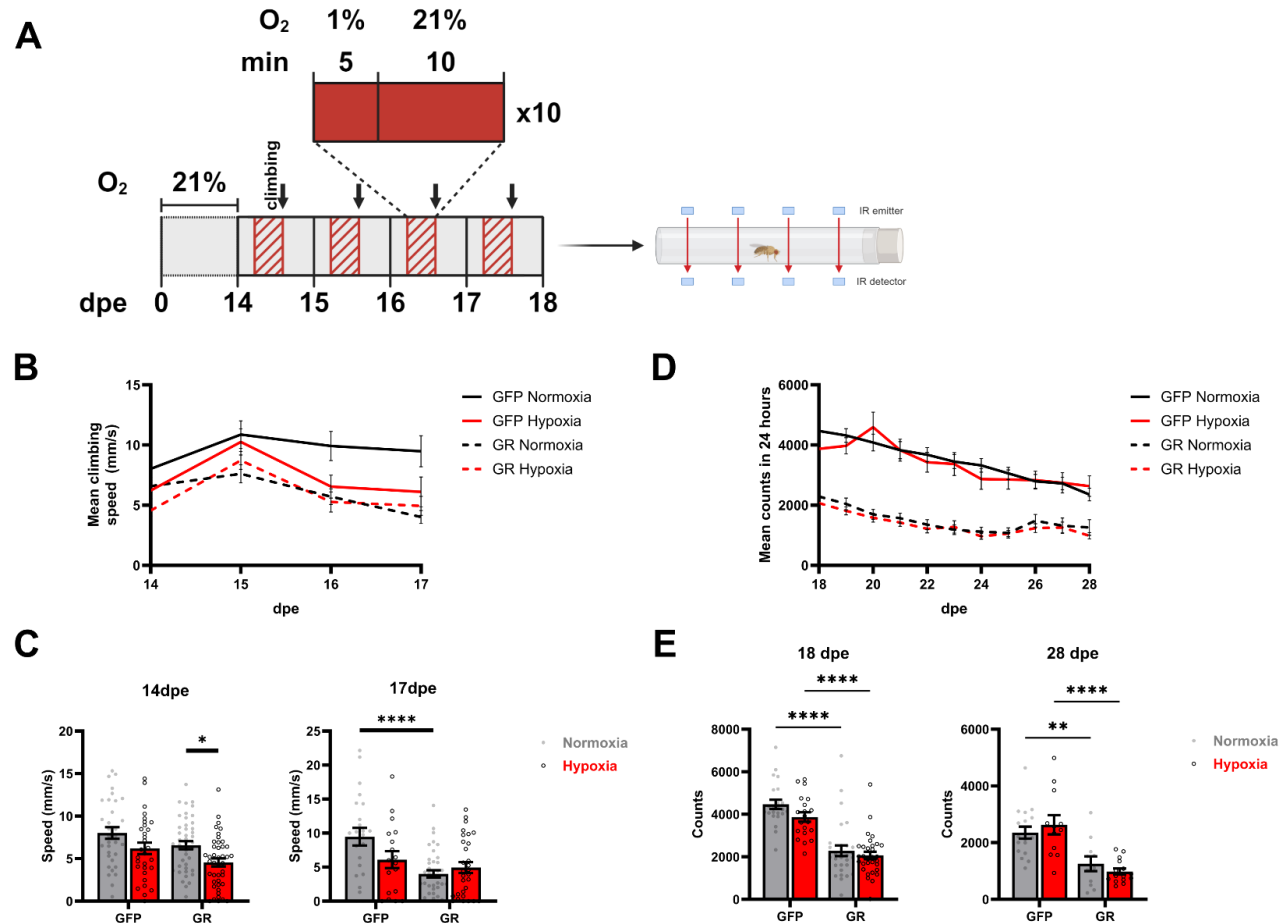


**Figure 5.4. Intermittent hypoxia does not cause or exacerbate motor phenotypes in *Drosophila*.** A) Schematic representation of intermittent hypoxia regime. Flies pan-neuronally (nSyb-Gal4 (III)) expressing GFP or GR1000 were used. Climbing (SING) assays were performed immediately following treatment per day of the regime. Activity assays were performed following the complete regime. Climbing data throughout the regime (B) and from first and final days of regime (C). Activity data for the full duration (D) and first and final days (E) following regime. Points represent individual flies; bars represent mean and error bars show SEM. Stats are two-way ANOVA with Šídák's multiple comparisons test of preselected pairs. \*  $p < 0.05$ , \*\*  $p < 0.01$ , \*\*\*  $p < 0.001$ , \*\*\*\*  $p < 0.0001$ . N = 3.

### 5.2.3. GR1000 disrupts the sensing of and/or response to hypoxia

During the intermittent hypoxia regime, we observed that flies of both genotypes were entering a hypoxic stupor under 1 % O<sub>2</sub> conditions. The hypoxic stupor is a physiological response in *Drosophila* to very low oxygen conditions. It is thought to occur as a protective mechanism to prevent excessive activity under low oxygen conditions from damaging cells and tissues. Upon initial observation, it appeared that flies pan-neuronally (nSyb-Gal4 (III)) expressing GFP or GR1000 were entering this stupor at different latencies. Therefore, we sought to replicate and quantify this phenotype. To do this we adapted an assay from Krishnan *et al.* (1997). Briefly, flies were assayed in transparent cages sealed with mesh to allow efficient gas exchange. Flies were left to settle at the top of the cage before the cages were transferred into a 1 % O<sub>2</sub> environment, resting between two pedestals to allow gas exchange through the mesh at the bottom. Flies were filmed and latency to enter hypoxic stupor was measured by time taken for flies to fall to the bottom of the cage. Given that this phenotype has not been observed previously in our model, we opted to study pan-neuronal (nSyb-Gal4 (III)) expression of all 4 DPR1000s and use both wild-type and GFP (*UAS-mCD8-GFP*) controls. Analysis revealed that flies pan-neuronally expressing GFP behaved similarly to wild-type (Fig. 5.5). Flies pan-neuronally expressing AP1000, GA1000 or GR1000 fell significantly earlier than GFP control flies (  $p = 0.0095$ ,  $< 0.0001$ ,  $0.0242$  respectively) (Fig. 5.5). GA1000-expressing flies fell first, followed by GR1000 and AP1000. PR1000-expressing flies did not behave significantly different to GFP control flies ( $p = 0.9644$ ).

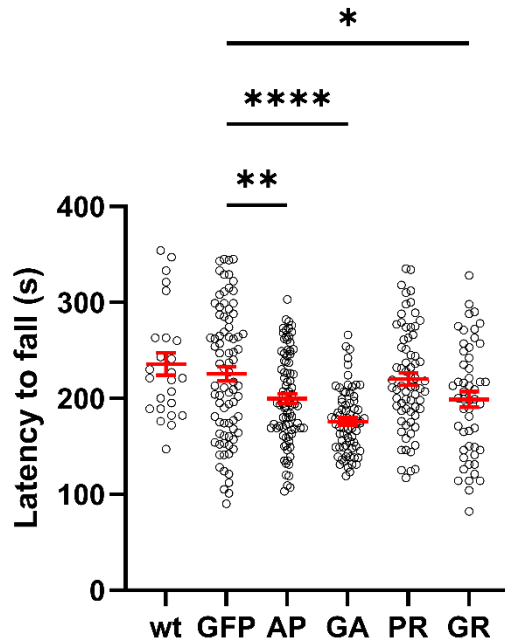


**Figure 5.5. The *Drosophila* hypoxic stupor response is perturbed by pan-neuronal expression of 1000-repeat DPRs.** Latency to enter the hypoxic stupor response was measured as latency to fall to the bottom of the cage in the hypoxic stupor assay in 14 dpe flies. wt flies are F<sub>1</sub> from CantonS crossed to OregonR, other genotypes are pan-neuronal (nSyb-Gal4 (III)) expression of noted DPR1000 or GFP. Points represent individual flies; lines represent mean and error bars show SEM. Stats are one-way ANOVA with Dunnett's multiple comparisons test of all genotypes to GFP. \* p < 0.05, \*\* p < 0.01, \*\*\* p < 0.001, \*\*\*\* p < 0.0001. N ≥ 2.

It is clear the pan-neuronal expression of GR1000 perturbs the *Drosophila* stupor response to acute hypoxia, however next we wanted to examine longer term changes in the response to hypoxia with more relevance to age-related neurodegenerative diseases such as FTD/ALS. As the master regulator of the primary cellular response to hypoxia, HIF1 $\alpha$  regulates transcriptional changes with long term effects in angiogenesis, erythropoiesis, metabolism and cell survival (Lee *et al.*, 2004). HIF1 $\alpha$  and the transcriptional response to hypoxia have already been implicated in wider ALS (Lambrechts *et al.*, 2003; Moreau *et al.*, 2011; Chen *et al.*, 2021), highlighting the importance of studying HIF1 $\alpha$  in our model. Given that HIF1 $\alpha$  function is partly governed by its export from the nucleus by XPO1, we hypothesised that GR1000 might cause changes in the HIF1 $\alpha$ -mediated transcriptional response to hypoxia.

Exposure of flies to 1 % O<sub>2</sub> for more than a few hours is lethal, so to study transcriptional responses to hypoxia we moved to a 24 hour, 5 % O<sub>2</sub> exposure. Bandarra *et al.* (2014) showed that with a 24 hour exposure to 5 % O<sub>2</sub> *Drosophila* demonstrate a transcriptional response in many hypoxia genes. With the response to a 24 hour, 5 % O<sub>2</sub> stimulus being previously characterised in wild-type flies, we sought to examine the response to the same

stimulus in flies pan-neuronally (nSyb-Gal4 (III)) expressing GFP or GR1000. Flies were exposed to normoxia or hypoxia (5 % O<sub>2</sub>) for 24 hours, finishing at 5 dpe or 28 dpe. RNA was collected from fly heads immediately following exposure and used in RT-qPCR to assess transcriptional changes in hypoxia genes. At 5 dpe, expression of HIF1 $\alpha$  was significantly ( $p = 0.0189$ ) increased 1.5-fold following exposure to hypoxia in flies pan-neuronally expressing GR1000 but not GFP ( $p = 0.8535$ ) (Fig. 5.6A). At 28 dpe, flies expressing GFP or GR1000 exhibited insignificant increases in HIF1 $\alpha$  expression following exposure to hypoxia ( $p = 0.9001$  and  $0.514$  respectively). Expression of lactate dehydrogenase (Ldh), a downstream transcriptional target of HIF1 $\alpha$ , was used to measure HIF1 $\alpha$  transcriptional activity. Following exposure to hypoxia in 5 dpe flies expressing GFP or GR1000, Ldh expression was increased ~2-fold ( $p = 0.2809$ ) and ~3-fold ( $p = 0.0085$ ) respectively (Fig. 5.6B). At 28 dpe, hypoxia increased expression of Ldh 3-fold and 4.8-fold in flies expressing GFP or GR1000 respectively, however these increases were not significant ( $p = 0.4745$  and  $0.06$  respectively).

In addition to activating HIF pathways, hypoxia also activates responses from other transcription factors. One such response is mediated through the highly conserved nuclear factor  $\kappa$ B (NF- $\kappa$ B) family of transcription factors. NF- $\kappa$ B controls a number of cell survival pathways, including metabolic, apoptotic, DNA damage, immune and inflammation pathways (Perkins, 2012; Tornatore *et al.*, 2012). As such, NF- $\kappa$ B activity has been associated with a number of diseases, including neurodegenerative diseases such as FTD/ALS. NF- $\kappa$ B activation has been observed in the affected cells and tissues of FTD/ALS patients (Swarup *et al.*, 2011; Frakes *et al.*, 2014; Prell *et al.*, 2014). Here we measure expression of *Drosophila* NF- $\kappa$ B, made up of Dorsal, Dif and Relish. We also measure NF- $\kappa$ B activation by downstream expression of the immune genes, anti-microbial peptides (AMPs): Drosomycin, Diptericin and Attacin A. NF- $\kappa$ B activation is mediated by a signalling cascade, including multiple points of negative regulation by proteins such as CYLD (dCYLD in *Drosophila*). Interestingly, mutations in CYLD have been associated with FTD/ALS (Dobson-Stone *et al.*, 2020) and CYLD expression is reduced in the motor neurons of ALS patients (Highley *et al.*, 2014; Cooper-Knock, Bury, *et al.*, 2015).

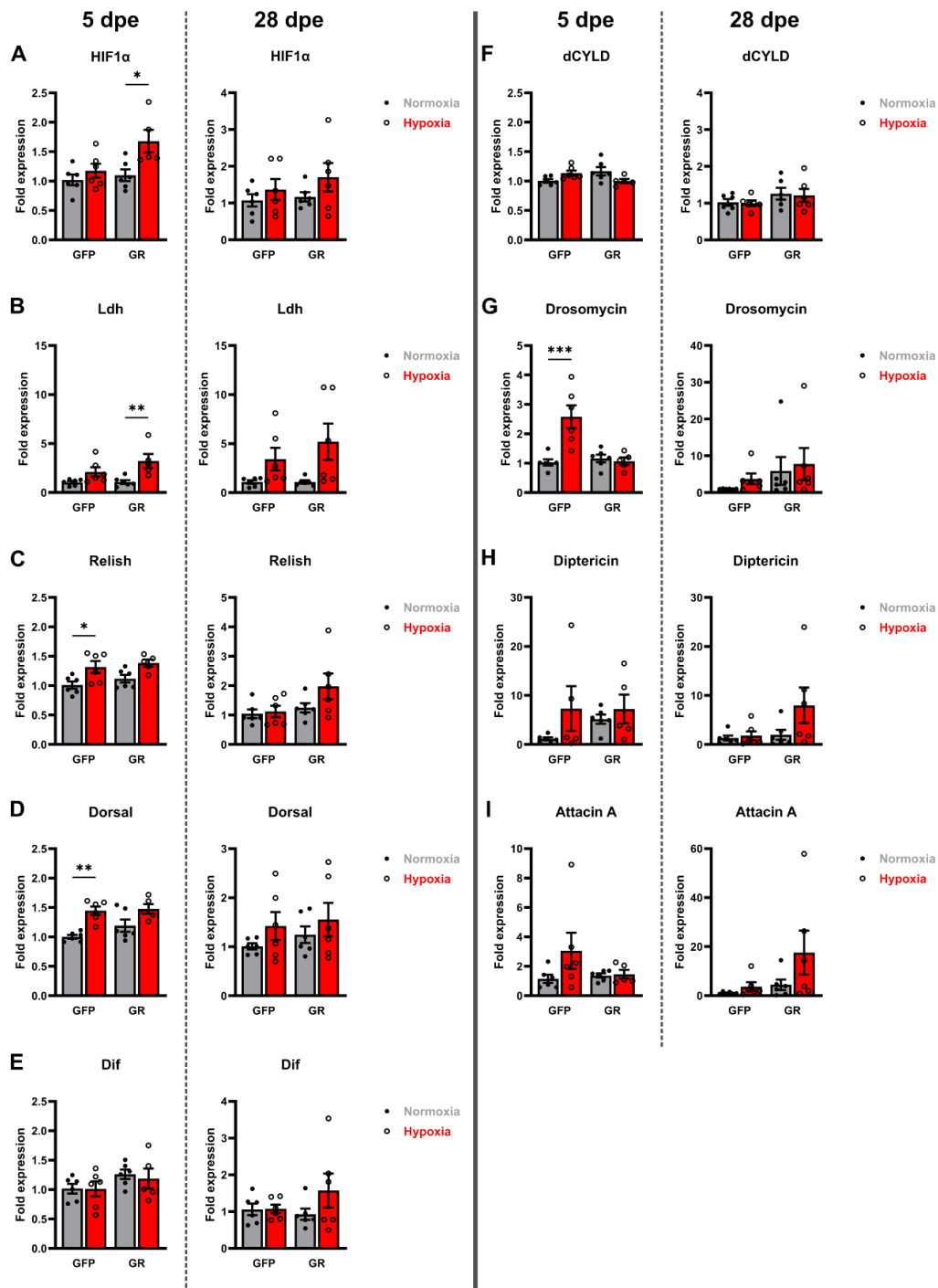
At 5 dpe, expression of Relish was significantly ( $p = 0.0327$ ) increased 1.3-fold in flies expressing GFP, following exposure to hypoxia (Fig 5.6C). A similar 1.2-fold increase in Relish expression following exposure to hypoxia in flies expressing GR1000, although this was insignificant ( $p = 0.0991$ ). At 5 dpe, expression of Dorsal was significantly ( $p = 0.002$ ) increased 1.4-fold following exposure to hypoxia in flies expressing GFP (Fig. 5.6D). While flies expressing GR1000 exhibited a 1.2-fold increase in Dorsal expression at 5 dpe following exposure to hypoxia, this effect was not significant ( $p = 0.0724$ ). At 28 dpe,

expression of Relish appeared increased, but not significantly ( $p = 0.2354$ ), following exposure to hypoxia in flies expressing GR1000 (Fig. 5.6C). At 28 dpe, expression of Dorsal was increased following exposure to hypoxia in flies expressing GFP or GR1000 but not significantly so ( $p = 0.6611$  and  $0.8409$  respectively) (Fig. 5.6D). At 5 dpe, expression of Dif appeared slightly but not significantly increased ( $p = 0.4701$ ) in flies expressing GR1000 compared to GFP under normoxia (Fig. 5.6E). Hypoxia-induced changes in Dif expression were not observed at 5 dpe. However, at 28 dpe, expression of Dif was increased 1.6-fold following exposure to hypoxia in flies expressing GR1000 but not GFP, although this effect was not significant ( $p = 0.3418$ ) (Fig. 5.6D). Under normoxia, expression of dCYLD appeared slightly but not significantly ( $p = 0.0835$ ) increased in flies expressing GR1000 compared to GFP at 5 dpe (Fig. 5.6F). No other differences in expression of dCYLD were observed between conditions at 5 or 28 dpe.

At 5 dpe, exposure to hypoxia caused a significant ( $p = 0.0004$ ) 2.6-fold increase in expression of Drosomycin in flies expressing GFP but not GR1000 (Fig. 5.6G). At 28 dpe, exposure to hypoxia did not cause a significant increase in Drosomycin expression in flies expressing GFP and GR1000 ( $p = 0.9469$  and  $0.9862$  respectively). Normoxic expression of Drosomycin was also increased ~6-fold, although not significantly ( $p = 0.7002$ ), in flies expressing GR1000 compared to GFP at 28 dpe (Fig. 5.6G). At 5 dpe, expression of Diptericin was not significantly increased following exposure to hypoxia in flies expressing GFP or GR1000 ( $p = 0.3408$  and  $0.9639$  respectively) (Fig. 5.6H). Expression of Diptericin was not significantly increased in flies expressing GR1000 under normoxia at 5 dpe ( $p = 0.6822$ ). At 28 dpe, expression of Diptericin was increased 4-fold following exposure to hypoxia in flies expressing GR1000 but not GFP, however this effect was not significant ( $p = 0.1575$ ) (Fig. 5.6H). At 5 dpe, exposure to hypoxia caused a 2.7-fold increase in expression of Attacin A in flies expressing GFP that was not observed in flies expressing GR1000, although this increase was not significant ( $p = 0.2073$ ) (Fig. 5.6I). At 28 dpe, exposure to hypoxia caused a 4-fold increase in expression of Attacin A in flies expressing GR1000 but not GFP, however this effect was not significant ( $p = 0.2257$ ) (Fig. 5.6I).

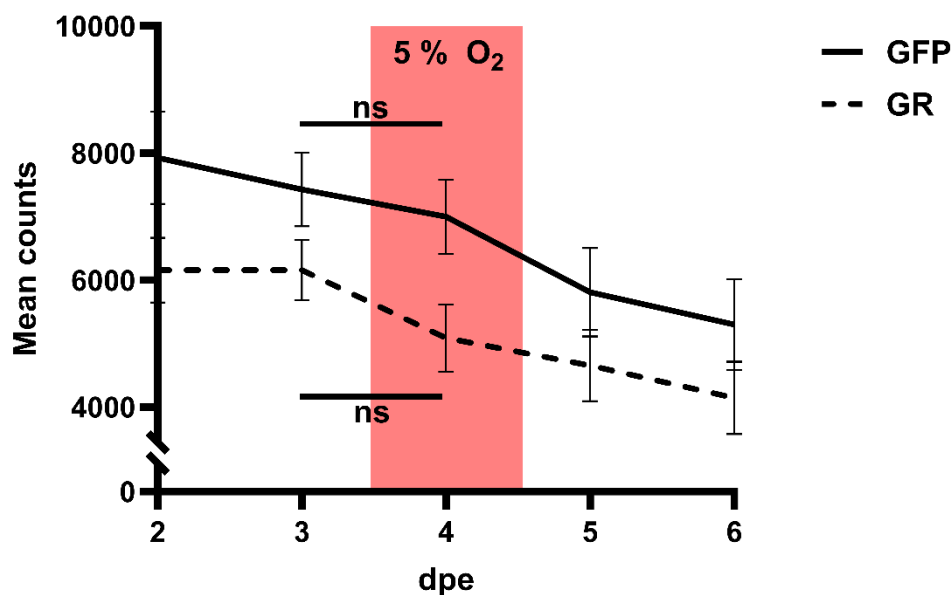
These data can be summarised by the findings that, at 5 dpe but not 28 dpe, GR flies exposed to hypoxia demonstrate significantly increased expression of HIF1a with a corresponding significant increase in Ldh expression. Similar effects were observed at 28 dpe although they were not significant. Conversely, Relish and Dorsal expression does not significantly increase following exposure to hypoxia in GR flies compared to control flies. This may be linked to the slightly elevated Relish and Dorsal expression in GR flies under normoxia. There was a corresponding effect observed in Drosomycin expression. No

significant effects were observed in expression of the other AMPs, but expression increased in GFP, but not GR, flies exposed to hypoxia. The inverse effect was observed at 28 dpe.



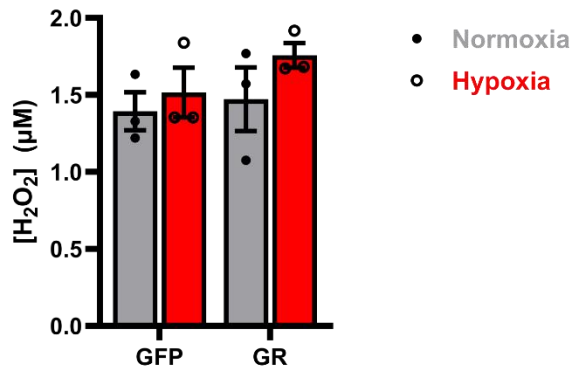
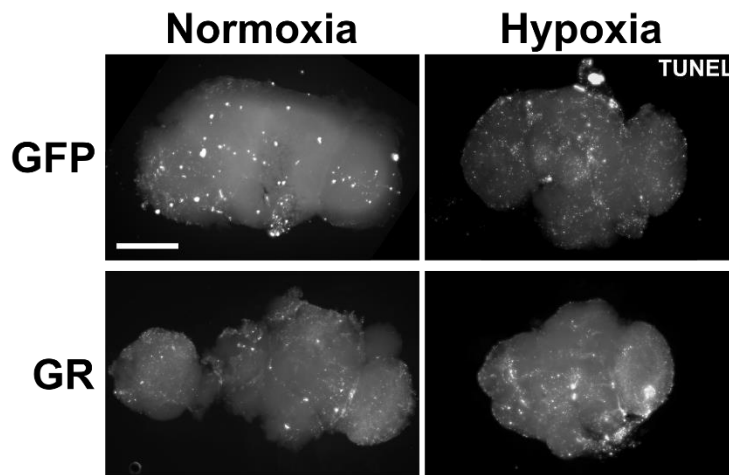
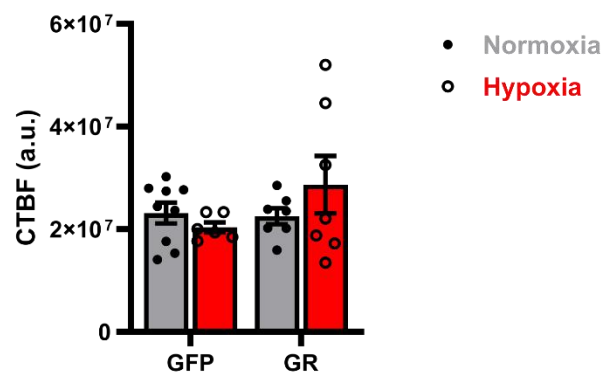
**Figure 5.6. Pan-neuronal expression of GR1000 perturbs the transcriptional response to hypoxia in *Drosophila*.** Fold expression of denoted genes was calculated from  $C_t$  values obtained in RT-qPCR using cDNA from 5 or 28 dpe flies pan-neuronally (nSyb-Gal4 (III)) expressing GFP or GR1000. Points represent biological replicates; lines represent mean and error bars show SEM. Stats are two-way ANOVA with Šídák's multiple comparisons test of preselected pairs. \*  $p < 0.05$ , \*\*  $p < 0.01$ , \*\*\*  $p < 0.001$ , \*\*\*\*  $p < 0.0001$ .  $N \geq 5$ .

Having demonstrated that flies pan-neuronally expressing GR1000 respond to hypoxia differently at the behavioural level, in their hypoxic stupor response, we wanted to determine whether these behavioural differences were driving the transcriptional changes we observed. At 5 % O<sub>2</sub>, flies do not enter the hypoxic stupor response but instead remain active. Therefore, we investigated whether pan-neuronal (nSyb-Gal4 (III)) expression of GR1000 leads to differences in activity under hypoxia. Using *Drosophila* activity monitors, we measured fly activity before, during and after a 24 hour 5 % O<sub>2</sub> exposure. Flies pan-neuronally expressing GR1000 demonstrated reduced activity compared to GFP controls at all timepoints (Fig. 5.7). However, GR1000-expressing flies exhibited the same slight but insignificant decrease in activity under hypoxia as GFP-expressing flies (GFP:  $p > 0.9999$ , GR:  $p = 0.9723$ ). Both genotypes exhibited a trend towards an age-related decline in activity post-hypoxia.



**Figure 5.7. Pan-neuronal expression of GR1000 does not affect activity under hypoxia in *Drosophila*.** Activity was measured as total counts in a 24 hour period. Flies pan-neuronally (nSyb-Gal4 (III)) expressing GFP or GR1000 were used. Activity assay was measured before, during and after a 24 hour exposure to 5 % O<sub>2</sub>. Stats are two-way ANOVA with Šídák's multiple comparisons test within genotypes. N = 2, n = 17 (GFP), 24 (GR).

Mitochondrial dysfunction has been identified as an early pathological event in ALS (Dafinca, Barbagallo and Talbot, 2021) and has been observed in *C9orf72* patient-derived cells (Onesto *et al.*, 2016; Mehta *et al.*, 2021). Research with models of GR toxicity have demonstrated mitochondrial dysfunction, through GR-protein interactions in mitochondria, leading to increased oxidative stress and DNA damage (Lopez-Gonzalez *et al.*, 2016; Choi *et al.*, 2019). Au *et al.* (2023) identified mitochondrial defects, oxidative stress and increased levels of reactive oxygen species (ROS), in the form of superoxide ( $O_2^-$ ) and hydrogen peroxide ( $H_2O_2$ ), in the brains of ( $G_4C_2$ )<sup>36</sup>, GR<sup>36</sup> and GR<sup>1000</sup>-expressing *Drosophila*. Genetic and pharmacological approaches to counteract these effects partially rescued  $G_4C_2$ /GR-mediated phenotypes in these models. Hypoxia is also associated with increased ROS and oxidative stress in humans (Magalhães *et al.*, 2004, 2005; Debevec *et al.*, 2014) and *Drosophila* (Malacrida *et al.*, 2022). With our understanding of the impaired transcriptional response to hypoxia in GR<sup>1000</sup>-expressing flies, we sought to investigate whether elevated ROS levels in GR<sup>1000</sup>-expressing flies were exacerbated by 24 hour, 5 %  $O_2$  exposure. Flies pan-neuronally (nSyb-Gal4 (III)) expressing GFP or GR<sup>1000</sup> were exposed to 21 % or 5 %  $O_2$  for 24 hours at 4 dpe. Immediately following exposure, brains were dissected from flies and incubated in media containing Amplex Red, which detects the ROS  $H_2O_2$ . Quantification revealed no significant differences in  $H_2O_2$  levels between conditions (two-way ANOVA with uncorrected Fisher's LSD test,  $p > 0.05$ ), despite noteworthy trends. Trends showed increased  $H_2O_2$  following hypoxic exposure, with a greater increase in flies expressing GR<sup>1000</sup> (Fig. 5.8A). There was also a trend towards a slight increase in  $H_2O_2$  in GR<sup>1000</sup>-expressing flies, compared to GFP-expressing flies, under normoxia.

**A****B****C**

**Figure 5.8. Pan-neuronal expression of GR1000 does not significantly exacerbate hypoxia-induced DNA damage or oxidative stress.** Flies pan-neuronally (nSyb-Gal4 (III)) expressing GFP or GR1000 were used. A) Quantification of  $\text{H}_2\text{O}_2$  in 5 dpe adult fly brains as measured in Amplex Red assays. B) Representative images of TUNEL staining in 5 dpe adult fly brains. Differences in brain morphology are due to mounting errors. Scale bar is 200 $\mu\text{m}$ . C) Quantification of TUNEL fluorescence as corrected total brain fluorescence (CTBF). Points represent biological replicates (A) or individual flies (C); lines represent mean and error bars show SEM. N = 3

Having demonstrated that hypoxic exposure is associated with aberrant transcription and trends towards increased ROS in young flies pan-neuronally expressing GR1000, we sought to examine whether these molecular changes are associated with cytotoxicity, cell death and neurodegeneration. To examine this, we utilised terminal deoxynucleotidyl transferase-dUTP nick end labelling (TUNEL) to detect DNA fragmentation, which is used as an indicator of apoptotic cells. Previous studies have demonstrated increased TUNEL signal in zebrafish embryos expressing GR100 (Riemslogh *et al.*, 2021) and *Drosophila* adult brains expressing GR1000 (unpublished data). Other methods have been also used to demonstrate increased DNA damage in C9 patient-derived motor neurons (Lopez-Gonzalez *et al.*, 2016). Hypoxic exposures of 0.1 % O<sub>2</sub> for 24 hours and 3 % O<sub>2</sub> for 48 hours have also been demonstrated to cause apoptosis, as measured by TUNEL signal, in primary cultures of rat neocortical neurons (Banasiak and Haddad, 1998).

Flies were exposed to 5 % O<sub>2</sub> for 24 hours at 4 dpe, before immediate dissection and fixation of brains for TUNEL staining. Imaging and quantification revealed no significant differences in TUNEL signal between conditions (Fig. 5.8B, C; two-way ANOVA with Šídák's multiple comparisons test,  $p > 0.05$ ). However, there was a clear trend towards increased TUNEL signal in GR1000-expressing flies exposed to hypoxia (Fig. 5.8B). No corresponding trend was observed in GFP control flies. Interestingly, GR1000 expression alone did not cause an increase in TUNEL signal compared to GFP. While TUNEL signal has previously been demonstrated to be increased in 28 dpe flies pan-neuronally expressing GR1000 (unpublished data), there are a number of reasons for this discrepancy with our findings. The first is that our data was collect from 5 dpe flies, so GR1000 may cause DNA damage and apoptosis in an age-related manner. Previous experiments were performed under different conditions which we know modify other GR1000 phenotypes. Additionally, a well-known pitfall of TUNEL is its high false positive rate, which may have affected our results (Arama and Steller, 2006).

#### **5.2.4. Continuous hypoxia does not potentiate GR1000 motor deficits**

Having observed a number of trends and significant differences in the molecular response of flies pan-neuronally expressing GR1000, following a 24 hour, 5 % O<sub>2</sub> exposure, we hypothesised that repeated induction of this aberrant response would be detrimental and exacerbate existing GR1000-induced motor phenotypes. To study this, we devised a repeated hypoxia regime, whereby flies pan-neuronally (nSyb-Gal4 (III)) expressing GFP or GR1000 are exposed to 21 % or 5 % O<sub>2</sub> for 24 hours, once every 7 dpe (Fig. 5.9). Following

exposure and a 48 hour recovery period, motor phenotypes are measured using climbing and activity assays.

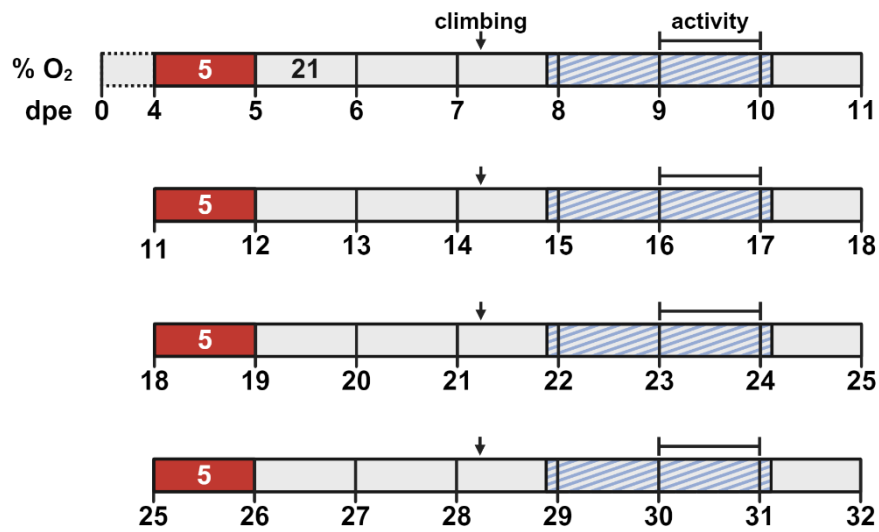


**Figure 5.9. Regime for repeated hypoxic exposure in *Drosophila*.** Flies are exposed to 5 % O<sub>2</sub> for 24 hours at 4, 11, 18 and 25 dpe. This exposure was selected based on its demonstrated effects on transcription at 4 dpe. Fly motor function is measured by climbing (SING) and activity assays at 7 and 9 dpe respectively, repeated every subsequent 7 dpe. Blue hatched blocks are time spent in activity tubes.

As in previous experiments, flies pan-neuronally expressing GR1000 demonstrated significantly reduced climbing ability compared to GFP controls from 14 dpe, regardless of exposure to hypoxia (Normoxia: 14 dpe;  $p = 0.0061$ , 21 dpe:  $p = 0.0044$ , 28 dpe;  $p = 0.0261$ , Hypoxia: 14 dpe;  $p < 0.0001$ , 21 dpe;  $p < 0.0001$ , 28 dpe;  $p < 0.0001$ ) (Fig. 5.10A, C, D, E). Exposure to hypoxia increased the climbing ability of flies pan-neuronally expressing GFP, but this effect was only significant at 7 and 14 dpe (7 dpe:  $p = 0.0386$ , 14 dpe:  $p = 0.0088$ , 21 dpe:  $p = 0.4101$ , 28 dpe:  $p = 0.4993$ ) (Fig. 5.10B, C). No such effect was observed in flies pan-neuronally expressing GR1000 (Fig. 5.10B, C).

Activity of flies pan-neuronally expressing GR1000 was significantly lower than GFP controls at all ages, regardless of exposure to hypoxia (Normoxia: 9 dpe;  $p = 0.0033$ , 16 dpe;  $p < 0.0001$ , 23 dpe:  $p < 0.0001$ , 30 dpe;  $p < 0.0001$ , Hypoxia: 9 dpe;  $p = 0.0313$ , 16 dpe;  $p = 0.0002$ , 23 dpe;  $p < 0.0001$ , 30 dpe;  $p < 0.0001$ ) (Fig. 5.11). Exposure to hypoxia caused a slight, insignificant decrease in the activity of flies pan-neuronally expressing GFP at all ages (9 dpe:  $p = 0.5874$ , 16 dpe:  $p = 0.2320$ , 23 dpe:  $p = 0.0641$ , 30 dpe:  $p = 0.3217$ ) (Fig. 5.11). No such effect was observed in flies pan-neuronally expressing GR1000 (Fig. 5.11).

In summary, exposure to hypoxia caused an increase in climbing ability of GFP flies that was significant at 7 and 14 dpe but not 21 and 28 dpe. Exposure to hypoxia had no effect on the climbing ability of GR flies at any age. Activity was significantly reduced in GR flies, regardless of treatment, compared to GFP controls at all ages. Exposure to hypoxia caused a slight decrease in the activity of GFP flies but did not cause significant changes in activity in either GFP or GR flies at any age.

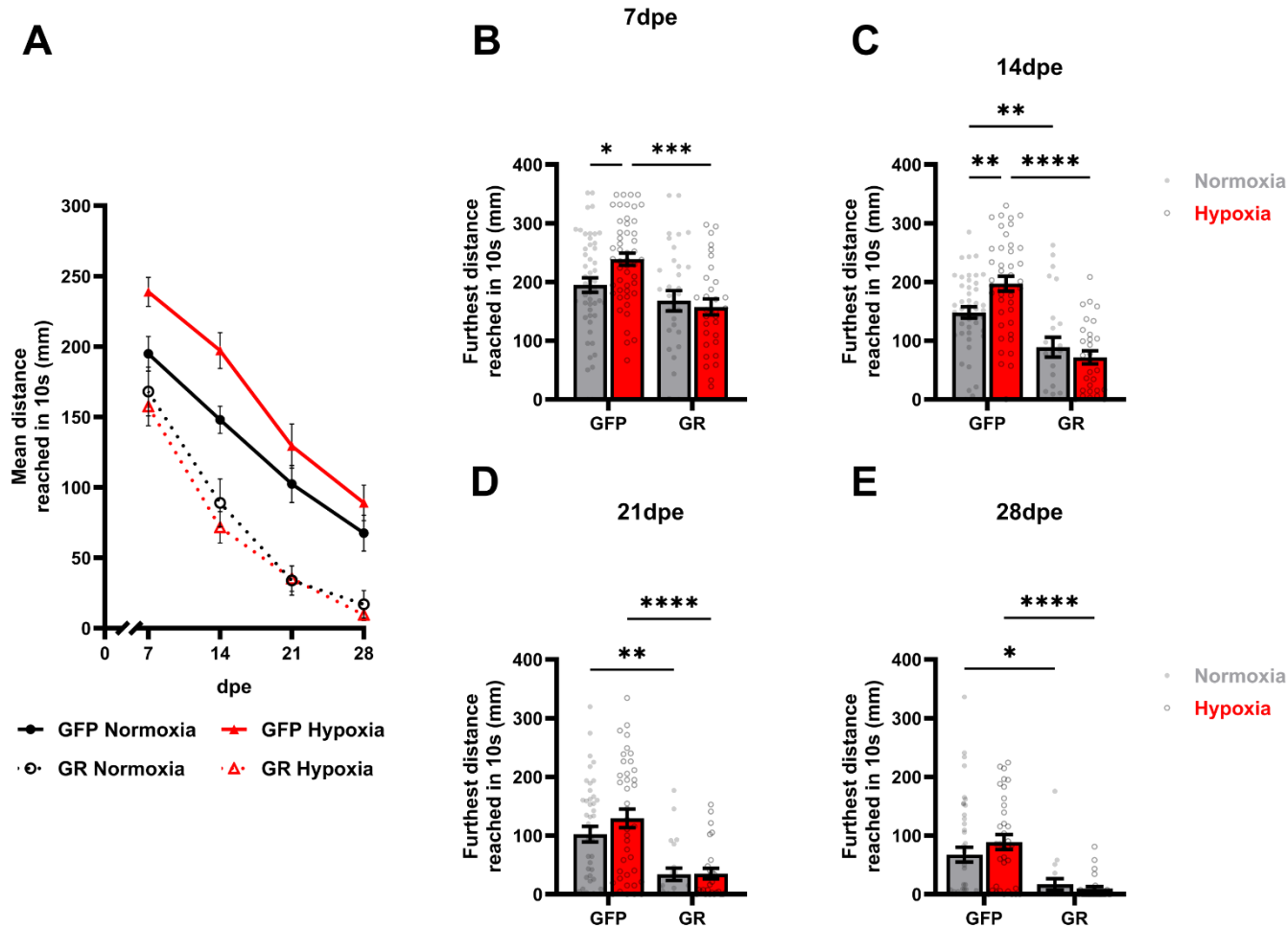


**Figure 5.10. Pan-neuronal expression of GR1000 prevents hypoxia-induced increases in climbing ability.** A) Quantification of fly climbing ability throughout the fly lifetime. Climbing ability was measured as the furthest distance reached in 10 seconds in SING assay at B) 7, C) 14, D) 21 and E) 28 dpe. Flies pan-neuronally (nSyb-Gal4 (III)) expressing GFP or GR1000 were repeatedly exposed to 21 % (normoxia) or 5 % (hypoxia) for 24 hours. Points represent individual flies; bars represent mean and error bars show SEM. Stats are two-way ANOVA with Šídák's multiple comparisons test of preselected pairs. \*  $p < 0.05$ , \*\*  $p < 0.01$ , \*\*\*  $p < 0.001$ , \*\*\*\*  $p < 0.0001$ . N = 3.

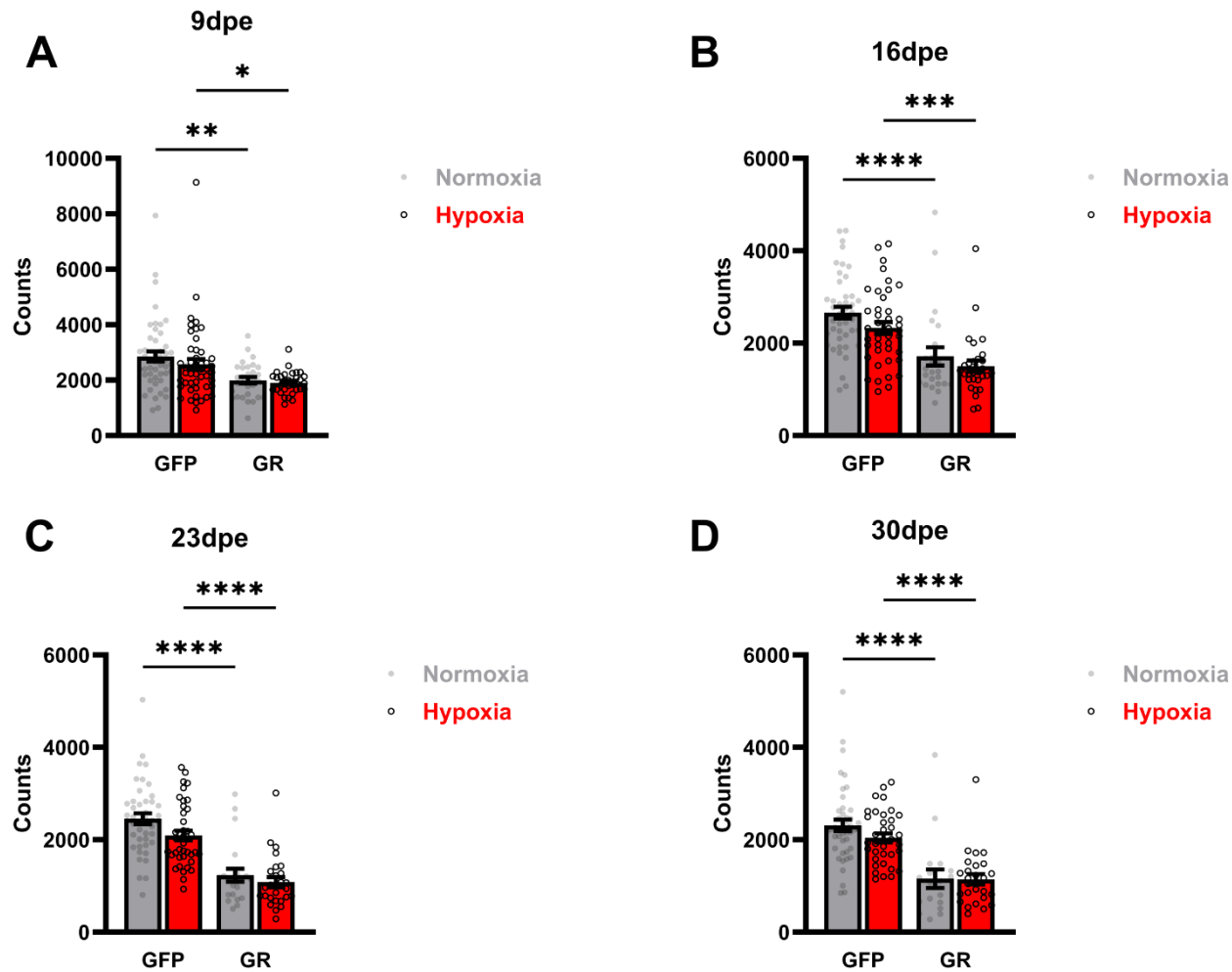


**Figure 5.11. Repeated exposure to hypoxia does not modify activity deficits in flies pan-neuronally expressing GR1000.** Activity was measured as total counts in a 24 hour period at A) 9, B) 16, C) 23 and D) 20 dpe. Flies pan-neuronally (nSyb-Gal4 (III)) expressing GFP or GR1000 were repeatedly exposed to 21 % (normoxia) or 5 % (hypoxia) for 24 hours. Points represent individual flies; bars represent mean and error bars show SEM. Stats are two-way ANOVA with Šídák's multiple comparisons test of preselected pairs. \*  $p < 0.05$ , \*\*  $p < 0.01$ , \*\*\*  $p < 0.001$ , \*\*\*\*  $p < 0.0001$ . N = 3.

### 5.2.5. Knockdown of HIF1 $\alpha$ does not facilitate hypoxia-induced effects on GR1000 motor phenotypes

Despite repeated induction of the aberrant transcriptional response, the motor function of flies pan-neuronally expressing GR1000 was unaffected by repeated hypoxic exposure. This leads us to believe that the aberrant transcriptional response observed in these flies is protective and/or compensatory, counteracting existing GR1000-induced deficits within the cell, rather than detrimental. To test this hypothesis, we measured the motor function of flies pan-neuronally (nSyb-Gal4 (II)) expressing GFP or GR1000 alongside RNAi knockdown of HIF1 $\alpha$  during our repeated hypoxia regime. With RNAi knockdown of HIF1 $\alpha$  we hope to counteract the hypoxia-induced increases in HIF1 $\alpha$  expression and activity that were observed in GR1000 flies.

Flies pan-neuronally expressing GFP and control RNAi did not exhibit the same repeated hypoxia induced increase in climbing ability demonstrated previously by flies pan-neuronally expressing GFP alone (Fig. 5.12A, B). This may be attributed to the titration of GAL4 by the control RNAi transgene in this experiment, or to the use of nSyb-Gal4 (II) in this experiment where nSyb-Gal4 (III) was used previously.

Knockdown of HIF1 $\alpha$ , compared to RNAi control, appeared to increase the climbing ability of flies exposed to normoxia and pan-neuronally expressing GFP at 7 and 28 dpe, although this was only significant at 28 dpe (7 dpe:  $p = 0.2020$ , 28 dpe:  $p = 0.0017$ ) (Fig. 5.12A, D). A similar but insignificant increase was observed with HIF1 $\alpha$  RNAi, compared to RNAi control, in flies exposed to hypoxia and pan-neuronally expressing GFP at all ages (7 dpe:  $p = 0.9711$ , 14 dpe:  $p = 0.8522$ , 21 dpe:  $p = 0.0567$ , 28 dpe:  $p = 0.0756$ ) (Fig. 5.12). Compared to RNAi control, knockdown of HIF1 $\alpha$  in flies pan-neuronally expressing GR1000 caused a decrease in climbing ability at 7 dpe, that was significant in flies exposed to hypoxia but not normoxia (Normoxia:  $p = 0.2334$ , Hypoxia:  $p = 0.0405$ ) (Fig. 5.12A). As in the previous experiment, repeated hypoxic exposure caused a slight but insignificant ( $p = 0.803$ ) decrease in the climbing ability of flies pan-neuronally expressing GR1000 alongside RNAi control at 14 dpe (Fig. 5.12B).

As in the previous experiment, repeated hypoxic exposure caused a slight but insignificant decrease in the activity of flies pan-neuronally expressing GFP alongside RNAi control at all ages (9 dpe:  $p = 0.6419$ , 16 dpe:  $p = 0.9677$ , 23 dpe:  $p = 0.6678$ , 30 dpe:  $p = 0.9175$ ) (Fig. 5.13). In contrast, the activity of GR1000-expressing flies showed no trends or differences in activity with repeated hypoxic exposure or knockdown of HIF1 $\alpha$  (Fig. 5.13).

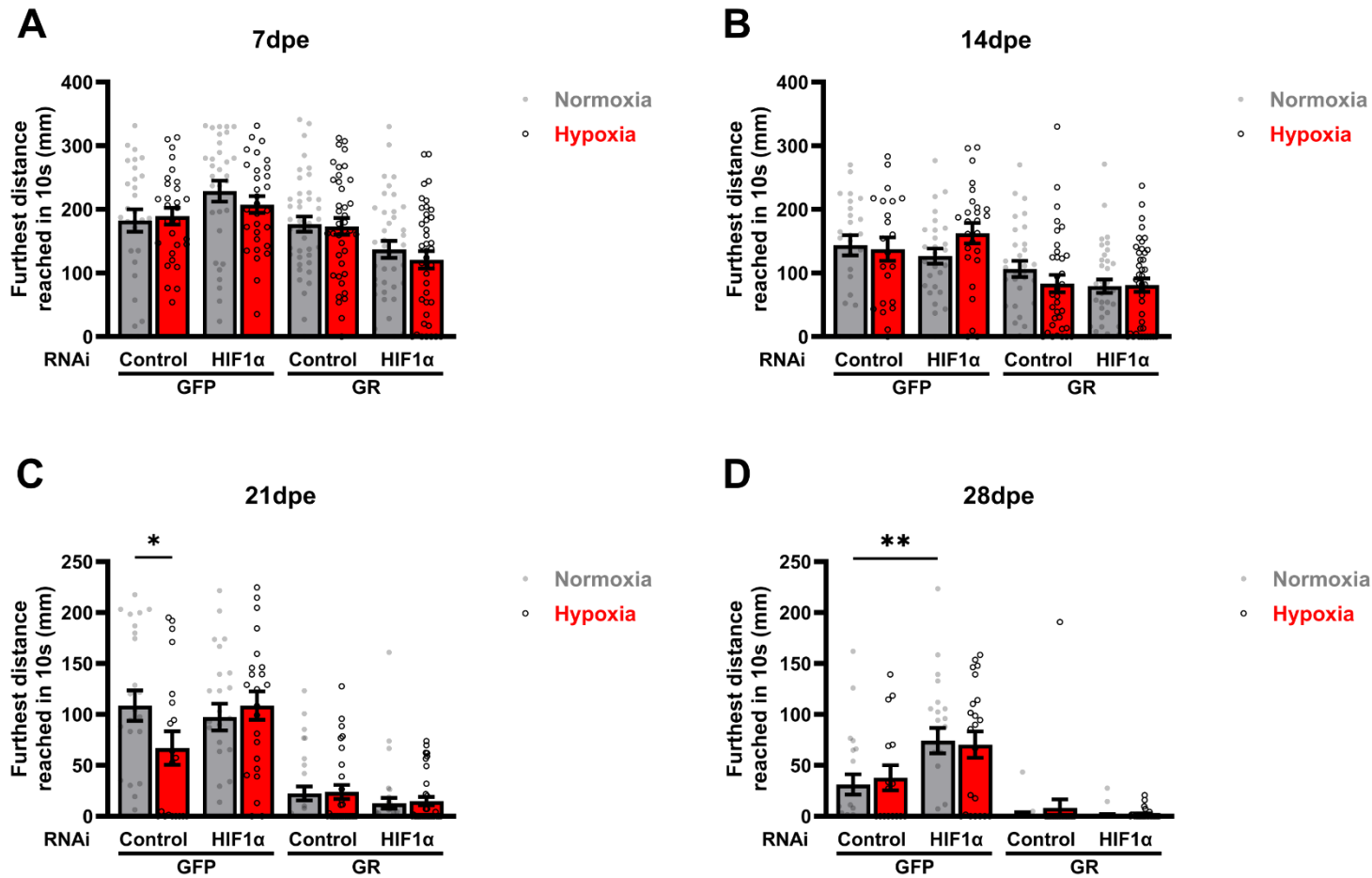


**Figure 5.12. Knockdown of HIF1 $\alpha$  does not affect *Drosophila* climbing ability following exposure to hypoxia.** Climbing ability was measured as the furthest distance reached in 10 seconds in SING assay at A) 7, B) 14, C) 21 and D) 28 dpe. Flies pan-neuronally (nSyb-Gal4 (II)) expressing GFP or GR1000, alongside mCherry-RNAi (control) or HIF1 $\alpha$ -RNAi, were repeatedly exposed to 21 % (normoxia) or 5 % (hypoxia) for 24 hours. Points represent individual flies; bars represent mean and error bars show SEM. Stats are two-way ANOVA with Šídák's multiple comparisons test of preselected pairs. \*  $p < 0.05$ , \*\*  $p < 0.01$ , \*\*\*  $p < 0.001$ , \*\*\*\*  $p < 0.0001$ . N = 3.

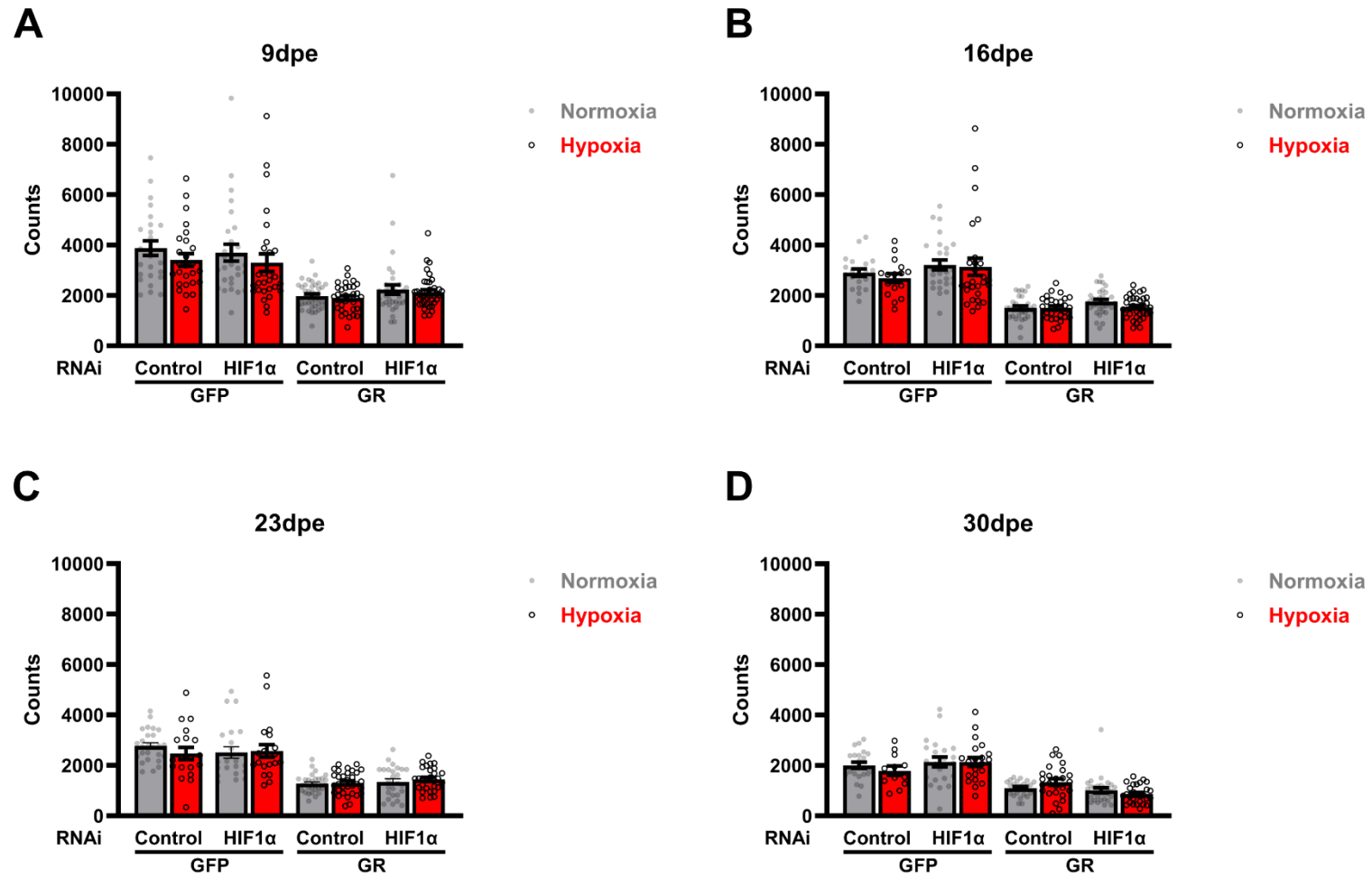


**Figure 5.13. Knockdown of HIF1 $\alpha$  does not affect *Drosophila* motor activity following exposure to hypoxia.** Activity was measured as total counts in a 24 hour period at A) 9, B) 16, C) 23 and D) 30 dpe. Flies pan-neuronally expressing (nSyb-Gal4 (II)) GFP or GR1000, alongside mCherry-RNAi (control) or HIF1 $\alpha$ -RNAi, were repeatedly exposed to 21 (normoxia) or 5 (hypoxia) % for 24 hours. Points represent individual flies; bars represent mean and error bars show SEM. N = 3.

### 5.3. Discussion

#### 5.3.1. Basal activity of HIF1 $\alpha$ under normoxic conditions is unaffected by GR1000

One of the key findings presented in this chapter is that HIF1 $\alpha$  expression and activity, measured by RT-qPCR, is not perturbed in GR1000-expressing flies under normoxic conditions. This indicates that HIF1 $\alpha$  is not driving the GR1000 toxicity that we and others have previously observed under normoxic conditions. While HIF1 $\alpha$  does not appear to mediate GR1000 toxicity, genetic manipulation of HIF $\alpha$  expression was able to modify GR1000-induced climbing deficits at young ages. We conclude from this that HIF1 $\alpha$  does not mediate GR1000 toxicity and phenotypes but is able to modify them, perhaps through regulation of HIF1 $\alpha$  transcriptional targets involved in cell survival processes (Lee *et al.*, 2004). We did not investigate the effects of HIF1 $\alpha$  knockdown or overexpression on downstream transcription of HIF1 $\alpha$  targets, such as Ldh. Using RT-qPCR, these effects should be studied in future work to shed light on possible mechanisms of HIF1 $\alpha$ -mediated modification of GR1000 phenotypes.

Despite continuous nuclear export of HIF1 $\alpha$  by XPO1, hypoxia causes a net movement of HIF1 $\alpha$  into the nucleus. Therefore, impairment of XPO1 function by GR1000 could lead to increased nuclear HIF1 $\alpha$  under hypoxia and an increased transcriptional response to hypoxia. Previous studies have shown that GR1000 flies exhibit increased ROS and oxidative stress, which have been shown to activate HIF1 $\alpha$  in a process known as pseudohypoxia (Hayashi *et al.*, 2019). Therefore, we had hypothesised that activation of HIF1 $\alpha$  would be observed in GR1000 flies even under hypoxia. However, our RT-qPCR data reveal little to no differences in transcription of hypoxia signalling genes between GFP and GR1000 flies under normoxia, even in older flies.

#### 5.3.2. GR1000 perturbs the hypoxic stupor response

In our intermittent hypoxia regime, we observed flies entering the hypoxic stupor response at different rates in a 1 % O<sub>2</sub> environment. When we investigated this effect with pan-neuronal expression of each of the 1000-repeat DPRs, we identified that AP, GA and GR all cause significantly earlier entry into the hypoxic stupor response. While we did not study this effect further, it does raise some interesting questions for further study.

The hypoxic stupor response has been proposed to be a protective response exhibited by many species, including *Drosophila*, to reduced energy consumption and production under hypoxia in order to prevent cellular damage (Krishnan *et al.*, 1997). It occurs through

silencing of motor neurons and is associated with decreases in carbohydrate metabolism (Krishnan *et al.*, 1997; Coquin *et al.*, 2008).

Apart from DPRs, the only reported modifier of rate of stupor onset is adenosine deaminase acting on RNA (ADAR), loss of function of which caused significantly earlier onset of the hypoxic stupor in *Drosophila* (Ma *et al.*, 2001). This effect is believed to occur through modulation of ion channels via ADAR-mediated RNA editing. This indicates that DPRs may cause similar electrophysiological defects that disrupt the neuronal silencing underlying the hypoxic stupor. However, previous study has only associated electrophysiological defects with AP1000 (West *et al.*, 2020), leaving GA and GR1000 hypoxic stupor phenotypes unexplained. This highlights the need for more in-depth electrophysiological study of neurons expressing 1000-repeat DPRs, including under hypoxia.

Existing evidence does not point to electrophysiological disruption in GA or GR1000, so there may be another mechanism through which DPRs can modify the onset of hypoxic stupor. DPR neurotoxicity undoubtedly causes reduced neuronal health and increased vulnerability to stressors. Given that the hypoxic stupor is a protective response, we believe that this vulnerability may lead to earlier onset of the hypoxic stupor to protect already unhealthy neurons from further damage. This could be tested using hypoxic stupor assays of flies induced with neuronal stress through a range of pharmacological or genetic means. This hypothesis may explain why PR1000 is the only DPR that does not modify the hypoxic stupor since it demonstrates the least severe motor phenotypes at 14 dpe, the age at which hypoxic stupor assays were performed (West *et al.*, 2020).

Rate of recovery from the hypoxic stupor is more commonly studied than rate of onset, with multiple modifiers having been identified (Haddad and Ma, 2001; Liu, Roy and Johnson, 2006; Mortimer and Moberg, 2013; Gleixner *et al.*, 2016). As such, we have a greater understanding of the mechanisms behind recovery, which include modulation of ion channels, oxygen metabolism and HIF1 activity. Unfortunately, we were unable to quantify latency to recovery with our experimental setup, due to insufficient video resolution. Future work should include studying the effects of DPR1000 expression on recovery, especially GR1000 since HIF1 activity has been implicated in the recovery process.

### 5.3.3. GR1000 motor phenotypes are unaffected by intermittent hypoxia

Previous studies have identified that occupations in which an individual is often exposed to hypoxia, such as professional athlete and firefighter, are associated with an increased ALS risk (Belli and Vanacore, 2005; Chiò *et al.*, 2005; Abel, 2007; Vanacore *et al.*, 2010). This occupational exposure to hypoxia would be classed as intermittent, rather than continuous. Interestingly, intermittent hypoxia has also been demonstrated to aggravate motor neuron degeneration and cognitive dysfunction in mouse models of SOD1 ALS (Kim *et al.*, 2013). These findings implicate intermittent hypoxic exposure as an environmental factor in the gene/environment/time hypothesis, whereby individuals with genetic susceptibility to ALS may increase their likelihood or rate of onset of disease through intermittent exposure to hypoxia. We attempted to replicate this with our intermittent hypoxia regime but were unable to elicit motor phenotypes in control flies or modify phenotypes in GR1000-expressing flies. One conclusion we could draw from this is that, despite evidence from mammalian studies, intermittent hypoxia does not play a role in motor dysfunction in *Drosophila*. *Drosophila* are particularly resistant to severely hypoxic conditions, capable of withstanding hours of anoxia without apparent damage to tissues (Haddad *et al.*, 1997), so may not exhibit the same negative effects of hypoxia as other organisms. However, it must be noted that GFP-expressing flies did demonstrate a trend towards decreased climbing ability after undergoing the intermittent regime. From this we can infer that intermittent hypoxia can disrupt motor function in *Drosophila*, but our regime was not sufficient to cause significant changes. To our knowledge, ours is the only study of *Drosophila* motor function following intermittent hypoxic exposure, so we do not have a validated protocol to which we can compare our data. Perhaps increasing the number or intensity of intermittent hypoxic exposures would be sufficient to evoke a significant decrease in fly motor function.

With this in mind, and in an effort to better recreate occupational hypoxia, future work could include regimes starting at younger ages and study the long term effects of these exposures on climbing ability in older flies. Alongside motor phenotypes, it would be interesting to examine the effects of intermittent hypoxia at the tissue, cellular and molecular level. Studying motor neuron degeneration as a result of intermittent hypoxia could provide a direct mechanism behind motor phenotypes, previously identified in and common to SOD1 ALS (Kim *et al.*, 2013).

While we identified an aberrant transcriptional response to continuous hypoxia in GR1000 flies, we did not examine transcriptional changes in response to intermittent hypoxia. Compared to continuous hypoxia, intermittent hypoxia has been shown to cause a different transcriptional response that is more heavily involved in NF- $\kappa$ B and immune signalling (Azad

*et al.*, 2009). Aberrant transcription was demonstrated in these pathways in our continuous hypoxia RT-qPCR data, highlighting the need for future work to study the transcriptional response to intermittent hypoxia.

Another question for future study is the role of the hypoxic stupor in protecting against intermittent hypoxia mediated damage. We demonstrated that flies pan-neuronally expressing GR1000 enter this protective stupor earlier than controls, which may explain why GR1000-expressing flies do not exhibit the same trend towards decreased climbing ability as controls. If we were able to 'rescue' the early stupor phenotype in GR1000 flies, we could determine whether loss of that protective effect facilitates intermittent hypoxia mediated effects on GR1000 motor phenotypes.

#### **5.3.4. GR1000 perturbs the transcriptional response to continuous hypoxia**

The most notable findings in this chapter are that pan-neuronal expression of GR1000 in *Drosophila* causes an aberrant response to hypoxia at the behavioural and transcriptional level. The transcriptional response to hypoxia is highly conserved between humans and flies. As such, these GR1000-mediated changes are highly relevant to C9 patients (Ismail *et al.*, 2013; Fomin *et al.*, 2018). While humans may not receive the equivalent to a 24 hour, 5 % O<sub>2</sub> exposure in *Drosophila*, they may experience shorter and less severe exposures on a more regular basis throughout their life, for example as a professional athlete or firefighter. Aberrant transcription in each of these 'micro'-exposures could result in cumulative downstream effects. However, it must be noted that repeated induction of this aberrant transcriptional response did not cause a decrease in fly motor function in our study.

The nature of the transcriptional differences themselves raised more questions than they answered. Hypoxia triggered a significant increase in the transcription of HIF1 $\alpha$  in GR1000 flies but not controls, which is unusual given that HIF1 $\alpha$  is predominantly regulated at the protein level (Lee *et al.*, 2004). Understanding what is driving this increase may provide an important link between GR1000 and dysregulation of the response to hypoxia. Transcription of HIF1 $\alpha$  is partly regulated by NF- $\kappa$ B (Rius *et al.*, 2008), but NF- $\kappa$ B transcription and activity was only significantly increased in GFP flies exposed to hypoxia. However, we cannot conclude from this that NF- $\kappa$ B is not driving the GR1000-mediated increases in HIF1 $\alpha$  transcription, because NF- $\kappa$ B activation in GR1000 flies may be occurring as HIF1 $\alpha$  transcription rather than AMP transcription. Further study could include investigating the transcriptional response to hypoxia in GR1000-expressing flies alongside knockdown or inhibition of NF- $\kappa$ B mediated HIF1 $\alpha$  transcription, shedding light on the driving force behind these GR1000-mediated changes.

Under normoxic conditions, overexpression of HIF1 $\alpha$  caused a slight increase in the motor function of young flies expressing GR1000 while knockdown of HIF1 $\alpha$  had the opposite effect. This demonstrates that HIF1 $\alpha$  expression affects the motor function of GR1000 flies, likely through some manner of mitigating GR1000 toxicity. Therefore, the increase in HIF1 $\alpha$  transcription may be a protective response exhibited by GR1000-expressing flies, which could be investigated by overexpression of HIF1 $\alpha$  alongside GR1000 in flies exposed to hypoxia. However, when we investigated this hypothesis by knocking down HIF1 $\alpha$  in GR1000 flies exposed to hypoxia, we saw no difference in their motor ability. Importantly though, we did not confirm that our HIF1 $\alpha$  RNAi line does cause sufficient knockdown to counteract hypoxia-induced changes in transcription. Validation of the effects of this RNAi on hypoxia-induced transcriptional changes would help us understand the protective nature of this effect. Another possibility is that this GR1000-associated, hypoxia-induced increase in HIF1 $\alpha$  transcription is a compensatory effect in an attempt to account for deficits in hypoxia signalling pathways. However, we also observed a corresponding increase in HIF1 $\alpha$  activity through transcription of HIF1 $\alpha$  target genes so there do not appear to be any deficits. This leads us to conclude that expression of GR1000 causes a hypersensitivity to hypoxia, occurring at either the sensing of or response to hypoxia. This conclusion is further supported by our observations of GR1000-expressing flies entering the hypoxic stupor response early, however we are cautious to draw direct comparisons between the stupor and transcriptional response given disparities in hypoxic stimulus, timeframe and mechanism. A key experiment in determining whether GR1000 causes hypersensitivity to hypoxia would be exposing GFP and GR1000 flies to a decreasing O<sub>2</sub> % or increasing exposure time and measuring the point at which flies begin to exhibit behavioural and transcriptional responses. Delineating dysfunction in the sensing or response to hypoxia would be more complicated and likely involve genetic disruption of different components of the hypoxia signalling pathway such as PHDs or VHL, alongside hypoxic exposure, to recreate the phenotypes observed in GR1000 flies.

Alongside significant increases in HIF1 $\alpha$  transcription, we also observed significantly increased HIF1 $\alpha$  transcriptional activity in GR1000 flies exposed to hypoxia. While this increase was only significant in young flies, a marked trend was observed in older flies too. Similar to our findings, Ilieva *et al.* (2003) identified sustained survival signalling in the spinal cord of SOD1 ALS mice following hypoxic exposure, although this signalling was not explicitly linked to HIF1 $\alpha$  activity. Interestingly, this contradicts findings from mouse models of SOD1 ALS which have all demonstrated reduced HIF1 $\alpha$  activity (Murakami *et al.*, 2003; Sato *et al.*, 2012; Nagara *et al.*, 2013). While these studies have not examined HIF1 $\alpha$  activity in response to hypoxia, they have all been performed in the spinal cord of these mice which

has been shown to be a hypoxic environment (Sato *et al.*, 2012). Importantly, our experiments were performed in the fly brain, rather than the thoracic ganglion (equivalent to spinal cord in *Drosophila*). This highlights the need for future work to examine the thoracic ganglion in our model, to better recapitulate the findings of previous studies. Reduced HIF1 $\alpha$  activity does not appear to be specific to SOD1 ALS, with Moreau *et al.* (2011) demonstrating that monocytes collected from sALS patients exhibit reduced HIF1 $\alpha$  activity after prolonged or acute hypoxic exposure. While there is clear evidence for dysregulation of HIF1 $\alpha$  expression and activity in ALS, our data highlight that the nature of dysregulation may vary between forms of the disease.

While we demonstrate an aberrant transcriptional response in young GR1000-expressing flies, no significant results were reported in older flies. Given that GR1000 is associated with phenotypes such as an age-related decline in climbing (West *et al.*, 2020), it is surprising to see the inverse effect here. To begin investigating this phenomenon, it would be useful to characterise the transcriptional response to hypoxia throughout the fly lifetime, rather than just young and old. Correlating this with other age-related phenotypes might shed light on the nature of these transcriptional effects.

### **5.3.5. Hypoxia may be associated with molecular changes in brains expressing GR1000**

In our study of the effects of hypoxic exposure on flies expressing GR1000, we also examined characteristic molecular changes associated with GR1000 expression in *Drosophila*. We identified trends towards increased ROS in the brains of young GR1000 flies exposed to hypoxia, which are understandable given the obvious links between hypoxia and oxidative stress (Magalhães *et al.*, 2004, 2005; Debevec *et al.*, 2014; Malacrida *et al.*, 2022). Where previous study identified increased ROS in 10 dpe fly brains expressing GR1000 even under normoxia (Au *et al.*, 2023), we did not observe such an effect at 5 dpe. This discrepancy may be due to differences in age, especially as we do not typically observe phenotypes in GR1000 flies at this early time point. Interestingly, Au *et al.*'s (2023) observations coincided with significant motor deficits while we observed no potentiation of motor deficits in GR1000 flies exposed to hypoxia. In addition to ROS, we also examined apoptosis in the *Drosophila* brain. Again, we observed a trend towards increased apoptosis in the brains of 5 dpe flies expressing GR1000 and exposed to hypoxia but in those exposed to normoxia. This contrasts our previous findings (unpublished data) which associated pan-neuronal expression of GR1000 alone with increased apoptosis in the brain, although this was only examined at 28 dpe.

Altogether it is clear from our study and its discrepancies with previous studies that further research is required into the effects of hypoxia on GR1000-associated increases in ROS and apoptosis in the fly brain. A full characterisation should be performed of ROS and apoptosis throughout the lifetime of flies expressing GR1000, alongside exposure to hypoxia. With this data, we would be able to determine whether hypoxic exposure accelerates or enhances GR1000-mediated effects. Combined with characterisation of GR1000-mediated aberrant transcriptional response to hypoxia throughout the fly lifetime, we may be able to correlate transcriptional effects to molecular changes and behavioural phenotypes. With these tools we would be able to better understand and further examine the mechanisms behind increased ROS and apoptosis in GR1000 flies exposed to hypoxia.

Importantly, it should be noted that the hypoxic exposure used in these experiments was not sufficient to affect GR1000-motor phenotypes so these molecular changes may not be entirely disease relevant. Studying these changes in a more intense hypoxia regime may overcome this issue.

### **5.3.6. Uncovering the effects of GR1000 on HIF1 $\alpha$ protein localisation and abundance**

Arguably the most important question that is not answered in this chapter is the effects of GR1000 expression on the HIF1 $\alpha$  protein. Using RT-qPCR we were able to quantify HIF1 $\alpha$  transcriptional activity, from which we can make inferences about HIF1 $\alpha$  localisation.

However, HIF1 $\alpha$  is primarily regulated at the protein level by its localisation and degradation. We sought to investigate HIF1 $\alpha$  localisation by IHC of larval salivary glands and Western blotting of nuclear and cytoplasmic protein fractions, but we were unable to achieve consistent HIF1 $\alpha$  staining with the antibodies available to us. This highlights the need for an antibody validated for staining *Drosophila* HIF1 $\alpha$  or fly lines carrying HIF1 $\alpha$  endogenously tagged with a fluorescent protein or protein tag, for which there are many well characterised antibodies.

Using these tools, future work would be able to ascertain how HIF1 $\alpha$  localisation is affected by the XPO1-GR1000 interaction and the implications of that on HIF1 $\alpha$  activity. Based on our previous observations, our hypothesis would be that GR1000-mediated impairment of XPO1 function leads to aberrant accumulation of HIF1 $\alpha$  in the nucleus, resulting in aberrant HIF1 $\alpha$  signalling. Measuring at a range of timepoints before, during and after hypoxic exposure would inform us on the dynamics of HIF1 $\alpha$  localisation in GR1000-expressing flies. If HIF1 $\alpha$  dynamics are disrupted at a specific stage, this data could shed light on whether GR1000-expressing flies are missensing or misresponding to hypoxia. Given that XPO1 provided the initial link between GR1000 and HIF1 $\alpha$ , we might expect that post-hypoxia

clearance of HIF1 $\alpha$  from the nucleus would be impaired by GR1000. This would be readily apparent by IHC and Western blot and could usefully be correlated to RT-qPCR data of HIF1 $\alpha$  transcriptional targets from matched timepoints.

### **5.3.7. GR1000 motor phenotypes are unaffected by continuous hypoxia**

Studying the cellular and molecular effects of GR1000 and hypoxia is incredibly useful from a mechanistic standpoint, but the most translational aspect of our work lies in motor phenotypes exhibited by our *Drosophila* model. One effect we observed was continuous hypoxia-mediated improvement in the motor function of control flies that was not exhibited by GR1000 flies. Although it is important to note that this effect was not replicated alongside expression of RNAi constructs in the subsequent experiment. Short-term hypoxia has previously been demonstrated to cause increases in motor function and motor cortex excitability (Katayama *et al.*, 2003; Szubski, Burtscher and Löscher, 2006; Dale, Ben Mabrouk and Mitchell, 2014), so this improvement was not unsurprising in our control flies. However, we did not see this improvement in GR1000 flies which leads us to believe that either: 1) GR1000-mediated disruption of hypoxia signalling pathways includes pathways mediating these improvements; or 2) GR1000-mediated decline in motor function is irreversible and thus cannot be improved upon or potentiated by hypoxic exposure.

Somewhat unexpectedly, repeated induction of the aberrant transcriptional response to hypoxia was not sufficient to affect motor function of flies expressing GR1000. Similar to our intermittent hypoxia experiments, it may be the case that our repeated hypoxia regime did not include sufficient hypoxic exposure to have any effects. As such, future work should seek to test a number of continuous hypoxia regimes to ascertain whether effects on motor function are possible. Alternatively, it may be the case that aberrant transcription is not detrimental to motor function at all. As discussed above, further study is required to determine the nature of this aberrant transcription, but it may be protective in some capacity.

### 5.3.8. NF- $\kappa$ B activity is modulated by GR1000

An intriguing observation from our RT-qPCR data was a trend towards increased expression and transcriptional activity of NF- $\kappa$ B in aged GR1000-expressing flies exposed to hypoxia. Similar trends were observed across multiple genes although no significant differences were reported, likely because of high variability between repeats. Activation of NF- $\kappa$ B by hypoxia occurs through calcium/calmodulin-dependent kinase 2 (CaMKII) activity, induced by cytoplasmic calcium influx (Hui *et al.*, 2006; Culver *et al.*, 2010). Given that NF- $\kappa$ B appears inactive in response to hypoxia in young GR1000-expressing flies, but appears hyperactive in older flies, neuronal calcium signalling may be disrupted by GR1000 in an age-related manner. Interestingly, a number of proteins involved in calcium ion transport and homeostasis were identified by our MS/MS screen as interacting with GR1000, providing a possible mechanism of disruption in calcium signalling.

Alternatively, NF- $\kappa$ B activity may be increased as a result of inflammation occurring in GR1000 flies under normoxia that is exacerbated by exposure to hypoxia. NF- $\kappa$ B is a key mediator of inflammatory responses, and hypoxia overlaps significantly with inflammation (Bartels, Grenz and Eltzschig, 2013; Liu *et al.*, 2017). While inflammation has never been examined in our model of GR1000 toxicity, it has understandably been linked to C9 disease (Masrori *et al.*, 2022).

However, it is important to note that NF- $\kappa$ B activity is activated by a number of stressors and that AMPs are primarily expressed as part of the immune response (Meister, Lemaitre and Hoffmann, 1997; Sun and Andersson, 2002). While biological replicates were raised under identical conditions, we did not explicitly control for immune stressors. Bacterial infections are not uncommon in lab *Drosophila* husbandry, so this may be what is driving the high expression in a few biological replicates.

## 5.4. Conclusions

In this chapter, we sought to investigate the role of HIF1 $\alpha$  and hypoxia in GR1000 toxicity. As an ALS-relevant XPO1 cargo protein, HIF1 $\alpha$  bears the potential to mediate GR1000 toxicity. We demonstrate that genetic manipulation of HIF1 $\alpha$  expression modifies cytotoxicity and motor phenotypes in control and GR1000 flies. We also used our model to study the potential causative or accelerative role of intermittent hypoxia in ALS and found an intermittent hypoxia regime caused trends towards motor defects in control flies but did not affect GR1000 flies. In doing so, we also identified that flies expressing GR1000 entered a protective hypoxic stupor significantly earlier than controls. This is a novel behavioural

phenotype in our model and represents GR1000-mediated missensing or misresponding to hypoxia. We demonstrated that this aberrant response to hypoxia is also present at the transcriptional level in HIF1 $\alpha$  and NF- $\kappa$ B expression and signalling. This aberrant response was also associated with trends towards increased ROS and apoptosis in adult fly brains. Despite these findings, GR1000 motor phenotypes were unaffected by repeated hypoxic exposure throughout the fly lifetime. However, control flies demonstrated hypoxia-mediated improvements in motor function, leading us to hypothesise that the aberrant response prevents these improvements in GR1000 flies. To investigate this, we attempted to counteract the aberrant transcriptional response to hypoxia by RNAi knockdown of HIF1 $\alpha$ . The motor phenotypes of flies expressing GR1000 remained unaffected by repeated exposure to hypoxia. While we demonstrate GR1000-mediated disruption to the behavioural and molecular response to hypoxia, our data do not indicate that this is associated with downstream neurotoxicity or motor impairment. However, our hypoxia regimes may not have been sufficient to cause changes in GR1000 motor function and future work should seek to investigate this further with more intense hypoxic exposures. Additionally, future work should include full characterisation of behavioural and molecular responses to hypoxia throughout the fly lifetime. Despite demonstrating an aberrant response to hypoxia in GR1000-expressing flies, we do not shed light on the underlying mechanisms of this. Lack of suitable tools prevented us from doing so, but future study of GR1000-mediated effects on HIF1 $\alpha$  protein would provide a great deal of insight into these mechanisms. Studying HIF1 $\alpha$  protein would also allow us to determine if and/or how the GR1000-XPO1 interaction leads to the observations we have reported here.

## 6. Discussion

Frontotemporal dementia (FTD) and amyotrophic lateral sclerosis (ALS) are two devastating neurodegenerative diseases, which share a high degree of clinical, pathological and genetic overlap (Ringholz *et al.*, 2005; Mackenzie *et al.*, 2007; Burrell *et al.*, 2011; DeJesus-Hernandez *et al.*, 2011; Renton *et al.*, 2011; Sieben *et al.*, 2012). As such FTD and ALS are considered to exist on a single disease spectrum. There is no known cure for either disease, and treatment options are currently limited. The most common genetic cause of both FTD and ALS is a hexanucleotide repeat expansion in the *C9orf72* (C9) gene, reaching up to 1000s of repeats in affected individuals (DeJesus-Hernandez *et al.*, 2011; Renton *et al.*, 2011). The most prominent driver of neurodegeneration downstream of this mutation is the bidirectional, RAN translation of the repeat to produce 5 toxic dipeptide repeat proteins (DPRs) (Mizielinska *et al.*, 2014; Tran *et al.*, 2015; Solomon *et al.*, 2018). Previous studies have highlighted the neurotoxicity of the DPRs, especially GR, but mechanisms of their toxicity remain somewhat unclear, partly due to the limitation of DPR repeat length (<100) in these studies. A key feature of the arginine-containing DPRs is their promiscuous protein-binding activity (Radwan *et al.*, 2020; Božič *et al.*, 2022), which could facilitate DPR-mediated disruption in a range of biological processes. Disruption in nucleocytoplasmic transport (NCT) has been associated with disease across the FTD/ALS spectrum, including C9 FTD/ALS (Freibaum *et al.*, 2015; Jovičić *et al.*, 2015; Zhang *et al.*, 2015). Exportin 1 (XPO1) is a nuclear export protein that has attracted particular attention in C9 FTD/ALS, primarily due to the conflicting evidence surrounding its role in C9 disease, including GR-mediated toxicity (Freibaum *et al.*, 2015; Vanneste *et al.*, 2019; Hutten *et al.*, 2020; Ramic *et al.*, 2021). Due to the intermediate nature of XPO1 in other biological processes, XPO1 disruption likely causes toxicity through impairment of its nuclear export cargo. Hypoxia-inducible factor 1  $\alpha$  (HIF1 $\alpha$ ) is an XPO1 cargo protein with a key role in the cellular response to hypoxia (Iyer *et al.*, 1998), dysfunction in which has been implicated as a pathological mechanism in non-C9 ALS (Sato *et al.*, 2012; Nagara *et al.*, 2013). Emerging evidence implicates a novel pathological role of hypoxia and hypoxia signalling in C9 FTD/ALS too (Fomin *et al.*, 2018; Julian *et al.*, 2021).

Therefore, the key aims of this research were to:

1. Identify GR1000-interacting proteins, such as XPO1, that act as modifiers of GR1000 toxicity *in vivo*
2. Characterise the effects of the GR1000-XPO1 interaction on XPO1 physiology
3. Investigate the effects of GR1000 expression on hypoxia signalling, a process downstream of XPO1
4. Elucidate the role of hypoxia and hypoxia signalling in GR1000 toxicity

## **6.1. Role of hypoxia in *C9orf72* FTD/ALS**

### **6.1.1. Exposure to hypoxia**

The nervous system is a major consumer of energy and, as such, is particularly vulnerable to the effects of hypoxia (Cervos-Navarro and Diemer, 1991). It is therefore unsurprising that a pathological role of hypoxia and hypoxia signalling has been identified in a range of neurodegenerative diseases, including ALS (Correia *et al.*, 2013; Mitroshina *et al.*, 2021). Specifically, previous studies have found occupational exposure to hypoxia to be associated with increased ALS risk (Belli and Vanacore, 2005; Chiò *et al.*, 2005; Vanacore *et al.*, 2010). Additionally, intermittent hypoxia has been shown to aggravate motor neuronal degeneration in ALS models (Kim *et al.*, 2013). Altogether these findings point towards a causative or accelerative role of occupational or intermittent exposure to hypoxia in ALS. While our intermittent hypoxia regime caused a trend towards motor deficits in healthy control flies, it did not accelerate motor decline in GR1000 flies. While this requires further study with more intensive regimes, these findings are an early indicator that the neurotoxicity of both GR1000 and intermittent hypoxia may occur through the same pathways. It is important to remember that, despite being one of the more abundant DPRs in patients, our GR overexpression model may not truly reflect the levels observed in patients. Therefore, pathways of toxicity that are activated in our model may only be partially activated in patients. However, simultaneous activation of these pathways by intermittent hypoxia and GR may cross a threshold of neurotoxicity.

The environmental nature of occupational and intermittent exposure to hypoxia raises some intriguing questions for future study, in how they affect *C9orf72* mutation carriers and contribute to disease progression, compared to carriers who are not exposed. To study these effects, patients need to be stratified by factors contributing to their lifetime hypoxic exposure, including occupation and physical activity. Post-mortem tissue may demonstrate pathological differences between strata; however, this is limited to end-point data and does

not necessarily inform us on disease progression. Epigenomic and transcriptomic analysis of blood samples throughout the patient lifetime would reveal some of the molecular effects of the interplay between the *C9orf72* mutation and hypoxic exposure. Further experiments could be conducted with induced neural progenitor cell (iNPC)-derived neurons from stratified patients, ideally collected at pre and post-symptomatic timepoints. Unlike induced pluripotent stem cell (iPSC)-derived cells, iNPC-derived cells retain the epigenetic profile of patients (Gatto *et al.*, 2020), which is particularly relevant when studying the effects of environmental factors such as exercise and hypoxia. In these iNPC-derived neurons we could examine in greater detail the cellular and molecular phenotypes that occur in response to intermittent hypoxia, with the full epigenetic background of patients who were exposed throughout their lifetime. This could shed light on any differences in the effects of hypoxic exposure between controls, patients without hypoxic exposures and patients with hypoxic exposures. An additional benefit of studying stratified patients is that it may reveal any confounding variables that segregate with occupational or intermittent hypoxic exposure, such as a genetic disposition towards intense activity.

### **6.1.2. HIF1 $\alpha$ -mediated response to hypoxia**

HIF1 $\alpha$  is a transcription factor that acts as the master regulator of the primary, transcriptional response to hypoxia (Iyer *et al.*, 1998). Dysfunction in HIF1 $\alpha$ -mediated hypoxia response pathways has been identified in studies of SOD1 and sALS, characterised by perturbed HIF1 $\alpha$  expression and downstream transcriptional activity (Moreau *et al.*, 2011; Sato *et al.*, 2012; Nagara *et al.*, 2013; Raman *et al.*, 2015; Nomura *et al.*, 2019). Applying these findings to C9 FTD/ALS, we demonstrated GR1000-mediated increases in HIF1 $\alpha$  expression and activity in response to hypoxia. To our knowledge, this is the first report of DPR-mediated disruption in hypoxia pathways. Our findings indicate that HIF1 $\alpha$  dysfunction, resulting in a perturbed transcriptional response to hypoxia, may be a common feature between causes of ALS.

Interestingly, knockdown of *C9orf72* has also been shown to cause increased NF- $\kappa$ B and hypoxia signalling (Fomin *et al.*, 2018). Therefore, studying the hypoxia response in iPSC-derived neurons from C9 FTD/ALS patients could provide interesting insight into the interplay between haploinsufficiency- and GR-mediated perturbations to hypoxia signalling. This could provide a clearer picture of what might be occurring in C9 FTD/ALS patients. Transcriptomic analysis of patient CSF and blood samples, collected at time of diagnosis and stratified by lifetime hypoxic exposure, could be used to assess environmental activation of aberrant hypoxia signalling in patients. Repeating this analysis on samples collected

throughout the course of the disease would provide further insight into the role of hypoxia signalling in disease progression. By studying HIF1 $\alpha$ -induced genes such as VEGF and ANG, known for their neuroprotective role (Lambrechts *et al.*, 2003; Sebastia *et al.*, 2009), we could also make inferences about the protective or detrimental effects of aberrant hypoxia signalling.

### 6.1.3. Tissue level hypoxia

Previous studies identified aberrant hypoxia signalling in the spinal cord of SOD1 ALS mice due to tissue level hypoxia, despite otherwise normoxic conditions (Sato *et al.*, 2012). Tissue level hypoxia combined with the GR-mediated aberrant response to hypoxia would result in continuous signalling and could confer toxicity. Our data demonstrate that GR does not perturb hypoxia signalling under normoxic conditions, although it must be noted that we looked in the brain rather than the thoracic ganglion (*Drosophila* equivalent to spinal cord). While our data suggest that GR does not cause tissue level hypoxia in *Drosophila*, we do not know if the other pathological mechanisms of the *C9orf72* mutation may contribute to tissue level hypoxia. Yamashita *et al.* (2021) used positron emission tomography (PET) to visualise hypoxic stress in the spinal cord of ALS patients, however it must be noted that this study was performed in Japan where SOD1 is the predominant cause of ALS and the *C9orf72* mutation is rare (Zou *et al.*, 2017). Using PET to examine hypoxic stress in C9 patients throughout disease progression could inform us on the temporal onset of hypoxia in patient tissue, therefore shedding light on the mechanistic role of tissue level hypoxia. This experiment could usefully be performed in patients stratified by lifetime hypoxic exposure, to provide further insight into how environmental factors interact with the *C9orf72* mutation to cause disease.

In SOD1 ALS, hypoxia in the spinal cord has been associated with vascular and blood flow changes (Miyazaki *et al.*, 2012). Vascular and blood flow changes remain relatively understudied in C9 FTD/ALS. Here, further study should take place in patient tissue and mammalian models because *Drosophila* do not possess vasculature in the same manner as mammals. Histological analysis of post-mortem patient tissue would provide us an insight into the degree of vascular changes in C9 FTD/ALS patients but would be limited to end point data only. Studying vascular changes in a mouse model would facilitate study throughout disease progression, informing us on the pathological role of these changes. Tissue hypoxia and vascular changes have previously been studied in the spinal cord in relation to ALS, but not FTD-relevant tissues. Therefore, studying these effects in relation to C9 FTD/ALS should include analysis of the frontal and temporal lobes.

#### 6.1.4. Hypoxia and astrocytes

Astrocytes are a subtype of glial cell found in the CNS, which function in partnership with neurons to facilitate physiological nervous system function (Ransom and Ransom, 2012). Astrocytes bear important metabolic, structural, homeostatic and neuroprotective functions and can act directly to affect neuronal health and survival. In C9 FTD/ALS, astrocytes exhibit TDP-43, RNA and DPR pathology and have been implicated in a key pathological role (Hsiung *et al.*, 2012; Stewart *et al.*, 2012; Mizielińska *et al.*, 2013). iPSC- and iNPC-derived astrocytes from C9 patients have even been shown to cause motor neuron pathophysiology (Meyer *et al.*, 2014; Zhao *et al.*, 2020). Due to time constraints, we were unable to study the effects of glial or astrocytic DPR expression in our *Drosophila* model. However, with the implication of hypoxia in DPR toxicity, it is important for future work to include the study of astrocytes. As part of their homeostatic function, astrocytes play a key role in the response to hypoxia in the CNS by modulating blood flow and maintaining energy levels (Marina *et al.*, 2016). Astrocytes also exhibit significant transcriptomic changes in response to hypoxia, resulting in dysfunction and dysregulation of mitochondria, metabolism and immune pathways (Allen *et al.*, 2020). Therefore, our findings of GR-mediated disruption to the transcriptional response may be particularly pertinent to astrocytes. Interestingly, astrocytic HIF1 $\alpha$  has been shown to mediate hypoxia-induced neuronal cell death while neuronal HIF1 $\alpha$  is neuroprotective (Vangeison *et al.*, 2008). These bidirectional effects of HIF1 $\alpha$  highlight the importance of studying GR-mediated effects on the hypoxia response in astrocytes. Future study of GR-mediated effects could take place in our *Drosophila* model, utilising astrocytic drivers (GMR86E01- or Alarm-Gal4) to express GR in astrocyte-like glial cells in the *Drosophila* nervous system (Kremer *et al.*, 2017). To study the combined effects of all *C9orf72* disease mechanisms, future experiments could be performed in iPSC-derived astrocytes and neurons from healthy controls and *C9orf72* FTD/ALS patients. By exposing mono- and co-cultures of these cells to hypoxia, we would be able to examine the astrocytic and neuronal responses to hypoxia, how they are affected by the *C9orf72* mutation and the hypoxia-induced effects of C9 astrocytes on both healthy and C9 neurons.

## 6.2. Role of XPO1 in *C9orf72* FTD/ALS

A number of studies have implicated NCT defects in C9 FTD/ALS (Freibaum *et al.*, 2015; Jovičić *et al.*, 2015; Zhang *et al.*, 2015). However, the nature of this dysfunction is debated, with evidence for disruption in both nuclear import and export pathways. The nuclear export protein XPO1 has received particular attention from researchers but evidence for its contribution to C9 FTD/ALS, particularly DPR toxicity, is conflicting (Freibaum *et al.*, 2015; Vanneste *et al.*, 2019; Hutten *et al.*, 2020; Ramic *et al.*, 2021). In our study of mechanisms of DPR toxicity, we demonstrated that XPO1 interacts with both 1000-repeat PR and GR. Further study of the effects of this interaction was hampered by a lack of appropriate tools. However, we were able to demonstrate that expression of GR causes trends towards nuclear accumulation of XPO1 cargo proteins, indicative of reduced XPO1 function. Our data provide further evidence for the relevance of XPO1 to C9 FTD/ALS. Following the further study to be performed in *Drosophila*, outlined in Chapter 4, it would be important to validate our findings in human cells. Additionally, it would be interesting to examine XPO1 localisation and function in both iPSC-derived neurons from *C9orf72* FTD/ALS patients and healthy neurons transfected with GR1000. Performing this experiment over time and correlating findings with FTD/ALS phenotypes, such as TDP-43 mislocalisation, would shed light on the XPO1-mediated accumulation of toxicity hypothesis hinted at by our data. This could be complimented with end-point data from C9 patient post-mortem tissue.

In addition to a physical interaction, we demonstrated a genetic interaction whereby partial knockdown of XPO1 delayed the onset of GR-mediated motor deficits in *Drosophila*. Previous studies have demonstrated neuroprotective effects of XPO1 downregulation or inhibition in models of FUS, TDP-43 and *C9orf72* FTD/ALS. Due its pathological role in a number of cancers, a number of XPO1 inhibitors have been developed. One compound, Selinexor (KPT-330), has already been approved by the FDA for treatment of multiple myeloma. Selinexor has demonstrated excellent blood-brain-barrier permeability (Green *et al.*, 2015) and related compounds have been shown to be beneficial in models of neurodegenerative disease, including FTD/ALS (Haines *et al.*, 2015; Grima *et al.*, 2017; Archbold *et al.*, 2018; Hightower *et al.*, 2020). Therefore, Selinexor is drug that could be repurposed to treat disease across the FTD/ALS spectrum.

## 6.3. Hypothesis of the GR-mediated aberrant response to hypoxia

Considering our findings altogether, we propose the mechanism linking the GR-XPO1 interaction with our hypoxia findings is based upon this interaction causing partial impairment of XPO1 function. Under hypoxia, HIF1 $\alpha$  is translocated to the nucleus and initiates the

transcriptional response to hypoxia. However, impaired XPO1 function leads to slowed clearing of HIF1 $\alpha$  from the nucleus after a return to normoxia. This results in prolonged HIF1 $\alpha$  signalling, which we observe as increased HIF1 $\alpha$  signalling in our experimental setup. The GR-XPO1 interaction also causes toxicity under normoxia, leading us to believe that non-HIF1 $\alpha$  pathways are also affected. These pathways may be affected by a separate gain-of-function mechanism, since reducing XPO1 expression ameliorated toxicity. Finally, we believe that the hypoxic stupor phenotype is caused through separate pathways altogether, as it was observed in GA and AP which demonstrate no interaction with XPO1.

#### **6.4. Implications for patients**

As researchers of human disease, it is important to consider the translational application of our findings, with the ultimate goal of improving outcomes for patients. With regards to the findings of this thesis and related work, we identify genetic and environmental factors that are associated with disease under the gene/environment/time hypothesis, and provide affected individuals with the information they need to make their own lifestyle choices. Previously, intermittent exposure to hypoxia has been an environmental factor linked to non-C9 ALS. Additionally, genetic variation in hypoxia genes, such as VEGF, has been associated with ALS more widely. Our findings, along with emerging studies, provide a novel link between hypoxia and C9 FTD/ALS. Demonstrating a role of hypoxia and hypoxia genes in C9 disease may have significant implications for genetic counselling of *C9orf72* mutation carriers and their families. Firstly, this highlights the need to screen suspected carriers for genetic variation in other disease risk genes, such as VEGF. With this information, individuals can gain a better understanding of their risk developing the disease. Secondly, identification of hypoxia as an environmental risk factor in C9 FTD/ALS would suggest the importance of informing carriers that occupations such as firefighter or professional athlete may increase their disease risk, especially if they carry genetic variants in hypoxia genes. With this information they would be able to make their own informed decisions on their lifestyle choices and if or how they want to manage their disease risk.

By identifying XPO1 impairment as a possible mechanism underlying perturbations in hypoxia pathways, we provide a potential therapeutic target in these pathways. Ours and others' findings, that modulation of XPO1 is beneficial in models of C9 FTD/ALS, provides evidence in support of XPO1 as a therapeutic target. Compounds targeting XPO1 are already approved for treating multiple myeloma patients, providing realistic opportunities for the repurposing of these therapies for FTD/ALS patients.

## 6.5. Conclusions

Building upon previous research, we demonstrated that GR1000 interacts with XPO1 and, while this doesn't affect XPO1 localisation, it causes trends towards impaired XPO1 function and nuclear accumulation of its cargo. Additionally, we demonstrate that partial knockdown of XPO1 expression causes a delay in the onset of GR1000-mediated motor deficits in flies, highlighting a mechanistic role of XPO1 in GR1000 toxicity. However, many questions remain unanswered on the nature of the GR-XPO1 interaction; its effects on XPO1 function; and its role in mediating GR toxicity. We identified HIF1 $\alpha$  as an XPO1 cargo protein that is relevant to FTD/ALS and demonstrated that altering its expression modifies motor function in *Drosophila*. While exact mechanisms of GR1000-mediated disruption in hypoxia pathways remain unclear, we show that expression of GR1000 causes an aberrant transcriptional response to hypoxia, characterised by increased HIF1 $\alpha$  expression and activity. Repeated induction of this response was associated with, but did not cause, an absence of hypoxia-induced improvements in motor function. Additionally, we found that pan-neuronal expression of AP, GA or GR1000 causes a perturbed behavioural response to hypoxia, in the form of early entry into the protective hypoxic stupor response. Despite perturbations in the behavioural and molecular responses to hypoxia, neither intermittent nor continuous hypoxic exposure were sufficient to modulate GR1000 motor deficits. In this thesis we built upon previous research to reinforce the case for previously identified mechanisms of DPR toxicity. By studying these mechanisms in further detail, we uncovered their implications on other biological processes and established disruption in these processes as a common link between causes of FTD/ALS. This led us to propose a mechanism whereby GR-mediated impairment of XPO1 leads to nuclear accumulation of HIF1 $\alpha$ , resulting in aberrant transcription in response to hypoxia. This work bolsters the case for XPO1 as a potential therapeutic target in FTD/ALS and highlights the importance of hypoxia as an environmental factor in disease across the FTD/ALS spectrum. However, our findings raise many further questions on the role of hypoxia and HIF1 $\alpha$  signalling, and the mechanisms underlying their disruption, in C9 FTD/ALS. Further work to validate and build upon our findings, in both *Drosophila* and mammalian models, will hopefully uncover these details and solidify the relevance of our findings to C9 FTD/ALS patients and their families.

## 6.6. Summary of key findings

1. GR1000 physically interacts with XPO1 in *Drosophila*
2. Partial knockdown of XPO1 delayed the onset of motor deficits in *Drosophila* pan-neuronally expressing GR1000
3. Expression of GR1000 did not appear to perturb XPO1 localisation or function
4. Genetic manipulation of HIF1 $\alpha$  expression modified *Drosophila* motor deficits
5. Pan-neuronal expression of GA, AP or GR1000 causes flies to enter the hypoxic stupor response significantly early
6. Expression of GR1000 causes an aberrant transcriptional response to hypoxia in the *Drosophila* brain, characterised by increased HIF1 $\alpha$  expression and activity and decreased NF- $\kappa$ B expression and activity
7. Pan-neuronal expression of GR1000 prevents hypoxia-induced increases in motor function in *Drosophila*
8. Counteracting GR1000-mediated, hypoxia-induced increases in HIF1 $\alpha$  expression does not facilitate hypoxia-induced motor improvement in *Drosophila*

## 7. Appendices

### 7.1. Proteins identified by tandem mass spectrometry as present in DPR but not GFP

**Table 7.1. Proteins identified by MS/MS as present in GA but not GFP**

<b>Accession number</b>	<b>Drosophila melanogaster protein</b>	<b>Fly Base ID</b>
A0A024E3A5_DROME	ND-39	FBgn0037001
A0A0B4JD18_DROME	RN-tre	FBgn0020620
A0A0B4K657_DROME	btsz	FBgn0266756
A0A0B4K6N4_DROME	tmod	FBgn0082582
A0A0B4KEG0_DROME	Nadk2	FBgn0033373
A0A0B4KET0_DROME	Uaf1	FBgn0033607
A0A0B4KFJ8_DROME	Kdm4B	FBgn0053182
A0A0B4KGI5_DROME	Ace	FBgn0000024
A0A0B4KHF3_DROME	puf	FBgn0039214
A0A0B4KHW1_DROME	SR	FBgn0037684
A0A0B4LEF8_DROME	Asap	FBgn0050372
A0A0B4LF64_DROME	TpnC47D	FBgn0010423
A0A0B4LG95_DROME	l(2)k09913	FBgn0021979
A0A0B4LIA3_DROME	Akt1	FBgn0010379
A0A0J9QT97_DROSI	shv	FBgn0031256
A0A0J9QTU1_DROSI	RFeSP	FBgn0021906
A0A0J9QTY9_DROSI	got2	FBgn0001125
A0A0J9QW48_DROSI	CG14034	FBgn0250847
A0A0J9R1H7_DROSI	Reps	FBgn0032341
A0A0J9R314_DROSI	bgm	FBgn0027348
A0A0J9R5Z3_DROSI	CG10417	FBgn0033021
A0A0J9R772_DROSI	didum	FBgn0261397
A0A0J9R866_DROSI	CSN7	FBgn0028836
A0A0J9R8V3_DROSI	drosha	FBgn0026722
A0A0J9R963_DROSI	RagC_D	FBgn0033272
A0A0J9RE19_DROSI	Trs31	FBgn0266723
A0A0J9RH71_DROSI	CG9346	FBgn0034572
A0A0J9RHP3_DROSI	MESK2	FBgn0043070
A0A0J9RL41_DROSI	CG2765	FBgn0035087
A0A0J9RLZ3_DROSI	Ctr9	FBgn0035205
A0A0J9RRS3_DROSI	rhea	FBgn0260442
A0A0J9RS21_DROSI	UGP	FBgn0035978
A0A0J9RTR2_DROSI	yps	FBgn0022959
A0A0J9TDR1_DROSI	sec24CD	FBgn0262126
A0A0J9UFJ2_DROSI	D19A	FBgn0022935

A0A0M3QXR2_DROBS	mRpL40	FBgn0037892
A0A0M4E6L4_DROBS	NTPase	FBgn0024947
A0A0M4EMX4_DROBS	CG42258	FBgn0259143
A0A0M4EPA3_DROBS	Pli	FBgn0025574
A0A0M5JDH0_DROBS	Gβ5	FBgn0030011
A0A0Q5T329_DROER	CG1552	FBgn0030258
A0A0Q5TIT0_DROER	Evi5	FBgn0262740
A0A0Q5WAA7_DROER	mRpS7	FBgn0032236
A0A0Q9WEL4_DROVI	Kyat	FBgn0037955
A0A0R1E5F9_DROYA	CG17726	FBgn0037880
A0A0R3NXB9_DROPS	pyd3	FBgn0037513
A0A0R3NZB2_DROPS	CG9281	FBgn0030672
A0A1W4UFH8_DROFC	holn1	FBgn0032250
A0A1W4UJW3_DROFC	CG18598	FBgn0038589
A0A1W4UZQ3_DROFC	Prosc1R	FBgn0050382
A0A1W4V0R6_DROFC	mRpL12	FBgn0011787
A0A1W4V8E0_DROFC	arg	FBgn0023535
A0A1W4VAC7_DROFC	Arpc4	FBgn0284255
A0A1W4VB23_DROFC	Srp14	FBgn0038808
A0A1W4VDF6_DROFC	RpL37A	FBgn0261608
A0A1W4VGT0_DROFC	EloC	FBgn0266711
A0A1W4VP61_DROFC	CG7747	FBgn0034109
A0A1W4VTP2_DROFC	CG3699	FBgn0040349
A0A1W4W0D2_DROFC	CG8507	FBgn0037756
A0A1W4W1U7_DROFC	sl	FBgn0003416
A0A1W4W229_DROFC	CG8032	FBgn0037606
A0ANI6_DROME	ocn	FBgn0041102
A0ZWP1_DROME	Tep2	FBgn0041182
A1Z6H6_DROME	CG7791	FBgn0033038
A1Z7K2_DROME	CG30349	FBgn0050349
A1Z8Z9_DROME	CG8834	FBgn0033733
A1Z9L3_DROME	pea	FBgn0086895
A1ZA73_DROME	Strn-Mlck	FBgn0265045
A4V4S5_DROME	car	FBgn0000257
A8E6K0_DROME	Gar1	FBgn0011824
A8JNN5_DROME	GAPcenA	FBgn0035879
A8JUV9_DROME	sgg	FBgn0003371
AGO2_DROME	AGO2	FBgn0087035
AIMP2_DROME	AIM	FBgn0024254
ATD3A_DROME	bor	FBgn0287225
B3DMT4_DROME	Spn75F	FBgn0052203
B3N662_DROER	nop5	FBgn0026196
B3N6C9_DROER	CG5958	FBgn0031913

B3NC82_DROER	Usp47	FBgn0016756
B3NFZ2_DROER	Ccz1	FBgn0035470
B3NI04_DROER	Prx1	FBgn0036490
B3NLI5_DROER	bonsai	FBgn0026261
B3NQG5_DROER	Nop60B	FBgn0259937
B3NTJ7_DROER	CG9213	FBgn0030655
B3NU86_DROER	CG1578	FBgn0030336
B3NX62_DROER	Had1	FBgn0286508
B3P2F2_DROER	Pi4KII $\alpha$	FBgn0037339
B3P626_DROER	CG3368	FBgn0039508
B3P788_DROER	slimp	FBgn0051133
B4HFB3_DROSE	Rassf	FBgn0039055
B4HJY4_DROSE	BckdhA	FBgn0037709
B4HME2_DROSE	mlt	FBgn0265512
B4HWT0_DROSE	CG17097	FBgn0265264
B4I080_DROSE	Fum2	FBgn0029890
B4I1I9_DROSE	Hsp60C	FBgn0031728
B4I2V4_DROSE	FASN1	FBgn0283427
B4I7C1_DROSE	Abcd3	FBgn0031069
B4I7I4_DROSE	cpa	FBgn0034577
B4I8H6_DROSE	Klp59D	FBgn0034827
B4IEB3_DROSE	CG6153	FBgn0032445
B4IIT9_DROSE	fln	FBgn0005633
B4IJ02_DROSE	$\gamma$ COP	FBgn0028968
B4IJ62_DROSE	CG14411	FBgn0030582
B4IJF0_DROSE	PQBP1	FBgn0039270
B4IL52_DROSE	snz	FBgn0029976
B4IWA4_DROYA	ARY	FBgn0058064
B4MZ98_DROWI	La	FBgn0011638
B4PAN7_DROYA	Hsl	FBgn0034491
B4PM39_DROYA	spr-C	FBgn0029768
B4QBS9_DROSI	PPO1	FBgn0283437
B4QHT0_DROSI	sec24AB	FBgn0033460
B4QMF1_DROSI	Agpat3	FBgn0036623
B4QUE5_DROSI	Wdr37	FBgn0038617
B4R4E3_DROSI	CG12177	FBgn0030510
C0PV71_DROME	T3dh	FBgn0017482
C28D1_DROME	Cyp28d1	FBgn0031689
E2QCZ3_DROME	dind	FBgn0286828
ELL_DROME	EII	FBgn0014037
F3YDB2_DROME	eIF2 $\beta$	FBgn0004926
H8F4R0_DROME	Myo61F	FBgn0010246
IF4E_DROME	eIF-4E	FBgn0015218

M9ND95_DROME	Mhc	FBgn0264695 !
M9NEP1_DROME	Mhc	FBgn0264695
M9PB96_DROME	CG6724	FBgn0032298
MP1_DROME	MP1	FBgn0027930
MTTF_DROME	mTTF	FBgn0028530
NAA25_DROME	psidin	FBgn0243511
NNRD_DROME	Naxd	FBgn0036848
O01350_DROME	gag	FBgn0286362
O46307_DROME	EG:8D8.4	FBgn0024364
O77287_DROME	Su(P)	FBgn0004465
Q2XYE0_DROME	CG8343	FBgn0040502
Q59E33_DROME	scaf6	FBgn0261872
Q6NL39_DROME	Spf45	FBgn0086683
Q6NLA0_DROME	Argk2	FBgn0035957
Q6NP11_DROME	did	FBgn0261519
Q6T2X3_DROSU	wupa	FBgn0283471
Q7JVH6_DROME	CG9436	FBgn0033101
Q7K0E6_DROME	AspRS	FBgn0002069
Q7K1U0_DROME	Arc1	FBgn0033926
Q7KK51_DROME	Mtmr6	FBgn0028497
Q7KMN4_DROME	Ulp1	FBgn0027603
Q7KN66_DROME	TBCD	FBgn0027509
Q7KSP6_DROME	Sbf	FBgn0025802
Q8I0S9_DROME	mcc	FBgn0039877
Q8IMK7_DROME	alph	FBgn0086361
Q8MR71_DROME	Reg-2	FBgn0016715
Q8MSW0_DROME	IleRS	FBgn0027086
Q8SYQ8_DROME	CG3420	FBgn0033100
Q8SZ36_DROME	vir-1	FBgn0043841
Q8T412_DROME	CG10749	FBgn0036328
Q8T4F0_DROME	gNacα	FBgn0031296
Q95RT3_DROME	CG5515	FBgn0039163
Q95RV6_DROME	RAF2	FBgn0036624
Q9VB10_DROME	HsdI2	FBgn0039537
Q9VBI0_DROME	CG14543	FBgn0039404
Q9VG07_DROME	CG7488	FBgn0038106
Q9VG86_DROME	CG10097	FBgn0038033
Q9VGQ8_DROME	Arfip	FBgn0037884
Q9VI08_DROME	CG10298	FBgn0037432
Q9VI66_DROME	CG31248	FBgn0051248
Q9VKB2_DROME	Ced-12	FBgn0032409
Q9VL16_DROME	Fundc1	FBgn0032200
Q9VL46_DROME	CG33301	FBgn0053301

Q9VL66_DROME	CG4592	FBgn0032162
Q9VLC4_DROME	CG4438	FBgn0032115
Q9VLJ7_DROME	Sgp	FBgn0032055
Q9VNH2_DROME	CG2100	FBgn0037369
Q9VXY3_DROME	Dbct	FBgn0030612
Q9VYT5_DROME	CG10347	FBgn0030342
Q9W196_DROME	CG3356	FBgn0034989
Q9W526_DROME	EG:67A9.2	FBgn0040394
Q9W5W6_DROME	CG9578	FBgn0031094
Q9XYW6_DROME	STUB1	FBgn0027052
Q9Y114_DROME	CG8042	FBgn0027554
Q9Y166_DROME	Dic1	FBgn0027610
T1W131_DROME	Uba5	FBgn0030305
UTP18_DROME	wcd	FBgn0262560
Y7065_DROME	CG7065	FBgn0030091

**Table 7.2. Proteins identified by MS/MS as present in AP but not GFP**

<b>Accession number</b>	<b>Drosophila melanogaster protein</b>	<b>Flybase ID</b>
A0A021WW64_DROME	CG17162	FBgn0039944
A0A023GPN7_DROME	CG4678	FBgn0030778
A0A024E3A5_DROME	ND-39	FBgn0037001
A0A075BNB9_DROME	Cyp6a2	FBgn0000473
A0A0A0RVF0_DROME	CYTB	FBgn0013678
A0A0B4JD18_DROME	RN-tre	FBgn0020620
A0A0B4K6N4_DROME	tmod	FBgn0082582
A0A0B4K851_DROME	RanBGM	FBgn0011766
A0A0B4KGN2_DROME	Mitofilin	FBgn0019960
A0A0B4KHW0_DROME	Axn	FBgn0026597
A0A0B4KHW1_DROME	JMJD6	FBgn0038948
A0A0B4KI69_DROME	Gprk2	FBgn0261988
A0A0B4LEY1_DROME	Sec31	FBgn0033339
A0A0B4LF64_DROME	TpnC47D	FBgn0010423
A0A0B4LF88_DROME	TppII	FBgn0020370
A0A0B4LG95_DROME	l(2)k09913	FBgn0021979
A0A0B4LIA3_DROME	Akt1	FBgn0069518
A0A0B4LIJ0_DROME	Rpt2	FBgn0015282
A0A0B7P9G0_DROME	uex	FBgn0262124
A0A0F6QCW0_DROME	bcn92	FBgn0013432
A0A0J9QUD1_DROSI	Cyp309a1	FBgn0031432
A0A0J9QUH6_DROSI	colt	FBgn0019830
A0A0J9QXE8_DROSI	Ziz	FBgn0260486
A0A0J9QXJ4_DROSI	ND-51	FBgn0031771
A0A0J9QZX9_DROSI	Mulk	FBgn0260750
A0A0J9R1H7_DROSI	Reps	FBgn0032341
A0A0J9R1I3_DROSI	B4	FBgn0023407
A0A0J9R2L7_DROSI	PRL-1	FBgn0024734
A0A0J9R3G0_DROSI	mdy	FBgn0004797
A0A0J9R5W9_DROSI	CG12567	FBgn0039958
A0A0J9R772_DROSI	didum	FBgn0261397
A0A0J9R866_DROSI	CSN7	FBgn0028836
A0A0J9R8V3_DROSI	drosha	FBgn0026722
A0A0J9RBM1_DROSI	CG8888	FBgn0033679
A0A0J9RDK9_DROSI	Vha36-1	FBgn0022097
A0A0J9RE92_DROSI	CG5065	FBgn0034145
A0A0J9RHP3_DROSI	MESK2	FBgn0043070
A0A0J9RMV0_DROSI	trio	FBgn0024277
A0A0J9RNP8_DROSI	ens	FBgn0264693
A0A0J9RQ14_DROSI	CG10077	FBgn0035720

A0A0J9RSJ9_DROSI	Arp3	FBgn0262716
A0A0J9RTR2_DROSI	yps	FBgn0022959
A0A0J9RUN8_DROSI	RpS12	FBgn0286213
A0A0J9RV83_DROSI	Sytbeta	FBgn0261090
A0A0J9RVT7_DROSI	DCP2	FBgn0036534
A0A0J9RXC1_DROSI	CG7564	FBgn0036734
A0A0J9RY67_DROSI	verm	FBgn0261341
A0A0J9RY90_DROSI	Fibp	FBgn0036911
A0A0J9RZ49_DROSI	CG3961	FBgn0036821
A0A0J9S0Y2_DROSI	Syt7	FBgn0039900
A0A0J9TQP4_DROSI	CG10333	FBgn0032690
A0A0M4E8F5_DROBS	mRpL51	FBgn0032053
A0A0M4EBG0_DROBS	Arl1	FBgn0000115
A0A0M4EBK5_DROBS	Rap2l	FBgn0283666
A0A0M4EJY6_DROBS	Vta1	FBgn0035251
A0A0M5J984_DROBS	Arpc1	FBgn0001961
A0A0M5JDH0_DROBS	Gβ5	FBgn0030011
A0A0P8XI16_DROAN	IA-2	FBgn0031294
A0A0P8XJT6_DROAN	S6klI	FBgn0262866
A0A0Q5T2M7_DROER	Tlk	FBgn0283657
A0A0Q5T329_DROER	CG1552	FBgn0030258
A0A0Q5T7I8_DROER	Stim	FBgn0045073
A0A0Q9W1U5_DROVI	wkd	FBgn0037917
A0A0R1E068_DROYA	Mpped	FBgn0036028
A0A0R1E434_DROYA	Pak	FBgn0267698
A0A0R1E493_DROYA	Efa6	FBgn0051158
A0A0R1E6I8_DROYA	modSP	FBgn0051217
A0A0R3NZB2_DROPS	CG9281	FBgn0030672
A0A1W4U4W7_DROFC	Tapδ	FBgn0021795
A0A1W4UB14_DROFC	Arp1	FBgn0011745
A0A1W4UJW3_DROFC	CG18598	FBgn0038589
A0A1W4ULI9_DROFC	CLIP-190	FBgn0020503
A0A1W4UNU9_DROFC	Ork1	FBgn0017561
A0A1W4UT00_DROFC	Ras85D	FBgn0003205
A0A1W4V0R6_DROFC	mRpL12	FBgn0011787
A0A1W4V381_DROFC	Rala	FBgn0015286
A0A1W4V3Q1_DROFC	CG7872	FBgn0030658
A0A1W4V4B4_DROFC	PCNA	FBgn0005655
A0A1W4VCC5_DROFC	Eaf	FBgn0033166
A0A1W4VDF6_DROFC	RpL37A	FBgn0261608
A0A1W4VGT0_DROFC	EloC	FBgn0266711
A0A1W4VP61_DROFC	CG11777	FBgn0033527
A0A1W4W036_DROFC	ND-30	FBgn0266582

A0A1W4W1U7_DROFC	sl	FBgn0003416
A0A1W4WDF0_DROFC	UQCR-14L	FBgn0039576
A1Z6H6_DROME	CG7791	FBgn0033038
A8E6R2_DROME	CG11241	FBgn0037186
A8JNN5_DROME	GAPcenA	FBgn0035879
A8JR57_DROME	CG31191	FBgn0051191
AGO2_DROME	AGO1	FBgn0262739
ATD3A_DROME	bor	FBgn0287225
B3N662_DROER	nop5	FBgn0026196
B3N7C1_DROER	CG13097	FBgn0032051
B3NDD2_DROER	CG7724	FBgn0036698
B3NJJ0_DROER	CG7137	FBgn0034422
B3NT15_DROER	Upf1	FBgn0030354
B3NT17_DROER	sicily	FBgn0030352
B3NTJ7_DROER	CG9213	FBgn0030655
B3NYB8_DROER	Mnr	FBgn0052521
B3P2F2_DROER	Pi4KIIalpha	FBgn0037339
B4HPV8_DROSE	Fmo-2	FBgn0033079
B4HQE9_DROSE	CG30159	FBgn0050159
B4HRB3_DROSE	CG8613	FBgn0033924
B4HT23_DROSE	GstT1	FBgn0050000
B4HYI2_DROSE	Mettl14	FBgn0032016
B4HYJ5_DROSE	CSN8	FBgn0261437
B4HZF3_DROSE	CG7789	FBgn0039698
B4I4I7_DROSE	CG1307	FBgn0026566
B4I7C1_DROSE	Pmp70	FBgn0031069
B4I7I4_DROSE	cpa	FBgn0034577
B4IEB3_DROSE	CG6153	FBgn0032445
B4IJ02_DROSE	gammaCOP	FBgn0028968
B4IJ62_DROSE	CG14411	FBgn0030582
B4IL51_DROSE	spidey	FBgn0029975
B4LXZ8_DROVI	CG6126	FBgn0038407
B4MZ98_DROWI	La	FBgn0011638
B4QFN1_DROSI	Isha	FBgn0034598
B4QI12_DROSI	CG8306	FBgn0034142
B4QMF1_DROSI	Agpat3	FBgn0036623
B4QUE5_DROSI	Wdr37	FBgn0038617
BOSS_DROME	boss	FBgn0000206
C12B2_DROME	Cyp12b2	FBgn0034387
C9QP43_DROME	Tango5	FBgn0052675
E1JIT4_DROME	Pfdn5	FBgn0038976
ELL_DROME	EII	FBgn0014037
F3YDB2_DROME	eIF2 $\beta$	FBgn0004926

IF4E_DROME	eIF-4E	FBgn0052016
LAM0_DROME	Lam	FBgn0002525
M9MRM4_DROME	Sac1	FBgn0194003
M9ND95_DROME	Mhc	FBgn0264695
M9NF46_DROME	Mhc	FBgn0264695 !
M9PB96_DROME	CG6724	FBgn0032298
MP1_DROME	MP1	FBgn0027930
MTTF_DROME	mTTF	FBgn0028530
O46112_DROME	toc	FBgn0015600
O46307_DROME	EG:8D8.4	FBgn0024364
P91616_DROME	CG5989	FBgn0017429
PARG_DROME	Parg	FBgn0023216
PPN_DROME	gpn	FBgn0003137
Q2XYE0_DROME	CG8343	FBgn0040502
Q3ZAP5_DROME	CG32017	FBgn0052017
Q6NP35_DROME	rho-5	FBgn0041723
Q7JVH6_DROME	CG9436	FBgn0033101
Q7K0F7_DROME	CG11200	FBgn0034500
Q7K1U0_DROME	Arc1	FBgn0033926
Q7K3E2_DROME	CG5080	FBgn0031313
Q7KJN6_DROME	gten	FBgn0026379
Q7KK51_DROME	Mtmr6	FBgn0028497
Q7KMN4_DROME	Ulp1	FBgn0027603
Q7KSP6_DROME	Sbf	FBgn0025802
Q8IMK7_DROME	alph	FBgn0086361
Q8INE8_DROME	Art3	FBgn0038306
Q8IQ51_DROME	SG50	FBgn0002490
Q8MR71_DROME	Reg-2	FBgn0016715
Q8MSW0_DROME	IleRS	FBgn0027086
Q8SZF2_DROME	ND-23	FBgn0283500
Q960Y8_DROME	alt	FBgn0038535
Q961E7_DROME	PhKy	FBgn0011754
Q9V9W4_DROME	CG1774	FBgn0039856
Q9VC87_DROME	CG18528	FBgn0039189
Q9VHB2_DROME	CG9396	FBgn0037714
Q9VL16_DROME	Fundc1	FBgn0032200
Q9VL66_DROME	CG4592	FBgn0032162
Q9VLC4_DROME	CG4438	FBgn0032115
Q9VLM7_DROME	CG13392	FBgn0032033
Q9VMA6_DROME	CG31633	FBgn0051633
Q9VVS6_DROME	Atg3	FBgn0036813
Q9VWD0_DROME	parvin	FBgn0052528
Q9VZF6_DROME	Sqor	FBgn0035515

Q9W501_DROME	temp	FBgn0027296
Q9W526_DROME	EG:67A9.2	FBgn0040394
Q9W5W6_DROME	CG9578	FBgn0031094
Q9XYW6_DROME	STUB1	FBgn0027052
Q9Y166_DROME	Dic1	FBgn0027610
T1W131_DROME	Uba5	FBgn0030305
UTP18_DROME	wcd	FBgn0262560
Y7065_DROME	CG7065	FBgn0030091

**Table 7.3. Proteins identified by MS/MS as present in PR but not GFP**

<b>Accession number</b>	<b>Drosophila melanogaster protein</b>	<b>FlyBase ID</b>
A0A023GPN7_DROME	CG4678	FBgn0030778
A0A024E3A5_DROME	ND-39	FBgn0037001
A0A075BNB9_DROME	Cyp6a2	FBgn0000473
A0A0A0RVF0_DROME	CYTB	FBgn0013678
A0A0B4J401_DROME	CG10737	FBgn0034420
A0A0B4JD02_DROME	gro	FBgn0001139
A0A0B4JD18_DROME	RN-tre	FBgn0020620
A0A0B4K657_DROME	btsz	FBgn0266756
A0A0B4K6A6_DROME	Calx	FBgn0013995
A0A0B4K6F9_DROME	Esyt2	FBgn0266758
A0A0B4K7Q6_DROME	mbc	FBgn0015513
A0A0B4K7V2_DROME	CG13743	FBgn0033368
A0A0B4KG17_DROME	CG8526	FBgn0037759
A0A0B4KGG6_DROME	CG1090	FBgn0037238
A0A0B4KGI5_DROME	Ace	FBgn0000024
A0A0B4KGN2_DROME	Mitofilin	FBgn0019960
A0A0B4KHX4_DROME	Nf1	FBgn0015269
A0A0B4KI71_DROME	Map205	FBgn0002645
A0A0B4LEU2_DROME	Cyp6w1	FBgn0033065
A0A0B4LEY1_DROME	Sec31	FBgn0033339
A0A0B4LEZ3_DROME	Not1	FBgn0085436
A0A0B4LF50_DROME	Mppe	FBgn0259985
A0A0B4LF88_DROME	TppII	FBgn0020370
A0A0B4LFR4_DROME	OstDelta	FBgn0034277
A0A0B4LG95_DROME	l(2)k09913	FBgn0021979
A0A0B4LGD3_DROME	kcc	FBgn0261794
A0A0B4LGJ9_DROME	Gpat4	FBgn0034971
A0A0B4LIA3_DROME	Akt1	FBgn0010379
A0A0B4LIJ0_DROME	Rpt2	FBgn0015282
A0A0B7P9G0_DROME	uex	FBgn0262124
A0A0J9QUW5_DROSI	CG17221	FBgn0031500
A0A0J9QVL8_DROSI	ine	FBgn0011603
A0A0J9QVU7_DROSI	smog	FBgn0051660
A0A0J9QW48_DROSI	CG14034	FBgn0250847
A0A0J9QYR0_DROSI	emb	FBgn0020497
A0A0J9QZL2_DROSI	CG5853	FBgn0032167
A0A0J9QZX9_DROSI	Mulk	FBgn0260750
A0A0J9R165_DROSI	Rab6	FBgn0015797

A0A0J9R1H7_DROSI	Reps	FBgn0032341
A0A0J9R1P1_DROSI	Tor	FBgn0021796
A0A0J9R1W1_DROSI	CG31729	FBgn0051729
A0A0J9R2L7_DROSI	PRL-1	FBgn0024734
A0A0J9R2Q9_DROSI	Cul3	FBgn0261268
A0A0J9R3G0_DROSI	mdy	FBgn0004797
A0A0J9R404_DROSI	CG10211	FBgn0032685
A0A0J9R438_DROSI	Cep104	FBgn0032800
A0A0J9R4N7_DROSI	sky	FBgn0032901
A0A0J9R5W9_DROSI	CG12567	FBgn0039958
A0A0J9R6C0_DROSI	Gfat1	FBgn0287209
A0A0J9R7Q2_DROSI	CG14762	FBgn0033250
A0A0J9R841_DROSI	pnut	FBgn0013726
A0A0J9R866_DROSI	CSN7	FBgn0028836
A0A0J9R8V3_DROSI	drosha	FBgn0026722
A0A0J9R963_DROSI	RagC-D	FBgn0033272
A0A0J9RAX3_DROSI	CG8841	FBgn0033713
A0A0J9RBM1_DROSI	CG8888	FBgn0033679
A0A0J9RCP8_DROSI	jef	FBgn0033958
A0A0J9RE92_DROSI	CG5065	FBgn0034145
A0A0J9RHP3_DROSI	MESK2	FBgn0043070
A0A0J9RMB1_DROSI	nSyb	FBgn0013342
A0A0J9RMV0_DROSI	trio	FBgn0024277
A0A0J9RNW8_DROSI	Hexo1	FBgn0041630
A0A0J9RNX8_DROSI	CG42540	FBgn0260657
A0A0J9RP14_DROSI	Dhc64C	FBgn0261797
A0A0J9RPJ3_DROSI	TM9SF3	FBgn0035622
A0A0J9RQ65_DROSI	ple	FBgn0005626
A0A0J9RQG6_DROSI	nAChRbeta1	FBgn0000038
A0A0J9RS21_DROSI	UGP	FBgn0035978
A0A0J9RTN7_DROSI	Pop2	FBgn0036239
A0A0J9RTR2_DROSI	yps	FBgn0022959
A0A0J9RXL5_DROSI	Tmx3	FBgn0036579
A0A0J9RZ49_DROSI	CG3961	FBgn0036821
A0A0J9RZD0_DROSI	CG6695	FBgn0039215
A0A0J9S0Q0_DROSI	Tsr1	FBgn0037073
A0A0J9TCA8_DROSI	CG3164	FBgn0288229
A0A0J9TCR4_DROSI	CG3662	FBgn0031285
A0A0J9TQP4_DROSI	CG10333	FBgn0032690
A0A0J9UJD7_DROSI	Gcat	FBgn0036208
A0A0M4E6M4_DROBS	Rpn11	FBgn0028694

A0A0M4EBG0_DROBS	Arl1	FBgn0000115
A0A0M4EGS4_DROBS	Cyt-b5	FBgn0264294
A0A0M4EJY6_DROBS	Vta1	FBgn0035251
A0A0M4FA16_DROBS	RSG7	FBgn0024941
A0A0M5J2W2_DROBS	Sec61beta	FBgn0010638
A0A0P8XI16_DROAN	IA-2	FBgn0031294
A0A0P8XJT6_DROAN	S6kII	FBgn0262866
A0A0Q5SU94_DROER	δCOP	FBgn0028969
A0A0Q5T4K5_DROER	eas	FBgn0000536
A0A0Q5TIT0_DROER	Evi5	FBgn0262740
A0A0Q9W1U5_DROVI	wkd	FBgn0037917
A0A0R1DM42_DROYA	Dgat2	FBgn0033215
A0A0R1E3D8_DROYA	Adgf-D	FBgn0038172
A0A0R1E6I8_DROYA	modSP	FBgn0051217
A0A0R1EB53_DROYA	sws	FBgn0003656
A0A0R3NH31_DROPS	sno	FBgn0265630
A0A0R3NZB2_DROPS	CG9281	FBgn0030672
A0A1W4U4W7_DROFC	Tapδ	FBgn0021795
A0A1W4UCE4_DROFC	eIF2Bα	FBgn0039726
A0A1W4UFH8_DROFC	holn1	FBgn0032250
A0A1W4UJB4_DROFC	Rab7	FBgn0015795
A0A1W4UJ13_DROFC	Rheb	FBgn0041191
A0A1W4UJW3_DROFC	CG18598	FBgn0038589
A0A1W4ULI8_DROFC	levy	FBgn0034877
A0A1W4UM98_DROFC	Plekhm1	FBgn0034694
A0A1W4UT00_DROFC	Ras85D	FBgn0003205
A0A1W4V2T8_DROFC	CG15211	FBgn0030234
A0A1W4V2X6_DROFC	Rab9	FBgn0032782
A0A1W4V381_DROFC	Rala	FBgn0015286
A0A1W4V4B4_DROFC	PCNA	FBgn0005655
A0A1W4V7F2_DROFC	wol	FBgn0261020
A0A1W4V9P3_DROFC	ogre	FBgn0004646
A0A1W4VDF6_DROFC	RpL37A	FBgn0261608
A0A1W4VGT0_DROFC	EloC	FBgn0266711
A0A1W4VKA7_DROFC	Cul2	FBgn0032956
A0A1W4VRM6_DROFC	OtopLa	FBgn0259994
A0A1W4VSJ1_DROFC	Tsp5D	FBgn0029837
A0A1W4W8T0_DROFC	CG10470	FBgn0032746
A0A1W4WDF0_DROFC	UQCR-14L	FBgn0039576
A0ANI6_DROME	ocn	FBgn0041102
A0AQ24_DROME	ND-PDSW	FBgn0021967

A1Z7H7_DROME	CG8586	FBgn0033320
A1Z863_DROME	Csgalnact	FBgn0033500
A1ZA73_DROME	Strn-Mlck	FBgn0265045
A1ZBE9_DROME	MetRS	FBgn0034401
A2TDT5_DROSI	COX4	FBgn0032833
A4V4I0_DROME	Gbeta13F	FBgn0001105
A7KX19_DROME	spp	FBgn0031260
A8JNN5_DROME	GAPcenA	FBgn0035879
AGO2_DROME	AGO2	FBgn0087035
AIMP2_DROME	AIMPE	FBgn0036515
ATD3A_DROME	bor	FBgn0287225
ATP5J_DROME	ATPsynCf6	FBgn0016119
B3DNM8_DROME	CG45002	FBgn0266354
B3M4G8_DROAN	Rpn12	FBgn0028693
B3MQN1_DROAN	CG14232	FBgn0031061
B3N323_DROER	Sec5	FBgn0266670
B3N662_DROER	nop5	FBgn0026196
B3N6C9_DROER	CG5958	FBgn0031913
B3N7D9_DROER	CatB	FBgn0032061
B3N9M1_DROER	Frmd5	FBgn0032225
B3NDD2_DROER	CG7724	FBgn0036698
B3NE23_DROER	Tom20	FBgn0036928
B3NKF9_DROER	Tim23	FBgn0267976
B3NT15_DROER	Upf1	FBgn0030354
B3NTH8_DROER	Pis	FBgn0030670
B3NUG9_DROER	Ost48	FBgn0014868
B3NXQ1_DROER	schlank	FBgn0040918
B3NY61_DROER	Mgstl	FBgn0025814
B3P243_DROER	atms	FBgn0010750
B3P2Y3_DROER	Sec15	FBgn0266674
B3P382_DROER	NP15.6	FBgn0027785
B3P7S7_DROER	stops	FBgn0086704
B3P8N8_DROER	CG5346	FBgn0038981
B4HAD4_DROPE	scramb2	FBgn0035390
B4HI97_DROSE	bumpel	FBgn0037895
B4HJ93_DROSE	gammaSnap2	FBgn0266721
B4HPV8_DROSE	Fmo-2	FBgn0033079
B4HQE9_DROSE	CG30159	FBgn0050159
B4HRB3_DROSE	CG8613	FBgn0033924
B4HVC2_DROSE	Rab26	FBgn0086913
B4HYP6_DROSE	Sema1a	FBgn0011259

B4HZF3_DROSE	CG7789	FBgn0039698
B4I478_DROSE	PSMG1	FBgn0037378
B4I558_DROSE	Cse1	FBgn0022213
B4I7C1_DROSE	Abcd3	FBgn0031069
B4ICY7_DROSE	Tspo	FBgn0031263
B4IGB9_DROSE	mRNA-cap	FBgn0030556
B4II25_DROSE	Pngl	FBgn0033050
B4IJ02_DROSE	$\gamma$ COP	FBgn0028968
B4IL51_DROSE	spidey	FBgn0029975
B4IL86_DROSE	Abcd1	FBgn0039890
B4K520_DROMO	asp	FBgn0000140
B4LXZ8_DROVI	CG6126	FBgn0038407
B4PNH1_DROYA	Scsd2	FBgn0038708
B4QFN1_DROSI	Isha	FBgn0034598
B4QI12_DROSI	CG8306	FBgn0034142
B4QMF1_DROSI	Agpat3	FBgn0036623
B4QTZ2_DROSI	PGS1	FBgn0038649
B4QUE5_DROSI	Wdr37	FBgn0038617
B4R4E3_DROSI	CG12177	FBgn0030510
B4ZJ97_DROME	Sfp33A3	FBgn0259964
B5RIL6_DROME	Arts	FBgn0042177
B5T1Z3_DROME	Cyp6a23	FBgn0033978
B7Z067_DROME	Nedd4	FBgn0259174
BOSS_DROME	boss	FBgn0000206
C12B2_DROME	Cyp12b2	FBgn0034387
C28A5_DROME	Cyp28a5	FBgn0028940
C28D1_DROME	Cyp28d1	FBgn0031689
C9QP43_DROME	Tango5	FBgn0052675
CP9B2_DROME	Cyp9b2	FBgn0015039
D2NUJ7_DROME	CG3566	FBgn0029854
E2QCZ3_DROME	dind	FBgn0286828
ECM29_DROME	CG8858	FBgn0033698
EXOC5_DROME	Sec10	FBgn0266673
F0JAJ1_DROME	$\alpha$ -Est3	FBgn0015571
F1DKP8_DROME	CG34034	FBgn0054034
F3YDB2_DROME	eIF2 $\beta$	FBgn0004926
G3P1_DROME	Gapdh1	FBgn0001091
G7H7Z0_DROME	LysRS	FBgn0027084
GRM_DROME	mGluR	FBgn0019985
GUTR1_DROME	Tre1	FBgn0046687
H8F4R0_DROME	Myo61F	FBgn0010246

H9XVP3_DROME	PlexA	FBgn0025741
IF4E_DROME	eIF-4E	FBgn0015218
KRH2_DROME	Kr-h2	FBgn0266449
LBR_DROME	LBR	FBgn0034657
LVA_DROME	Iva	FBgn0029688
M9MRM4_DROME	Sac1	FBgn0283500
M9NDL5_DROME	trol	FBgn0284408
M9PB96_DROME	CG6724	FBgn0032298
MP1_DROME	MP1	FBgn0027930
NFU1_DROME	CG32500	FBgn0285970
NNRD_DROME	Naxd	FBgn0036848
O46112_DROME	toc	FBgn0015600
O77287_DROME	Su(P)	FBgn0004465
O96306_DROME	Ac3	FBgn0023416
PPN_DROME	Ppn	FBgn0003137
PSB4_DROME	Prosbeta7	FBgn0250746
PTCD3_DROME	Ptcd3	FBgn0033816
Q24506_DROME	ScpX	FBgn0015808
Q2XYE0_DROME	CG8343	FBgn0040502
Q3ZAP5_DROME	CG32017	FBgn0052017
Q5LJX8_DROME	zyd	FBgn0265767
Q6NLA0_DROME	Argk2	FBgn0035957
Q6NP11_DROME	did	FBgn0261519
Q6NP35_DROME	rho-5	FBgn0041723
Q7JV39_DROME	CG11400	FBgn0034198
Q7JYH3_DROME	ND-B14.7	FBgn0034576
Q7K0E6_DROME	AspRS	FBgn0002069
Q7K1U0_DROME	Arc1	FBgn0033926
Q7K3E2_DROME	CG5080	FBgn0031313
Q7K3T3_DROME	CG1441	FBgn0033464
Q7KAK2_DROME	Fpps	FBgn0025373
Q7KJN6_DROME	Pten	FBgn0026379
Q7KK51_DROME	Mtmr6	FBgn0028497
Q7KMM4_DROME	GCS2alpha	FBgn0027588
Q7KSP6_DROME	Sbf	FBgn0025802
Q7KTG2_DROME	Apoltp	FBgn0032136
Q7KTW9_DROME	AsnS	FBgn0270926
Q7PLL6_DROME	I(3)80Fj	FBgn0287182
Q8IMT3_DROME	CG31436	FBgn0051436
Q8MR71_DROME	Reg-2	FBgn0016715
Q8MSS3_DROME	rumpel	FBgn0029950

Q8MSW0_DROME	IleRS	FBgn0027086
Q8S XK2_DROME	ArgRS-m	FBgn0037526
Q8SYQ8_DROME	CG3420	FBgn0033100
Q8SZ36_DROME	vir-1	FBgn0043841
Q8SZF2_DROME	ND-23	FBgn0017567
Q8T412_DROME	CG10749	FBgn0036328
Q960Y8_DROME	alt	FBgn0038535
Q961E7_DROME	Phkgamma	FBgn0011754
Q9V3N6_DROME	TM9SF4	FBgn0028541
Q9VC87_DROME	CG18528	FBgn0039189
Q9VCS2_DROME	CG13833	FBgn0039040
Q9VD14_DROME	CG13850	FBgn0038961
Q9VEM4_DROME	CG5265	FBgn0038486
Q9VG33_DROME	CG12279	FBgn0038080
Q9VG86_DROME	CG10097	FBgn0038033
Q9VGQ8_DROME	Arfip	FBgn0037884
Q9VHB2_DROME	CG9396	FBgn0037714
Q9VI66_DROME	CG31248	FBgn0051248
Q9VJD1_DROME	GCS2beta	FBgn0032643
Q9VL16_DROME	Fundc1	FBgn0032200
Q9VLJ7_DROME	Sgp	FBgn0032055
Q9VLM7_DROME	CG13392	FBgn0032033
Q9VP06_DROME	Alg11	FBgn0037108
Q9VV87_DROME	Baldspot	FBgn0260960
Q9VVS6_DROME	Atg3	FBgn0036813
Q9VW3_DROME	Sfxn2	FBgn0036843
Q9VWI2_DROME	Naa15-16	FBgn0031020
Q9VXY3_DROME	Dbct	FBgn0030612
Q9W196_DROME	CG3356	FBgn0034989
Q9W2J4_DROME	Ugt49B1	FBgn0027073
Q9W350_DROME	c11.1	FBgn0040236
Q9W3M6_DROME	Dhdds	FBgn0029980
Q9W501_DROME	temp	FBgn0027296
Q9W5T4_DROME	CG12547	FBgn0250830
Q9XYW6_DROME	STUB1	FBgn0027052
Q9XZ61_DROME	Uch-L5	FBgn0011327
Q9Y137_DROME	mino	FBgn0027579
Q9Y166_DROME	Dic1	FBgn0027610
SNP25_DROME	Snap25	FBgn0011288
T1W131_DROME	Uba5	FBgn0030305

**Table 7.4. Proteins identified by MS/MS as present in GR but not GFP**

<b>Accession Number</b>	<b>Drosophila melanogaster protein</b>	<b>Fly Base ID</b>
A0A023GQA5_DROME	I(2)37Cc	FBgn0002031
A0A023JPB4_DROSN	COX5B	FBgn0031830
A0A024E3A5_DROME	ND-39	FBgn0037001
A0A075BNB9_DROME	Cyp6a2	FBgn0000473
A0A0A0RVF0_DROME	CYTB	FBgn0013678
A0A0B4J401_DROME	CG10737	FBgn0034420
A0A0B4JD18_DROME	RN-tre	FBgn0020620
A0A0B4K657_DROME	btsz	FBgn0266756
A0A0B4K664_DROME	mssp	FBgn0027948
A0A0B4K6A6_DROME	Calx	FBgn0013995
A0A0B4K6F9_DROME	Esyt2	FBgn0266758
A0A0B4KGC5_DROME	P5cr-2	FBgn0038516
A0A0B4KGG6_DROME	CG1090	FBgn0037238
A0A0B4KGN2_DROME	Mitofilin	FBgn0019960
A0A0B4LEU2_DROME	Cyp6w1	FBgn0033065
A0A0B4LEY1_DROME	Sec31	FBgn0033339
A0A0B4LEZ3_DROME	Not1	FBgn0085436
A0A0B4LF50_DROME	Mppe	FBgn0259985
A0A0B4LFR4_DROME	OstDelta	FBgn0034277
A0A0B4LG95_DROME	I(2)k09913	FBgn0021979
A0A0B4LGD3_DROME	kcc	FBgn0261794
A0A0B4LGJ9_DROME	Gpat4	FBgn0034971
A0A0B4LH53_DROME	Nsf2	FBgn0266464
A0A0B4LIJ0_DROME	Rpt2	FBgn0015282
A0A0B7P9G0_DROME	uex	FBgn0262124
A0A0J9QTU1_DROSI	RFeSP	FBgn0021906
A0A0J9QUC6_DROSI	ninaA	FBgn0002936
A0A0J9QUUD1_DROSI	Cyp309a1	FBgn0031432
A0A0J9QUH6_DROSI	colt	FBgn0019830
A0A0J9QVL8_DROSI	ine	FBgn0011603
A0A0J9QVU7_DROSI	Smog	FBgn0051660
A0A0J9QXJ4_DROSI	ND-51	FBgn0031771
A0A0J9QXS0_DROSI	santa-maria	FBgn0025697
A0A0J9QYR0_DROSI	emb	FBgn0020497
A0A0J9QZX9_DROSI	Mulk	FBgn0260750
A0A0J9R165_DROSI	Rab6	FBgn0015797
A0A0J9R1W1_DROSI	CG31729	FBgn0051729
A0A0J9R2Q9_DROSI	Cul3	FBgn0261268

A0A0J9R3G0_DROSI	mdy	FBgn0004797
A0A0J9R4N7_DROSI	sky	FBgn0032901
A0A0J9R6C0_DROSI	Gfat1	FBgn0287209
A0A0J9R6G6_DROSI	sxc	FBgn0261403
A0A0J9R7Q2_DROSI	CG14762	FBgn0033250
A0A0J9R7S3_DROSI	Tmem63	FBgn0033259
A0A0J9R963_DROSI	RagC-D	FBgn0033272
A0A0J9RAX3_DROSI	CG8841	FBgn0033713
A0A0J9RBM1_DROSI	CG8888	FBgn0033679
A0A0J9RCP8_DROSI	jef	FBgn0033958
A0A0J9RE92_DROSI	CG5065	FBgn0034145
A0A0J9RHP3_DROSI	MESK2	FBgn0043070
A0A0J9RLZ2_DROSI	Gk2	FBgn0035266
A0A0J9RMB1_DROSI	nSyb	FBgn0013342
A0A0J9RMV0_DROSI	trio	FBgn0024277
A0A0J9RNX8_DROSI	CG42540	FBgn0260657
A0A0J9RP14_DROSI	Dhc64C	FBgn0261797
A0A0J9RPJ3_DROSI	TM9SF3	FBgn0035622
A0A0J9RQ65_DROSI	ple	FBgn0005626
A0A0J9RQG6_DROSI	nAChR $\beta$ 1	FBgn0000038
A0A0J9RTN7_DROSI	Pop2	FBgn0036239
A0A0J9RUH6_DROSI	Klc	FBgn0010235
A0A0J9RUN8_DROSI	RpS12	FBgn0286213
A0A0J9RX11_DROSI	Sec3	FBgn0266669
A0A0J9RY53_DROSI	Lon	FBgn0036892
A0A0J9RYJ5_DROSI	rdgC	FBgn0265959
A0A0J9RZ49_DROSI	CG3961	FBgn0036821
A0A0J9RZQ0_DROSI	Oct-TyrR	FBgn0004514
A0A0J9S0Y2_DROSI	Syt7	FBgn0039900
A0A0J9TCA8_DROSI	CG3164	FBgn0288229
A0A0J9TCR4_DROSI	CG3662	FBgn0031285
A0A0J9TLV6_DROSI	ThrRS	FBgn0027081
A0A0J9TVE2_DROSI	CG1598	FBgn0033191
A0A0J9TXV3_DROSI	CG1371	FBgn0033482
A0A0J9U9F1_DROSI	Pde8	FBgn0266377
A0A0M3QV50_DROBS	SmD3	FBgn0023167
A0A0M4E6L4_DROBS	NTPase	FBgn0024947
A0A0M4E6M4_DROBS	Rpn11	FBgn0028694
A0A0M4EBG0_DROBS	Arl1	FBgn0000115
A0A0M4EG31_DROBS	Vamp7	FBgn0266186
A0A0M4EGS4_DROBS	Cyt-b5	FBgn0264294

A0A0M4FA16_DROBS	RSG7	FBgn0024941
A0A0M5IXP2_DROBS	roh	FBgn0250838
A0A0M5J0V3_DROBS	Stt3A	FBgn0031149
A0A0M5JCG6_DROBS	Nup93-2	FBgn0038274
A0A0M5JDD1_DROBS	snf	FBgn0003449
A0A0M5JDH0_DROBS	Gβ5	FBgn0030011
A0A0P8XI16_DROAN	IA-2	FBgn0031294
A0A0Q5SU94_DROER	δCOP	FBgn0028969
A0A0Q5T4K5_DROER	eas	FBgn0000536
A0A0Q5T6Y3_DROER	CG12531	FBgn0031064
A0A0Q5TI48_DROER	Lrp4	FBgn0030706
A0A0Q9W1U5_DROVI	wkd	FBgn0037917
A0A0R1E3D8_DROYA	Adgf-D	FBgn0038172
A0A0R1E5N5_DROYA	Cdep	FBgn0265082
A0A0R1EB53_DROYA	sws	FBgn0003656
A0A0R3NZB2_DROPS	CG9281	FBgn0030672
A0A0S0WFE8_DROME	Dscam2	FBgn0265296
A0A140SRF8_DROME	CG11857	FBgn0039303
A0A1W4U4W7_DROFC	Tapδ	FBgn0021795
A0A1W4UB14_DROFC	Arp1	FBgn0011745
A0A1W4UGS1_DROFC	CG14258	FBgn0039482
A0A1W4UJ76_DROFC	jagn	FBgn0037374
A0A1W4UJ13_DROFC	Rheb	FBgn0041191
A0A1W4UJW3_DROFC	CG18598	FBgn0038589
A0A1W4UM98_DROFC	Plekhm1	FBgn0034694
A0A1W4UT00_DROFC	Ras85D	FBgn0003205
A0A1W4V117_DROFC	Cyp4g15	FBgn0030304
A0A1W4V1L8_DROFC	VhaAC39-1	FBgn0285910
A0A1W4V1N7_DROFC	baf	FBgn0031977
A0A1W4V2T8_DROFC	CG15211	FBgn0030234
A0A1W4V2X6_DROFC	Rab9	FBgn0032782
A0A1W4V7F2_DROFC	wol	FBgn0261020
A0A1W4V9P3_DROFC	ogre	FBgn0004646
A0A1W4VDF6_DROFC	RpL37A	FBgn0261608
A0A1W4VER2_DROFC	PpV	FBgn0003139
A0A1W4VGT0_DROFC	EloC	FBgn0266711
A0A1W4VKA7_DROFC	Cul2	FBgn0032956
A0A1W4VRM6_DROFC	OtopLa	FBgn0259994
A0A1W4VS60_DROFC	Rab18	FBgn0015794
A0A1W4VSE5_DROFC	ND-B16.6	FBgn0029868
A0A1W4W3Q7_DROFC	CG7888	FBgn0036116

A0A1W4WCK4_DROFC	ATPsynF	FBgn0035032
A0A1W4WDF0_DROFC	UQCR-14L	FBgn0039576
A0AQ24_DROME	ND-PDSW	FBgn0021967
A1Z6G9_DROME	CG8245-RA	FBgn0033031
A1Z863_DROME	Csgalnact	FBgn0033500
A2TDT5_DROSI	COX4	FBgn0032833
A4V4I0_DROME	Gbeta13F	FBgn0001105
A7KX19_DROME	spp	FBgn0031260
A8Y4V5_DROME	CG40498	FBgn0069969
AGO2_DROME	AGO2	FBgn0087035
AIMP2_DROME	AIMP2	FBgn0036515
ATD3A_DROME	bor	FBgn0040237
ATP5J_DROME	ATPsynCf6	FBgn0016119
B3DNM8_DROME	CG45002	FBgn0266354
B3M4G8_DROAN	Rpn12	FBgn0028693
B3MDE7_DROAN	Sec6	FBgn0266671
B3MQN1_DROAN	CG14232	FBgn0031061
B3N323_DROER	Sec5	FBgn0266670
B3N662_DROER	nop5	FBgn0026196
B3N6C9_DROER	CG5958	FBgn0031913
B3N9M1_DROER	FrmD5	FBgn0032225
B3NFZ2_DROER	Ccz1	FBgn0035470
B3NKF9_DROER	Tim23	FBgn0267976
B3NQG5_DROER	Nop60B	FBgn0259937
B3NT15_DROER	Upf1	FBgn0030354
B3NTH8_DROER	Pis	FBgn0030670
B3NUG9_DROER	Ost48	FBgn0014868
B3NVI8_DROER	Pp2B-14D	FBgn0011826
B3NXQ1_DROER	schlank	FBgn0040918
B3NY61_DROER	Mgstl	FBgn0025814
B3P2F2_DROER	Pi4KII $\alpha$	FBgn0037339
B3P2Y3_DROER	Sec15	FBgn0266674
B3P382_DROER	NP15.6	FBgn0027785
B3P7I9_DROER	pinta	FBgn0038966
B3P7S7_DROER	stops	FBgn0086704
B3P8X3_DROER	ND-B14.5A	FBgn0025839
B4HI97_DROSE	bumpel	FBgn0037895
B4HJY4_DROSE	BckdhA	FBgn0037709
B4HQE9_DROSE	CG30159	FBgn0050159
B4HU31_DROSE	CG1265	FBgn0035517
B4HVV2_DROSE	CG7879	FBgn0035235

B4HWD9_DROSE	CG4658	FBgn0032170
B4HYP6_DROSE	Sema1a	FBgn0011259
B4I3X0_DROSE	Vps37B	FBgn0037299
B4I7C1_DROSE	Abcd3	FBgn0031069
B4IC16_DROSE	Exo84	FBgn0266668
B4ICY7_DROSE	Tspo	FBgn0031263
B4II25_DROSE	Pngl	FBgn0033050
B4IJ02_DROSE	γCOP	FBgn0028968
B4IL51_DROSE	spidey	FBgn0029975
B4IL86_DROSE	Abcd1	FBgn0039890
B4K520_DROMO	asp	FBgn0000140
B4LXZ8_DROVI	CG6126	FBgn0038407
B4PL10_DROYA	CG6178	FBgn0039156
B4QFN1_DROSI	Isha	FBgn0034598
B4QI12_DROSI	CG8306	FBgn0034142
B4QJK9_DROSI	Fbp1	FBgn0000639
B4QMF1_DROSI	Agpat3	FBgn0036623
B4QTZ2_DROSI	PGS1	FBgn0038649
B4QUE5_DROSI	Wdr37	FBgn0038617
B4R4E3_DROSI	CG12177	FBgn0030510
B5RIL6_DROME	Arts	FBgn0042177
B5T1Z3_DROME	Cyp6a23	FBgn0033978
B7Z067_DROME	Nedd4	FBgn0259174
BOSS_DROME	boss	FBgn0000206
BRUN_DROME	brun	FBgn0261787
C12B2_DROME	Cyp12b2	FBgn0034387
C28A5_DROME	Cyp28a5	FBgn0028940
C28D1_DROME	Cyp28d1	FBgn0031689
C9QP43_DROME	Tango5	FBgn0052675
CP9B2_DROME	Cyp9b2	FBgn0015039
E2QCZ3_DROME	dind	FBgn0038639
ECM29_DROME	CG8858	FBgn0033698
EXOC5_DROME	Sec10	FBgn0266673
F3YDB2_DROME	eIF-2beta-RA	FBgn0004926
GUTR1_DROME	Tre1	FBgn0046687
H9XVP3_DROME	PlexA	FBgn0025741
IF4E_DROME	eIF-4E	FBgn0015218
KRH2_DROME	Kr-h2	FBgn0266449
LAM0_DROME	Lam	FBgn0002525
M9MRM4_DROME	Sac1	FBgn0283500
M9NDL5_DROME	trol	FBgn0284408

MP1_DROME	MP1	FBgn0027930
MTTF_DROME	mTTF	FBgn0028530
O18407_DROME	vkg	FBgn0016075
O77287_DROME	Su(P)	FBgn0004465
O96306_DROME	Ac3	FBgn0023416
Q0E9L2_DROME	Dscam1	FBgn0033159
Q5LJX8_DROME	zyd	FBgn0265767
Q6NP35_DROME	rho-5	FBgn0041723
Q7JYH3_DROME	ND-B14.7	FBgn0034576
Q7K0E6_DROME	AspRS	FBgn0002069
Q7K1R6_DROME	CG10916	FBgn0034312
Q7K3T3_DROME	CG1441	FBgn0033464
Q7KMM4_DROME	GCS2alpha	FBgn0027588
Q7KSP6_DROME	Sbf	FBgn0025802
Q7KTG2_DROME	Apoltp	FBgn0032136
Q7PLL6_DROME	I(3)80Fj	FBgn0039959
Q8IMT3_DROME	CG31436	FBgn0051436
Q8MR71_DROME	Reg-2	FBgn0016715
Q8MSS3_DROME	rumpel	FBgn0029950
Q8MSW0_DROME	IleRS	FBgn0027086
Q8SWZ9_DROME	Ldsdh1	FBgn0029994
Q8S XK2_DROME	ArgRS-m	FBgn0037526
Q8SYQ8_DROME	CG3420	FBgn0033100
Q8SZF2_DROME	ND-23	FBgn0017567
Q960Y8_DROME	alt	FBgn0038535
Q961E7_DROME	PhKgamma	FBgn0011754
Q9VB10_DROME	Hsdl2	FBgn0039537
Q9VC87_DROME	CG18528	FBgn0039189
Q9VCS2_DROME	CG13833	FBgn0039040
Q9VD14_DROME	CG13850	FBgn0038961
Q9VHB2_DROME	CG9396	FBgn0037714
Q9VHJ4_DROME	RagA-B	FBgn0037647
Q9VI66_DROME	CG31248	FBgn0051248
Q9VJD1_DROME	GCS2beta	FBgn0032643
Q9VL16_DROME	Fundc1	FBgn0032200
Q9VLM7_DROME	CG13392	FBgn0032033
Q9VP06_DROME	Alg11	FBgn0037108
Q9VV87_DROME	Baldspot	FBgn0260960
Q9W196_DROME	CG3356	FBgn0034989
Q9W2J4_DROME	Ugt49B1	FBgn0027073
Q9W350_DROME	c11.1	FBgn0040236

Q9W3M6_DROME	Dhdds	FBgn0029980
Q9W501_DROME	temp	FBgn0027296
Q9Y137_DROME	mino	FBgn0027579
Q9Y166_DROME	Dic1	FBgn0027610
RT26_DROME	mRpS26	FBgn0036774
SNP25_DROME	Snap25	FBgn0011288

## 7.2. Proteins identified by tandem mass spectrometry as significantly higher in DPR than GFP

**Table 7.5. Proteins identified by MS/MS as significantly higher in GA than GFP**

<b>Accession</b>	<b>Drosophila melanogaster protein</b>	<b>FlyBase ID</b>
A0A0B4KGX1_DROME	jar	FBgn0011225
A0A0J9R3D8_DROSI	Mhc	FBgn0264695
A0A0J9R3U1_DROSI	CLIP-190	FBgn0020503
A0A0J9RL63_DROSI	zip	FBgn0287873
A0A0M4EPH2_DROBS	$\beta$ Tub85D	FBgn0003889
A1ZA73_DROME	Strn-Mlck	FBgn0265045
A8JUV9_DROME	sgg	FBgn0003371
B4I2V4_DROSE	FASN1	FBgn0283427
B4QBS9_DROSI	PPO1	FBgn0283437
E1JHJ4_DROME	Mhc	FBgn0264695
M9ND95_DROME	Mhc	FBgn0264695
M9NEP1_DROME	Mhc	FBgn0264695

**Table 7.6. Proteins identified by MS/MS as significantly higher in AP than GFP**

<b>Accession</b>	<b>Drosophila melanogaster protein</b>	<b>FlyBase ID</b>
A0A0B4KGX1_DROME	jar	FBgn0011225
A0A0B4LF88_DROME	TppII	FBgn0020370
A0A0B4LH50_DROME	Act87E	FBgn0000046
A0A0J9R3D8_DROSI	Mhc	FBgn0264695
A0A0J9R3U1_DROSI	CLIP-190	FBgn0020503
A0A0J9R772_DROSI	didum	FBgn0261397
A0A0J9RL63_DROSI	zip	FBgn0287873
A0A1W4ULI9_DROFC	CLIP-190	FBgn0020503
A0A1W4VML6_DROFC	Gyc88E	FBgn0038295
A4V1N8_DROME	Prm	FBgn0003149
B3N6C8_DROER	muc	FBgn0283658
B3NTJ7_DROER	CG9213	FBgn0030655
CL190_DROME	CLIP-190	FBgn0020503
E1JHJ4_DROME	Mhc	FBgn0264695
M9ND95_DROME	Mhc	FBgn0264695
M9NF46_DROME	Mhc	FBgn0264695
NINAC_DROME	ninaC	FBgn0002938
Q7K3E2_DROME	C5080	FBgn0031313
Q7KSP6_DROME	Sbf	FBgn0025802
Q8MR71_DROME	Reg-2	FBgn0016715

**Table 7.7. Proteins identified by MS/MS as significantly higher in PR than GFP**

<b>Accession number</b>	<b>Drosophila melanogaster protein</b>	<b>FlyBase ID</b>
A0A024E3A5_DROME	ND-39	FBgn0037001
A0A075BNB9_DROME	Cyp6a2	FBgn0000473
A0A0B4KFA6_DROME	CD98hc	FBgn0037533
A0A0B4KFE4_DROME	AcsI	FBgn0263120
A0A0B4LF88_DROME	TpplI	FBgn0020370
A0A0B4LGD3_DROME	kcc	FBgn0261794
A0A0B4LIJ0_DROME	Rpt2	FBgn0015282
A0A0J9QVU7_DROSI	smog	FBgn0051660
A0A0J9QYR0_DROSI	emb	FBgn0020497
A0A0J9RBM1_DROSI	CG8888	FBgn0033679
A0A0J9RP14_DROSI	Dhc64C	FBgn0261797
A0A0R3NZB2_DROPS	CG9281	FBgn0030672
A0A1W4VGT0_DROFC	EloC	FBgn0266711
A1Z784_DROME	ACC	FBgn0033246
AIMP2_DROME	AIMP2	FBgn0036515
APLP_DROME	apolpp	FBgn0087002
B3N6C8_DROER	muc	FBgn0283658
B4HZR1_DROSE	aralar1	FBgn0028646
B4I2M5_DROSE	Drp1	FBgn0026479
B4IJ02_DROSE	γCOP	FBgn0028968
B7Z001_DROME	FASN1	FBgn0283427
C28A5_DROME	Cyp28a5	FBgn0028940
C28D1_DROME	Cyp28d1	FBgn0031689
E1JIR4_DROME	Atpalpha	FBgn0002921
E1JJA4_DROME	shi	FBgn0003392
ECM29_DROME	CG8858	FBgn0033698
G3P1_DROME	Gapdh1	FBgn0001091
M9NDL5_DROME	trol	FBgn0284408
Q24506_DROME	ScpX	FBgn0015808
Q6NP35_DROME	rho-5	FBgn0041723
Q7K3E2_DROME	CT16297	FBgn0031313
Q7KMM4_DROME	GCS2alpha	FBgn0027588
Q8MR71_DROME	Reg-2	FBgn0016715
Q8MSW0_DROME	IleRS	FBgn0027086
Q9VP06_DROME	Alg11	FBgn0037108
Q9W196_DROME	CG3356	FBgn0034989
Q9Y166_DROME	Dic1	FBgn0027610

**Table 7.8. Proteins identified by MS/MS as significantly higher in GR than GFP**

<b>Accession</b>	<b>Drosophila melanogaster protein</b>	<b>FlyBase ID</b>
A0A024E3A5_DROME	ND-39	FBgn0037001
A0A075BNB9_DROME	Cyp6a2	FBgn0000473
A0A0A0RZ60_DROME	mt:Coll	FBgn0013675
A0A0B4J401_DROME	CG10737	FBgn0034420
A0A0B4K6F9_DROME	Esyt2	FBgn0266758
A0A0B4KFA6_DROME	CD98hc	FBgn0037533
A0A0B4KFE4_DROME	Acsi	FBgn0263120
A0A0B4LEY1_DROME	Sec31	FBgn0033339
A0A0B4LEZ3_DROME	Not1	FBgn0085436
A0A0B4LG95_DROME	l(2)k09913	FBgn0021979
A0A0B4LGD3_DROME	kcc	FBgn0261794
A0A0B4LGJ9_DROME	Gpat4	FBgn0034971
A0A0B4LH53_DROME	Nsf2	FBgn0266464
A0A0J9QVU7_DROSI	Smog	FBgn0051660
A0A0J9QYR0_DROSI	emb	FBgn0020497
A0A0J9QZX9_DROSI	Mulk	FBgn0260750
A0A0J9R029_DROSI	Cand1	FBgn0027568
A0A0J9R165_DROSI	Rab6	FBgn0015797
A0A0J9R1W1_DROSI	CG31729	FBgn0051729
A0A0J9R4N7_DROSI	sky	FBgn0032901
A0A0J9RBM1_DROSI	CG8888	FBgn0033679
A0A0J9RCP8_DROSI	jef	FBgn0033958
A0A0J9RK49_DROSI	SERCA	FBgn0263006
A0A0J9RMV0_DROSI	trio	FBgn0024277
A0A0J9RP14_DROSI	Dhc64C	FBgn0261797
A0A0J9TCR4_DROSI	CG3662	FBgn0031285
A0A0J9TSR4_DROSI	nrv3	FBgn0032946
A0A0P8XI16_DROAN	IA-2	FBgn0031294
A0A0R3NZB2_DROPS	CG9281	FBgn0030672
A0A1W4VGT0_DROFC	EloC	FBgn0266711
A0A1W4VKA7_DROFC	Cul2	FBgn0032956
A0A1W4W959_DROFC	Tps1	FBgn0027560
A1Z784_DROME	ACC	FBgn0033246
A4V4I0_DROME	Gbeta13F	FBgn0001105
A4V4U5_DROME	slgA	FBgn0003423
AIMP2_DROME	AIMP2	FBgn0036515
APLP_DROME	apolpp	FBgn0087002
B3N6C9_DROER	CG5958	FBgn0031913

B3N9M1_DROER	FrmD5	FBgn0032225
B3NVI8_DROER	Pp2B-14D	FBgn0011826
B3NXJ2_DROER	Chc	FBgn0000319
B4HYP6_DROSE	Sema1a	FBgn0011259
B4HZ72_DROSE	Rpn2	FBgn0028692
B4HZR1_DROSE	aralar1	FBgn0028646
B4I2M5_DROSE	Drp1	FBgn0026479
B4IDU1_DROSE	sesB	FBgn0003360
B4II25_DROSE	Pngl	FBgn0033050
B4IIV9_DROSE	PMCA	FBgn0259214
B4IJ02_DROSE	$\gamma$ COP	FBgn0028968
B4QI12_DROSI	CG8306	FBgn0034142
B4QJK9_DROSI	Fbp1	FBgn0000639
B4QMF1_DROSI	Agpat3	FBgn0036623
B5T1Z3_DROME	Cyp6a23	FBgn0033978
B6IDR5_DROME	Sc2	FBgn0035471
B7Z001_DROME	FASN1	FBgn0283427
C28A5_DROME	Cyp28a5	FBgn0028940
C28D1_DROME	Cyp28d1	FBgn0031689
E1JHE4_DROME	Fatp	FBgn0267828
E1JIR4_DROME	Atpalpha	FBgn0002921
E1JJA4_DROME	shi	FBgn0003392
ECM29_DROME	CG8858	FBgn0033698
H9XVP3_DROME	PlexA	FBgn0025741
M9PB68_DROME	poe	FBgn0011230
M9PH10_DROME	comt	FBgn0000346
O61380_DROME	eIF4G1	FBgn0023213
O77287_DROME	Su(P)	FBgn0004465
O96306_DROME	Ac3	FBgn0023416
Q0E8E8_DROME	Mpcp2	FBgn0026409
Q6NP35_DROME	rho-5	FBgn0041723
Q7JQH9_DROME	whd	FBgn0261862
Q7KMM4_DROME	GCS2alpha	FBgn0027588
Q7KSP6_DROME	Sbf	FBgn0025802
Q7KSQ0_DROME	sea	FBgn0037912
Q7KTC7_DROME	MRP	FBgn0032456
Q7KTG2_DROME	Apoltp	FBgn0032136
Q7PLL6_DROME	CG17514	FBgn0039959
Q8MM39_DROME	Spn42Da	FBgn0265137
Q8MR71_DROME	Reg-2	FBgn0016715
Q8MSW0_DROME	IleRS	FBgn0027086

Q9VAJ9_DROME	CG1907	FBgn0039674
Q9VD14_DROME	GH07286p	FBgn0038961
Q9VJD1_DROME	GCS2beta	FBgn0032643
Q9VL16_DROME	Fundc1	FBgn0032200
Q9VLM7_DROME	CG13392	FBgn0032033
Q9VN44_DROME	Karybeta3	FBgn0087013
Q9VP06_DROME	Alg11	FBgn0037108
Q9W196_DROME	CG3356	FBgn0034989
Q9W2J4_DROME	Ugt49B1	FBgn0027073
Q9W2M4_DROME	CG10527	FBgn0034583
Q9W350_DROME	c11.1	FBgn0040236
Q9Y166_DROME	Dic1	FBgn0027610
SYEP_DROME	GluProRS	FBgn0005674
TRP_DROME	trp	FBgn0003861

### 7.3. Whole blots for Figure 4.5

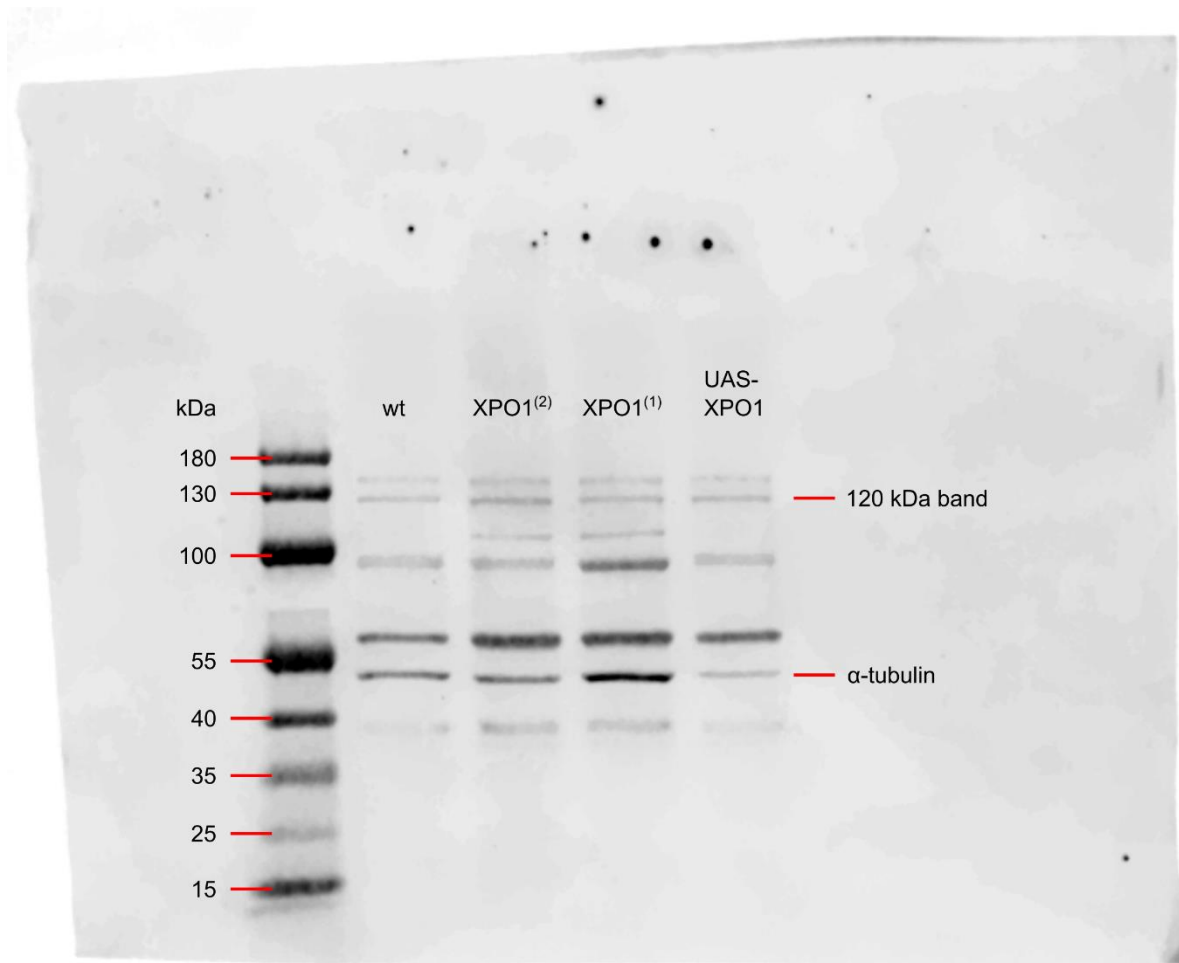


**Figure 7.1. Annotated whole blot of Figure 4.5A.** Molecular weights of PageRuler™ Plus Prestained Protein Ladder labelled on the left. Bands shown and discussed in main body labelled on the right. All bands except α-tubulin appeared as a result of anti-XPO1.

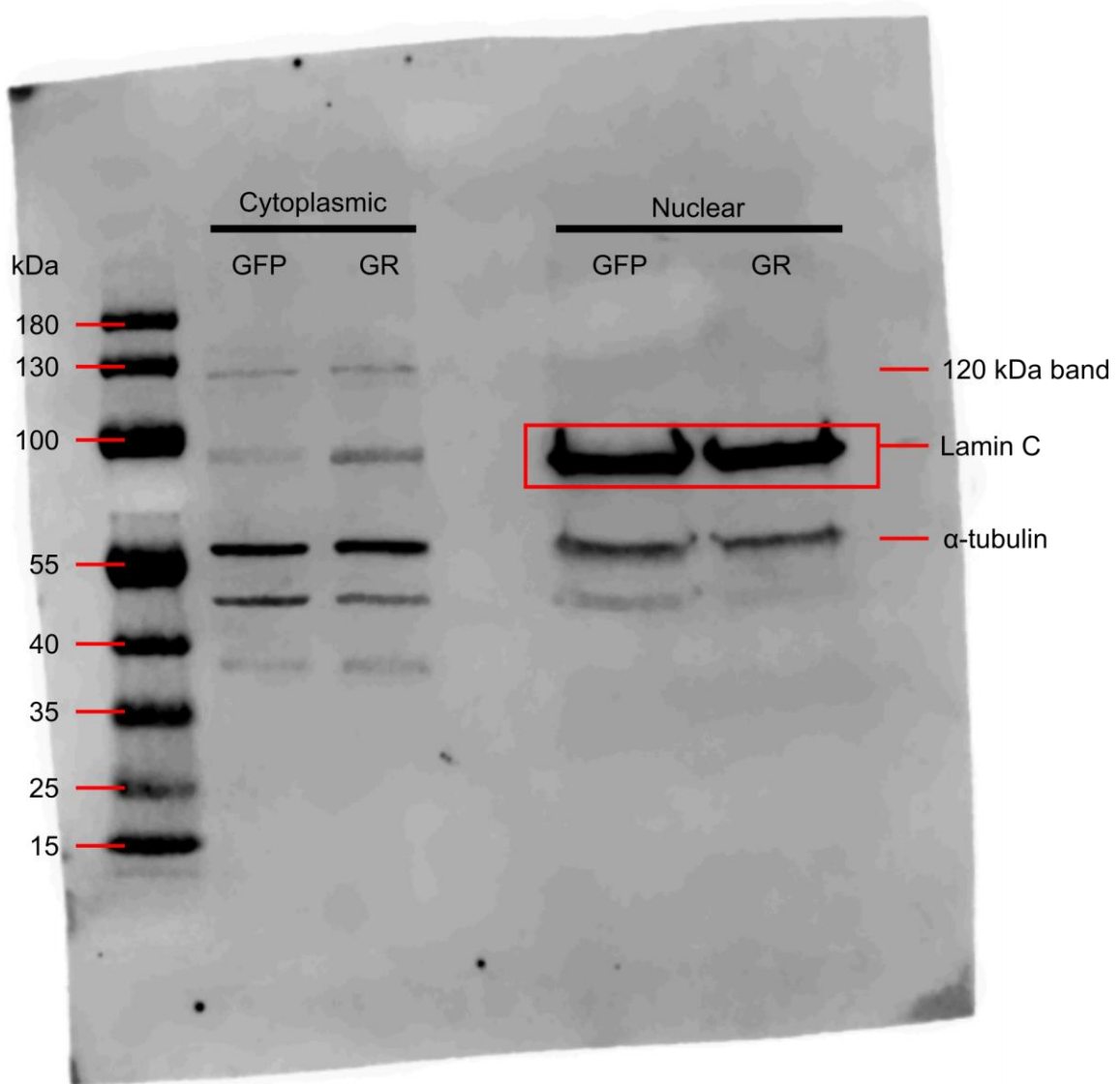


**Figure 7.2. Annotated whole blot of Figure 4.5C.** Molecular weights of PageRuler™ Plus Prestained Protein Ladder labelled on the left. Bands shown and discussed in main body labelled on the right. All bands except α-tubulin and Lamin C appeared as a result of anti-XPO1.

## 8. Bibliography

- Abel, E. L. (2007) 'Amyotrophic lateral sclerosis', *Perceptual and Motor Skills*, 104, pp. 1251–1254. doi: 10.1016/S0140-6736(07)60944-1.
- Abu-Shaar, M., Ryoo, H. D. and Mann, R. S. (1999) 'Control of the nuclear localization of Extradenticle by competing nuclear import and export signals', *Genes and Development*, 13(8), pp. 935–945. doi: 10.1101/gad.13.8.935.
- Aizawa, H. *et al.* (2019) 'Impaired Nucleoporins Are Present in Sporadic Amyotrophic Lateral Sclerosis Motor Neurons that Exhibit Mislocalization of the 43-kDa TAR DNA-Binding Protein', *Journal of Clinical Neurology*, 15(1), p. 62. doi: 10.3988/JCN.2019.15.1.62.
- Al-Chalabi, A. and Hardiman, O. (2013) 'The epidemiology of ALS: a conspiracy of genes, environment and time', *Nature Reviews Neurology*, 9, pp. 617–628.
- Al-Sarraj, S. *et al.* (2011) 'P62 positive, TDP-43 negative, neuronal cytoplasmic and intranuclear inclusions in the cerebellum and hippocampus define the pathology of C9orf72-linked FTLN and MND/ALS', *Acta Neuropathologica*, 122(6), pp. 691–702. doi: 10.1007/S00401-011-0911-2.
- Allen, S. P. *et al.* (2020) 'Transcriptomic analysis of human astrocytes in vitro reveals hypoxia-induced mitochondrial dysfunction, modulation of metabolism, and dysregulation of the immune response', *International Journal of Molecular Sciences*, 21(21), pp. 1–22. doi: 10.3390/ijms21218028.
- Alvarez-Mora, M. I. *et al.* (2022) 'Bioenergetic and Autophagic Characterization of Skin Fibroblasts from C9orf72 Patients', *Antioxidants*, 11(6), pp. 1–14. doi: 10.3390/antiox11061129.
- Amick, J., Roczniak-Ferguson, A. and Ferguson, S. M. (2016) 'C9orf72 binds SMCR8, localizes to lysosomes, and regulates mTORC1 signaling', *Molecular Biology of the Cell*, 27(20), pp. 3040–3051. doi: 10.1091/mbc.E16-01-0003.
- Andersen, P. M. and Al-Chalabi, A. (2011) 'Clinical genetics of amyotrophic lateral sclerosis: what do we really know?', *Nature Reviews Neurology*, 7(11), pp. 603–615. doi: 10.1038/nrneurol.2011.150.
- Aoki, Y. *et al.* (2017) 'C9orf72 and RAB7L1 regulate vesicle trafficking in amyotrophic lateral sclerosis and frontotemporal dementia', *Brain*, 140(4), pp. 887–897. doi: 10.1093/BRAIN/AWX024.
- Arama, E. and Steller, H. (2006) 'Detection of apoptosis by terminal deoxynucleotidyl

transferase-mediated dUTP nick-end labeling and acridine orange in *Drosophila* embryos and adult male gonads', *Nature Protocols*, 1(4), pp. 1725–1731. doi: 10.1038/nprot.2006.235.

Archbold, H. C. *et al.* (2018) 'TDP43 nuclear export and neurodegeneration in models of amyotrophic lateral sclerosis and frontotemporal dementia', *Scientific Reports*, 8(1), pp. 1–18. doi: 10.1038/s41598-018-22858-w.

Ash, P. E. A. *et al.* (2013) 'Unconventional Translation of C9ORF72 GGGGCC Expansion Generates Insoluble Polypeptides Specific to c9FTD/ALS', *Neuron*, 77(4), pp. 639–646. doi: 10.1016/j.neuron.2013.02.004.

Atanasio, A. *et al.* (2016) 'C9orf72 ablation causes immune dysregulation characterized by leukocyte expansion, autoantibody production, and glomerulonephropathy in mice', *Scientific Reports*, 6(November 2015), pp. 1–14. doi: 10.1038/srep23204.

Au, W. H. *et al.* (2023) 'Activation of the Keap1 / Nrf2 pathway suppresses mitochondrial dysfunction in C9orf72 ALS / FTD in vivo models and patient iNeurons', *bioRxiv*.

Azad, P. *et al.* (2009) 'Distinct Mechanisms Underlying Tolerance to Intermittent and Constant Hypoxia in *Drosophila melanogaster*', *PLOS ONE*, 4(4), p. e5371. doi: 10.1371/JOURNAL.PONE.0005371.

Baade, I. and Kehlenbach, R. H. (2019) 'The cargo spectrum of nuclear transport receptors', *Current Opinion in Cell Biology*, 58, pp. 1–7. doi: 10.1016/J.CEB.2018.11.004.

Baborie, A. *et al.* (2015) 'Accumulation of dipeptide repeat proteins predates that of TDP-43 in frontotemporal lobar degeneration associated with hexanucleotide repeat expansions in C9ORF72 gene', *Neuropathology and Applied Neurobiology*, 41(5), pp. 601–612. doi: 10.1111/nan.12178.

Balendra, R. *et al.* (2023) 'Transcriptome-wide RNA binding analysis of C9orf72 poly(PR) dipeptides', *Life Science Alliance*, 6(9), pp. 1–11. doi: 10.26508/lsa.202201824.

Banasiak, K. J. and Haddad, G. G. (1998) 'Hypoxia-induced apoptosis: Effect of hypoxic severity and role of p53 in neuronal cell death', *Brain Research*, 797(2), pp. 295–304. doi: 10.1016/S0006-8993(98)00286-8.

Bandarra, D. *et al.* (2014) 'Hypoxia activates IKK-NF-κB and the immune response in *Drosophila melanogaster*', *Bioscience Reports*, 34(4), pp. 429–440. doi: 10.1042/BSR20140095.

Bang, J., Spina, S. and Miller, B. L. (2015) 'Frontotemporal dementia', *The Lancet*,

386(10004), pp. 1672–1682. doi: 10.1016/S0140-6736(15)00461-4.

Baralle, M., Buratti, E. and Baralle, F. E. (2013) 'The role of TDP-43 in the pathogenesis of ALS and FTL D', *Biochemical Society Transactions*, 41(6), pp. 1536–1540. doi: 10.1042/BST20130186.

Bartels, K., Grenz, A. and Eltzschig, H. K. (2013) 'Hypoxia and inflammation are two sides of the same coin', *Proceedings of the National Academy of Sciences of the United States of America*, 110(46), pp. 18351–18352. doi: 10.1073/pnas.1318345110.

Beck, J. *et al.* (2013) 'Large C9orf72 hexanucleotide repeat expansions are seen in multiple neurodegenerative syndromes and are more frequent than expected in the UK population', *American Journal of Human Genetics*, 92(3), pp. 345–353. doi: 10.1016/j.ajhg.2013.01.011.

Beckers, J. *et al.* (2023) 'A toxic gain-of-function mechanism in C9orf72 ALS impairs the autophagy-lysosome pathway in neurons', *Acta Neuropathologica Communications*, 11(1), pp. 1–22. doi: 10.1186/s40478-023-01648-0.

Belli, S. and Vanacore, N. (2005) 'Proportionate mortality of Italian soccer players: Is amyotrophic lateral sclerosis an occupational disease?', *European Journal of Epidemiology*, 20(3), pp. 237–242. doi: 10.1007/s10654-004-6879-7.

Belzil, V. V. *et al.* (2013) 'Reduced C9orf72 gene expression in c9FTD/ALS is caused by histone trimethylation, an epigenetic event detectable in blood', *Acta Neuropathologica*, 126(6), pp. 895–905. doi: 10.1007/s00401-013-1199-1.

Benajiba, L. *et al.* (2009) 'TARDBP mutations in motoneuron disease with frontotemporal lobar degeneration', *Annals of Neurology*, 65(4), pp. 470–473. doi: 10.1002/ANA.21612.

Benderro, G. F. and Lamanna, J. C. (2011) 'Hypoxia-induced angiogenesis is delayed in aging mouse brain', *Brain Research*, 1389, pp. 50–60. doi: 10.1016/j.brainres.2011.03.016.

Bennett, C. L. *et al.* (2023) 'Senataxin helicase, the causal gene defect in ALS4, is a significant modifier of C9orf72 ALS G4C2 and arginine-containing dipeptide repeat toxicity', *Acta Neuropathologica Communications*, 11(1), pp. 1–18. doi: 10.1186/s40478-023-01665-z.

Le Ber, I. (2013) 'Genetics of frontotemporal lobar degeneration: An up-date and diagnosis algorithm', *Revue Neurologique*, 169(10), pp. 811–819. doi: 10.1016/J.NEUROL.2013.07.014.

Bharathi, V., Girdhar, A. and Patel, B. K. (2021) 'Role of CNC1 gene in TDP-43 aggregation-induced oxidative stress-mediated cell death in *S. cerevisiae* model of ALS', *Biochimica et Biophysica Acta (BBA) - Molecular Cell Research*, 1868(6), p. 118993. doi:

10.1016/J.BBAMCR.2021.118993.

Blair, I. P. *et al.* (2010) 'FUS mutations in amyotrophic lateral sclerosis: Clinical, pathological, neurophysiological and genetic analysis', *Journal of Neurology, Neurosurgery and Psychiatry*, 81(6), pp. 639–645. doi: 10.1136/jnnp.2009.194399.

van Blitterswijk, M. *et al.* (2013) 'Association between repeat sizes and clinical and pathological characteristics in carriers of C9ORF72 repeat expansions (Xpansize-72): a cross-sectional cohort study', *The Lancet Neurology*, 12(10), pp. 978–988. doi: 10.1016/S1474-4422(13)70210-2.

van Blitterswijk, M. *et al.* (2015) 'Novel clinical associations with specific C9ORF72 transcripts in patients with repeat expansions in C9ORF72', *Acta Neuropathologica*, 130(6), pp. 863–876. doi: 10.1007/s00401-015-1480-6.

Van Blitterswijk, M. *et al.* (2012) 'Evidence for an oligogenic basis of amyotrophic lateral sclerosis', *Human Molecular Genetics*, 21(17), pp. 3776–3784. doi: 10.1093/HMG/DDS199.

Boeve, B. F. *et al.* (2012) 'Characterization of frontotemporal dementia and/or amyotrophic lateral sclerosis associated with the GGGGCC repeat expansion in C9ORF72', *Brain*, 135(3), pp. 765–783. doi: 10.1093/BRAIN/AWS004.

Boeynaems, S. *et al.* (2016) 'Drosophila screen connects nuclear transport genes to DPR pathology in c9ALS/FTD', *Scientific Reports*, 6(1), pp. 1–8. doi: 10.1038/srep20877.

Van Den Bosch, L. *et al.* (2004) 'Effects of vascular endothelial growth factor (VEGF) on motor neuron degeneration', *Neurobiology of Disease*, 17(1), pp. 21–28. doi: 10.1016/j.nbd.2004.06.004.

Boxer, A. L. *et al.* (2011) 'Clinical, neuroimaging and neuropathological features of a new chromosome 9p-linked FTD-ALS family', *Journal of neurology, neurosurgery, and psychiatry*, 82(2), p. 196. doi: 10.1136/JNNP.2009.204081.

Božič, J. *et al.* (2022) 'Interactome screening of C9orf72 dipeptide repeats reveals VCP sequestration and functional impairment by polyGA', *Brain*, 145(2), pp. 684–699. doi: 10.1093/BRAIN/AWAB300.

Brand, A. H. and Perrimon, N. (1993) 'Targeted gene expression as a means of altering cell fates and generating dominant phenotypes', *Development*, 118(2), pp. 401–415.

Brockington, A. *et al.* (2006) 'Expression of vascular endothelial growth factor and its receptors in the central nervous system in amyotrophic lateral sclerosis', *Journal of Neuropathology and Experimental Neurology*, 65(1), pp. 26–36. doi:

10.1097/01.jnen.0000196134.51217.74.

Broustal, O. *et al.* (2010) 'FUS mutations in frontotemporal lobar degeneration with amyotrophic lateral sclerosis', *Journal of Alzheimer's Disease*, 22(3), pp. 765–769. doi: 10.3233/JAD-2010-100837.

Bruick, R. K. and McKnight, S. L. (2001) 'A conserved family of prolyl-4-hydroxylases that modify HIF', *Science*, 294(5545), pp. 1337–1340. doi: 10.1126/science.106637.

Brujin, L. I. *et al.* (1997) 'ALS-linked SOD1 mutant G85R mediates damage to astrocytes and promotes rapidly progressive disease with SOD1-containing inclusions', *Neuron*, 18(2), pp. 327–338. doi: 10.1016/S0896-6273(00)80272-X.

Burguete, A. S. *et al.* (2015) 'GGGGCC microsatellite RNA is neuritically localized, induces branching defects, and perturbs transport granule function', *eLife*, 4, pp. 1–23. doi: 10.7554/eLife.08881.

Burrell, J. R. *et al.* (2011) 'Motor Neuron dysfunction in frontotemporal dementia', *Brain*, 134(9), pp. 2582–2594. doi: 10.1093/brain/awr195.

Byrne, S. *et al.* (2011) 'Rate of familial amyotrophic lateral sclerosis: a systematic review and meta-analysis', *Journal of Neurology, Neurosurgery & Psychiatry*, 82(6), pp. 623–627. doi: 10.1136/JNNP.2010.224501.

C. Correia, S. *et al.* (2013) 'Defective HIF Signaling Pathway and Brain Response to Hypoxia in Neurodegenerative Diseases: Not an "Iffy" Question!', *Current Pharmaceutical Design*, 19(38), pp. 6809–6822. doi: 10.2174/1381612811319380013.

Cafaro, R. P. (1960) 'Hypoxia: Its Causes and Symptoms.', *Journal of the American Dental Society of Anesthesiology*, 7(4), pp. 4–8. Available at: <http://www.ncbi.nlm.nih.gov/pubmed/19598857> <http://www.pubmedcentral.nih.gov/articlerender.fcgi?artid=PMC2067517>.

Cai, W. *et al.* (2017) 'Dysfunction of the neurovascular unit in ischemic stroke and neurodegenerative diseases: An aging effect', *Ageing Research Reviews*, 34, pp. 77–87. doi: 10.1016/j.arr.2016.09.006.

Cairns, N. J. *et al.* (2007) 'TDP-43 in Familial and Sporadic Frontotemporal Lobar Degeneration with Ubiquitin Inclusions', *The American Journal of Pathology*, 171(1), pp. 227–240. doi: 10.2353/AJPATH.2007.070182.

Callister, J. B. *et al.* (2016) 'Modelling C9orf72 dipeptide repeat proteins of a physiologically relevant size', *Human Molecular Genetics*, 25(23), pp. 5069–5082. doi:

10.1093/hmg/ddw327.

Cao, W. *et al.* (2008) 'Identification of novel genes that modify phenotypes induced by Alzheimer's  $\beta$ -amyloid overexpression in *Drosophila*', *Genetics*, 178(3), pp. 1457–1471. doi: 10.1534/genetics.107.078394.

Celona, B. *et al.* (2017) 'Suppression of c9orf72 RNA repeat-induced neurotoxicity by the ALS-associated RNA-binding protein Zfp106', *eLife*, 6, pp. 1–17. doi: 10.7554/eLife.19032.

Cervos-Navarro, J. and Diemer, N. H. (1991) 'Selective vulnerability in brain hypoxia', *Critical Reviews in Neurobiology*, 6(3), pp. 149–182.

Česnik, A. B. *et al.* (2019) 'Nuclear RNA foci from C9ORF72 expansion mutation form paraspeckle-like bodies', *Journal of Cell Science*, 132(5), pp. 1–10. doi: 10.1242/jcs.224303.

Chang, J. C. and Morton, D. B. (2017) '*Drosophila* lines with mutant and wild type human TDP-43 replacing the endogenous gene reveals phosphorylation and ubiquitination in mutant lines in the absence of viability or lifespan defects', *PLoS ONE*, 12(7), pp. 1–24. doi: 10.1371/journal.pone.0180828.

Chen, H. *et al.* (2021) 'The Potential Role of Hypoxia-Inducible Factor-1 in the Progression and Therapy of Central Nervous System Diseases', *Current Neuropharmacology*, 20(9), pp. 1651–1666. doi: 10.2174/1570159x19666210729123137.

Chio, A. *et al.* (2012) 'Extensive genetics of ALS : A population-based study in Italy', *Neurology*, 79(19), pp. 1983–1989. doi: 10.1212/WNL.0B013E3182735D36.

Chiò, A. *et al.* (2005) 'Severely increased risk of amyotrophic lateral sclerosis among Italian professional football players', *Brain*, 128(3), pp. 472–476. doi: 10.1093/brain/awh373.

Chiò, A. *et al.* (2015) 'Development and evaluation of a clinical staging system for amyotrophic lateral sclerosis', *Journal of Neurology, Neurosurgery & Psychiatry*, 86(1), pp. 38–44. doi: 10.1136/JNNP-2013-306589.

Chiò, A. *et al.* (2018) 'The multistep hypothesis of ALS revisited', *Neurology*, 91(7), pp. e635–e642. doi: 10.1212/WNL.0000000000005996.

Chitiprolu, M. *et al.* (2018) 'A complex of C9ORF72 and p62 uses arginine methylation to eliminate stress granules by autophagy', *Nature Communications*, 9(1), pp. 1–18. doi: 10.1038/s41467-018-05273-7.

Choi, S. Y. *et al.* (2019) 'C9ORF72-ALS/FTD-associated poly(GR) binds Atp5a1 and compromises mitochondrial function in vivo', *Nature Neuroscience*, 22(6), pp. 851–862. doi: 10.1038/s41593-019-0397-0.

- Chou, C. C. *et al.* (2018) 'TDP-43 pathology disrupts nuclear pore complexes and nucleocytoplasmic transport in ALS/FTD', *Nature Neuroscience*, 21(2), pp. 228–239. doi: 10.1038/s41593-017-0047-3.
- Chow, T. W. *et al.* (1999) 'Inheritance of Frontotemporal Dementia', *Archives of Neurology*, 56(7), pp. 817–822. doi: 10.1001/ARCHNEUR.56.7.817.
- Christos Samakovlis *et al.* (1996) 'Development of the Drosophila tracheal system occurs by a series of morphologically distinct but genetically coupled branching events', *Development*, 1407, pp. 1395–1407.
- Cirelli, C. and Bushey, D. (2008) 'Sleep and wakefulness in Drosophila melanogaster', *Annals of the New York Academy of Sciences*, 1129, pp. 323–329. doi: 10.1196/ANNALS.1417.017.
- Ciura, S. *et al.* (2013) 'Loss of function of C9orf72 causes motor deficits in a zebrafish model of amyotrophic lateral sclerosis', *Annals of Neurology*, 74(2), pp. 180–187. doi: 10.1002/ana.23946.
- Cloutier, M. M. and Thrall, R. S. (2009) 'Physiology', in Koeppe, B. M. and Stanton, B. A. (eds) *Physiology*. 6th edn. Elsevier Health Sciences, p. 464.
- Collier, S. *et al.* (2000) 'The Drosophila embargoed Gene Is Required for Larval Progression and Encodes the Functional Homolog of Schizosaccharomyces Crm1', *Genetics*, 155(4), pp. 1799–1807. doi: 10.1093/GENETICS/155.4.1799.
- Cook, C. N. *et al.* (2020) 'C9orf72 poly(GR) aggregation induces TDP-43 proteinopathy', *Science Translational Medicine*, 12(559), pp. 1–11. doi: 10.1126/SCITRANSLMED.ABB3774.
- Cooper-Knock, J. *et al.* (2012) 'Clinico-pathological features in amyotrophic lateral sclerosis with expansions in C9ORF72', *Brain*, 135(3), pp. 751–764. doi: 10.1093/BRAIN/AWR365.
- Cooper-Knock, J. *et al.* (2014) 'Sequestration of multiple RNA recognition motif-containing proteins by C9orf72 repeat expansions', *Brain*, 137(7), pp. 2040–2051. doi: 10.1093/BRAIN/AWU120.
- Cooper-Knock, J., Higginbottom, A., *et al.* (2015) 'Antisense RNA foci in the motor neurons of C9ORF72-ALS patients are associated with TDP-43 proteinopathy', *Acta Neuropathologica*, 130(1), pp. 63–75. doi: 10.1007/s00401-015-1429-9.
- Cooper-Knock, J., Bury, J. J., *et al.* (2015) 'C9ORF72 GGGGCC Expanded Repeats Produce Splicing Dysregulation which Correlates with Disease Severity in Amyotrophic

- Lateral Sclerosis', *PLoS ONE*, 10(5). doi: 10.1371/JOURNAL.PONE.0127376.
- Coquin, L. *et al.* (2008) 'Metabolomic and flux-balance analysis of age-related decline of hypoxia tolerance in *Drosophila* muscle tissue', *Molecular Systems Biology*, 4(233). doi: 10.1038/msb.2008.71.
- Cronin, S. *et al.* (2008) 'Screening of hypoxia-inducible genes in sporadic ALS', *Amyotrophic Lateral Sclerosis*, 9, pp. 299–305. doi: 10.1080/17482960802160297.
- Cruts, M. *et al.* (2006) 'Null mutations in progranulin cause ubiquitin-positive frontotemporal dementia linked to chromosome 17q21', *Nature*, 442(24), pp. 920–924. doi: 10.1038/nature05017.
- Cruts, M., Theuns, J. and Van Broeckhoven, C. (2012) 'Locus-specific mutation databases for neurodegenerative brain diseases', *Human Mutation*, 33(9), pp. 1340–1344. doi: 10.1002/HUMU.22117.
- Culver, C. *et al.* (2010) 'Mechanism of Hypoxia-Induced NF- $\kappa$ B', *Molecular and Cellular Biology*, 30(20), pp. 4901–4921. doi: 10.1128/mcb.00409-10.
- Cunningham, K. M. *et al.* (2020) 'Tfeb/mitf links impaired nuclear import to autophagolysosomal dysfunction in c9-als', *eLife*, 9, pp. 1–35. doi: 10.7554/ELIFE.59419.
- Curtis, A. F. *et al.* (2017) 'Sex differences in the prevalence of genetic mutations in FTD and ALS: A meta-analysis', *Neurology*, 89(15), p. 1633. doi: 10.1212/WNL.0000000000004494.
- Cushman-Nick, M., Bonini, N. M. and Shorter, J. (2013) 'Hsp104 Suppresses Polyglutamine-Induced Degeneration Post Onset in a *Drosophila* MJD/SCA3 Model', *PLoS Genetics*, 9(9). doi: 10.1371/journal.pgen.1003781.
- Cykowski, M. D. *et al.* (2019) 'Dipeptide repeat (DPR) pathology in the skeletal muscle of ALS patients with C9ORF72 repeat expansion', *Acta Neuropathologica*, 138(4), pp. 667–670. doi: 10.1007/S00401-019-02050-8/FIGURES/1.
- Dafinca, R., Barbagallo, P. and Talbot, K. (2021) 'The Role of Mitochondrial Dysfunction and ER Stress in TDP-43 and C9ORF72 ALS', *Frontiers in Cellular Neuroscience*, 15, p. 653688. doi: 10.3389/FNCEL.2021.653688.
- Dale, E. A., Ben Mabrouk, F. and Mitchell, G. S. (2014) 'Unexpected benefits of intermittent hypoxia: Enhanced respiratory and nonrespiratory motor function', *Physiology*, 29(1), pp. 39–48. doi: 10.1152/physiol.00012.2013.
- Daneshvar, D. H. *et al.* (2021) 'Incidence of and Mortality from Amyotrophic Lateral Sclerosis in National Football League Athletes', *JAMA Network Open*, 4(12), pp. 1–11. doi:

10.1001/jamanetworkopen.2021.38801.

Darling, A. L. *et al.* (2019) 'Repeated repeat problems: Combinatorial effect of C9orf72-derived dipeptide repeat proteins', *International Journal of Biological Macromolecules*, 127, pp. 136–145. doi: 10.1016/j.ijbiomac.2019.01.035.

Davidson, Y. S. *et al.* (2014) 'Brain distribution of dipeptide repeat proteins in frontotemporal lobar degeneration and motor neurone disease associated with expansions in C9ORF72', *Acta Neuropathologica Communications*, 2(70), pp. 1–13. doi: 10.1186/20515960168.

Debevec, T. *et al.* (2014) 'Moderate exercise blunts oxidative stress induced by normobaric hypoxic confinement', *Medicine and Science in Sports and Exercise*, 46(1), pp. 33–41. doi: 10.1249/MSS.0b013e31829f87ef.

Debray, S. *et al.* (2013) 'Frequency of C9orf72 repeat expansions in amyotrophic lateral sclerosis: a Belgian cohort study', *Neurobiology of Aging*, 34(12), pp. 2890.e7-2890.e12. doi: 10.1016/J.NEUROBIOLAGING.2013.06.009.

Debska-Vielhaber, G. *et al.* (2021) 'Impairment of mitochondrial oxidative phosphorylation in skin fibroblasts of SALS and FALS patients is rescued by in vitro treatment with ROS scavengers', *Experimental Neurology*, 339(December 2020), p. 113620. doi: 10.1016/j.expneurol.2021.113620.

Dedeene, L. *et al.* (2019) 'Circadian sleep/wake-associated cells show dipeptide repeat protein aggregates in C9orf72-related ALS and FTLD cases', *Acta Neuropathologica Communications*, 7(1), p. 189. doi: 10.1186/S40478-019-0845-9.

Van Deerlin, V. M. *et al.* (2008) 'TARDBP mutations in amyotrophic lateral sclerosis with TDP-43 neuropathology: a genetic and histopathological analysis', *Lancet Neurology*, 7(5), p. 409. doi: 10.1016/S1474-4422(08)70071-1.

DeJesus-Hernandez, M. *et al.* (2011) 'Expanded GGGGCC Hexanucleotide Repeat in Noncoding Region of C9ORF72 Causes Chromosome 9p-Linked FTD and ALS', *Neuron*, 72(2), pp. 245–256. doi: 10.1016/j.neuron.2011.09.011.

DeJesus-Hernandez, M. *et al.* (2017) 'In-depth clinico-pathological examination of RNA foci in a large cohort of C9ORF72 expansion carriers', *Acta Neuropathologica*, 134(2), pp. 255–269. doi: 10.1007/s00401-017-1725-7.

Depienne, C. and Mandel, J. L. (2021) '30 years of repeat expansion disorders: What have we learned and what are the remaining challenges?', *American Journal of Human Genetics*, 108(5), pp. 764–785. doi: 10.1016/j.ajhg.2021.03.011.

- Devenney, E. M. *et al.* (2021) 'Factors That Influence Non-Motor Impairment Across the ALS-FTD Spectrum: Impact of Phenotype, Sex, Age, Onset and Disease Stage', *Frontiers in Neurology*, 12, p. 743688. doi: 10.3389/FNEUR.2021.743688/BIBTEX.
- Dickson, D. W. (1998) 'Pick's disease: A modern approach', *Brain Pathology*, 8(2), pp. 339–354. doi: 10.1111/j.1750-3639.1998.tb00158.x.
- Dickson, D. W. *et al.* (2011) 'Neuropathology of Frontotemporal Lobar Degeneration–Tau (FTLD-Tau)', *Journal of Molecular Neuroscience*, 45(3), pp. 384–389. doi: 10.1007/S12031-011-9589-0.
- Dickson, D. W. *et al.* (2019) 'Extensive transcriptomic study emphasizes importance of vesicular transport in C9orf72 expansion carriers', *Acta Neuropathologica Communications*, 7(1), pp. 1–21. doi: 10.1186/S40478-019-0797-0.
- Dobson-Stone, C. *et al.* (2012) 'C9ORF72 repeat expansion in clinical and neuropathologic frontotemporal dementia cohorts', *Neurology*, 79(10), p. 995. doi: 10.1212/WNL.0B013E3182684634.
- Dobson-Stone, C. *et al.* (2013) 'C9ORF72 Repeat Expansion in Australian and Spanish Frontotemporal Dementia Patients', *PLOS ONE*, 8(2), p. e56899. doi: 10.1371/JOURNAL.PONE.0056899.
- Dobson-Stone, C. *et al.* (2020) 'CYLD is a causative gene for frontotemporal dementia – amyotrophic lateral sclerosis', *Brain*, 143(3), pp. 783–799. doi: 10.1093/BRAIN/AWAA039.
- Dols-Icardo, O. *et al.* (2014) 'Characterization of the repeat expansion size in C9orf72 in amyotrophic lateral sclerosis and frontotemporal dementia', *Human Molecular Genetics*, 23(3), pp. 749–754. doi: 10.1093/HMG/DDT460.
- Donnelly, C. J. *et al.* (2013) 'RNA Toxicity from the ALS/FTD C9ORF72 Expansion Is Mitigated by Antisense Intervention', *Neuron*, 80(2), pp. 415–428. doi: 10.1016/j.neuron.2013.10.015.
- Ebbert, M. T. W. *et al.* (2018) 'Long-read sequencing across the C9orf72 "GGGGCC" repeat expansion: implications for clinical use and genetic discovery', *Molecular Neurodegeneration*, 13(1), p. 46. Available at: <https://molecularneurodegeneration.biomedcentral.com/articles/10.1186/s13024-018-0274-4>.
- Edwards-Lee, T. *et al.* (1997) 'The temporal variant of frontotemporal dementia', *Brain*,

120(6), pp. 1027–1040. doi: 10.1093/brain/120.6.1027.

Elden, A. C. *et al.* (2011) 'Ataxin-2 intermediate-length polyglutamine expansions are associated with increased risk for ALS', *Nature*, 466(7310), pp. 1069–1075. doi: 10.1038/nature09320.Ataxin-2.

Elisa, R. *et al.* (2012) 'SQSTM1 mutations in frontotemporal lobar degeneration and amyotrophic lateral sclerosis', *Neurology*, 79(15), pp. 1556–1562. doi: 10.1212/WNL.0B013E31826E25DF.

Ema, M. *et al.* (1997) 'A novel bHLH-PAS factor with close sequence similarity to hypoxia-inducible factor 1 $\alpha$  regulates the VEGF expression and is potentially involved in lung and vascular development', *Proceedings of the National Academy of Sciences of the United States of America*, 94(9), pp. 4273–4278. doi: 10.1073/pnas.94.9.4273.

Epstein, A. C. R. *et al.* (2001) 'C. elegans EGL-9 and mammalian homologs define a family of dioxygenases that regulate HIF by prolyl hydroxylation', *Cell*, 107(1), pp. 43–54. doi: 10.1016/S0092-8674(01)00507-4.

Van Es, M. A. *et al.* (2009) 'Genome-wide association study identifies 19p13.3 (UNC13A) and 9p21.2 as susceptibility loci for sporadic amyotrophic lateral sclerosis', *Nature Genetics*, 41(10), pp. 1083–1087. doi: 10.1038/ng.442.

Etchin, J. *et al.* (2013) 'KPT-330 inhibitor of CRM1 (XPO1)-mediated nuclear export has selective anti-leukaemic activity in preclinical models of T-cell acute lymphoblastic leukaemia and acute myeloid leukaemia', *British Journal of Haematology*, 161(1), pp. 117–127. doi: 10.1111/bjh.12231.

Fang, T. *et al.* (2018) 'Stage at which riluzole treatment prolongs survival in patients with amyotrophic lateral sclerosis: a retrospective analysis of data from a dose-ranging study', *The Lancet Neurology*, 17(5), pp. 416–422. doi: 10.1016/S1474-4422(18)30054-1.

Farg, M. A. *et al.* (2014) 'C9ORF72, implicated in amyotrophic lateral sclerosis and frontotemporal dementia, regulates endosomal trafficking', *Human Molecular Genetics*, 23(13), pp. 3579–3595. doi: 10.1093/hmg/ddu068.

Fasken, M. B. *et al.* (2000) 'A leptomycin B-sensitive homologue of human CRM1 promotes nuclear export of nuclear export sequence-containing proteins in Drosophila cells', *Journal of Biological Chemistry*, 275(3), pp. 1878–1886. doi: 10.1074/jbc.275.3.1878.

Feany, M. B. and Bender, W. W. (2000) 'A Drosophila model of Parkinson's disease', *Nature*, 404, pp. 394–398.

- Feldman, E. L. *et al.* (2022) 'Amyotrophic lateral sclerosis', *The Lancet*, 400(10360), pp. 1363–1380. doi: 10.1016/S0140-6736(22)01272-7.
- Fernández Martínez, M. *et al.* (2008) 'Prevalence of Neuropsychiatric Symptoms in Elderly Patients with Dementia in Mungialde County (Basque Country, Spain)', *Dementia and Geriatric Cognitive Disorders*, 25(2), pp. 103–108. doi: 10.1159/000112215.
- Figuroa-Romero, C. *et al.* (2020) 'Early life metal dysregulation in amyotrophic lateral sclerosis', *Annals of Clinical and Translational Neurology*, 7(6), pp. 872–882. doi: 10.1002/acn3.51006.
- Fomin, V. *et al.* (2018) 'The C9ORF72 Gene, Implicated in Amyotrophic Lateral Sclerosis and Frontotemporal Dementia, Encodes a Protein That Functions in Control of Endothelin and Glutamate Signaling', *Molecular and Cellular Biology*, 38(22). doi: 10.1128/MCB.00155-18.
- Fornerod, M. *et al.* (1997) 'CRM1 is an export receptor for leucine-rich nuclear export signals', *Cell*, 90(6), pp. 1051–1060. doi: 10.1016/S0092-8674(00)80371-2.
- Forsberg, K. *et al.* (2019) 'Misfolded SOD1 inclusions in patients with mutations in C9orf72 and other ALS/FTD-associated genes', *Journal of Neurology, Neurosurgery, and Psychiatry*, 90(8), p. 869. doi: 10.1136/JNNP-2018-319386.
- Frakes, A. E. *et al.* (2014) 'Microglia induce motor neuron death via the classical NF- $\kappa$ B pathway in amyotrophic lateral sclerosis', *Neuron*, 81(5), pp. 1009–1023. doi: 10.1016/j.neuron.2014.01.013.
- Fratta, P. *et al.* (2012) 'C9orf72 hexanucleotide repeat associated with amyotrophic lateral sclerosis and frontotemporal dementia forms RNA G-quadruplexes', *Scientific Reports*, 2, pp. 1–6. doi: 10.1038/srep01016.
- Fratta, P. *et al.* (2013) 'Homozygosity for the C9orf72 GGGGCC repeat expansion in frontotemporal dementia', *Acta Neuropathologica*, 126(3), pp. 401–409. doi: 10.1007/s00401-013-1147-0.
- Freibaum, B. D. *et al.* (2015) 'GGGGCC repeat expansion in C9orf72 compromises nucleocytoplasmic transport', *Nature*, 525(7567), pp. 129–133. doi: 10.1038/nature14974.
- Frick, P. *et al.* (2018) 'Novel antibodies reveal presynaptic localization of C9orf72 protein and reduced protein levels in C9orf72 mutation carriers', *Acta Neuropathologica Communications*, 6(1), p. 72. doi: 10.1186/S40478-018-0579-0.
- Fu, S. C. *et al.* (2013) 'ValidNESs: A database of validated leucine-rich nuclear export

- signals', *Nucleic Acids Research*, 41(D1), pp. 338–343. doi: 10.1093/nar/gks936.
- Galimberti, D. *et al.* (2013) 'Autosomal Dominant Frontotemporal Lobar Degeneration Due to the C9ORF72 Hexanucleotide Repeat Expansion: Late-Onset Psychotic Clinical Presentation', *Biological Psychiatry*, 74(5), pp. 384–391. doi: 10.1016/J.BIOPSYCH.2013.01.031.
- Gatto, N. *et al.* (2020) 'Directly converted astrocytes retain the ageing features of the donor fibroblasts and elucidate the astrocytic contribution to human CNS health and disease', *Aging Cell*, 20(1), pp. 1–22. doi: 10.1111/acer.13281.
- Ge, S. X. *et al.* (2020) 'ShinyGO: A graphical gene-set enrichment tool for animals and plants', *Bioinformatics*, 36(8), pp. 2628–2629. doi: 10.1093/bioinformatics/btz931.
- Geevasinga, N. *et al.* (2015) 'Axonal ion channel dysfunction in C9orf72 familial amyotrophic lateral sclerosis', *JAMA Neurology*, 72(1), pp. 49–57. doi: 10.1001/jamaneurol.2014.2940.
- Gellera, C. *et al.* (2012) 'Ubiquilin 2 mutations in Italian patients with amyotrophic lateral sclerosis and frontotemporal dementia', *Journal of Neurology, Neurosurgery & Psychiatry*. doi: 10.1136/jnnp-2012-303433.
- Gendron, T. F. *et al.* (2013) 'Antisense transcripts of the expanded C9ORF72 hexanucleotide repeat form nuclear RNA foci and undergo repeat-associated non-ATG translation in c9FTD/ALS', *Acta Neuropathologica*, 126(6), pp. 829–844. doi: 10.1007/S00401-013-1192-8.
- Gershoni-Emek, N. *et al.* (2016) 'Proteomic analysis of dynein-interacting proteins in amyotrophic lateral sclerosis synaptosomes reveals alterations in the RNA-binding protein staufen', *Molecular and Cellular Proteomics*, 15(2), pp. 506–522. doi: 10.1074/mcp.M115.049965.
- Giblin, A. *et al.* (2024) 'Neuronal polyunsaturated fatty acids are protective in FTD/ALS', *bioRxiv*, p. 2024.01.16.575677. Available at: <https://www.biorxiv.org/content/10.1101/2024.01.16.575677v1>.
- Gijssels, I. *et al.* (2015) 'The C9orf72 repeat size correlates with onset age of disease, DNA methylation and transcriptional downregulation of the promoter', *Molecular Psychiatry*, 21(8), pp. 1112–1124. doi: 10.1038/mp.2015.159.
- Gillingham, A. K. *et al.* (2014) 'Toward a Comprehensive Map of the Effectors of Rab GTPases', *Developmental Cell*, 31(3), p. 358. doi: 10.1016/j.devcel.2014.10.007.
- Gleixner, E. *et al.* (2016) 'Knockdown of Drosophila hemoglobin suggests a role in O2

- homeostasis', *Insect Biochemistry and Molecular Biology*, 72, pp. 20–30. doi: 10.1016/j.ibmb.2016.03.004.
- Gobrecht, P. *et al.* (2014) 'Sustained GSK3 activity markedly facilitates nerve regeneration', *Nature Communications*, 5. doi: 10.1038/ncomms5561.
- Godfrey, R. K. *et al.* (2023) 'Modelling TDP-43 proteinopathy in *Drosophila* uncovers shared and neuron-specific targets across ALS and FTD relevant circuits', *Acta Neuropathologica Communications*, 11(1), pp. 1–25. doi: 10.1186/S40478-023-01656-0.
- Gomez-Deza, J. *et al.* (2015) 'Dipeptide repeat protein inclusions are rare in the spinal cord and almost absent from motor neurons in C9ORF72 mutant amyotrophic lateral sclerosis and are unlikely to cause their degeneration', *Acta Neuropathologica Communications*, 3(1), p. 38. doi: 10.1186/S40478-015-0218-Y.
- Gómez-Tortosa, E. *et al.* (2013) 'C9ORF72 hexanucleotide expansions of 20-22 repeats are associated with frontotemporal deterioration', *Neurology*, 80(4), pp. 366–370. doi: 10.1212/WNL.0B013E31827F08EA.
- Goodman, L. D. *et al.* (2019) 'Toxic expanded GGGGCC repeat transcription is mediated by the PAF1 complex in C9orf72-associated FTD', *Nature Neuroscience*, 22(6), pp. 863–874. doi: 10.1038/s41593-019-0396-1.Toxic.
- Gorno-Tempini, M. L. *et al.* (2004) 'Cognition and Anatomy in Three Variants of Primary Progressive Aphasia', *Annals of Neurology*, 55, pp. 335–346.
- Gorno-Tempini, M. L. *et al.* (2006) 'Anatomical correlates of early mutism in progressive nonfluent aphasia', *Neurology*, 67, pp. 1849–1851.
- Gorno-Tempini, M. L. *et al.* (2011) 'Classification of primary progressive aphasia and its variants', *Neurology*, 76(11), pp. 1006–1014. doi: 10.1212/WNL.0B013E31821103E6.
- Gorr, T. A., Gassmann, M. and Wappner, P. (2006) 'Sensing and responding to hypoxia via HIF in model invertebrates', *Journal of Insect Physiology*, 52(4), pp. 349–364. doi: 10.1016/j.jinsphys.2006.01.002.
- Goutman, S. A. *et al.* (2019) 'High plasma concentrations of organic pollutants negatively impact survival in amyotrophic lateral sclerosis', *Journal of Neurology, Neurosurgery and Psychiatry*, 90(8), pp. 907–912. doi: 10.1136/jnnp-2018-319785.
- Graff-Radford, N. R. *et al.* (1990) 'Progressive aphasia in a patient with Pick's disease: A neuropsychological, radiologic, and anatomic study', *Neurology*, 40(4), pp. 620–626. doi: 10.1212/wnl.40.4.620.

- Green, A. L. *et al.* (2015) 'Preclinical antitumor efficacy of selective exportin 1 inhibitors in glioblastoma', *Neuro-Oncology*, 17(5), pp. 697–707. doi: 10.1093/neuonc/nou303.
- Gregory, J. M. *et al.* (2020) 'Genetics of Amyotrophic Lateral Sclerosis', *Current Genetic Medicine Reports*, 8, pp. 121–131. doi: 10.1007/s40142-020-00194-8.
- Grima, J. C. *et al.* (2017) 'Mutant Huntingtin Disrupts the Nuclear Pore Complex', *Neuron*, 94(1), pp. 93-107.e6. doi: 10.1016/j.neuron.2017.03.023.
- Gu, Y. Z. *et al.* (1998) 'Molecular characterization and chromosomal localization of a third  $\alpha$ -class hypoxia inducible factor subunit, HIF3 $\alpha$ ', *Gene Expression*, 7(3), pp. 205–213.
- Guarnieri, B. *et al.* (2012) 'Prevalence of Sleep Disturbances in Mild Cognitive Impairment and Dementing Disorders: A Multicenter Italian Clinical Cross-Sectional Study on 431 Patients', *Dementia and Geriatric Cognitive Disorders*, 33(1), pp. 50–58. doi: 10.1159/000335363.
- Guerreiro, R. J. *et al.* (2013) 'Using Exome Sequencing to Reveal Mutations in TREM2 Presenting as a Frontotemporal Dementia-like Syndrome Without Bone Involvement', *JAMA Neurology*, 70(1), pp. 78–84. doi: 10.1001/JAMANEUROL.2013.579.
- Gusarova, G. A. *et al.* (2011) 'Hypoxia Leads to Na,K-ATPase Downregulation via Ca<sup>2+</sup> Release-Activated Ca<sup>2+</sup> Channels and AMPK Activation', *Molecular and Cellular Biology*, 31(17), pp. 3546–3556. doi: 10.1128/mcb.05114-11.
- Haddad, G. G. *et al.* (1997) 'Genetic basis of tolerance to O<sub>2</sub> deprivation in *Drosophila melanogaster*', *Proceedings of the National Academy of Sciences of the United States of America*, 94(20), pp. 10809–10812. doi: 10.1073/pnas.94.20.10809.
- Haddad, G. G. and Ma, E. (2001) 'Neuronal tolerance to O<sub>2</sub> deprivation in *Drosophila*: Novel approaches using genetic models', *Neuroscientist*, 7(6), pp. 538–550. doi: 10.1177/107385840100700610.
- Haeusler, A. R. *et al.* (2014) 'C9orf72 nucleotide repeat structures initiate molecular cascades of disease', *Nature*, 507(7491), pp. 195–200. doi: 10.1038/nature13124.
- Haines, J. D. *et al.* (2015) 'Nuclear export inhibitors avert progression in preclinical models of inflammatory demyelination', *Nature Neuroscience*, 18(4), pp. 511–520. doi: 10.1038/nn.3953.
- Hao, Z. *et al.* (2019) 'Motor dysfunction and neurodegeneration in a C9orf72 mouse line expressing poly-PR', *Nature Communications*, 10(1). doi: 10.1038/s41467-019-10956-w.
- Harms, M. B. *et al.* (2013) 'Lack of C9ORF72 coding mutations supports a gain of function

- for repeat expansions in amyotrophic lateral sclerosis', *Neurobiology of Aging*, 34(9), pp. 2234.e13-2234.e19. doi: 10.1016/j.neurobiolaging.2013.03.006.
- Hartmann, H. *et al.* (2018) 'Proteomics and C9orf72 neuropathology identify ribosomes as poly-GR/PR interactors driving toxicity', *Life Science Alliance*, 1(2), pp. 1–13. doi: 10.26508/lsa.201800070.
- Hayashi, Y. *et al.* (2019) 'Hypoxia/pseudohypoxia-mediated activation of hypoxia-inducible factor-1 $\alpha$  in cancer', *Cancer Science*, 110(5), pp. 1510–1517. doi: 10.1111/cas.13990.
- Hayes, L. R. *et al.* (2020) 'C9orf72 arginine-rich dipeptide repeat proteins disrupt karyopherin-mediated nuclear import', *eLife*, 9, pp. 1–29. doi: 10.7554/eLife.51685.
- He, F. *et al.* (2014) 'TDP-43 suppresses CGG repeat-induced neurotoxicity through interactions with HnRNP A2/B1', *Human Molecular Genetics*, 23(19), pp. 5036–5051. doi: 10.1093/hmg/ddu216.
- Higashi, S. *et al.* (2007) 'Concurrence of TDP-43, tau and  $\alpha$ -synuclein pathology in brains of Alzheimer's disease and dementia with Lewy bodies', *Brain Research*, 1184(1), pp. 284–294. doi: 10.1016/J.BRAINRES.2007.09.048.
- Highley, J. R. *et al.* (2014) 'Loss of nuclear TDP-43 in amyotrophic lateral sclerosis (ALS) causes altered expression of splicing machinery and widespread dysregulation of RNA splicing in motor neurones', *Neuropathology and Applied Neurobiology*, 40(6), pp. 670–685. doi: 10.1111/NAN.12148.
- Hightower, R. M. *et al.* (2020) 'The SINE Compound KPT-350 Blocks Dystrophic Pathologies in DMD Zebrafish and Mice', *Molecular Therapy*, 28(1), pp. 189–201. doi: 10.1016/j.ymthe.2019.08.016.
- Hogan, D. B. *et al.* (2016) 'The prevalence and incidence of frontotemporal dementia: A systematic review', *Canadian Journal of Neurological Sciences*, 43(S1), pp. S96–S109. doi: 10.1017/cjn.2016.25.
- Hopkins, S. R. (2007) 'Exercise-induced Hypoxemia (EIH): Causes and Consequences', in Roach, R., Wagner, P. D., and Hackett, P. (eds) *Hypoxia and Exercise*. Volume 588. Springer Science and Business Media, pp. 17–31.
- Hornbein, T. F. (1992) 'Long Term Effects of High Altitude on Brain Function', *International Journal of Sports Medicine*, 13, pp. 43–45.
- Hsiung, G. Y. R. *et al.* (2012) 'Clinical and pathological features of familial frontotemporal dementia caused by C9ORF72 mutation on chromosome 9p', *Brain*, 135(3), pp. 709–722.

doi: 10.1093/BRAIN/AWR354.

Hu, Y. *et al.* (2011) 'An integrative approach to ortholog prediction for disease-focused and other functional studies', *BMC Bioinformatics*, 12. doi: 10.1186/1471-2105-12-357.

Huang, L. E. *et al.* (1998) 'Regulation of hypoxia-inducible factor 1 $\alpha$  is mediated by an O<sub>2</sub>-dependent degradation domain via the ubiquitin-proteasome pathway', *Proceedings of the National Academy of Sciences of the United States of America*, 95(14), pp. 7987–7992. doi: 10.1073/pnas.95.14.7987.

Hui, A. S. *et al.* (2006) 'Calcium signaling stimulates translation of HIF- $\alpha$  during hypoxia', *The FASEB Journal*, 20(3), pp. 466–475. doi: 10.1096/fj.05-5086com.

Hutten, S. *et al.* (2020) 'Nuclear Import Receptors Directly Bind to Arginine-Rich Dipeptide Repeat Proteins and Suppress Their Pathological Interactions', *Cell Reports*, 33(12), p. 108538. doi: 10.1016/j.celrep.2020.108538.

Hutton, M. *et al.* (1998) 'Association of missense and 5'-splice-site mutations in tau with the inherited dementia FTDP-17', *Nature*, 393, pp. 702–705.

Hyder, F., Rothman, D. L. and Bennett, M. R. (2013) 'Cortical energy demands of signaling and nonsignaling components in brain are conserved across mammalian species and activity levels', *Proceedings of the National Academy of Sciences of the United States of America*, 110(9), pp. 3549–3554. doi: 10.1073/pnas.1214912110.

Iacoangeli, A. *et al.* (2019) 'C9orf72 intermediate expansions of 24-30 repeats are associated with ALS', *Acta Neuropathologica Communications*, 7(1), p. 115. doi: 10.1186/S40478-019-0724-4.

Ilieva, E. V. *et al.* (2007) 'Oxidative and endoplasmic reticulum stress interplay in sporadic amyotrophic lateral sclerosis', *Brain*, 130(12), pp. 3111–3123. doi: 10.1093/brain/awm190.

Ilieva, H. *et al.* (2003) 'Sustained induction of survival p-AKT and p-ERK signals after transient hypoxia in mice spinal cord with G93A mutant human SOD1 protein', *Journal of the Neurological Sciences*, 215(1–2), pp. 57–62. doi: 10.1016/S0022-510X(03)00186-2.

Irisarri, M. *et al.* (2009) 'Central Role of the Oxygen-dependent Degradation Domain of Drosophila HIF $\alpha$ /Sima in Oxygen-dependent Nuclear Export', *Molecular Biology of the Cell*, 20, pp. 3878–3887. doi: 10.1091/mbc.E09.

Irwin, D. J. *et al.* (2013) 'Cognitive decline and reduced survival in C9orf72 expansion Frontotemporal degeneration and Amyotrophic lateral sclerosis', *Journal of Neurology, Neurosurgery, and Psychiatry*, 84(2), p. 163. doi: 10.1136/JNNP-2012-303507.

- Irwin, D. J. *et al.* (2016) 'Deep clinical and neuropathological phenotyping of Pick disease', *Annals of Neurology*, 79(2), pp. 272–287. doi: 10.1002/ana.24559.
- Ishiura, H. and Tsuji, S. (2015) 'Epidemiology and molecular mechanism of frontotemporal lobar degeneration/amyotrophic lateral sclerosis with repeat expansion mutation in C9orf72', *Journal of Neurogenetics*, 29(2–3), pp. 85–94. doi: 10.3109/01677063.2015.1085980.
- Ismail, A. *et al.* (2013) 'Concurrence of multiple sclerosis and amyotrophic lateral sclerosis in patients with hexanucleotide repeat expansions of C9ORF72', *Journal of Neurology, Neurosurgery and Psychiatry*, 84(1), pp. 79–87. doi: 10.1136/jnnp-2012-303326.
- Ismailov, S. M. *et al.* (2014) 'Experimental approach to the gene therapy of motor neuron disease with the use of genes hypoxia-inducible factors', *Russian Journal of Genetics*, 50(5), pp. 518–527. doi: 10.1134/S1022795414050056.
- Ito, K. *et al.* (2011) 'The role of the CNOT1 subunit of the CCR4-NOT complex in mRNA deadenylation and cell viability', *Protein and Cell*, 2(9), pp. 755–763. doi: 10.1007/s13238-011-1092-4.
- Iyer, N. V. *et al.* (1998) 'Cellular and developmental control of O<sub>2</sub> homeostasis by hypoxia-inducible factor 1 $\alpha$ ', *Genes and Development*, 12(2), pp. 149–162. doi: 10.1101/gad.12.2.149.
- Jaakkola, P. *et al.* (2001) 'Targeting of HIF- $\alpha$  to the von Hippel-Lindau ubiquitylation complex by O<sub>2</sub>-regulated prolyl hydroxylation', *Science*, 292(5516), pp. 468–472. doi: 10.1126/science.1059796.
- Jafarinia, H., van der Giessen, E. and Onck, P. R. (2020) 'Phase Separation of Toxic Dipeptide Repeat Proteins Related to C9orf72 ALS/FTD', *Biophysical Journal*, 119(4), pp. 843–851. doi: 10.1016/j.bpj.2020.07.005.
- Jafarinia, H., Van der Giessen, E. and Onck, P. R. (2022) 'Molecular basis of C9orf72 poly-PR interference with the  $\beta$ -karyopherin family of nuclear transport receptors', *Scientific Reports*, 12(1), pp. 1–11. doi: 10.1038/s41598-022-25732-y.
- Jensen, B. K. *et al.* (2020) 'Synaptic dysfunction induced by glycine-alanine dipeptides in C9orf72- ALS / FTD is rescued by SV2 replenishment', *EMBO Molecular Medicine*, 12(5). doi: 10.15252/EMMM.201910722.
- Jewell, U. R. *et al.* (2001) 'Induction of HIF-1 $\alpha$  in response to hypoxia is instantaneous', *The FASEB Journal*, 15(7), pp. 1312–1314. doi: 10.1096/fj.00-0732fje.
- Jo, Y. *et al.* (2022) 'Poly-dipeptides produced from C9orf72 hexanucleotide repeats cause

selective motor neuron hyperexcitability in ALS', *Proceedings of the National Academy of Sciences of the United States of America*, 119(11), pp. 1–11. doi: 10.1073/pnas.2113813119.

Johnson, J. K. *et al.* (2005) 'Frontotemporal Lobar Degeneration: Demographic Characteristics of 353 Patients', *Archives of Neurology*, 62(6), pp. 925–930. doi: 10.1001/ARCHNEUR.62.6.925.

Jovičić, A. *et al.* (2015) 'Modifiers of C9orf72 dipeptide repeat toxicity connect nucleocytoplasmic transport defects to FTD/ALS', *Nature Neuroscience*, 18(9), pp. 1226–1229. doi: 10.1038/nn.4085.

Julian, T. H. *et al.* (2021) 'Physical exercise is a risk factor for amyotrophic lateral sclerosis: Convergent evidence from Mendelian randomisation, transcriptomics and risk genotypes', *EBioMedicine*, 68, p. 103397. doi: 10.1016/j.ebiom.2021.103397.

Just, N. *et al.* (2007) 'High erythropoietin and low vascular endothelial growth factor levels in cerebrospinal fluid from hypoxemic ALS patients suggest an abnormal response to hypoxia', *Neuromuscular Disorders*, 17(2), pp. 169–173. doi: 10.1016/j.nmd.2006.10.004.

Kabashi, E. *et al.* (2008) 'TARDBP mutations in individuals with sporadic and familial amyotrophic lateral sclerosis', *Nature Genetics*, 40(5), pp. 572–574. doi: 10.1038/ng.132.

Kaivorinne, A. *et al.* (2013) 'Clinical Characteristics of C9ORF72 -Linked Frontotemporal Lobar Degeneration', pp. 251–262. doi: 10.1159/000351859.

Kakidani, H. and Ptashne, M. (1988) 'GAL4 activates gene expression in mammalian cells', *Cell*, 52(1), pp. 161–167.

Kallio, P. J. *et al.* (1999) 'Regulation of the hypoxia-inducible transcription factor 1 $\alpha$  by the ubiquitin-proteasome pathway', *Journal of Biological Chemistry*, 274(10), pp. 6519–6525. doi: 10.1074/jbc.274.10.6519.

Kanekura, K. *et al.* (2016) 'Poly-dipeptides encoded by the C9ORF72 repeats block global protein translation', *Human Molecular Genetics*, 25(9), pp. 1803–1813. doi: 10.1093/hmg/ddw052.

Katayama, K. *et al.* (2003) 'Intermittent Hypoxia Improves Endurance Performance and Submaximal Exercise Efficiency', *High Altitude Medicine & Biology*, 4(3).

Katsani, K. R. *et al.* (2008) 'In vivo dynamics of Drosophila nuclear envelope components', *Molecular Biology of the Cell*, 19(9), pp. 3652–3666. doi: 10.1091/MBC.E07-11-1162.

Kehlenbach, R. H. *et al.* (2001) 'Stimulation of Nuclear Export and Inhibition of Nuclear

Import by a Ran Mutant Deficient in Binding to Ran-binding Protein 1', *Journal of Biological Chemistry*, 276(17), pp. 14524–14531. doi: 10.1074/jbc.M011087200.

Keller, A. D. *et al.* (2002) 'Empirical statistical model to estimate the accuracy of protein identifications made by MS/MS and database search', *Analytical Chemistry*, 74(20), pp. 5383–5392.

Kent-Braun, J. A. *et al.* (1998) 'Functional significance of upper and lower motor neuron impairment in amyotrophic lateral sclerosis', *Muscle and Nerve*, 21(6), pp. 762–768. doi: 10.1002/(SICI)1097-4598(199806)21:6<762::AID-MUS8>3.0.CO;2-5.

Kety, S. S. (1957) 'The general metabolism of the brain in vivo', *Metabolism of the Nervous System*, pp. 221–237.

Khosravi, B. *et al.* (2017) 'Cytoplasmic poly-GA aggregates impair nuclear import of TDP-43 in C9orf72 ALS/FTLD', *Human Molecular Genetics*, 26(4), pp. 790–800. doi: 10.1093/hmg/ddw432.

Khosravi, B. *et al.* (2020) 'Cell-to-cell transmission of C9orf72 poly-(Gly-Ala) triggers key features of ALS / FTD', *The EMBO Journal*, 39(8), pp. 1–19. doi: 10.15252/embj.2019102811.

Kim, H. *et al.* (2003) 'Analysis of the effect of aging on the response to hypoxia by cDNA microarray', *Mechanisms of Ageing and Development*, 124(8–9), pp. 941–949. doi: 10.1016/S0047-6374(03)00166-0.

Kim, K. S. *et al.* (2016) 'Oxidative stress-induced telomere length shortening of circulating leukocyte in patients with obstructive sleep apnea', *Ageing and Disease*, 7(5), pp. 604–613. doi: 10.14336/AD.2016.0215.

Kim, S.-M. *et al.* (2013) 'Intermittent Hypoxia Can Aggravate Motor Neuronal Loss and Cognitive Dysfunction in ALS Mice', *PLOS ONE*, 8(11), p. e81808. doi: 10.1371/JOURNAL.PONE.0081808.

Kim, W.-Y. *et al.* (2006) 'Essential roles for GSK-3s and GSK-3 primed substrates in neurotrophin-induced and hippocampal axon growth', *Neuron*, 52(6), pp. 981–996. doi: 10.1016/j.neuron.2006.10.031.Essential.

Kinoshita, Y. *et al.* (2009) 'Nuclear Contour Irregularity and Abnormal Transporter Protein Distribution in Anterior Horn Cells in Amyotrophic Lateral Sclerosis', *Journal of Neuropathology & Experimental Neurology*, 68(11), pp. 1184–1192. doi: 10.1097/NEN.0B013E3181BC3BEC.

- Kırlı, K. *et al.* (2015) 'A deep proteomics perspective on CRM1-mediated nuclear export and nucleocytoplasmic partitioning', *eLife*, 4(DECEMBER2015), pp. 1–28. doi: 10.7554/eLife.11466.
- Kneussel, M. and Wagner, W. (2013) 'Myosin motors at neuronal synapses: Drivers of membrane transport and actin dynamics', *Nature Reviews Neuroscience*, 14(4), pp. 233–247. doi: 10.1038/nrn3445.
- Knopman, D. S. and Roberts, R. O. (2011) 'Estimating the number of persons with frontotemporal lobar degeneration in the US population', *Journal of Molecular Neuroscience*, 45(3), pp. 330–335. doi: 10.1007/S12031-011-9538-Y.
- Koppers, M. *et al.* (2015) 'C9orf72 ablation in mice does not cause motor neuron degeneration or motor deficits', *Annals of Neurology*, 78(3), pp. 426–438. doi: 10.1002/ana.24453.
- Koumenis, C. *et al.* (2002) 'Regulation of Protein Synthesis by Hypoxia via Activation of the Endoplasmic Reticulum Kinase PERK and Phosphorylation of the Translation Initiation Factor eIF2 $\alpha$ ', *Molecular and Cellular Biology*, 22(21), pp. 7405–7416. doi: 10.1128/mcb.22.21.7405-7416.2002.
- Kremer, M. C. *et al.* (2017) 'The glia of the adult *Drosophila* nervous system', *Glia*, 65(4), pp. 606–638. doi: 10.1002/glia.23115.
- Kriachkov, V. *et al.* (2023) 'Arginine-rich C9ORF72 ALS proteins stall ribosomes in a manner distinct from a canonical ribosome-associated quality control substrate', *Journal of Biological Chemistry*, 299(1), p. 102774. doi: 10.1016/j.jbc.2022.102774.
- Krishnan, S. N. *et al.* (1997) 'Behavioural and Electrophysiologic Responses of *Drosophila melanogaster* to Prolonged Periods of Anoxia', *Journal of Insect Physiology*, 43(3), pp. 203–210.
- Kuznetsov, D. *et al.* (2023) 'OrthoDB v11: annotation of orthologs in the widest sampling of organismal diversity', *Nucleic Acids Research*, 51(1 D), pp. D445–D451. doi: 10.1093/nar/gkac998.
- Laaksovirta, H. *et al.* (2010) 'Chromosome 9p21 in Amyotrophic Lateral Sclerosis in Finland: A Genome-Wide Association Study', *Lancet Neurology*, 9(10), p. 978. doi: 10.1016/S1474-4422(10)70184-8.
- Lagier-Tourenne, C. *et al.* (2013) 'Targeted degradation of sense and antisense C9orf72 RNA foci as therapy for ALS and frontotemporal degeneration', *Proceedings of the National*

*Academy of Sciences of the United States of America*, 110(47). doi:  
10.1073/pnas.1318835110.

Lambrechts, D. *et al.* (2003) 'VEGF is a modifier of amyotrophic lateral sclerosis in mice and humans and protects motoneurons against ischemic death', *Nature Genetics*, 34(4), pp. 383–394. doi: 10.1038/ng1211.

Lanata, S. C. and Miller, B. L. (2016) 'The behavioural variant frontotemporal dementia (bvFTD) syndrome in psychiatry', *Journal of Neurology, Neurosurgery and Psychiatry*, 87(5), pp. 501–511. doi: 10.1136/jnnp-2015-310697.

Lando, D. *et al.* (2002) 'FIH-1 is an asparaginyl hydroxylase enzyme that regulates the transcriptional activity of hypoxia-inducible factor', *Genes and Development*, 16(12), pp. 1466–1471. doi: 10.1101/gad.991402.

Landqvist Waldö, M. *et al.* (2015) 'Psychotic symptoms in frontotemporal dementia: a diagnostic dilemma?', *International Psychogeriatrics / Ipa*, 27(4), p. 531. doi:  
10.1017/S1041610214002580.

Lanson, N. A. *et al.* (2011) 'A Drosophila model of FUS-related neurodegeneration reveals genetic interaction between FUS and TDP-43', *Human Molecular Genetics*, 20(13), pp. 2510–2523. doi: 10.1093/hmg/ddr150.

Lapalombella, R. *et al.* (2012) 'Selective inhibitors of nuclear export show that CRM1/XPO1 is a target in chronic lymphocytic leukemia', *Blood*, 120(23), pp. 4621–4634. doi:  
10.1182/blood-2012-05-429506.

Lashley, T. *et al.* (2015) 'Review: An update on clinical, genetic and pathological aspects of frontotemporal lobar degenerations', *Neuropathology and Applied Neurobiology*, 41(7), pp. 858–881. doi: 10.1111/NAN.12250.

Laszlo, Z. I. *et al.* (2022) 'Synaptic proteomics reveal distinct molecular signatures of cognitive change and C9ORF72 repeat expansion in the human ALS cortex', *Acta Neuropathologica Communications*, 10(1), pp. 1–20. doi: 10.1186/s40478-022-01455-z.

Latallo, M. J. *et al.* (2023) 'Single-molecule imaging reveals distinct elongation and frameshifting dynamics between frames of expanded RNA repeats in C9ORF72-ALS/FTD', *Nature Communications*, 14(1). doi: 10.1038/s41467-023-41339-x.

Lavista-Llanos, S. *et al.* (2002) 'Control of the Hypoxic Response in Drosophila melanogaster by the Basic Helix-Loop-Helix PAS Protein Similar', *Molecular and Cellular Biology*, 22(19), p. 6842. doi: 10.1128/MCB.22.19.6842-6853.2002.

- Law, W. J., Cann, K. L. and Hicks, G. G. (2006) 'TLS, EWS and TAF15: A model for transcriptional integration of gene expression', *Briefings in Functional Genomics and Proteomics*, 5(1), pp. 8–14. doi: 10.1093/bfgp/ell015.
- Le, M. U. T. *et al.* (2023) 'Monitoring lipid alterations in Drosophila heads in an amyotrophic lateral sclerosis model with time-of-flight secondary ion mass spectrometry', *Analyst*, 149(3), pp. 846–858. doi: 10.1039/d3an01670f.
- Lederer, C. W. *et al.* (2007) 'Pathways and genes differentially expressed in the motor cortex of patients with sporadic amyotrophic lateral sclerosis', *BMC Genomics*, 8, pp. 1–26. doi: 10.1186/1471-2164-8-26.
- Lee, A. *et al.* (2023) 'Proteomic investigation of ALS motor cortex identifies known and novel pathogenetic mechanisms', *Journal of the Neurological Sciences*, 452, p. 120753. doi: 10.1016/J.JNS.2023.120753.
- Lee, E. B. *et al.* (2017) 'Expansion of the classification of FTLTD-TDP: distinct pathology associated with rapidly progressive frontotemporal degeneration', *Acta Neuropathologica*, 134(1), pp. 65–78. doi: 10.1007/s00401-017-1679-9.
- Lee, J.-W. *et al.* (2004) 'Hypoxia-inducible factor (HIF-1) $\alpha$ : its protein stability and biological functions', *Experimental and Molecular Medicine*, 36(1), pp. 1–12. Available at: <https://www.nature.com/articles/emm20041>.
- Lee, K. H. *et al.* (2016) 'C9orf72 Dipeptide Repeats Impair the Assembly, Dynamics, and Function of Membrane-Less Organelles', *Cell*, 167(3), pp. 774-788.e17. doi: 10.1016/j.cell.2016.10.002.
- Lee, S. and Huang, E. J. (2017) 'Modeling ALS and FTD with iPSC-derived Neurons Sebum', *Brain Research*, 1(1656), pp. 88–97. doi: 10.1016/j.brainres.2015.10.003.Modeling.
- Lee, Y.-B. *et al.* (2017) 'C9orf72 poly GA RAN-translated protein plays a key role in amyotrophic lateral sclerosis via aggregation and toxicity', *Human Molecular Genetics*, 26(24), pp. 4765–4777. doi: 10.1093/hmg/ddx350.
- Leigh, P. N. *et al.* (1991) 'Ubiquitin-immunoreactive intraneuronal inclusions in amyotrophic lateral sclerosis: morphology, distribution, and specificity', *Brain*, 114(2), pp. 775–788. doi: 10.1093/BRAIN/114.2.775.
- Levine, T. P. *et al.* (2013) 'The product of C9orf72, a gene strongly implicated in neurodegeneration, is structurally related to DENN Rab-GEFs', *Bioinformatics*, 29(4), pp. 499–503. doi: 10.1093/BIOINFORMATICS/BTS725.

- Li, H. *et al.* (2022) 'Fly Cell Atlas: A single-nucleus transcriptomic atlas of the adult fruit fly', *Science*, 375(6584). doi: 10.1126/science.abk2432.
- Li, L. B. *et al.* (2008) 'RNA toxicity is a component of ataxin-3 degeneration in *Drosophila*', *Nature*, 453(7198), pp. 1107–1111. doi: 10.1038/nature06909.
- Liu, E. Y. *et al.* (2014) 'C9orf72 hypermethylation protects against repeat expansion-associated pathology in ALS/FTD', *Acta Neuropathologica*, 128(4), pp. 525–541. doi: 10.1007/s00401-014-1286-y.
- Liu, F. *et al.* (2022) 'Proximity proteomics of C9orf72 dipeptide repeat proteins identifies molecular chaperones as modifiers of poly-GA aggregation', *Acta Neuropathologica Communications* 2022 10:1, 10(1), pp. 1–18. doi: 10.1186/S40478-022-01322-X.
- Liu, G., Roy, J. and Johnson, E. A. (2006) 'Identification and function of hypoxia-response genes in *Drosophila melanogaster*', *Physiological Genomics*, 25(1), pp. 134–141. doi: 10.1152/physiolgenomics.00262.2005.
- Liu, T. *et al.* (2017) 'NF- $\kappa$ B signaling in inflammation', *Signal Transduction and Targeted Therapy*, 2(April). doi: 10.1038/sigtrans.2017.23.
- Liz, M. A. *et al.* (2014) 'Neuronal deletion of GSK3 $\beta$  increases microtubule speed in the growth cone and enhances axon regeneration via CRMP-2 and independently of MAP1B and CLASP2', *BMC Biology*, 12(1), pp. 1–19. doi: 10.1186/1741-7007-12-47.
- Lomen-Hoerth, C., Anderson, T. and Miller, B. (2002) 'The overlap of amyotrophic lateral sclerosis and frontotemporal dementia', *Neurology*, 59(7), pp. 1077–1079. doi: 10.1212/WNL.59.7.1077.
- Lopez-Gonzalez, R. *et al.* (2016) 'Poly(GR) in C9ORF72-Related ALS/FTD Compromises Mitochondrial Function and Increases Oxidative Stress and DNA Damage in iPSC-Derived Motor Neurons', *Neuron*, 92(2), pp. 383–391. doi: 10.1016/j.neuron.2016.09.015.
- Loveland, A. B. *et al.* (2022) 'Ribosome inhibition by C9ORF72-ALS/FTD-associated poly-PR and poly-GR proteins revealed by cryo-EM', *Nature Communications*, 13(1), pp. 1–13. doi: 10.1038/s41467-022-30418-0.
- Lyall, R. A. *et al.* (2001) 'Respiratory muscle strength and ventilatory failure in amyotrophic lateral sclerosis', *Brain*, 124(10), pp. 2000–2013. doi: 10.1093/brain/124.10.2000.
- Ma, E. *et al.* (2001) 'Mutation in pre-mRNA adenosine deaminase markedly attenuates neuronal tolerance to O<sub>2</sub> deprivation in *Drosophila melanogaster*', *Journal of Clinical Investigation*, 107(6), pp. 685–693. doi: 10.1172/JCI11625.

- MacKenzie, I. R. *et al.* (2013) 'Dipeptide repeat protein pathology in C9ORF72 mutation cases: Clinico-pathological correlations', *Acta Neuropathologica*, 126(6), pp. 859–879. doi: 10.1007/S00401-013-1181-Y.
- Mackenzie, I. R. A. *et al.* (2007) 'Pathological TDP-43 distinguishes sporadic amyotrophic lateral sclerosis from amyotrophic lateral sclerosis with SOD1 mutations', *Annals of Neurology*, 61(5), pp. 427–434. doi: 10.1002/ANA.21147.
- Mackenzie, I. R. A. *et al.* (2011) 'A harmonized classification system for FTLTDP pathology', *Acta Neuropathologica*, 122(1), pp. 111–113. doi: 10.1007/S00401-011-0845-8.
- Mackenzie, I. R. A. *et al.* (2015) 'Quantitative analysis and clinico-pathological correlations of different dipeptide repeat protein pathologies in C9ORF72 mutation carriers', *Acta Neuropathologica*, 130(6), pp. 845–861. doi: 10.1007/s00401-015-1476-2.
- MacKenzie, I. R. A. *et al.* (2010) 'Nomenclature and nosology for neuropathologic subtypes of frontotemporal lobar degeneration: An update', *Acta Neuropathologica*, 119(1), pp. 1–4. doi: 10.1007/S00401-009-0612-2.
- MacKenzie, I. R. A. *et al.* (2011) 'Distinct pathological subtypes of FTLTDP-FUS', *Acta Neuropathologica*, 121(2), pp. 207–218. doi: 10.1007/S00401-010-0764-0.
- Mackenzie, I. R. A., Frick, P. and Neumann, M. (2014) 'The neuropathology associated with repeat expansions in the C9ORF72 gene', *Acta Neuropathologica*, 127(3), pp. 347–357. doi: 10.1007/S00401-013-1232-4.
- MacKenzie, I. R. A. and Neumann, M. (2012) 'FET proteins in frontotemporal dementia and amyotrophic lateral sclerosis', *Brain Research*, 1462, pp. 40–43. doi: 10.1016/j.brainres.2011.12.010.
- Magalhães, J. *et al.* (2004) 'Oxidative Stress in Humans During and After 4 Hours of Hypoxia at a Simulated Altitude of 5500 m', *Aviation, Space and Environment Medicine*, 75(1), pp. 16–22.
- Magalhães, J. *et al.* (2005) 'Acute and severe hypobaric hypoxia increases oxidative stress and impairs mitochondrial function in mouse skeletal muscle', *Journal of Applied Physiology*, 99(4), pp. 1247–1253. doi: 10.1152/JAPPLPHYSIOL.01324.2004.
- Maharjan, N. *et al.* (2017) 'C9ORF72 Regulates Stress Granule Formation and Its Deficiency Impairs Stress Granule Assembly, Hypersensitizing Cells to Stress', *Molecular Neurobiology*, 54(4), pp. 3062–3077. doi: 10.1007/S12035-016-9850-1/.
- Malacrida, S. *et al.* (2022) 'Lifespan and ROS levels in different *Drosophila melanogaster*

strains after 24 h hypoxia exposure', *Biology Open*, 11(6). doi: 10.1242/BIO.059386/275522.

Manalo, D. J. *et al.* (2005) 'Transcriptional regulation of vascular endothelial cell responses to hypoxia by HIF-1', *Blood*, 105(2), pp. 659–669. doi: 10.1182/blood-2004-07-2958.

Mandelkow, E. M. and Mandelkow, E. (2012) 'Biochemistry and Cell Biology of Tau Protein in Neurofibrillary Degeneration', *Cold Spring Harbor Perspectives in Medicine*, 2(7), pp. 1–25. doi: 10.1101/CSHPERSPECT.A006247.

Mann, D. M. *et al.* (2013) 'Dipeptide repeat proteins are present in the p62 positive inclusions in patients with frontotemporal lobar degeneration and motor neurone disease associated with expansions in C9ORF72', *Acta Neuropathologica Communications*, 1(1), p. 68. doi: 10.1186/2051-5960-1-68.

Marchi, P. M. *et al.* (2022) 'C9ORF72-derived poly-GA DPRs undergo endocytic uptake in iAstrocytes and spread to motor neurons', *Life Science Alliance*, 5(9), pp. 1–19. doi: 10.26508/lsa.202101276.

Marin, B. *et al.* (2015) 'Clinical and demographic factors and outcome of amyotrophic lateral sclerosis in relation to population ancestral origin', *European Journal of Epidemiology* 2015 31:3, 31(3), pp. 229–245. doi: 10.1007/S10654-015-0090-X.

Marina, N. *et al.* (2016) 'Astrocytes and Brain Hypoxia', in *Hypoxia*. Boston, MA: Springer, pp. 201–227.

Marogianni, C. *et al.* (2019) 'The role of C9orf72 in neurodegenerative disorders: a systematic review, an updated meta-analysis, and the creation of an online database', *Neurobiology of Aging*, 84, pp. 238.e25-238.e34. doi: 10.1016/J.NEUROBIOLAGING.2019.04.012.

Masi, R. De and Orlando, S. (2022) 'GANAB and N-Glycans Substrates Are Relevant in Human Physiology, Polycystic Pathology and Multiple Sclerosis: A Review', *International Journal of Molecular Sciences* 2022, Vol. 23, Page 7373, 23(13), p. 7373. doi: 10.3390/IJMS23137373.

Masrori, P. *et al.* (2022) 'The role of inflammation in neurodegeneration: novel insights into the role of the immune system in C9orf72 HRE-mediated ALS/FTD', *Molecular Neurodegeneration*, 17(1), pp. 1–23. doi: 10.1186/s13024-022-00525-z.

Masrori, P. and Van Damme, P. (2020) 'Amyotrophic lateral sclerosis: a clinical review', *European Journal of Neurology*, 27(10), pp. 1918–1929. doi: 10.1111/ene.14393.

Masters, C. L. *et al.* (1985) 'Amyloid plaque core protein in Alzheimer disease and Down

syndrome', *Proceedings of the National Academy of Sciences of the United States of America*, 82(12), pp. 4245–4249. doi: 10.1073/pnas.82.12.4245.

Maxwell, Patrick H. Wiesener, M. S. *et al.* (1999) 'The tumour suppressor protein VHL targets hypoxia-inducible factors for oxygen-dependent proteolysis', *Nature*, 399(1997), pp. 271–275. Available at: doi: 10.1038/20459.

May, S. *et al.* (2014) 'C9orf72 FTL/ALS-associated Gly-Ala dipeptide repeat proteins cause neuronal toxicity and Unc119 sequestration', *Acta Neuropathologica*, 128(4), pp. 485–503. doi: 10.1007/s00401-014-1329-4.

McEachin, Z. T. *et al.* (2020) 'Chimeric Peptide Species Contribute to Divergent Dipeptide Repeat Pathology in c9ALS/FTD and SCA36', *Neuron*, 107(2), pp. 292-305.e6. doi: 10.1016/j.neuron.2020.04.011.

McGurk, L. *et al.* (2021) 'Toxicity of pathogenic ataxin-2 in *Drosophila* shows dependence on a pure CAG repeat sequence', *Human Molecular Genetics*, 30(19), pp. 1797–1810. doi: 10.1093/hmg/ddab148.

McLaughlin, L. R., Vajda, A. and Hardiman, O. (2015) 'Heritability of amyotrophic lateral sclerosis insights from disparate numbers', *JAMA Neurology*, 72(8), pp. 857–858. doi: 10.1001/jamaneurol.2014.4049.

McMillan, C. T. *et al.* (2015) 'C9orf72 promoter hypermethylation is neuroprotective', *Neurology*, 84(16), pp. 1622–1630. doi: 10.1212/WNL.0000000000001495.

Mehta, A. R. *et al.* (2021) 'Mitochondrial bioenergetic deficits in C9orf72 amyotrophic lateral sclerosis motor neurons cause dysfunctional axonal homeostasis', *Acta Neuropathologica*, 141(2), p. 257. doi: 10.1007/S00401-020-02252-5.

Mehta, P. R. *et al.* (2019) 'Younger age of onset in familial amyotrophic lateral sclerosis is a result of pathogenic gene variants, rather than ascertainment bias', *Journal of Neurology, Neurosurgery & Psychiatry*, 90(3), pp. 268–271. doi: 10.1136/JNNP-2018-319089.

Meister, M., Lemaitre, B. and Hoffmann, J. A. (1997) 'Antimicrobial peptide defense in *Drosophila*', *BioEssays*, 19(11), pp. 1019–1026. doi: 10.1002/bies.950191112.

Meulener, M. *et al.* (2005) '*Drosophila* DJ-1 mutants are selectively sensitive to environmental toxins associated with Parkinson's disease', *Current Biology*, 15(17), pp. 1572–1577. doi: 10.1016/j.cub.2005.07.064.

Meulener, M. C. *et al.* (2006) 'Mutational analysis of DJ-1 in *Drosophila* implicates functional inactivation by oxidative damage and aging', *Proceedings of the National Academy of*

*Sciences of the United States of America*, 103(33), pp. 12517–12522. doi: 10.1073/pnas.0601891103.

Meyer, K. *et al.* (2014) 'Direct conversion of patient fibroblasts demonstrates non-cell autonomous toxicity of astrocytes to motor neurons in familial and sporadic ALS', *Proceedings of the National Academy of Sciences of the United States of America*, 111(2), pp. 829–832. doi: 10.1073/pnas.1314085111.

Miklossy, J. *et al.* (2008) 'Enduring involvement of tau,  $\beta$ -amyloid,  $\alpha$ -synuclein, ubiquitin and TDP-43 pathology in the amyotrophic lateral sclerosis/parkinsonism-dementia complex of Guam (ALS/PDC)', *Acta Neuropathologica*, 116(6), pp. 625–637. doi: 10.1007/S00401-008-0439-2/FIGURES/7.

Mitroshina, E. V. *et al.* (2021) 'Hypoxia-Inducible Factor (HIF) in Ischemic Stroke and Neurodegenerative Disease', *Frontiers in Cell and Developmental Biology*, 9(July), pp. 1–14. doi: 10.3389/fcell.2021.703084.

Miyazaki, K. *et al.* (2012) 'Early and progressive impairment of spinal blood flow-glucose metabolism coupling in motor neuron degeneration of ALS model mice', *Journal of Cerebral Blood Flow and Metabolism*, 32(3), pp. 456–467. doi: 10.1038/jcbfm.2011.155.

Mizielinska, S. *et al.* (2013) 'C9orf72 frontotemporal lobar degeneration is characterised by frequent neuronal sense and antisense RNA foci', *Acta Neuropathologica*, 126(6), pp. 845–857. doi: 10.1007/S00401-013-1200-Z.

Mizielinska, S. *et al.* (2014) 'C9orf72 repeat expansions cause neurodegeneration in *Drosophila* through arginine-rich proteins', *Science*, 345(6201), pp. 1192–1194. doi: 10.1126/science.1256800.

Mizielinska, S. *et al.* (2017) 'Bidirectional nucleolar dysfunction in C9orf72 frontotemporal lobar degeneration', *Acta Neuropathologica Communications*, 5(1), p. 29. doi: 10.1186/s40478-017-0432-x.

Moens, T. G. *et al.* (2018) 'Sense and antisense RNA are not toxic in *Drosophila* models of C9orf72-associated ALS/FTD', *Acta Neuropathologica*, 135(3), pp. 445–457. doi: 10.1007/s00401-017-1798-3.

Moens, T. G. *et al.* (2019) 'C9orf72 arginine-rich dipeptide proteins interact with ribosomal proteins in vivo to induce a toxic translational arrest that is rescued by eIF1A', *Acta Neuropathologica*, 137(3), pp. 487–500. doi: 10.1007/S00401-018-1946-4.

Morahan, J. M. *et al.* (2009) 'A genome-wide analysis of brain DNA methylation identifies

new candidate genes for sporadic amyotrophic lateral sclerosis', *Amyotrophic Lateral Sclerosis*, 10(5–6), pp. 418–429. doi: 10.3109/17482960802635397.

Moreau, C. *et al.* (2006) 'Paradoxical response of VEGF expression to hypoxia in CSF of patients with ALS', *Journal of Neurology, Neurosurgery and Psychiatry*, 77(2), pp. 255–257. doi: 10.1136/jnnp.2005.070904.

Moreau, C. *et al.* (2011) 'Deregulation of the hypoxia inducible factor-1 $\alpha$  pathway in monocytes from sporadic amyotrophic lateral sclerosis patients', *Neuroscience*, 172, pp. 110–117. doi: 10.1016/j.neuroscience.2010.10.040.

Mori, K., Arzberger, T., *et al.* (2013) 'Bidirectional transcripts of the expanded C9orf72 hexanucleotide repeat are translated into aggregating dipeptide repeat proteins', *Acta Neuropathologica*, 126(6), pp. 881–893. doi: 10.1007/S00401-013-1189-3/FIGURES/6.

Mori, K., Weng, S.-M., *et al.* (2013) 'The C9orf72 GGGGCC Repeat Is Translated into Aggregating Dipeptide-Repeat Proteins in FTL/ALS', *Science*, 339(6125), pp. 1335–1338. doi: 10.1126/science.1232927.

Morita, M. *et al.* (2006) 'A locus on chromosome 9p confers susceptibility to ALS and frontotemporal dementia', *Neurology*, 66(6), pp. 839–844. doi: 10.1212/01.wnl.0000200048.53766.b4.

Morón-Oset, J. *et al.* (2019) 'Glycine-Alanine dipeptide repeats spread rapidly in a repeat length-and age-dependent manner in the fly brain', *Acta Neuropathologica Communications*, 7(1), pp. 1–14. doi: 10.1186/S40478-019-0860-X.

Mortimer, N. T. and Moberg, K. H. (2013) 'The Archipelago Ubiquitin Ligase Subunit Acts in Target Tissue to Restrict Tracheal Terminal Cell Branching and Hypoxic-Induced Gene Expression', *PLoS Genetics*, 9(2), pp. 21–24. doi: 10.1371/journal.pgen.1003314.

Munoz, D. G. *et al.* (2009) 'FUS pathology in basophilic inclusion body disease', *Acta Neuropathologica*, 118(5), pp. 617–627. doi: 10.1007/s00401-009-0598-9.

Murakami, T. *et al.* (2003) 'Hypoxic induction of vascular endothelial growth factor is selectively impaired in mice carrying the mutant SOD1 gene', *Brain Research*, 989(2), pp. 231–237. doi: 10.1016/S0006-8993(03)03374-2.

Murray, M. E. *et al.* (2011) 'Clinical and neuropathologic heterogeneity of c9FTD/ALS associated with hexanucleotide repeat expansion in C9ORF72', *Acta Neuropathologica*, 122(6), pp. 673–690. doi: 10.1007/S00401-011-0907-Y.

Nagara, Y. *et al.* (2013) 'Impaired Cytoplasmic–Nuclear Transport of Hypoxia-Inducible

Factor-1 $\alpha$  in Amyotrophic Lateral Sclerosis', *Brain Pathology*, 23(5), pp. 534–546. doi: 10.1111/BPA.12040.

Neary, D. *et al.* (1994) 'Clinical and neuropathological criteria for frontotemporal dementia. The Lund and Manchester Groups.', *Journal of Neurology, Neurosurgery, and Psychiatry*, 57(4), p. 416. doi: 10.1136/JNNP.57.4.416.

Neary, D. *et al.* (1998) 'Frontotemporal lobar degeneration: A consensus on clinical diagnostic criteria', *Neurology*, 51, pp. 1546–1554.

Nelson, T. O. *et al.* (1990) 'Cognition and metacognition at extreme altitudes on Mount Everest.', *Journal of Experimental Psychology*, 119(4), pp. 367–374.

Nesvizhskii, A. I. *et al.* (2003) 'A statistical model for identifying proteins by tandem mass spectrometry', *Analytical Chemistry*, 75(17), pp. 4646–4658. doi: 10.1021/ac0341261.

Neumann, M. *et al.* (2006a) 'Ubiquitinated TDP-43 in frontotemporal lobar degeneration and amyotrophic lateral sclerosis', *Science*, 314(5796), pp. 130–133. doi: 10.1126/science.1134108.

Neumann, M. *et al.* (2006b) 'Ubiquitinated TDP-43 in frontotemporal lobar degeneration and amyotrophic lateral sclerosis', *Science*, 314(5796), pp. 130–133. doi: 10.1126/SCIENCE.1134108.

Neumann, M., Rademakers, R., *et al.* (2009) 'A new subtype of frontotemporal lobar degeneration with FUS pathology', *Brain*, 132(11), pp. 2922–2931. doi: 10.1093/brain/awp214.

Neumann, M., Roeber, S., *et al.* (2009) 'Abundant FUS-immunoreactive pathology in neuronal intermediate filament inclusion disease', *Acta Neuropathologica*, 118(5), pp. 605–616. doi: 10.1007/s00401-009-0581-5.

Neumann, M. *et al.* (2011) 'FET proteins TAF15 and EWS are selective markers that distinguish FTLD with FUS pathology from amyotrophic lateral sclerosis with FUS mutations', *Brain*, 134(9), pp. 2595–2609. doi: 10.1093/brain/awr201.

Nihei, Y. *et al.* (2020) 'Poly-glycine–alanine exacerbates C9orf72 repeat expansion-mediated DNA damage via sequestration of phosphorylated ATM and loss of nuclear hnRNPA3', *Acta Neuropathologica*, 139(1), pp. 99–118. doi: 10.1007/S00401-019-02082-0.

Nomura, E. *et al.* (2019) 'Imaging Hypoxic Stress and the Treatment of Amyotrophic Lateral Sclerosis with Dimethyloxalylglycine in a Mice Model', *Neuroscience*, 415, pp. 31–43. doi: 10.1016/J.NEUROSCIENCE.2019.06.025.

- Nonaka, T. *et al.* (2018) 'C9ORF72 dipeptide repeat poly-GA inclusions promote intracellular aggregation of phosphorylated TDP-43', *Human Molecular Genetics*, 27(15), pp. 2658–2670. doi: 10.1093/hmg/ddy174.
- Nordin, A. *et al.* (2015) 'Extensive size variability of the GGGGCC expansion in C9orf72 in both neuronal and non-neuronal tissues in 18 patients with ALS or FTD', *Human Molecular Genetics*, 24(11), pp. 3133–3142. doi: 10.1093/HMG/DDV064.
- Okamoto, K., Mizuno, Y. and Fujita, Y. (2008) 'Bunina bodies in amyotrophic lateral sclerosis', *Neuropathology*, 28(2), pp. 109–115. doi: 10.1111/j.1440-1789.2007.00873.x.
- Okazaki, R., Yamazoe, K. and Inoue, Y. H. (2020) 'Nuclear Export of Cyclin B Mediated by the Nup62 Complex Is Required for Meiotic Initiation in Drosophila Males', *Cells*, 9(2). doi: 10.3390/cells9020270.
- Olzscha, H. *et al.* (2011) 'Amyloid-like aggregates sequester numerous metastable proteins with essential cellular functions', *Cell*, 144(1), pp. 67–78. doi: 10.1016/j.cell.2010.11.050.
- Onesto, E. *et al.* (2016) 'Gene-specific mitochondria dysfunctions in human TARDBP and C9ORF72 fibroblasts', *Acta Neuropathologica Communications*, 4(1), p. 47. doi: 10.1186/S40478-016-0316-5.
- Oosthuysen, B. *et al.* (2001) 'Deletion of the hypoxia-response element in the vascular endothelial growth factor promoter causes motor neuron degeneration', *Nature Genetics*, 28(2), pp. 131–138. doi: 10.1038/88842.
- Otomo, A., Pan, L. and Hadano, S. (2012) 'Dysregulation of the autophagy-endolysosomal system in amyotrophic lateral sclerosis and related motor neuron diseases', *Neurology Research International*, 2012. doi: 10.1155/2012/498428.
- Owen, R. and Gordon-Weeks, P. R. (2003) 'Inhibition of glycogen synthase kinase 3 $\beta$  in sensory neurons in culture alters filopodia dynamics and microtubule distribution in growth cones', *Molecular and Cellular Neuroscience*, 23(4), pp. 626–637. doi: 10.1016/S1044-7431(03)00095-2.
- Pandey, U. B. *et al.* (2007) 'HDAC6 rescues neurodegeneration and provides an essential link between autophagy and the UPS', *Nature*, 447(7146), pp. 859–863. doi: 10.1038/nature05853.
- Park, J. *et al.* (2023) 'Poly(GR) interacts with key stress granule factors promoting its assembly into cytoplasmic inclusions', *Cell Reports*, 42(8). doi: 10.1016/j.celrep.2023.112822.

- Parkinson, N. *et al.* (2006) 'ALS phenotypes with mutations in CHMP2B (charged multivesicular body protein 2B)', *Neurology*, 67, pp. 1074–1077. doi: 10.1136/jnnp-2013-306573.22.
- Perkins, E. M. *et al.* (2021) 'Altered network properties in C9ORF72 repeat expansion cortical neurons are due to synaptic dysfunction', *Molecular Neurodegeneration*, 16(1), pp. 1–16. doi: 10.1186/s13024-021-00433-8.
- Perkins, N. D. (2012) 'The diverse and complex roles of NF- $\kappa$ B subunits in cancer', *Nature Reviews Cancer*, 12(2), pp. 121–132. doi: 10.1038/nrc3204.
- Peters, S. *et al.* (2021) 'Blood Metal Levels and Amyotrophic Lateral Sclerosis Risk: A Prospective Cohort', *Annals of Neurology*, 89(1), pp. 125–133. doi: 10.1002/ana.25932.
- Phukan, J. *et al.* (2012) 'The syndrome of cognitive impairment in amyotrophic lateral sclerosis: a population-based study', *Journal of Neurology, Neurosurgery & Psychiatry*, 83(1), pp. 102–108. doi: 10.1136/JNNP-2011-300188.
- Pick, A. (1892) 'Über die Beziehungen der senilen Hirnatrophie zur Aphasie', *Prager Medizinische Wochenschrift*, 17, pp. 165–167. Available at: <https://cir.nii.ac.jp/crid/1571135649794907264.bib?lang=en> (Accessed: 16 January 2024).
- Porath, B. *et al.* (2016) 'Mutations in GANAB, Encoding the Glucosidase II $\alpha$  Subunit, Cause Autosomal-Dominant Polycystic Kidney and Liver Disease', *American Journal of Human Genetics*, 98(6), pp. 1193–1207. doi: 10.1016/j.ajhg.2016.05.004.
- Prell, T. *et al.* (2014) 'Endoplasmic reticulum stress is accompanied by activation of NF- $\kappa$ B in amyotrophic lateral sclerosis', *Journal of Neuroimmunology*, 270(1–2), pp. 29–36. doi: 10.1016/j.jneuroim.2014.03.005.
- Pronto-Laborinho, A. C., Pinto, S. and De Carvalho, M. (2014) 'Roles of vascular endothelial growth factor in amyotrophic lateral sclerosis', *BioMed Research International*, 2014. doi: 10.1155/2014/947513.
- Pu, M. *et al.* (2022) 'The contribution of proteasomal impairment to autophagy activation by C9orf72 poly-GA aggregates', *Cellular and Molecular Life Sciences*, 79(9), pp. 1–23. doi: 10.1007/S00018-022-04518-5.
- Quaegebeur, A. *et al.* (2020) 'Soluble and insoluble dipeptide repeat protein measurements in C9orf72-frontotemporal dementia brains show regional differential solubility and correlation of poly-GR with clinical severity', *Acta Neuropathologica Communications*, 8(1), p. 184. doi: 10.1186/s40478-020-01036-y.

- Radwan, M. *et al.* (2020) 'Arginine in C9ORF72 Dipolypeptides Mediates Promiscuous Proteome Binding and Multiple Modes of Toxicity', *Molecular & Cellular Proteomics*, 19(4), pp. 640–654. doi: 10.1074/MCP.RA119.001888.
- Raji, J. I. and Potter, C. J. (2021) 'The number of neurons in Drosophila and mosquito brains', *PLoS ONE*, 16(5 May), pp. 1–11. doi: 10.1371/journal.pone.0250381.
- Raman, R. *et al.* (2015) 'Gene expression signatures in motor neurone disease fibroblasts reveal dysregulation of metabolism, hypoxia-response and RNA processing functions', *Neuropathology and Applied Neurobiology*, 41(2), p. 201. doi: 10.1111/NAN.12147.
- Ramic, M. *et al.* (2021) 'Epigenetic Small Molecules Rescue Nucleocytoplasmic Transport and DNA Damage Phenotypes in C9ORF72 ALS/FTD', *Brain Sciences*, 11(11), p. 1543. doi: 10.3390/brainsci11111543.
- Ransom, B. R. and Ransom, C. B. (2012) *Astrocytes: Multitalented stars of the central nervous system*, *Methods in Molecular Biology*. doi: 10.1007/978-1-61779-452-0\_1.
- Rascovsky, K. *et al.* (2011) 'Sensitivity of revised diagnostic criteria for the behavioural variant of frontotemporal dementia', *Brain*, 134(9), pp. 2456–2477. doi: 10.1093/brain/awr179.
- Ratti, A. *et al.* (2012) 'C9ORF72 repeat expansion in a large Italian ALS cohort: evidence of a founder effect', *Neurobiology of Aging*, 33(10), pp. 2528.e7–2528.e14. doi: 10.1016/J.NEUROBIOLAGING.2012.06.008.
- Reiter, L. T. *et al.* (2001) 'A systematic analysis of human disease-associated gene sequences in *Drosophila melanogaster*', *Genome Research*, 11(6), pp. 1114–1125. doi: 10.1101/gr.169101.
- Renton, A. E. *et al.* (2011) 'A hexanucleotide repeat expansion in C9ORF72 is the cause of chromosome 9p21-linked ALS-FTD', *Neuron*, 72(2), pp. 257–268. doi: 10.1016/j.neuron.2011.09.010.A.
- Riemsлагh, F. W. *et al.* (2021) 'Reduction of oxidative stress suppresses poly-GR-mediated toxicity in zebrafish embryos', *Disease Models & Mechanisms*, 14(11). doi: 10.1242/DMM.049092/272601.
- Ringholz, G. M. *et al.* (2005) 'Prevalence and patterns of cognitive impairment in sporadic ALS', *Neurology*, 65(4), pp. 586–590. doi: 10.1212/01.WNL.0000172911.39167.B6.
- Ritson, G. P. *et al.* (2010) 'TDP-43 mediates degeneration in a novel *Drosophila* model of disease caused by mutations in VCP/p97', *Journal of Neuroscience*, 30(22), pp. 7729–7739.

doi: 10.1523/JNEUROSCI.5894-09.2010.

Rius, J. *et al.* (2008) 'NF- $\kappa$ B links innate immunity to the hypoxic response through transcriptional regulation of HIF-1 $\alpha$ ', *Nature*, 453(7196), pp. 807–811. doi: 10.1038/nature06905.

Rizzu, P. *et al.* (2016) 'C9orf72 is differentially expressed in the central nervous system and myeloid cells and consistently reduced in C9orf72, MAPT and GRN mutation carriers', *Acta Neuropathologica Communications*, 4(1), p. 37. doi: 10.1186/s40478-016-0306-7.

Rohrer, J. D. *et al.* (2009) 'The heritability and genetics of frontotemporal lobar degeneration', *Neurology*, 73(18), pp. 1451–1456. doi: 10.1212/WNL.0b013e3181bf997a.

Rossi, A. *et al.* (2021) 'Neural stem cells alter nucleocytoplasmic partitioning and accumulate nuclear polyadenylated transcripts during quiescence', *bioRxiv*. Available at: <https://doi.org/10.1101/2021.01.06.425462>.

Roth, P. *et al.* (2003) 'The Drosophila nucleoporin DNup88 localizes DNup214 and CRM1 on the nuclear envelope and attenuates NES-mediated nuclear export', *The Journal of Cell Biology*, 163(4), p. 701. doi: 10.1083/JCB.200304046.

Rowland, L. P. (1998) 'Diagnosis of amyotrophic lateral sclerosis', *Journal of the Neurological Sciences*, 160(SUPPL. 1), pp. S6–S24. doi: 10.1016/S0022-510X(98)00193-2.

Russ, J. *et al.* (2015) 'Hypermethylation of repeat expanded C9orf72 is a clinical and molecular disease modifier', *Acta Neuropathologica*, 129(1), pp. 39–52. doi: 10.1007/s00401-014-1365-0.

Ryan, S. *et al.* (2022) 'C9orf72 dipeptides disrupt the nucleocytoplasmic transport machinery and cause TDP-43 mislocalisation to the cytoplasm', *Scientific Reports*, 12(1), pp. 1–13. doi: 10.1038/s41598-022-08724-w.

Saberi, S. *et al.* (2015) 'Neuropathology of Amyotrophic Lateral Sclerosis and Its Variants', *Neurologic Clinics*, 33(4), pp. 855–876. doi: 10.1016/j.ncl.2015.07.012.

Saberi, S. *et al.* (2018) 'Sense-encoded poly-GR dipeptide repeat proteins correlate to neurodegeneration and uniquely co-localize with TDP-43 in dendrites of repeat-expanded C9orf72 amyotrophic lateral sclerosis', *Acta Neuropathologica*, 135(3), pp. 459–474. doi: 10.1007/s00401-017-1793-8.

Sahana, T. G. and Zhang, K. (2021) 'Mitogen-activated protein kinase pathway in amyotrophic lateral sclerosis', *Biomedicines*, 9(8). doi: 10.3390/biomedicines9080969.

Sakae, N. *et al.* (2018) 'Poly-GR dipeptide repeat polymers correlate with neurodegeneration

and clinicopathological subtypes in C9ORF72-related brain disease', *Acta Neuropathologica Communications*, 6(1), p. 63. doi: 10.1186/s40478-018-0564-7.

Sasaki, S. *et al.* (1990) 'Ultrastructure of swollen proximal axons of anterior horn neurons in motor neuron disease', *Journal of the Neurological Sciences*, 97(2–3), pp. 233–240. doi: 10.1016/0022-510X(90)90221-8.

Sato, K. *et al.* (2012) 'Impaired response of hypoxic sensor protein HIF-1 $\alpha$  and its downstream proteins in the spinal motor neurons of ALS model mice', *Brain Research*, 1473, pp. 55–62. doi: 10.1016/J.BRAINRES.2012.07.040.

Satoh, J.-I. *et al.* (2014) 'Molecular Network Analysis Suggests a Logical Hypothesis for the Pathological Role of C9orf72 in Amyotrophic Lateral Sclerosis/Frontotemporal Dementia', *Journal of Central Nervous System Disease*, 6. doi: 10.4137/JCNSD.S18103.

Schipper, L. J. *et al.* (2016) 'Prevalence of brain and spinal cord inclusions, including dipeptide repeat proteins, in patients with the C9ORF72 hexanucleotide repeat expansion: a systematic neuropathological review', *Neuropathology and Applied Neurobiology*, 42(6), pp. 547–560. doi: 10.1111/NAN.12284.

Schludi, M. H. *et al.* (2017) 'Spinal poly-GA inclusions in a C9orf72 mouse model trigger motor deficits and inflammation without neuron loss', *Acta Neuropathologica*, 134(2), pp. 241–254. doi: 10.1007/s00401-017-1711-0.

Schmidt, J. *et al.* (2013) 'Genome-wide studies in multiple myeloma identify XPO1/CRM1 as a critical target validated using the selective nuclear export inhibitor KPT-276', *Leukemia*, 27(12), pp. 2357–2365. doi: 10.1038/leu.2013.172.Genome-wide.

Schymick, J. C. *et al.* (2007) 'Progranulin mutations and amyotrophic lateral sclerosis or amyotrophic lateral sclerosis–frontotemporal dementia phenotypes', *Journal of Neurology, Neurosurgery, and Psychiatry*, 78(7), p. 754. doi: 10.1136/JNNP.2006.109553.

Sebastià, J. *et al.* (2009) 'Angiogenin protects motoneurons against hypoxic injury', *Cell Death & Differentiation* 2009 16:9, 16(9), pp. 1238–1247. doi: 10.1038/cdd.2009.52.

Seeley, W. W. *et al.* (2005) 'The natural history of temporal variant frontotemporal dementia', *Neurology*, 64(8), p. 1384. doi: 10.1212/01.WNL.0000158425.46019.5C.

Sellier, C. *et al.* (2016) 'Loss of C9ORF72 impairs autophagy and synergizes with polyQ Ataxin-2 to induce motor neuron dysfunction and cell death', *The EMBO Journal*, 35(12), pp. 1276–1297. doi: 10.15252/EMBJ.201593350.

Selvaraj, B. T. *et al.* (2018) 'C9ORF72 repeat expansion causes vulnerability of motor

- neurons to Ca<sup>2+</sup>-permeable AMPA receptor-mediated excitotoxicity', *Nature Communications*, 9(1). doi: 10.1038/s41467-017-02729-0.
- Sendoel, A. and Hengartner, M. O. (2014) 'Apoptotic cell death under hypoxia', *Physiology*, 29(3), pp. 168–176. doi: 10.1152/physiol.00016.2013.
- Shang, J. *et al.* (2017) 'Aberrant distributions of nuclear pore complex proteins in ALS mice and ALS patients', *Neuroscience*, 350, pp. 158–168. doi: 10.1016/J.NEUROSCIENCE.2017.03.024.
- Shao, Q. *et al.* (2019) 'C9orf72 deficiency promotes motor deficits of a C9ALS/FTD mouse model in a dose-dependent manner', *Acta neuropathologica communications*, 7(1), p. 32. doi: 10.1186/s40478-019-0685-7.
- Sharpe, J. L. *et al.* (2021) 'Modeling C9orf72-Related Frontotemporal Dementia and Amyotrophic Lateral Sclerosis in Drosophila', *Frontiers in Cellular Neuroscience*, 15, p. 424. doi: 10.3389/FNCEL.2021.770937.
- Shatunov, A. *et al.* (2010) 'Chromosome 9p21 in sporadic amyotrophic lateral sclerosis in the UK and seven other countries: A genome-wide association study', *Lancet Neurology*, 9(10), pp. 986–994. doi: 10.1016/S1474-4422(10)70197-6.
- Shi, Y. *et al.* (2018) 'Haploinsufficiency leads to neurodegeneration in C9ORF72 ALS/FTD human induced motor neurons', *Nature Medicine*, 24(3), pp. 313–325. doi: 10.1038/nm.4490.
- Shiota, T. *et al.* (2022) 'C9orf72-Derived Proline:Arginine Poly-Dipeptides Modulate Cytoskeleton and Mechanical Stress Response', *Frontiers in Cell and Developmental Biology*, 10, p. 750829. doi: 10.3389/FCCELL.2022.750829/BIBTEX.
- Shulman, J. M. and Feany, M. B. (2003) 'Genetic Modifiers of Tauopathy in Drosophila', *Genetics*, 165(3), pp. 1233–1242. doi: 10.1093/genetics/165.3.1233.
- Sieben, A. *et al.* (2012) 'The genetics and neuropathology of frontotemporal lobar degeneration', *Acta Neuropathologica* 2012 124:3, 124(3), pp. 353–372. doi: 10.1007/S00401-012-1029-X.
- Silva, R. F. O. *et al.* (2022) 'Automated analysis of activity, sleep, and rhythmic behaviour in various animal species with the Rtivity software', *Scientific Reports*, 12(1), pp. 1–11. doi: 10.1038/s41598-022-08195-z.
- Simón-Sánchez, J. *et al.* (2012) 'The clinical and pathological phenotype of C9ORF72 hexanucleotide repeat expansions', *Brain*, 135(3), pp. 723–735. doi:

10.1093/BRAIN/AWR353.

Sirtori, R. *et al.* (2024) 'Altered nuclear envelope homeostasis is a key pathogenic event in C9ORF72-linked ALS/FTD', *bioRxiv*, 1. Available at: <https://doi.org/10.1101/2024.02.01.578318>.

Sivadasan, R. *et al.* (2016) 'C9ORF72 interaction with cofilin modulates actin dynamics in motor neurons', *Nature Neuroscience*, 19(12), pp. 1610–1618. doi: 10.1038/nn.4407.

Skibinski, G. *et al.* (2005) 'Mutations in the endosomal ESCRTIII-complex subunit CHMP2B in frontotemporal dementia', *Nature Genetics*, 37(8), pp. 806–808. doi: 10.1038/ng1609.

Smeyers, J., Banchi, E. G. and Latouche, M. (2021) 'C9ORF72: What It Is, What It Does, and Why It Matters', *Frontiers in Cellular Neuroscience*, 15. doi: 10.3389/FNCEL.2021.661447/BIBTEX.

Snowden, J. S. *et al.* (2011) 'The most common type of FTL-D-FUS (aFTLD-U) is associated with a distinct clinical form of frontotemporal dementia but is not related to mutations in the FUS gene', *Acta Neuropathologica*, 122(1), pp. 99–110. doi: 10.1007/s00401-011-0816-0.

Snowden, J. S. *et al.* (2012) 'Distinct clinical and pathological characteristics of frontotemporal dementia associated with C9ORF72 mutations', *Brain*, 135(3), pp. 693–708. doi: 10.1093/BRAIN/AWR355.

Snowden, J. S., Neary, D. and Mann, D. M. A. (2002) 'Frontotemporal dementia', *British Journal of Psychiatry*, 180, pp. 140–143. doi: 10.1007/978-1-84996-011-3\_6.

Solomon, D. A. *et al.* (2018) 'A feedback loop between dipeptide-repeat protein, TDP-43 and karyopherin- $\alpha$  mediates C9orf72-related neurodegeneration', *Brain*, 141(10), pp. 2908–2924. doi: 10.1093/brain/awy241.

Sowa, A. S. *et al.* (2018) 'Karyopherin  $\alpha$ -3 is a key protein in the pathogenesis of spinocerebellar ataxia type 3 controlling the nuclear localization of ataxin-3', *Proceedings of the National Academy of Sciences of the United States of America*, 115(11), pp. E2624–E2633. doi: 10.1073/pnas.1716071115.

Spillantini, M. G. *et al.* (1997) 'a-Synuclein In Lewy Bodies.', *Nature*, 388, pp. 839–840.

Sreedharan, J. *et al.* (2015) 'Age-dependent TDP-43-mediated Motor Neuron Degeneration Requires GSK3, Hat-trick, and Xmas-2', *Current Biology*, 25(16), pp. 2130–2136. doi: 10.1016/j.cub.2015.06.045.Age-dependent.

Srikanth, S., Nagaraja, A. V. and Ratnavalli, E. (2005) 'Neuropsychiatric symptoms in dementia-frequency, relationship to dementia severity and comparison in Alzheimer's

- disease, vascular dementia and frontotemporal dementia', *Journal of the Neurological Sciences*, 236(1–2), pp. 43–48. doi: 10.1016/J.JNS.2005.04.014.
- Stade, K. *et al.* (1997) 'Exportin 1 (Crm1p) is an essential nuclear export factor', *Cell*, 90(6), pp. 1041–1050. doi: 10.1016/S0092-8674(00)80370-0.
- Stewart, H. *et al.* (2012) 'Clinical and pathological features of amyotrophic lateral sclerosis caused by mutation in the C9ORF72 gene on chromosome 9p', *Acta Neuropathologica*, 123(3), pp. 409–417. doi: 10.1007/S00401-011-0937-5/FIGURES/1.
- Steyaert, J. *et al.* (2018) 'FUS-induced neurotoxicity in *Drosophila* is prevented by downregulating nucleocytoplasmic transport proteins', *Human Molecular Genetics*, 27(23), pp. 4103–4116. doi: 10.1093/HMG/DDY303.
- Su, F. C. *et al.* (2016) 'Association of environmental toxins with amyotrophic lateral sclerosis', *JAMA Neurology*, 73(7), pp. 803–811. doi: 10.1001/jamaneurol.2016.0594.
- Suh, E. R. *et al.* (2015) 'Semi-automated quantification of C9orf72 expansion size reveals inverse correlation between hexanucleotide repeat number and disease duration in frontotemporal degeneration', *Acta Neuropathologica*, 130(3), pp. 363–372. doi: 10.1007/S00401-015-1445-9.
- Sullivan, P. M. *et al.* (2016) 'The ALS/FTLD associated protein C9orf72 associates with SMCR8 and WDR41 to regulate the autophagy-lysosome pathway', *Acta Neuropathologica Communications*, 4(1), p. 51. doi: 10.1186/S40478-016-0324-5/FIGURES/10.
- Sun, Z. and Andersson, R. (2002) 'NF- $\kappa$ B Activation and Inhibition: A Review', *Shock*, 18(2), pp. 99–106. doi: 10.1177/1461444810365020.
- Suzuki, H. and Matsuoka, M. (2021) 'Proline-arginine poly-dipeptide encoded by the C9orf72 repeat expansion inhibits adenosine deaminase acting on RNA', *Journal of Neurochemistry*, 158(3), pp. 753–765. doi: 10.1111/jnc.15445.
- Swaminathan, A. *et al.* (2018) 'Expression of C9orf72-related dipeptides impairs motor function in a vertebrate model', *Human Molecular Genetics*, 27(10), pp. 1754–1762. doi: 10.1093/hmg/ddy083.
- Swarup, V. *et al.* (2011) 'Deregulation of TDP-43 in amyotrophic lateral sclerosis triggers nuclear factor  $\kappa$ B-mediated pathogenic pathways', *Journal of Experimental Medicine*, 208(12), pp. 2429–2447. doi: 10.1084/jem.20111313.
- Swinnen, B. *et al.* (2018) 'A zebrafish model for C9orf72 ALS reveals RNA toxicity as a pathogenic mechanism', *Acta Neuropathologica*, 135(3), pp. 427–443. doi: 10.1007/s00401-

017-1796-5.

Szubski, C., Burtscher, M. and Löscher, W. N. (2006) 'The effects of short-term hypoxia on motor cortex excitability and neuromuscular activation', *Journal of Applied Physiology*, 101(6), pp. 1673–1677. doi: 10.1152/jappphysiol.00617.2006.

Tada, S. *et al.* (2019) 'Single injection of sustained-release prostacyclin analog ONO-1301-MS ameliorates hypoxic toxicity in the murine model of amyotrophic lateral sclerosis', *Scientific Reports*, 9(1), pp. 1–9. doi: 10.1038/s41598-019-41771-4.

Tao, Z. *et al.* (2015) 'Nucleolar stress and impaired stress granule formation contribute to C9orf72 RAN translation-induced cytotoxicity', *Human Molecular Genetics*, 24(9), pp. 2426–2441. doi: 10.1093/hmg/ddv005.

Therrien, M. *et al.* (2013) 'Deletion of C9ORF72 results in motor neuron degeneration and stress sensitivity in *C. elegans*', *PLoS ONE*, 8(12), pp. 1–10. doi: 10.1371/journal.pone.0083450.

Thomas, F. and Kutay, U. (2003) 'Biogenesis and nuclear export of ribosomal subunits in higher eukaryotes depend on the CRM1 export pathway', *Journal of Cell Science*, 116(12), pp. 2409–2419. doi: 10.1242/jcs.00464.

Thomason, P. A., King, J. S. and Insall, R. H. (2017) 'Mroh1, a lysosomal regulator localized by WASH-generated actin', *Journal of Cell Science*, 130(10), pp. 1785–1795. doi: 10.1242/jcs.197210.

Thompson, S. A., Patterson, K. and Hodges, J. R. (2003) 'Left/right asymmetry of atrophy in semantic dementia: Behavioral-cognitive implications', *Neurology*, 61(9), pp. 1196–1203. doi: 10.1212/01.WNL.0000091868.28557.B8.

Tootle, T. L., Lee, P. S. and Rebay, I. (2003) 'CRM1-mediated nuclear export and regulated activity of the Receptor Tyrosine Kinase antagonist YAN require specific interactions with MAE', *Development*, 130(5), pp. 845–857. doi: 10.1242/DEV.00312.

Tornatore, L. *et al.* (2012) 'The nuclear factor kappa B signaling pathway: Integrating metabolism with inflammation', *Trends in Cell Biology*, 22(11), pp. 557–566. doi: 10.1016/j.tcb.2012.08.001.

Tran, H. *et al.* (2015) 'Differential Toxicity of Nuclear RNA Foci versus Dipeptide Repeat Proteins in a *Drosophila* Model of C9ORF72 FTD/ALS', *Neuron*, 87(6), pp. 1207–1214. doi: 10.1016/j.neuron.2015.09.015.

Tu, W. Y. *et al.* (2023) 'C9orf72 poly-GA proteins impair neuromuscular transmission',

*Zoological Research*, 44(2), p. 331. doi: 10.24272/J.ISSN.2095-8137.2022.356.

Urwin, H. *et al.* (2010) 'FUS pathology defines the majority of tau-and TDP-43-negative frontotemporal lobar degeneration', *Acta Neuropathologica*, 120(1), pp. 33–41. doi: 10.1007/s00401-010-0698-6.

Uy, G. *et al.* (2024) 'The Effects of poly-GA and poly-PR C9orf72 Dipeptide Repeats on Sleep Patterns in *Drosophila melanogaster*', *MicroPublication Biology*, (C). Available at: 10.17912/micropub.biology.000973.

Vanacore, N. *et al.* (2010) 'Job strain, hypoxia and risk of amyotrophic lateral sclerosis: Results from a death certificate study', *Amyotrophic Lateral Sclerosis*, 11(5), pp. 430–434. doi: 10.3109/17482961003605796.

Vance, C. *et al.* (2006) 'Familial amyotrophic lateral sclerosis with frontotemporal dementia is linked to a locus on chromosome 9p13.2–21.3', *Brain*, 129(4), pp. 868–876. doi: 10.1093/BRAIN/AWL030.

Vance, C. *et al.* (2009) 'Mutations in FUS, an RNA processing protein, cause familial Amyotrophic Lateral Sclerosis type 6', *Science*, 323, pp. 1208–1211.

Vangeison, G. *et al.* (2008) 'The good, the bad, and the cell type-specific roles of hypoxia inducible factor-1 $\alpha$  in neurons and astrocytes', *Journal of Neuroscience*, 28(8), pp. 1988–1993. doi: 10.1523/JNEUROSCI.5323-07.2008.

Vanneste, J. *et al.* (2019) 'C9orf72-generated poly-GR and poly-PR do not directly interfere with nucleocytoplasmic transport', *Scientific Reports*, 9(1), pp. 1–10. doi: 10.1038/s41598-019-52035-6.

Vieira, R. T. *et al.* (2013) 'Epidemiology of early-onset dementia: a review of the literature', *Clinical Practice & Epidemiology in Mental Health*, 9(1), pp. 88–95. doi: 10.2174/1745017901309010088.

Viodé, A. *et al.* (2018) 'New antibody-free mass spectrometry-based quantification reveals that C9ORF72 long protein isoform is reduced in the frontal cortex of hexanucleotide-repeat expansion carriers', *Frontiers in Neuroscience*, 12(AUG), pp. 1–11. doi: 10.3389/fnins.2018.00589.

Vissers, L. E. L. M. *et al.* (2020) 'De Novo Variants in CNOT1, a Central Component of the CCR4-NOT Complex Involved in Gene Expression and RNA and Protein Stability, Cause Neurodevelopmental Delay', *American Journal of Human Genetics*, 107(1), pp. 164–172. doi: 10.1016/j.ajhg.2020.05.017.

- Vlahopoulos, S. and Zoumpourlis, V. C. (2004) 'JNK: A key modulator of intracellular signaling', *Biochemistry (Moscow)*, 69(8), pp. 844–854. doi: 10.1023/B:BIRY.0000040215.02460.45.
- Vucic, S. *et al.* (2020) 'ALS is a multistep process in South Korean, Japanese, and Australian patients', *Neurology*, 94(15), pp. E1657–E1663. doi: 10.1212/WNL.00000000000009015.
- Wainger, B. J. and Cudkovicz, M. E. (2015) 'Cortical hyperexcitability in amyotrophic lateral sclerosis C9Orf72 repeats', *JAMA Neurology*, 72(11), pp. 1235–1236. doi: 10.1001/jamaneurol.2015.2197.
- Waite, A. J. *et al.* (2014) 'Reduced C9orf72 protein levels in frontal cortex of amyotrophic lateral sclerosis and frontotemporal degeneration brain with the C9ORF72 hexanucleotide repeat expansion', *Neurobiology of Aging*, 35(7), pp. 1779.e5-1779.e13. doi: 10.1016/j.neurobiolaging.2014.01.016.
- Wang, M. *et al.* (2020) 'C9orf72 associates with inactive Rag GTPases and regulates mTORC1-mediated autophagosomal and lysosomal biogenesis', *Aging Cell*, 19(4), pp. 1–14. doi: 10.1111/accel.13126.
- Wang, R. *et al.* (2019) 'Poly-PR in C9ORF72-Related Amyotrophic Lateral Sclerosis/Frontotemporal Dementia Causes Neurotoxicity by Clathrin-Dependent Endocytosis', *Neuroscience Bulletin*, 35(5), pp. 889–900. doi: 10.1007/s12264-019-00395-4.
- Wang, T. *et al.* (2021) 'C9orf72 regulates energy homeostasis by stabilizing mitochondrial complex I assembly', *Cell Metabolism*, 33(3), pp. 531-546.e9. doi: 10.1016/j.cmet.2021.01.005.
- Wappner, P. *et al.* (2003) 'The hypoxic response in *Drosophila* depends on the bHLH-PAS protein similar and the prolyl-4-hydroxylase, fatiga, that operates as an oxygen sensor.', *Developmental Biology*, 259(2), p. 520.
- Watson, M. R. *et al.* (2008) 'A *Drosophila* model for amyotrophic lateral sclerosis reveals motor neuron damage by human SOD1', *Journal of Biological Chemistry*, 283(36), pp. 24972–24981. doi: 10.1074/jbc.M804817200.
- Watts, G. D. J. *et al.* (2004) 'Inclusion body myopathy associated with Paget disease of bone and frontotemporal dementia is caused by mutant valosin-containing protein', *Nature Genetics*, 36(4), pp. 377–381. doi: 10.1038/ng1332.
- Webster, C. P. *et al.* (2016) 'The C9orf72 protein interacts with Rab1a and the ULK 1

complex to regulate initiation of autophagy', *The EMBO Journal*, 35(15), pp. 1656–1676. doi: 10.15252/embj.201694401.

Webster, N. *et al.* (1988) 'The yeast UASG is a transcriptional enhancer in human hela cells in the presence of the GAL4 trans-activator', *Cell*, 52(2), pp. 169–178. doi: 10.1016/0092-8674(88)90505-3.

Weil, J. V. (2003) 'Variation in human ventilatory control - Genetic influence on the hypoxic ventilatory response', *Respiratory Physiology and Neurobiology*, 135(2–3), pp. 239–246. doi: 10.1016/S1569-9048(03)00048-X.

Wen, X. *et al.* (2014) 'Antisense proline-arginine RAN dipeptides linked to C9ORF72-ALS/FTD form toxic nuclear aggregates that initiate invitro and invivo neuronal death', *Neuron*, 84(6), pp. 1213–1225. doi: 10.1016/j.neuron.2014.12.010.

Wenger, R. H., Stiehl, D. P. and Camenisch, G. (2005) 'Integration of oxygen signaling at the consensus HRE.', *Science's STKE*, 2005(306), pp. 1–13. doi: 10.1126/stke.3062005re12.

West, R. J. H. *et al.* (2018) 'The pro-apoptotic JNK scaffold POSH/SH3RF1 mediates CHMP2BIntron5-associated toxicity in animal models of frontotemporal dementia', *Human Molecular Genetics*, 27(8), pp. 1382–1395. doi: 10.1093/hmg/ddy048.

West, Ryan J H *et al.* (2020) 'Co-expression of C9orf72 related dipeptide-repeats over 1000 repeat units reveals age- and combination-specific phenotypic profiles in Drosophila', *Acta Neuropathologica Communications*, 8(158), pp. 1–19. doi: 10.1186/s40478-020-01028-y.

West, Ryan J.H. *et al.* (2020) 'Neuroprotective activity of ursodeoxycholic acid in CHMP2BIntron5 models of frontotemporal dementia', *Neurobiology of Disease*, 144(August), p. 105047. doi: 10.1016/j.nbd.2020.105047.

Westeneng, H. J. *et al.* (2021) 'Associations between lifestyle and amyotrophic lateral sclerosis stratified by C9orf72 genotype: a longitudinal, population-based, case-control study', *The Lancet Neurology*, 20(5), pp. 373–384. doi: 10.1016/S1474-4422(21)00042-9.

White, M. R. *et al.* (2019) 'C9orf72 Poly(PR) Dipeptide Repeats Disturb Biomolecular Phase Separation and Disrupt Nucleolar Function', *Molecular Cell*, 74(4), pp. 713-728.e6. doi: 10.1016/J.MOLCEL.2019.03.019.

Wiesner, D. *et al.* (2013) 'Fumaric Acid Esters Stimulate Astrocytic VEGF Expression through HIF-1 $\alpha$  and Nrf2', *PLoS ONE*, 8(10), pp. 1–10. doi: 10.1371/journal.pone.0076670.

Wittenberg, R. *et al.* (2020) 'Projections of care for older people with dementia in England: 2015 to 2040', *Age and Ageing*, 49(2), pp. 264–269. doi: 10.1093/ageing/afz154.

Woolley, J. D. *et al.* (2011) 'The diagnostic challenge of psychiatric symptoms in neurodegenerative disease; rates of and risk factors for prior psychiatric diagnosis in patients with early neurodegenerative disease', *The Journal of Clinical Psychiatry*, 72(2), pp. 126–133. doi: 10.4088/JCP.10M06382OLI.

World Health Organization (2020) *The top 10 causes of death*. Available at: <https://www.who.int/news-room/fact-sheets/detail/the-top-10-causes-of-death>.

World Health Organization (2023) 'Dementia Fact Sheet'. Available at: <https://www.who.int/news-room/fact-sheets/detail/dementia>.

Xiao, S. *et al.* (2015) 'Isoform-specific antibodies reveal distinct subcellular localizations of C9orf72 in amyotrophic lateral sclerosis', *Annals of Neurology*, 78(4), pp. 568–583. doi: 10.1002/ana.24469.

Xiong, Z. *et al.* (2021) 'In vivo proteomic mapping through gfp-directed proximity-dependent biotin labelling in zebrafish', *eLife*, 10, pp. 1–21. doi: 10.7554/ELIFE.64631.

Xu, D., Grishin, N. V. and Chook, Y. M. (2012) 'NESdb: A database of NES-containing CRM1 cargoes', *Molecular Biology of the Cell*, 23(18), pp. 3673–3676. doi: 10.1091/mbc.E12-01-0045.

Xu, L. *et al.* (2020) 'Global variation in prevalence and incidence of amyotrophic lateral sclerosis: a systematic review and meta-analysis', *Journal of Neurology*, 267(4), pp. 944–953. doi: 10.1007/S00415-019-09652-Y.

Xu, L. *et al.* (2023) 'C9orf72 poly(PR) aggregation in nucleus induces ALS/FTD-related neurodegeneration in cynomolgus monkeys', *Neurobiology of Disease*, 184(April), p. 106197. doi: 10.1016/j.nbd.2023.106197.

Xu, W. and Xu, J. (2018) 'C9orf72 dipeptide repeats cause selective neurodegeneration and cell-autonomous excitotoxicity in Drosophila glutamatergic neurons', *Journal of Neuroscience*, 38(35), pp. 7741–7752. doi: 10.1523/JNEUROSCI.0908-18.2018.

Xu, Z. *et al.* (2013) 'Expanded GGGGCC repeat RNA associated with amyotrophic lateral sclerosis and frontotemporal dementia causes neurodegeneration', *Proceedings of the National Academy of Sciences of the United States of America*, 110(19), pp. 7778–7783. doi: 10.1073/pnas.1219643110.

Xue, X. *et al.* (2023) 'ERVW-1 Activates ATF6-Mediated Unfolded Protein Response by Decreasing GANAB in Recent-Onset Schizophrenia', *Viruses*, 15(6), p. 1298. doi: 10.3390/V15061298/S1.

- Yamakawa, M. *et al.* (2015) 'Characterization of the dipeptide repeat protein in the molecular pathogenesis of c9FTD/ALS', *Human Molecular Genetics*, 24(6), pp. 1630–1645. doi: 10.1093/hmg/ddu576.
- Yamashita, T. *et al.* (2021) 'Hypoxic stress visualized in the cervical spinal cord of ALS patients', *Neurological Research*, 43(6), pp. 429–433. doi: 10.1080/01616412.2020.1866383.
- Yang, D. *et al.* (2015) 'FTD/ALS-associated poly(GR) protein impairs the Notch pathway and is recruited by poly(GA) into cytoplasmic inclusions', *Acta Neuropathologica*, 130(4), pp. 525–535. doi: 10.1007/s00401-015-1448-6.
- Yang, M. *et al.* (2016) 'A C9ORF72/SMCR8-containing complex regulates ULK1 and plays a dual role in autophagy', *Science Advances*, 2(9), pp. 1–17. doi: 10.1126/sciadv.1601167.
- Yoshimura, S. I. *et al.* (2010) 'Family-wide characterization of the DENN domain Rab GDP-GTP exchange factors', *Journal of Cell Biology*, 191(2), pp. 367–381. doi: 10.1083/JCB.201008051.
- Yu, F. *et al.* (2001) 'HIF-1 $\alpha$  binding to VHL is regulated by stimulus-sensitive proline hydroxylation', *Proceedings of the National Academy of Sciences of the United States of America*, 98(17), pp. 9630–9635. doi: 10.1073/pnas.181341498.
- Zerial, M. and McBride, H. (2001) 'Rab proteins as membrane organizers', *Nature Reviews Molecular Cell Biology*, 2(2), pp. 107–117. doi: 10.1038/35052055.
- Zhang, K. *et al.* (2013) 'Novel selective inhibitors of nuclear export CRM1 antagonists for therapy in mantle cell lymphoma', *Experimental Hematology*, 41(1), pp. 67–78.e4. doi: 10.1016/j.exphem.2012.09.002.
- Zhang, K. *et al.* (2015) 'The C9orf72 repeat expansion disrupts nucleocytoplasmic transport', *Nature*, 525(7567), pp. 56–61. doi: 10.1038/nature14973.
- Zhang, M. *et al.* (2017) 'DNA methylation age-acceleration is associated with disease duration and age at onset in C9orf72 patients', *Acta Neuropathologica*, 134(2), pp. 271–279. doi: 10.1007/s00401-017-1713-y.
- Zhang, Y. J. *et al.* (2014) 'Aggregation-prone c9FTD/ALS poly(GA) RAN-translated proteins cause neurotoxicity by inducing ER stress', *Acta Neuropathologica*, 128(4), pp. 505–524. doi: 10.1007/s00401-014-1336-5.
- Zhang, Y. J. *et al.* (2016) 'C9ORF72 poly(GA) aggregates sequester and impair HR23 and nucleocytoplasmic transport proteins', *Nature Neuroscience*, 19(5), pp. 668–677. doi:

10.1038/nn.4272.

Zhang, Y. J. *et al.* (2018) 'Poly(GR) impairs protein translation and stress granule dynamics in C9orf72-associated frontotemporal dementia and amyotrophic lateral sclerosis', *Nature Medicine*, 24(8), pp. 1136–1142. doi: 10.1038/s41591-018-0071-1.

Zhang, Y. J. *et al.* (2019) 'Heterochromatin anomalies and double-stranded RNA accumulation underlie C9orf72 poly(PR) toxicity', *Science*, 363(6428). doi: 10.1126/science.aav2606.

Zhao, C. *et al.* (2020) 'Mutant C9orf72 human iPSC-derived astrocytes cause non-cell autonomous motor neuron pathophysiology', *Glia*, 68(5), pp. 1046–1064. doi: 10.1002/glia.23761.

Zheng, C. *et al.* (2004) 'Vascular endothelial growth factor prolongs survival in a transgenic mouse model of ALS', *Annals of Neurology*, 56(4), pp. 564–567. doi: 10.1002/ana.20223.

Zhong, Z. *et al.* (2008) 'ALS-causing SOD1 mutants generate vascular changes prior to motor neuron degeneration', *Nature Neuroscience*, 11(4), pp. 420–422. doi: 10.1038/nn2073.

Zou, Z. Y. *et al.* (2017) 'Genetic epidemiology of amyotrophic lateral sclerosis: a systematic review and meta-analysis', *Journal of Neurology, Neurosurgery & Psychiatry*, 88(7), pp. 540–549. doi: 10.1136/JNNP-2016-315018.